Anomalous Charged-Particle Transport in Organic and Soft-Condensed Matter

Thesis submitted by

Peter Stokes BSc(Hons)

in April 2018

for the degree of Doctor of Philosophy

in the College of Science and Engineering

James Cook University

Statement of Access

I, the undersigned, the author of this thesis, understand the James Cook University will make it available for use within the University Library and, by microfilm or other means, allow access to users in other approved libraries. All users consulting with this thesis will have to sign the following statement:

> In consulting this thesis I agree not to copy or closely paraphrase it in whole or in part without the written consent of the author; and to make proper written acknowledgement for any assistance which I have obtained from it.

Beyond this, I do not wish to place any restriction on access to this thesis.

23/04/2018

Peter Stokes — Date

Sources Declaration

I declare that this thesis is my own work and has not been submitted in any form for another degree or diploma at any university or other institute of tertiary education. Information derived from the published and unpublished work of others has been acknowledged in the text and a list of references is given.

23/04/2018

Peter Stokes — Date

Statement of the Contribution of Others

I gratefully acknowledge the following contributions.

Funding support was provided by an Australian Government Research Training Program Scholarship and the James Cook University Graduate Research Scheme.

Contributions to co-authored publications that form the basis of chapters in this thesis were made by the co-authors listed at the start of each chapter.

Editorial assistance was provided in general by Prof Ronald White, Dr Bronson Philippa, and Mr Mitchell Greenberg. For chapters based on co-authored publications, editorial assistance was provided by all listed co-authors.

Acknowledgements

To my supervisor Professor Ronald White, I thank you for your endless support, wisdom and patience during the completion of this work.

To Bronson Philippa and Daniel Cocks, I thank you both for your continued insight and assistance.

To Rob Robson and Nathan Garland, I thank each of you for the fruitful transport theory conversations we shared.

Lastly, to my parents, my brother, and my sister — I am forever grateful for your support and encouragement throughout the course of my studies.

Abstract

A general phase-space kinetic model for non-equilibrium charged particle transport through combined localised and delocalised states is presented that accounts for scattering, trapping/detrapping and recombination loss processes in organic and soft-condensed matter. The model takes the form of a generalised Boltzmann equation, for which an analytical solution is found in Fourier-Laplace space. A Chapman-Enskog-type perturbative solution technique is also applied, confirming the analytical results and highlighting the emergence of a density gradient series representation in the weak-gradient hydrodynamic regime. This representation validates Fick's law for this model, providing expressions for the flux transport coefficients of drift velocity and diffusion. By applying Fick's law, a generalised diffusion equation with a unique global time operator is shown to arise that coincides with both the standard diffusion equation and the Caputo fractional diffusion equation in the respective limits of normal and dispersive transport. A subordination transformation is used to efficiently solve the generalised diffusion equation by mapping from the solution of a corresponding classical diffusion equation.

From the aforementioned density gradient expansion, we extend Fick's law to consider also the third-order transport coefficient of skewness. This extension is in turn applied to yield a corresponding generalised advection-diffusion-skewness equation. Negative skewness is observed and a physical interpretation is provided in terms of the processes of trapping and detrapping. By analogy with the generalised Einstein relation, a relationship between skewness, diffusion, mobility and temperature is also formed.

The phase-space model is generalised further by introducing energy-dependence in the collision, trapping and loss frequencies. The solution of this resulting model is explored indirectly through balance equations for particle continuity, momentum and energy. Generalised Einstein relations (GER) are developed that enable the anisotropic nature of diffusion to be determined in terms of the measured field-dependence of the mobility. Interesting phenomena such as negative differential conductivity (NDC) and recombination heating/cooling are shown to arise from recombination loss processes and the localised and delocalised nature of transport. Fractional generalisations of the GER and mobility are also explored.

Finally, a planar organic semiconductor device simulation is presented that makes use of the aforementioned generalised advection-diffusion equation to account for the trapping and detrapping of charge carriers. In this simulation, we use Poisson's equation to account for space-charge effects and Kirchhoff's circuit laws to account for RC effects. These considerations allow for a variety of charge transport experiments to be simulated in a planar geometry, including time of flight (TOF), charge extraction by linearly increasing voltage (CELIV) and resistance-dependent photovoltage (RPV) experiments. The simulation is used to explore a proposed experimental technique for the characterisation of the recombination coefficient, as well as to study what effects traps would have on the measured current.

List of Publications

This thesis contains content that has been published in the following journal articles:

[1] Peter W. Stokes, Bronson Philippa, Wayne Read, and Ronald D. White. Efficient numerical solution of the time fractional diffusion equation by mapping from its Brownian counterpart. *Journal of Computational Physics*, **282**, 334 (2015). doi:10.1016/j.jcp.2014.11.023

[2] Peter W. Stokes, Bronson Philippa, Daniel Cocks, and Ronald D. White. Solution of a generalized Boltzmann's equation for nonequilibrium charged-particle transport via localized and delocalized states. *Physical Review E*, **93**, 032119 (2016). doi:10.1103/PhysRevE.93.032119

[3] Peter W. Stokes, Bronson Philippa, Daniel Cocks, and Ronald D. White. Generalized balance equations for charged particle transport via localized and delocalized states: Mobility, generalized Einstein relations, and fractional transport. *Physical Review E*, **95**, 042119 (2017). doi:10.1103/PhysRevE.95.042119

[4] Peter W. Stokes, Ilija Simonović, Bronson Philippa, Daniel Cocks, Saša Dujko, and Ronald D. White. Third-order transport coefficients for localised and delocalised charged-particle transport. *Scientific Reports*, **8**, 2226 (2018). doi:10.1038/s41598-018-19711-5

[5] R. D. White, D. G. Cocks, G. Boyle, M. Casey, N. A. Garland, D. Konovalov, B. Philippa, P. Stokes, J. de Urquijo, O. González-Magaña, R. P McEachran, S. J. Buckman, M. J. Brunger, G. Garcia, S. Dujko, and Z. L. Petrovic. Electron transport in biomolecular gaseous and liquid systems: Theory, experiment and self-consistent cross-sections. *Plasma Sources Science and Technology* (2018). doi:10.1088/1361-6595/aabdd7

Conference presentations

- Ronald White, Peter Stokes, and Bronson Philippa. Efficient numerical solution of the time fractional diffusion equation by mapping from its Brownian counterpart. *XXVI IUPAP Conference on Computational Physics (CCP)*, United States, poster presentation (2014).
- Peter W. Stokes, Bronson Philippa, Daniel Cocks, and Ronald D. White. Trapping vs. Scattering: Impact on Charge Transport in Organic Semiconductors. *IUMRS International Conference on Electronic Materials (ICEM)*, Singapore, poster presentation (2016).
- Peter Stokes. A Generalised Boltzmann Equation for Non-Equilibrium Charged Particle Transport via Localised and Delocalised States. *28th Summer School and*

International Symposium on the Physics of Ionized Gases (SPIG) – 4th International Workshop on Non-Equilibrium Processes (NonEqProc), Serbia, invited lecture (2016).

- Peter W. Stokes, Ilija Simonović, Bronson Philippa, Daniel Cocks, Saša Dujko, and Ronald D. White. Combined localised and delocalised transport phenomena. *XX International Symposium on Electron-Molecule Collisions and Swarms (POSMOL)*, Australia, poster presentation (2017).

Contents

List of Figures

1 Introduction

1.1 Dispersive transport in disordered systems

Semiconductors are fundamental to the operation of modern electronic devices, with applications to computing, lighting and solar energy production. Recent research has focused on organic semiconductors to their unique electronic properties, mechanical flexibility, light weight and cost effective processing [7–9]. There thus exists a huge space of potential organic molecules which can, in principle, be tailored to specific applications. In this tailoring process, it is important to be able to characterise the charge carrier transport in these materials. Unlike inorganic semiconductors that are crystalline in nature, many organic materials are disordered and consequently exhibit a fundamentally slower type of charge transport, known as "dispersive transport" [7, 10].

In normal charge transport, as could be described by the diffusion equation, the mean squared displacement of charge carriers increases in linear proportion to time, t. Dispersive transport, however, is characterised by a mean squared displacement that scales sublinearly, proportional to t^{α} where $0 < \alpha < 1$ [11]. Due in part to this non-integer power-law dependence, dispersive transport is also known as "fractional transport".

Physically, dispersive transport arises due to the presence of traps causing particles to become immobilised (localised states) for extended periods of time and resulting in fundamentally slower transport [12]. A number of physical systems have the potential to exhibit dispersive transport. For example, in organic semiconductors, and other disordered media, trapped states arise due to local imperfections or variation in the energetic landscape [12–16]. Trapped states also exist in organic-inorganic metal-halide perovskites and influence the delocalised nature of transport in these materials [17].

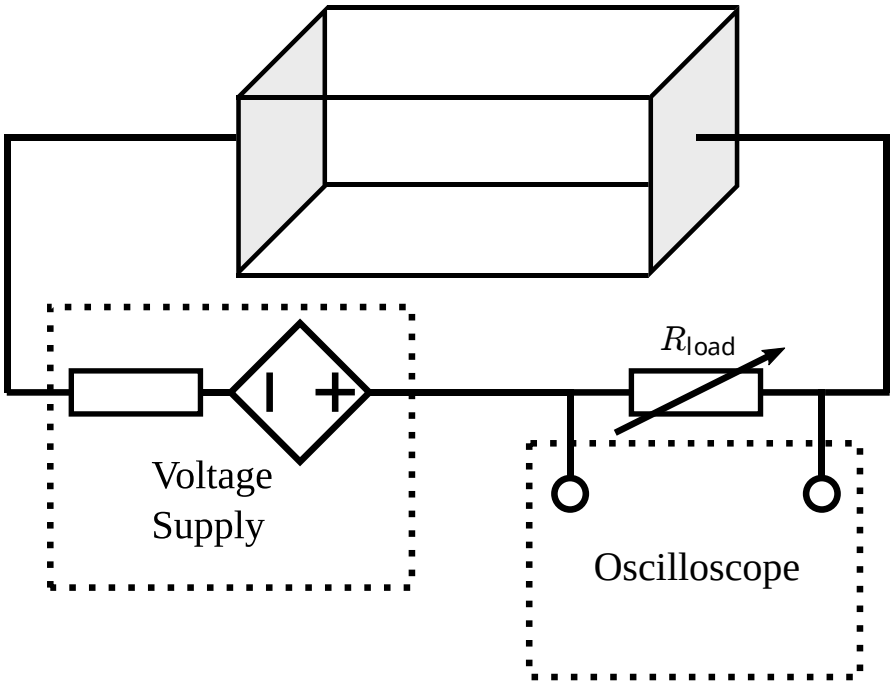

Figure 1.1: Typical charge transport experiment configuration.

Electron transport in certain liquids can be influenced through electrons becoming trapped in (localised) bubble states (see e.g. [18,19]), giving rise to dispersive electronic transport in liquid neon [20]. Similar trapping processes occur for positronium in bubbles (see e.g. [21–23]) and positrons annihilation on induced clusters (see e.g. [24]). The combined localised/delocalised nature of charged transport occurring in many materials warrants the development of a new transport theory to treat and explore the problem, and this represents the theme of this thesis.

1.2 Characterising charge transport experimentally

A number of experiments have been introduced to determine the nature of charged-particle transport in different systems, including in some systems which exhibit dispersive transport. Figure 1.1 illustrates the typical configuration used in many charge transport experiments.

1.2.1 Time Of Flight (TOF)

The Time Of Flight (TOF) experiment, or transient photoconductivity experiment, was introduced in 1957 by Spear [12, 25, 26] to study charge carrier transport in thin evaporated films of amorphous selenium. As illustrated in Figure 1.1, the TOF experiment places a semiconductor sample between two electrodes with a large DC voltage difference. One of the electrodes is transparent, allowing for a brief flash of laser light to photogenerate a thin sheet of charge carriers near the transparent electrode. This sheet then begins to drift due to the electrode potential difference and diffuse due to the temperature . The total time taken for the sheet to traverse and leave the sample

is known as the transit time, t_{tr}, and is observable on the measured current trace. Although described here in terms of semiconductors, TOF is a very general technique that has also been used to determine charged particle transit times in both gaseous and liquid systems.

Accurately determining the transit time is important as it provides the charge carrier drift velocity $\mathbf{W}$, which in turn allows for the calculation of the the charge carrier mobility, μ (the constant of proportionality between drift velocity and electric field, $\mathbf{E}$, satisfying $\mathbf{W} \equiv \mu\mathbf{E}$). However, in the case of dispersive transport, the sheet of drifting charge disperses longitudinally due to repeated trapping events, obfuscating this transit time. For this reason, disordered organic semiconductors are difficult to study with experiments like TOF. It is evident that alternative techniques are required to aid with the classification of organic semiconductors.

1.2.2 Charge Extraction by Linearly Increasing Voltage (CELIV)

The Charge Extraction via Linearly Increasing Voltage (CELIV) experiment was introduced in 2000 by Juška *et al.* [27], in part, to overcome the shortcomings of other methods, like TOF. As with TOF, the CELIV experiment configuration is described by Figure 1.1, except that, rather than using an applied DC voltage, the CELIV experiment uses a pulse of linearly increasing voltage. This has the benefit of producing current traces with easily discernible features, including in the case where transport is dispersive.

There are two types of CELIV experiments which can be performed [27]:

Photo-CELIV — Extraction of photogenerated charge carriers in undoped semiconductors.

Dark-CELIV — Extraction of thermally generated charge carriers in doped semiconductors.

The Photo-CELIV experiment is thus very similar to a TOF experiment, differing only in the voltage applied.

1.2.3 Resistance-dependent PhotoVoltage (RPV)

The Resistance-dependent PhotoVoltage (RPV) experiment was introduced in 2014 by Philippa *et al.* [28] to overcome various limitations of the charge transport experiments described above. For example, CELIV current traces are often difficult to interpret accurately without comparing to a corresponding numerical simulation.

As depicted in Figure 1.1, the RPV experiment uses an identical experiment configuration to TOF, with charge initially photogenerated using a brief flash of laser light. What distinguishes RPV from TOF is the variation of the load resistance, R, over many orders of magnitude. The resulting transients of the voltage on this resistance reveal the transit time of each charge carrier as a "shoulder" in the voltage transient. In turn, this allows for the calculation of the mobility of each charge carrier.

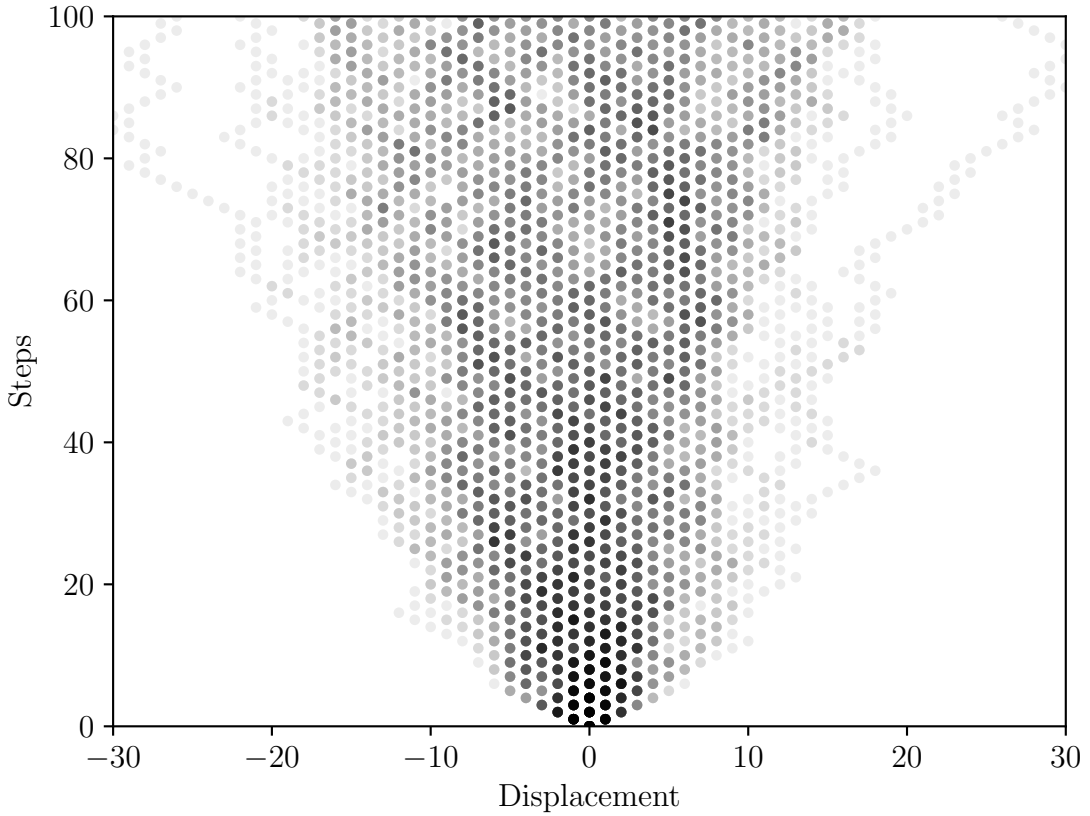

Figure 1.2: One-hundred instances of the classical random walk described by Eq. 1.1 for steps of length $l = 1$.

1.3 Existing models for dispersive transport

Mathematical models for charge transport can be used to design and interpret charge transport experiments, like those discussed in the previous section and depicted in Figure 1.1. Applying any of these charge transport experiments to organic devices thus requires models capable of describing transport that is dispersive. There are a number of dispersive transport models that exist in the literature. We outline some of the main ones in this section, in order of increasing sophistication.

1.3.1 Continuous-time random walks

Both normal and dispersive transport have stochastic formulations in terms of random walk processes [11]. For example, the classical random walk is a simple model for normal transport that consists of a random walker that steps repeatedly in directions sampled from a discrete probability distribution. Consider, for instance, a random walker in one dimension that performs steps of length l with equal likelihood in each direction. In this case, the displacement of each step is sampled uniformly, $\Delta x \in \{-l, l\}$. Figure 1.2 overlays one-hundred instances of this random walk, hinting at the average behaviour of the walker.

To study this simple random walk, we consider a random sequence of N steps, $\{\Delta x_1, \ldots, \Delta x_N\}$. The overall displacement of the random walker from the origin is

then simply the sum of displacements due to each step [29]:

$$x_N = \sum_{i=1}^{N} \Delta x_i. \tag{1.1}$$

As a step in each direction is equally likely, the average displacement of each step is zero $\langle \Delta x_i \rangle = 0$ and thus the expected displacement overall is also zero [29]:

$$\langle x_N \rangle = 0. \tag{1.2}$$

This can be seen in Figure 1.2 as the symmetry about the origin. This figure also strongly suggests a mean squared displacement that increases monotonically. Indeed, we can confirm using Eq. (1.1) that we have the mean squared displacement [29]

$$\left\langle x_N^2 \right\rangle = Nl^2, \tag{1.3}$$

which increases with the number of steps N. Note that N can be thought of as an operational time for the random walker. If we enforce that the random walker has an average speed W, then the mean squared displacement (1.3) can be shown to be proportional to the physical time t [29]:

$$\left\langle x_N^2 \right\rangle = Wlt. \tag{1.4}$$

This property is indicative of normal transport and thus classical random walks are applicable to modelling phenomena where transport is normal. Consequently, classical random walks cannot be applied successfully to modelling cases of dispersive transport where the mean squared displacement increases sublinearly with time.

Montroll and Weiss [30] introduced a generalisation of classical random walks that samples both the jump length and the waiting time between jumps from continuous distributions. This so-called continuous-time random walk (CTRW) is defined entirely by a probability density function $\Psi(t, x)$, introduced such that $\Psi(t, x)\,\mathrm{d}t\mathrm{d}x$ is the infinitesimal probability of jumping a distance between x and $x + \mathrm{d}x$ after waiting for a time between t and $t + \mathrm{d}t$. From this general distribution, we can state separate PDFs for the respective jump length and waiting time [30]:

$$\lambda(x) \equiv \int_0^\infty \Psi(t, x)\,\mathrm{d}t, \tag{1.5}$$

$$w(t) \equiv \int_{-\infty}^\infty \Psi(t, x)\,\mathrm{d}x. \tag{1.6}$$

When it comes to modelling phenomena with a CTRW it can be shown that the precise form of the waiting time and jump length distributions is rarely important and that the model is specified entirely by the moments of the above distributions [11], including

the characteristic waiting time

$$T \equiv \int_0^\infty t w(t)\,\mathrm{d}t, \tag{1.7}$$

the characteristic jump length

$$\chi \equiv \int_{-\infty}^\infty x \lambda(x)\,\mathrm{d}x, \tag{1.8}$$

and the jump length variance

$$\sigma^2 \equiv \int_{-\infty}^\infty x^2 \lambda(x)\,\mathrm{d}x. \tag{1.9}$$

CTRWs have been applied to modelling dispersive transport in disordered semiconductors by Scher and Montroll [12] who proposed a waiting time distribution with a power law tail of the form [12]:

$$w(t) \sim \left(\frac{\tau}{t}\right)^{1+\alpha}, \quad 0 < \alpha < 1, \tag{1.10}$$

where τ is a scaling parameter for the distribution and α describes the severity of trapping, with smaller values corresponding to longer-lived traps. A distribution of this form lacks a characteristic waiting time and so is ideal for modelling dispersive transport where trapping times span many orders of magnitude. Indeed, Scher and Montroll [12] were able to confirm that a heavy-tailed waiting time distribution of this results in a CTRW with a mean squared displacement that scales sublinearly:

$$\left\langle x^2(t) \right\rangle \propto t^\alpha, \tag{1.11}$$

indicating dispersive transport.

1.3.2 Fractional advection-diffusion equation

In addition to stochastic formulations in terms of random walk processes, both normal and dispersive transport have deterministic formulations using diffusion equations [11]. Indeed, the linear time-scaling of the mean squared displacement (1.4) in a classical random walk is indicative of the diffusion equation. In fact, it is known that the probability density function, $n(t, x)$, which describes the likelihood of finding the classical random walker within a certain region of space during a certain interval of time satisfies the diffusion equation [29]:

$$\frac{\partial n}{\partial t} - D\frac{\partial^2 n}{\partial x^2} = 0, \tag{1.12}$$

where D is a diffusion coefficient, proportional to the variance of the classical random walker.

In the case of dispersive transport, the power-law scaling of mean squared displacement (1.11) is distinct from, but reminiscent of, the linear scaling of the diffusion

equation. This suggests that we may be able to describe a dispersive CTRW with a differential equation that is similar in form to the diffusion equation. We can explore the nature of such a generalisation by studying the probability density function $n(t,x)$ in the context of a CTRW. For general CTRWs, the form of $n(t,x)$ is known in Fourier-Laplace space $(t,x) \rightarrow (p,k)$ [31]:

$$n(p,k) \equiv \frac{1-w(p)}{p} \frac{n(0,k)}{1-\lambda(k)\,w(p)}, \tag{1.13}$$

where $n(p,k) \equiv \int_0^\infty \mathrm{d}t \int_{-\infty}^\infty \mathrm{d}x \mathrm{e}^{-(pt+\imath kx)} n(t,x)$. At late times, a waiting time distribution of the form of Eq. (1.10) can be approximated in Laplace-space as [31]

$$w(p) \approx 1-(\tau p)^\alpha . \tag{1.14}$$

Similarly, far from the origin, we can approximate the jump length distribution as [31]

$$\lambda(k) \approx 1+\chi\imath k-\frac{1}{2}\sigma^2 k^2, \tag{1.15}$$

so long as it has a defined jump length variance σ, as is the case considered by Scher and Montroll [12]. Substituting these approximate expressions into Eq. (1.13) and omitting higher order terms (as we are not interested in transient effects) results in the Fourier-Laplace-transformed equation:

$$(\tau p)^{\alpha-1}\left[pn(p,k)-n(0,k)\right]-\frac{\chi}{\tau}\imath k n(p,k)+\frac{\sigma^2}{2\tau}k^2 n(p,k)=0. \tag{1.16}$$

Performing the inverse Fourier-Laplace transform and making use of the convolution theorem yields

$$\tau^{\alpha-1}\frac{t^{-\alpha}}{\Gamma(1-\alpha)} * \frac{\partial n}{\partial t}+W\frac{\partial n}{\partial x}-D\frac{\partial^2 n}{\partial x^2}=0. \tag{1.17}$$

where we have introduced the drift velocity

$$W \equiv \frac{\chi}{\tau}, \tag{1.18}$$

and diffusivity

$$D \equiv \frac{\sigma^2}{2\tau}. \tag{1.19}$$

This is a generalised advection-diffusion equation that describes dispersive transport. The new time operator present is known as the Caputo fractional derivative of order $0<\alpha<1$ and is defined:

$${}_0^{\mathrm{C}}\mathcal{D}_t^\alpha n(t,x) \equiv \frac{\tau^{\alpha-1}}{\Gamma(1-\alpha)}\int_0^t (t-\tau)^{-\alpha}\frac{\partial n}{\partial t}\mathrm{d}\tau. \tag{1.20}$$

Fractional derivatives and fractional calculus in general, are described in more detail in Chapter 2. This generalisation of the advection-diffusion equation is known as a

"fractional advection-diffusion" equation:

$$ {}_{0}^{\mathrm{C}}\mathcal{D}_{t}^{\alpha} n + W_{\alpha} \frac{\partial n}{\partial x} - D_{\alpha} \frac{\partial^2 n}{\partial x^2} = 0, \tag{1.21} $$

with fractional transport coefficients:

$$ W_{\alpha} \equiv \tau^{1-\alpha} W, \tag{1.22} $$

$$ D_{\alpha} \equiv \tau^{1-\alpha} D. \tag{1.23} $$

As the Caputo fractional derivative coincides with ordinary differentiation when $\alpha = 1$, the above fractional advection-diffusion equation evidently coincides with the classical one as $\alpha \to 1$. Importantly, this is consistent with the power-law time-scaling of the mean squared displacement (1.11).

Note that in the above derivation there is an explicit assumption of small spatial gradients in the number density, which manifests implicitly in the fractional advection-diffusion equation (1.21) as the drift-diffusion spatial operator. At the same time, the Caputo fractional derivative is a global time operator can potentially cause initially large spatial gradients to persist for all time. This inconsistency challenges the validity of fractional diffusion equations. In the following section, as an alternative, we describe phase-space kinetic models for dispersive transport that make no such assumptions on the size of spatial gradients [32, 33].

1.3.3 Generalised Boltzmann equation

In 1872, Ludwig Boltzmann introduced the following kinetic equation [34]:

$$ \left(\frac{\partial}{\partial t} + \mathbf{v} \cdot \frac{\partial}{\partial \mathbf{r}} + \mathbf{a} \cdot \frac{\partial}{\partial \mathbf{v}} \right) f\left(t, \mathbf{r}, \mathbf{v}\right) = \left(\frac{\partial f}{\partial t} \right)_{\mathrm{coll}}, \tag{1.24} $$

where $f\left(t, \mathbf{r}, \mathbf{v}\right)$ is a distribution function of particles in phase-space. Here $\mathbf{v} \cdot \frac{\partial f}{\partial \mathbf{r}}$ describes the movement of particles in configuration space due to having a velocity $\mathbf{v}$ and $\mathbf{a} \cdot \frac{\partial f}{\partial \mathbf{v}}$ describes the movement of particles in velocity space due to the applied acceleration $\mathbf{a}$. The $\left(\frac{\partial f}{\partial t}\right)_{\mathrm{coll}}$ term is an operator that describes changes in particle velocity due to binary elastic collisions. For example, for the collision of two particle species "1" and "2" the Boltzmann collision term is

$$ \left(\frac{\partial f}{\partial t} \right)_{\mathrm{coll}}^{(1,2)} = \int \mathrm{d}\mathbf{v}_2 \int \mathrm{d}\Omega_{\mathbf{g}'} g \sigma\left(\mathbf{g}, \mathbf{g}'\right) \left[f_1\left(\mathbf{v}_1'\right) f_2\left(\mathbf{v}_2'\right) - f_1\left(\mathbf{v}_1\right) f_2\left(\mathbf{v}_2\right) \right], \tag{1.25} $$

where numbers denote respective particle quantities, primes denote post-collision quantities, $\mathbf{g} = \mathbf{v}_1 - \mathbf{v}_2$ is the relative velocity between particles, $\mathrm{d}\Omega_{\mathbf{g}'} = \sin\chi \mathrm{d}\chi \mathrm{d}\psi$ is the solid angle of scattering in terms of χ and ψ, the polar angles of $\mathbf{g}'$, and $\sigma\left(\mathbf{g}, \mathbf{g}'\right)$ is the differential cross section defined by [35]

$$ \sigma\left(\mathbf{g}, \mathbf{g}'\right) \mathrm{d}\Omega_{\mathbf{g}'} \equiv \frac{\text{number of particles scattered into solid angle } \mathrm{d}\Omega_{\mathbf{g}'}}{\text{incident particle flux}}. \tag{1.26} $$

The Boltzmann collision integral relies on the assumption that the distribution functions of colliding particles are uncorrelated, known as the collision hypothesis, or *Stosszahlansatz*. As this assumption is no longer true after collision, Boltzmann has thus introduced an "arrow of time" through the formalism of his calculation.

A common simplification of the Boltzmann collision integral is the Bhatnagar-Gross-Krook (BGK) collision operator [36] for collisions between a species of particle and its surrounding medium:

$$\left(\frac{\partial f}{\partial t}\right)_{\text{coll}} = -\nu_{\text{coll}}\left[f\left(t,\mathbf{r},\mathbf{v}\right) - n\left(t,\mathbf{r}\right)w\left(\alpha,v\right)\right], \tag{1.27}$$

where the particle number density in configuration space is given by $n\left(t,\mathbf{r}\right) \equiv \int \mathrm{d}\mathbf{v} f\left(t,\mathbf{r},\mathbf{v}\right)$. The BGK operator describes the relaxation of the distribution function at the collision frequency ν_{coll} to the Maxwellian equilibrium distribution:

$$w\left(\alpha,v\right) \equiv \left(\frac{\alpha^2}{2\pi}\right)^{\frac{3}{2}} \exp\left(-\frac{\alpha^2 v^2}{2}\right), \tag{1.28}$$

$$\alpha^2 \equiv \frac{m}{k_{\text{B}}T}, \tag{1.29}$$

where m is the particle mass, T is the background temperature and $k_{\text{B}}$is the Boltzmann constant. Alternatively, the Boltzmann equation with BGK operator can be thought of as a rate equation in phase space with a loss of incident particles at the rate $\nu_{\text{coll}} f\left(t,\mathbf{r},\mathbf{v}\right)$ and an instantaneous gain of scattered particles at the rate $\nu_{\text{coll}} n\left(t,\mathbf{r}\right) w\left(\alpha,v\right)$. Although generally introduced in this sort of *ad hoc* fashion, the BGK operator can be derived rigorously for the case of resonant charge exchange with a polarisation potential [37]. Due to its simplicity, the BGK collision operator has been applied extensively in the literature on crystalline semiconductors [38]. The use of the BGK collision operator also has the benefit of making the Boltzmann equation amenable to analytical solution techniques [39].

In the weak-gradient hydrodynamic regime, for both of the collision operators above, the Boltzmann equation coincides with the diffusion equation and so cannot be used to describe dispersive transport. With the goal of modelling dispersive transport in organic semiconductors, Philippa *et al.* introduced a new operator that generalises the BGK collision operator to describe trapping and detrapping rather than collisions and scattering, respectively [33]:

$$\left(\frac{\partial f}{\partial t}\right)_{\text{trap/detrap}} = -\nu_{\text{trap}}\left[f\left(t,\mathbf{r},\mathbf{v}\right) - \phi\left(t\right) * n\left(t,\mathbf{r}\right)w\left(\alpha,v\right)\right]. \tag{1.30}$$

Here, similar to the BGK operator, particles are lost at a constant rate (according to the trapping frequency ν_{trap}). However, unlike BGK, this operator does not return scattered particles immediately, but rather after a delay defined by the distribution of trapping times $\phi\left(t\right)$, as depicted in Figure 1.3. As in CTRW theory, choosing a distribution of trapping times with the power-law tail as in Eq. (1.10) results in transport that is dispersive [33]. In particular, Philippa *et al.* considered a multiple

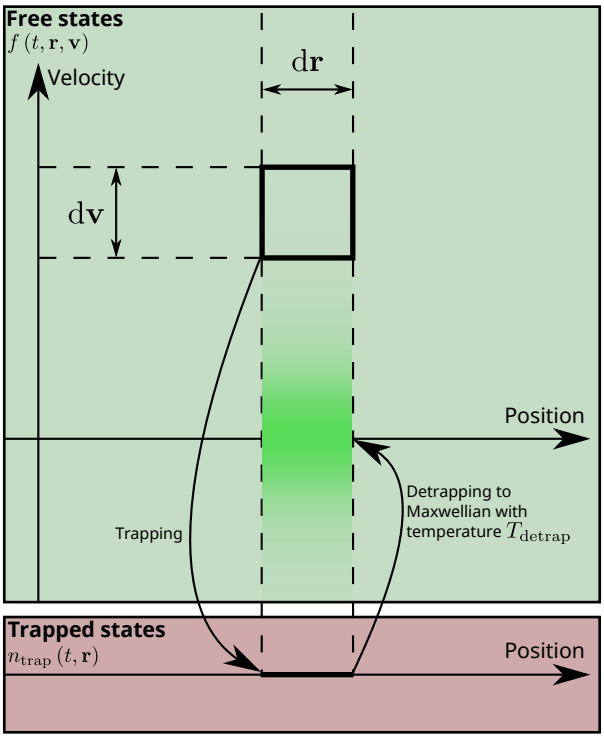

Figure 1.3: Phase space diagram depicting the trapping and detrapping processes modelled by the BGK-type operator (1.30).

trapping model with a uniform trapping cross-section for charge carriers [40], which results in the dispersive trapping time distribution [33]:

$$\phi(t) = \alpha\nu_0 (\nu_0 t)^{-\alpha-1} \gamma(\alpha+1, \nu_0 t), \tag{1.31}$$

where $\gamma(a, z) \equiv \int_0^z \mathrm{d}\zeta\, \zeta^{a-1}\mathrm{e}^{-\zeta}$ is the lower incomplete Gamma function and ν_0 is a frequency characterising the rate of escape from traps. In this case, the trap severity has a physical interpretation as the ratio $\alpha \equiv T/T_\mathrm{c}$, where T is the temperature and T_c is a characteristic temperature that describes the width of the density of trapped states. The delayed BGK operator (1.30) in conjunction with the heavy-tailed trapping time distribution (1.31) will be used extensively throughout this thesis to model dispersive transport due to traps.

1.4 Thesis outline

In Chapter 2 of this thesis, we introduce fractional calculus and outline a technique for the efficient solution of fractional advection-diffusion equations. Chapter 3 introduces and explores a generalised Boltzmann equation that considers collisions, trapping and recombination, and is capable of describing dispersive transport. Chapter 4 continues the investigation of this model by studying the form of its third-order transport coefficient of skewness. Chapter 5 introduces energy-dependence to the aforementioned model and explores a variety of displayed energy-dependent phenomena includ-

ing particle heating/cooling, generalised Einstein relations and NDC. Chapter 6 applies the kinetic model to a simulation of charge transport experiments on planar organic semiconducting devices. Finally, Chapter 7 presents the conclusion and recommendations for future work.

2

Fractional transport

This chapter contains material that has been published in the following journal article:

[1] Peter W. Stokes, Bronson Philippa, Wayne Read, and Ronald D. White. Efficient numerical solution of the time fractional diffusion equation by mapping from its Brownian counterpart. *Journal of Computational Physics*, **282**, 334 (2015). doi:10.1016/j.jcp.2014.11.023

2.1 Introduction

A consequence of dispersive systems, especially those with long-lived traps, is their dependence on their history. The diffusion equation, which uses a local time operator, is fundamentally incapable of describing such memory effects. Mathematically, an adequate model for dispersive transport requires a global time operator that acts on the entire history of the system. In the previous chapter we outlined one successful approach for modelling dispersive transport that involves replacing the the local time derivative in the diffusion equation with a global fractional time derivative of order α [41, 42]. This resulting fractional diffusion equation describes memory effects while also satisfying the required sublinear scaling of the mean squared displacement. This is one of many examples where derivatives of non-integer order have been particularly successful in describing a variety of complex processes with memory effects. Other applications arise in statistical finance [43], economic modelling [44], image processing [45], quantum systems [46] and kinetics [13, 33, 47–51].

In this chapter, we are concerned with the numerical solution of a Caputo fractional advection diffusion model. In particular, for the application toward modelling the

current in a time-of-flight experiment for a disordered semiconductor [13, 49, 52–54]. The Caputo fractional advection diffusion equation is

$$ {}_0^{\mathrm{C}}\mathcal{D}_t^{\alpha} u(t,x) = D\frac{\partial^2}{\partial x^2}u(t,x) - W\frac{\partial}{\partial x}u(t,x), \tag{2.1} $$

where W is a generalised drift velocity, D_{L} is a generalised diffusion coefficient and the operator for Caputo fractional differentiation of order $0 < \alpha < 1$ is defined in terms of the convolution integral [55]

$$ {}_0^{\mathrm{C}}\mathcal{D}_t^{\alpha} f(t) \equiv \frac{1}{\Gamma(1-\alpha)}\int_0^t \mathrm{d}\tau\,(t-\tau)^{-\alpha} f'(\tau). \tag{2.2} $$

Note that the normal advection diffusion equation can be recovered in the relevant limit of no trapping

$$ \lim_{\alpha\to 1} {}_0^{\mathrm{C}}\mathcal{D}_t^{\alpha} u(t,x) = \frac{\partial}{\partial t}u(t,x). \tag{2.3} $$

Numerous methods exist [56–62] for finding the numerical solution of fractional differential equations of the form of Eq. (2.1). Many of these are direct analogues to approaches that are also applicable to integer order differential equations. This is to be expected with the definition of fractional differentiation (2.2) defined in terms of both differentiation and integration. Unfortunately, when solving fractional differential equations numerically there is an increase [63] in time computational complexity over that encountered when solving differential equations of integer order. This is due to the global nature of fractional differentiation and, as in the case of anomalous diffusion, can be interpreted as a result of the system having memory. Consequently, any numerical algorithm that computes the solution at a present point in time requires the entire solution history to do so. In the context of an N-point finite difference time discretisation, this causes a time computational complexity increase from $O(N)$ to $O\left(N^2\right)$ [64].

A number of approaches have been proposed to accelerate the computation of the numerical solution of fractional differential equations [63–67]. As this added computational complexity stems from the memory inherent to the system, many of these approaches involve restricting this memory in some way. Podlubny [63] considered this approach by introducing the *fixed memory principle*, which amounts to truncating the convolution integral in the definition of fractional differentiation (2.2). In effect, this restricts the memory of the system to a fixed interval of time into the past, subsequently allowing for the solution to be found numerically in $O(N)$ in exchange for some loss in solution accuracy. Unfortunately, the only way to guarantee the accuracy of a numerical method used in conjunction with the fixed memory principle is to choose a fixed interval of time that encompasses the entire history of the solution, returning the computational complexity to $O\left(N^2\right)$. Ford and Simpson [64] demonstrated exactly this and, as an alternative, introduced the *logarithmic memory principle*, which samples from the solution history in a logarithmic fashion, allowing for the solution to be found in $O(N\ln N)$ without compromise in solution accuracy. Finally, a number

of parallel computing algorithms have also been introduced [66, 67]. These approaches are viable ways for accelerating the computation of the solution although, as they often involve splitting the problem into smaller problems of the same computational complexity, they are ultimately still of $O\left(N^2\right)$.

In Section 2.2, we briefly introduce fractional calculus and the operators of fractional integration and differentiation. Section 2.3 compares the analytical solution of the fractional diffusion equation (2.1) for a particular order $0 < \alpha < 1$ to the classical diffusion case where $\alpha = 1$. In Section 2.4, we show that the solution to the fractional advection diffusion equation (2.1) can be related to the solution of the normal advection diffusion equation through a linear mapping in time. This mapping relationship, which takes the form of a matrix multiplication, provides an approach for the numerical acceleration of the fractional solution. In Section 2.5, an algorithm for the computation of the matrix that defines the linear mapping is presented that utilises the fast Fourier transform. Additionally, we show that many elements of this matrix may contribute negligibly to the solution and so can be neglected, subsequently allowing for even further acceleration. In Section 2.5.3, we demonstrate the accuracy of this mapping approach by benchmarking the numerical solution of a fractional relaxation equation against its exact analytic solution. In Section 2.6, this mapping is applied successfully to accelerate the fitting of Eq. (2.1) to experimental data for a time-of-flight experiment. Finally, in Section 2.7, we present conclusions and briefly list possible applications of our approach to various generalisations of the considered fractional-order problem.

2.2 Fractional calculus

Fractional calculus is a generalisation of calculus that considers differentiation and integration to arbitrary real or complex orders [63]. Although not as well-known as calculus, fractional calculus has a long history with origins in a 1695 exchange of letters between l'Hôpital and Leibniz, a mere decade after calculus was published by Leibniz in his *Nova Methodus* [68, 69]. In this correspondence, while referencing Leibniz's notation for n-th order differentiation, $\frac{\mathrm{d}^n}{\mathrm{d}x^n}$, l'Hôpital asked "What if n is $\frac{1}{2}$?" [68]. Leibniz responds that there arises "an apparent paradox from which one day, useful consequences will be drawn" [68]. The paradox Leibniz refers to is an unexpected ambiguity in fractional differentiation, akin to the ambiguity of indefinite integration. That is, in general, fractional differentiation is a global operator that acts on an interval [70]. It is only when the order of fractional differentiation is a non-negative integer that fractional differentiation becomes ordinary differentiation and acts locally on a single point [63].

2.2.1 Fractional integration

Fractional integration follows directly from Cauchy's formula for repeated integration [63]:

$$\begin{aligned} {}_0\mathcal{D}_t^{-n} f(t) &\equiv \int_0^t \mathrm{d}\tau_n \int_0^{\tau_n} \mathrm{d}\tau_{n-1} \cdots \int_0^{\tau_1} \mathrm{d}\tau_1 f(\tau_1) \\ &\equiv \frac{1}{(n-1)!} \int_0^t (t-\tau)^{n-1} f(\tau)\, \mathrm{d}\tau \\ &\equiv \frac{t^{n-1}}{(n-1)!} * f(t), \end{aligned} \tag{2.4}$$

where the operator ${}_0\mathcal{D}_t^{-n}$ denotes n-fold integration over the interval $[0, t]$, and $*$ denotes a convolution over that same interval. We can relax the requirement that n be an integer through use of the Gamma function. Thus, we define α-fold fractional integration as

$$\begin{aligned} {}_0\mathcal{D}_t^{-\alpha} f(t) &\equiv \frac{1}{\Gamma(\alpha)} \int_0^t (t-\tau)^{\alpha-1} f(\tau)\, \mathrm{d}\tau \\ &\equiv \frac{t^{\alpha-1}}{\Gamma(\alpha)} * f(t), \end{aligned} \tag{2.5}$$

where α is an arbitrary positive real number. This definition of fractional integration can be extended to non-negative real orders through the identity operation:

$${}_0\mathcal{D}_t^{0} f(t) \equiv \lim_{\alpha \to 0} {}_0\mathcal{D}_t^{-\alpha} f(t) \equiv f(t). \tag{2.6}$$

This operator, ${}_0\mathcal{D}_t^{-\alpha}$, is also known as the Riemann-Liouville fractional integral [63].

It should be noted that Riemann-Liouville fractional integration has the desirable semigroup property [63]:

$${}_0\mathcal{D}_t^{-\alpha}\, {}_0\mathcal{D}_t^{-\beta} \equiv {}_0\mathcal{D}_t^{-(\alpha+\beta)}, \tag{2.7}$$

where α and β are non-negative real numbers.

2.2.2 Fractional differentiation

Fractional differentiation follows naturally by drawing inspiration from the semigroup property (2.7) and applying both fractional integration and integer-order differentiation in succession. In what follows, we will consider only fractional derivatives of orders $0 < \alpha < 1$, as these are what typically arise in fractional calculus models for dispersive transport. Fractional differentiation of order α can thus be achieved by performing ordinary differentiation of order 1 followed by fractional integration of order

$1-\alpha$. This results in the Caputo fractional derivative [55]:

$$\begin{aligned} {}^{\mathrm{C}}_{0}\mathcal{D}^{\alpha}_{t} f(t) &\equiv {}_{0}\mathcal{D}^{-(1-\alpha)}_{t} \mathcal{D}^{1} f(t) \\ &\equiv \frac{1}{\Gamma(1-\alpha)} \int_{0}^{t} \mathrm{d}\tau \, (t-\tau)^{-\alpha} \left. \frac{\partial f}{\partial t} \right|_{t=\tau} \\ &\equiv \frac{t^{-\alpha}}{\Gamma(1-\alpha)} * \frac{\partial f}{\partial t}. \end{aligned} \tag{2.8}$$

Alternatively, we could have first performed fractional integration followed then by differentiation. Since integer-order differentiation and fractional integration do not commute [63], this would have resulted in an alternative definition for fractional differentiation known as the Riemann-Liouville fractional derivative. When present in initial value problems, the Riemann-Liouville fractional derivative requires initial conditions to be specified in terms of fractional integrals, which are difficult to interpret physically. For this reason, we will exclusively use the Caputo fractional derivative (2.8).

2.3 Direct solution of the fractional diffusion equation

The classical diffusion equation is

$$\frac{\partial}{\partial t} u(t,x) = D \frac{\partial^{2}}{\partial x^{2}} u(t,x), \tag{2.9}$$

where D is the diffusion coefficient. A fractional diffusion equation simply has one or both of the above integer-order derivatives replaced with fractional derivatives. In 1989, Schneider and Wyss introduced a so-called time-fractional diffusion equation where the time derivative in the classical diffusion equation (2.9) had been replaced with a Caputo fractional derivative (2.8) of order α [71]:

$${}_{0}\mathcal{D}^{\alpha}_{t} n(t,x) = D_{\alpha} \frac{\partial^{2}}{\partial x^{2}} n(t,x), \tag{2.10}$$

where D_{α} denotes a generalised diffusion coefficient with fractional units of time. Unlike the classical diffusion equation (2.9) that describes Brownian motion, the fractional diffusion equation (2.10) describes transport that is dispersive. We can thus compare both kinds of transport by comparing the solutions of each diffusion equation. Using Fourier-Laplace transform techniques, it is straightforward to find an analytical expression for the solution of the fractional diffusion equation (2.10). In the case of an impulse initial condition centred at the origin, $n(0,x) \equiv \delta(x)$, we have the fundamental solution [63]:

$$n(t,x) = \frac{1}{2\sqrt{D_{\alpha} t^{\alpha}}} W\left(-\frac{|x|}{\sqrt{D_{\alpha} t^{\alpha}}}; -\frac{\alpha}{2}, 1-\frac{\alpha}{2} \right), \tag{2.11}$$

where the Wright function is defined

$$W\left(z;\alpha,\beta\right)\equiv\sum_{k=0}^{\infty}\frac{z^{k}}{k!\Gamma\left(\alpha k+\beta\right)},\quad\Re\left(\alpha\right)>-1,\,\beta\in\mathbb{C}. \tag{2.12}$$

By choosing $\alpha=1$, we recover the well-known fundamental Gaussian solution of the classical diffusion equation (2.9):

$$u\left(t,x\right)=\frac{1}{2\sqrt{\pi Dt}}\exp\left[-\left(\frac{x}{2\sqrt{Dt}}\right)^{2}\right]. \tag{2.13}$$

We now compare normal and dispersive transport by plotting in Figure 2.1 the fundamental solution (2.11) at various times for $\alpha=1$ and $\alpha=\frac{1}{2}$. This figure shows the fundamental slowness of dispersive transport in comparison to normal transport. Additionally, in the case of fractional diffusion, the impulse initial condition persists as a cusp at the origin. This memory of the location of the initial impulse manifests mathematically as the global time operator (2.8) of fractional differentiation acting on the entire solution history.

2.4 Mapping between normal and fractional diffusion

In this section we will explore accelerating the numerical solution of the fractional advection-diffusion equation (2.1) by relating it to the solution of the normal advection diffusion equation

$$\frac{\partial}{\partial t}v\left(t,x\right)=D\frac{\partial^{2}}{\partial x^{2}}v\left(t,x\right)-W\frac{\partial}{\partial x}v\left(t,x\right). \tag{2.14}$$

By enforcing both equivalent initial conditions and boundary conditions, we can relate these solutions using the known integral transform [41, 72–75]

$$u\left(t,x\right)=\int_{0}^{\infty}\mathrm{d}\tau A\left(\tau,t\right)v\left(\tau,x\right), \tag{2.15}$$

which also holds true for any other shared *linear spatial* operator in the considered advection diffusion equations. Here, the kernel is defined

$$A\left(\tau,t\right)\equiv\mathcal{L}^{-1}\left\{s^{\alpha-1}\mathrm{e}^{-s^{\alpha}\tau}\right\}=\frac{\partial}{\partial\tau}\left[1-L_{\alpha}\left(\frac{t}{\sqrt[\alpha]{\tau}}\right)\right], \tag{2.16}$$

where $\mathcal{L}$ denotes the Laplace transform and $L_{\alpha}\left(t\right)$ is the one-sided Lévy distribution, which is expressible in terms of the one-sided Lévy density $l_{\alpha}\left(t\right)$ as

$$L_{\alpha}\left(t\right)\equiv\int_{0}^{t}\mathrm{d}\tau l_{\alpha}\left(t\right),\quad\mathcal{L}l_{\alpha}\left(t\right)\equiv\mathrm{e}^{-s^{\alpha}}. \tag{2.17}$$

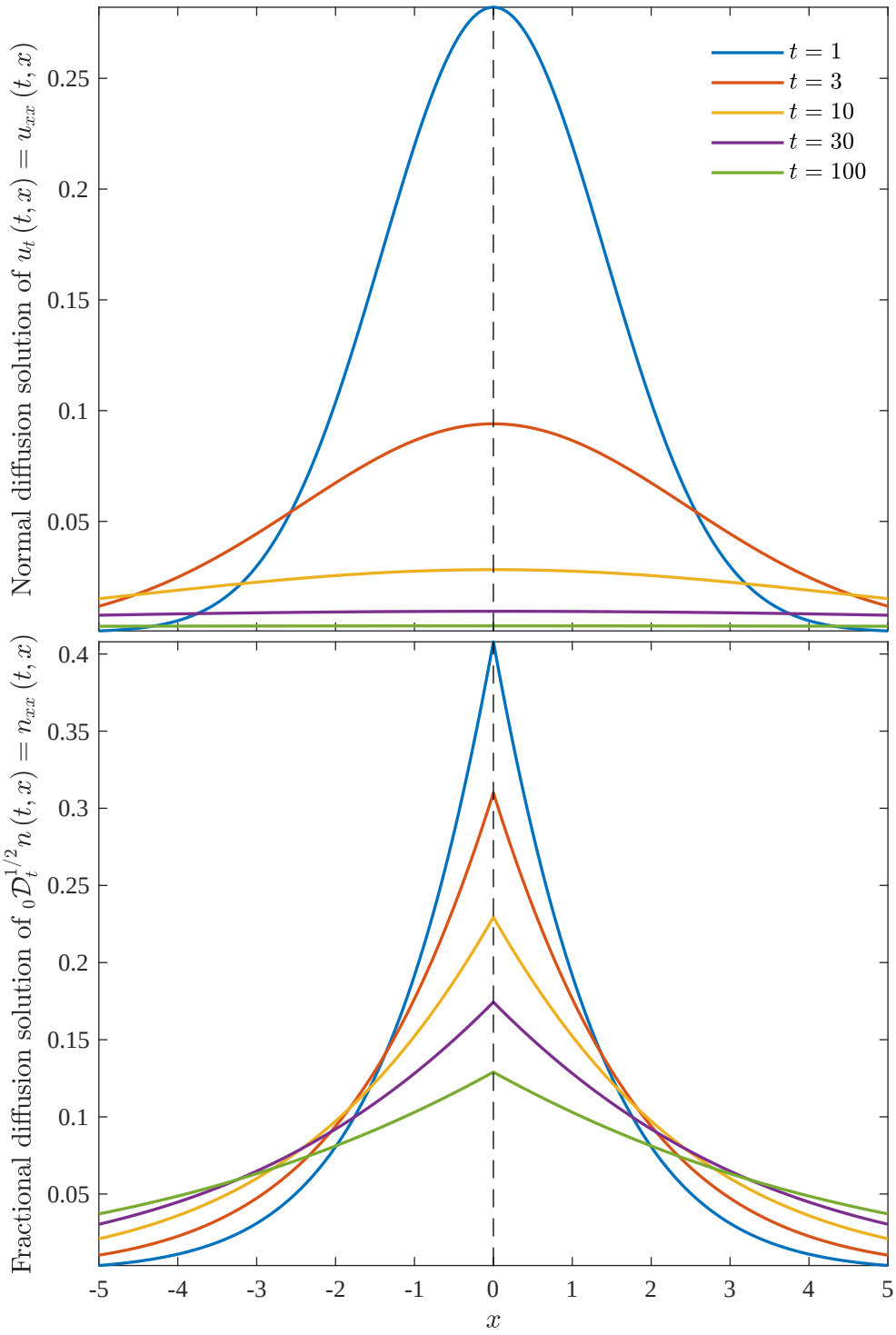

Figure 2.1: Plots of the fundamental solutions, (2.13) and (2.11), of the normal and fractional diffusion equations. The vertical dotted line denotes the location of the impulse initial condition at the origin. The persisting cusp at this location in the fractional solution is due to the memory effects of dispersive transport and the corresponding global nature of fractional differentiation.

This integral relationship is known as a subordination transformation, where $A(\tau, t)$ is the probability distribution function providing subordination of the random process governed by Eq. (2.1) on the physical time scale t to that governed by Eq. (2.14) on the operational time scale τ [76].

In order to determine the fractional order solution numerically, we wish to find a discrete analogue of this transform. We note that this relationship acts on time alone, independent of space. As such, in what follows, we shall consider the solutions $u(t, x)$ and $v(t, x)$ solely as functions of time and reintroduce spatial dependence at a later point. Performing separation of variables, we can instead consider the ordinary time differential equations

$$ {}_0^{\mathrm{C}}\mathcal{D}_t^{\alpha} u(t) = \lambda u(t), \tag{2.18} $$

$$ \frac{\partial}{\partial t} v(t) = \lambda v(t), \tag{2.19} $$

where λ is the separation constant or eigenvalue of the shared spatial operator. We will now perform a finite difference time discretisation of these ordinary differential equations. We will denote time steps by superscripts $u^n \equiv u(n\Delta t)$, where Δt is the time step size and $n = 0, \ldots, N$ is the time step number with N being the total number of time steps and $t \equiv N\Delta t$ being the present point in time. To numerically approximate the fractional time derivative we will make use of the L1 algorithm [77], which was introduced by Oldham and Spanier to approximate the Riemann-Liouville fractional derivative. This algorithm has since been applied by a number of authors [56,57,78–80] to the Caputo fractional derivative, resulting in the approximation

$$ {}_0^{\mathrm{C}}\mathcal{D}_t^{\alpha} u(t) = \Delta t^{-\alpha} \sum_{n=1}^{N} w_n \left(u^{N-n+1} - u^{N-n} \right) + O(\Delta t), \tag{2.20} $$

where we have the quadrature weights defined

$$ w_n \equiv \frac{n^{1-\alpha} - (n-1)^{1-\alpha}}{\Gamma(2-\alpha)}. \tag{2.21} $$

This discretisation of the Caputo fractional derivative includes the limiting case where $\alpha \to 1$ from which we can recover the Euler method

$$ \frac{\partial}{\partial t} v(t) = \frac{v^N - v^{N-1}}{\Delta t} + O(\Delta t). \tag{2.22} $$

Applying these discretisations to the ordinary differential equations (2.18) and (2.19) yields recurrence relationships for the approximate finite difference solutions

$$ \left(1 - \lambda \frac{\Delta t^{\alpha}}{w_1}\right) u^N = \hat{w}_N u^0 + \sum_{n=1}^{N-1} \left(\hat{w}_n - \hat{w}_{n+1}\right) u^{N-n}, \tag{2.23} $$

$$ (1 - \lambda \Delta t) v^N = v^{N-1}, \tag{2.24} $$

where we have introduced the normalised quadrature weights $\hat{w}_n \equiv w_n/w_1$. As expected, the fractional order solution at each time step depends on the entire solution history, while the integer order solution depends only the nearest prior point in the neighbourhood of the present. We can solve these recurrence relationships analytically for the present time step in terms of their respective initial conditions

$$u^N = \sum_{n=1}^{N} a_{Nn} \frac{u^0}{\left(1 - \lambda \frac{\Delta t^\alpha}{w_1}\right)^n}, \tag{2.25}$$

$$v^N = \frac{v^0}{(1 - \lambda \Delta t)^N}, \tag{2.26}$$

where a_{Nn}, which is yet to be determined, denotes the n-th weight in the weighted sum for the fractional order solution at the N-th time step. If we choose the integer order initial condition to coincide with the fractional one $v^0 = u^0$ and also choose a time step size for the integer order case of $\Delta t^\alpha / w_1$ we can relate the solution to the fractional order problem directly to the solution of the integer order one as

$$u^N = \sum_{n=1}^{N} a_{Nn} v^n. \tag{2.27}$$

This is a discrete analogue of the continuous integral relationship (2.15) and so the weights a_{Nn} can be interpreted as quadrature weights. We should expect this discrete analogue to coincide with the continuous relationship in the limit of many time steps N. Most generally, reintroducing spatial dependence and considering all time steps, we can write each weighted sum in the form of Eq. (2.27) using the matrix multiplication

$$\mathbf{U} = \mathbf{A}\mathbf{V}, \tag{2.28}$$

where we have the matrix of quadrature weights

$$\mathbf{A} = \begin{bmatrix} a_{11} & 0 & 0 \\ \vdots & \ddots & 0 \\ a_{N1} & \cdots & a_{NN} \end{bmatrix}, \tag{2.29}$$

which allows for mapping from the integer order solution matrix

$$\mathbf{V} = \begin{bmatrix} — & \mathbf{v}^1 & — \\ & \vdots & \\ — & \mathbf{v}^N & — \end{bmatrix}, \tag{2.30}$$

to the fractional order solution matrix

$$\mathbf{U} = \begin{bmatrix} — & \mathbf{u}^1 & — \\ & \vdots & \\ — & \mathbf{u}^N & — \end{bmatrix}, \tag{2.31}$$

where the rows of these solution matrices correspond to the spatial solution at each time step for the same spatial points. As the mapping matrix $\mathbf{A}$ is lower triangular, determining the solution matrix $\mathbf{U}$ using this matrix multiplication is of $O\left(N^2\right)$. This is no better than directly applying Eq. (2.23) to find the solution recursively. Fortunately, this is only the case if we absolutely require the solution at *every* time step. Indeed, if we are content with the solution at a subset of the overall time steps, we can partially perform the matrix multiplication in Eq. (2.28) in $O\left(N\right)$. Consider, for example, stability limitations such as the Courant-Friedrichs-Lewy condition [81] that arise in explicit finite difference schemes and may require time steps smaller than would otherwise be needed. In such a situation, we can solve the integer order problem with sufficiently small time steps (to satisfy the stability criterion), and then map it onto the fractional problem using sparser time steps. Of course, the usefulness of this approach also depends on the computational complexity of computing the required rows of the mapping matrix. Fortunately, as the solution mapping depends solely on the operator of fractional differentiation, the mapping matrix can be precomputed for a given value of α and used repeatedly. The precise computational complexity of computing the mapping matrix will be considered in Section 2.5.

2.5 The solution mapping matrix $\mathbf{A}$

In the following sections, we address the problem of efficiently computing and applying the mapping matrix $\mathbf{A}$, present in Eq. (2.28) for the numerical relationship between integer and fractional order solutions.

2.5.1 Computation using the fast Fourier transform

Substitution of the fractional finite difference solution approximation (2.25) back into its recurrence relationship (2.23) allows us to express the elements of the mapping matrix $\mathbf{A}$ in the form of a generating function recurrence relationship

$$A_n\left(x\right) = \Omega\left(x\right) A_{n-1}\left(x\right), \tag{2.32}$$

where we have the generating function for the n-th column of the mapping matrix

$$A_n\left(x\right) \equiv \sum_{m\geq 1} a_{mn} x^m, \tag{2.33}$$

with the first column given by the initial condition weights from Eq. (2.23)

$$A_1\left(x\right) \equiv \sum_{m\geq 1} \hat{w}_m x^m, \tag{2.34}$$

and the generating function of past time step weights from Eq. (2.23)

$$\Omega\left(x\right) \equiv \sum_{m\geq 1} \left(\hat{w}_m - \hat{w}_{m+1}\right) x^m. \tag{2.35}$$

The Cauchy product [82] allows us to write this generating function recurrence relationship explicitly using a discrete linear convolution

$$\begin{bmatrix} a_{nn} \\ \vdots \\ a_{Nn} \end{bmatrix} = \begin{bmatrix} \hat{w}_1 - \hat{w}_2 \\ \vdots \\ \hat{w}_{N-n+1} - \hat{w}_{N-n+2} \end{bmatrix} * \begin{bmatrix} a_{n-1,n-1} \\ \vdots \\ a_{N-1,n-1} \end{bmatrix}, \tag{2.36}$$

where the initial column vector is provided by its generating function $A_1(x)$

$$\begin{bmatrix} a_{11} \\ \vdots \\ a_{N1} \end{bmatrix} = \begin{bmatrix} \hat{w}_1 \\ \vdots \\ \hat{w}_N \end{bmatrix}. \tag{2.37}$$

This convolution representation can be implemented using the fast Fourier transform, allowing for the computation of an $N \times N$ mapping matrix in $O\left(N^2 \ln N\right)$. Evidently, determining the mapping matrix alone is more computationally intensive than finding the finite difference solution recursively in only $O\left(N^2\right)$. Certain situations exist, however, where the mapping matrix may be precomputed and reused, allowing for computational benefit even with this larger computational complexity. One such situation is the focus of Section 2.6, where the least squares fit of a fractional order model to experimental data is considered. Fortunately, as described in the following section, we are not limited to only these situations when it comes to useful application of this solution mapping.

2.5.2 Column truncation

The magnitude of the elements of the mapping matrix $\mathbf{A}$ is illustrated in Figure 2.2 for various values of the fractional differentiation order α. It can be seen that, as α decreases, fewer elements are likely to contribute to the solution mapping. This suggests that we can truncate the mapping matrix at some point during its column-wise computation described by Eq. (2.36). Here, we will specifically consider truncating the weighted sum (2.27) corresponding to the solution at the last time step. As a simplification, we will take both integer and fractional order solutions to be constant and hence equal, allowing us to remove all solution dependence and focus on truncating the summation

$$\sum_{n>0} a_{Nn} = 1. \tag{2.38}$$

This expression can also be derived from the generating function representation (2.32) and is equivalent to stating that the rows of the mapping matrix sum to unity. Now, by introducing a truncation tolerance $0 < \varepsilon < 1$, which is proportional to the absolute error incurred by the truncation, we can define the number of columns in the truncated mapping matrix as the smallest integer N_{trunc} that satisfies

$$\sum_{n>N_{\text{trunc}}} a_{Nn} \leq \varepsilon. \tag{2.39}$$

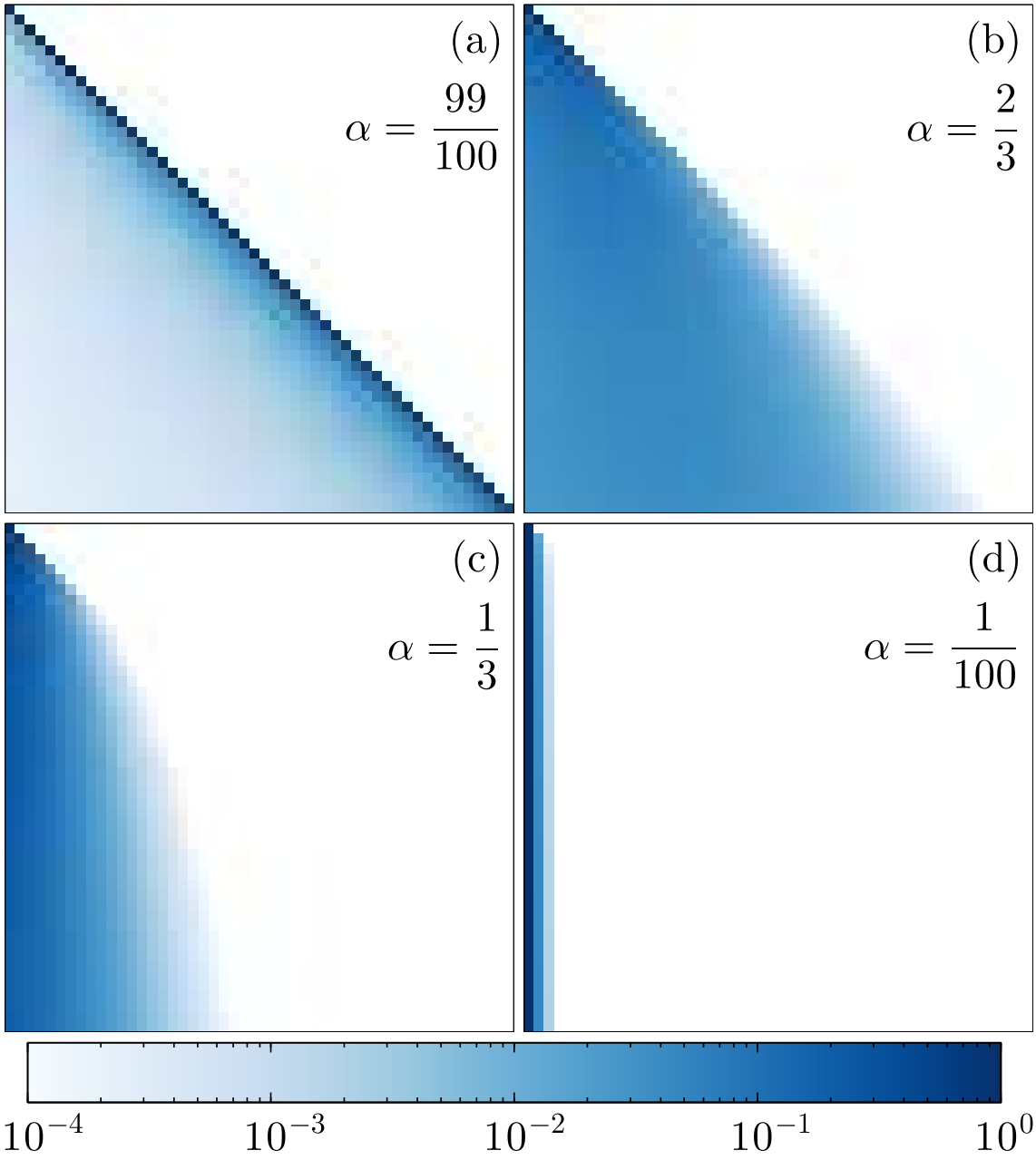

Figure 2.2: Illustration of the matrix $\mathbf{A}$ that maps from the solution of the normal diffusion equation (2.14) to the solution of the order α fractional diffusion equation (2.1). Each matrix is of size 50×50 with elements that have been coloured according to their magnitude on a logarithmic scale. (a) As $\alpha \to 1$, the identity matrix is recovered, corresponding to the fractional and integer order solutions coinciding. (b-c) As α decreases, the matrix is dominated by elements with a lower column number, indicating that the early time solution to the integer order problem becomes increasingly significant. (d) As $\alpha \to 0$, the matrix approaches having only an initial column of ones, which corresponds to a time-invariant solution. This rapid decrease in element magnitude suggests the possibility of column-wise truncation of the mapping matrix, allowing for improved efficiency in both its computation and application, especially for small values of α.

Evidently, to determine N_{trunc} using this inequality requires computation of matrix elements that will ultimately be truncated. Fortunately, using the row summation identity (2.38), we can restate this inequality using known matrix elements

$$\sum_{1\leq n\leq N_{\text{trunc}}} a_{Nn} \geq 1-\varepsilon. \tag{2.40}$$

We can gain some insight into the asymptotic form of N_{trunc}, and hence any computational benefit of this truncation, by considering the continuous analogue of this solution mapping, provided by Eq. (2.15). As before, by choosing an integer order solution that is constant, we find that

$$\int_0^\infty \mathrm{d}\tau A(\tau,t) = 1, \tag{2.41}$$

which is evident from the Laplace space representation (2.16) of $A(\tau,t)$ as being the normalisation condition for an exponential distribution in τ. By nondimensionalising in terms of the finite difference time step indices, that is taking $t = N\Delta t$ and $\tau = n\Delta t^\alpha/w_1$, we find the continuous analogue to the row summation identity (2.38)

$$\int_0^\infty \mathrm{d}n a_{Nn} = 1, \quad a_{Nn} \equiv \frac{\Delta t^\alpha}{w_1} A\left(\frac{n\Delta t^\alpha}{w_1}, N\Delta t\right), \tag{2.42}$$

where both n and a_{Nn} are continuous here. Continuing with the analogy, we can now choose to truncate this integral at the point $n = N_{\text{trunc}}$, resulting in the continuous analogue to truncation tolerance definition (2.39)

$$\varepsilon \equiv \int_{N_{\text{trunc}}}^\infty \mathrm{d}n a_{Nn} = L_\alpha \sqrt[\alpha]{\frac{w_1 N^\alpha}{N_{\text{trunc}}}}, \tag{2.43}$$

where we have made use of the Lévy distribution representation (2.16) of the kernel $A(\tau,t)$. It is evident here that we can make this truncation tolerance an arbitrarily small constant that is independent of N by choosing that N_{trunc} is directly proportional to N^α. As the discrete truncation tolerance coincides with this continuous one in the limit of large N, we should expect to find the asymptotic behaviour $N_{\text{trunc}} \sim N^\alpha$ for the continuous case. Indeed, Figure 2.3 shows precisely this as the size of the mapping matrix is increased for select values of α. Therefore, when truncated, an $N \times N$ mapping matrix becomes of size $N \times O(N^\alpha)$, allowing for column-wise computation of it using the recurrence relationship (2.36) in only $O\left(N^{1+\alpha}\ln N\right)$. Similarly, we can now find the fractional order solution at particular instants in time in $O(N^\alpha)$. Finally, with this truncation, it should be noted that we are no longer required to precompute the mapping matrix in order to obtain a solution in a computational complexity better than $O\left(N^2\right)$.

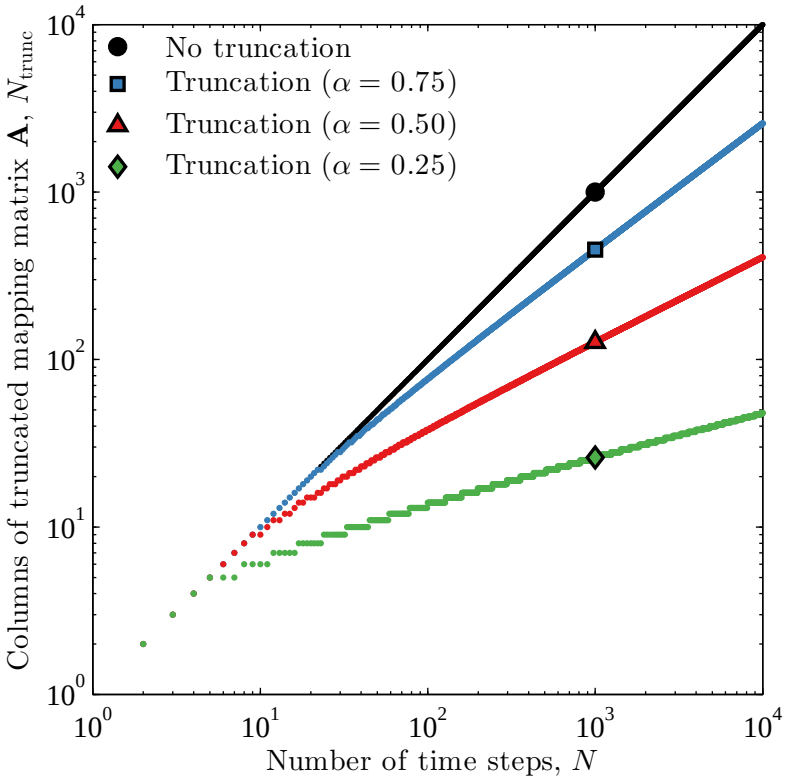

Figure 2.3: The number of columns in the mapping matrix $\mathbf{A}$, truncated according to the inequality (2.40) with a truncation tolerance of $\varepsilon = 10^{-2}$. The gradient of each case approaches α as the number of time steps N grow large, suggesting the asymptotic form $N_{\text{trunc}} \sim N^{\alpha}$.

2.5.3 Benchmarking the truncated mapping

In this section, we will demonstrate the expected accuracy of the truncated mapping solution described in Section 2.5 relative to the direct finite difference solution provided either recursively or by the full mapping introduced in Section 2.4. Specifically, we will consider the solution of the fractional relaxation equation [11]

$$ {}_{0}^{\mathrm{C}}\mathcal{D}_{t}^{\frac{1}{2}} u(t) = u(t), \quad u(0) = 1, \tag{2.44} $$

which we chose because it has the exact analytic solution [83]

$$ u(t) = \mathrm{e}^{t}\left(1 + \operatorname{erf}\sqrt{t}\right), \tag{2.45} $$

where $\operatorname{erf}(x) \equiv \frac{2}{\sqrt{\pi}} \int_0^x \mathrm{d}\xi \mathrm{e}^{-\xi^2}$ is the Gauss error function. Additionally, the finite difference solution here can be found recursively by simply taking Eqs. (2.23) and (2.24) with $\alpha = 1/2$ and $\lambda = 1$.

Figure 2.4 shows that the truncated mapping can be applied to find the solution to the fractional relaxation equation (2.44) to an accuracy comparable to the finite difference method, while still maintaining an improved computational complexity.

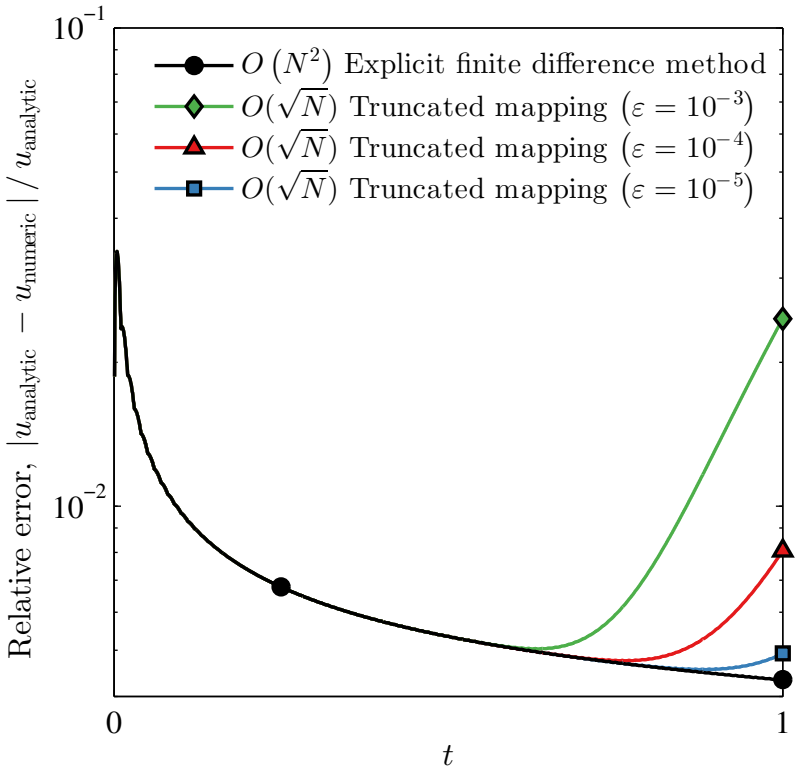

Figure 2.4: The error of an $N = 100$ point finite difference solution of the fractional relaxation equation (2.44) relative to its analytic solution (2.45). The truncated solution mapping described in Section 2.5 is applied for decreasing values of the truncation tolerance ε. Note how the truncated mapping can be made to be arbitrarily accurate, while still retaining its $O\left(\sqrt{N}\right)$ computational complexity. The divergence in accuracy for late times stems from the truncation of more terms at later time steps. To perform this plot, a truncated mapping matrix $\mathbf{A}$ was precomputed in $O\left(N^{\frac{3}{2}} \ln N\right)$ and then truncated further as required.

2.6 Efficient fitting of experimental data via solution mapping

The solution mapping outlined in Sections 2.4 and 2.5 is ideally suited to the acceleration of curve-fitting problems where the solution defining the curve must be found repeatedly and at relatively few points. In this section we will demonstrate this by fitting a fractional-order model to experimental data for the current in a time-of-flight experiment for a disordered semiconductor. As stated in Section 2.1, this can be described by the fractional advection diffusion model (2.1). This model describes the charge carrier density in a thin sample held between two large plane-parallel boundaries with all spatial variation occurring normal to these boundaries. It will be assumed that the boundaries are perfectly absorbing, providing the Dirichlet boundary conditions

$$u\left(t, 0\right) = 0 = u\left(t, L\right), \tag{2.46}$$

where L is the thickness of the sample. We will choose the initial distribution of charge carriers to be governed by the Beer-Lambert law resulting in the exponential initial condition

$$u\left(0,x\right) \propto \mathrm{e}^{-ax}, \tag{2.47}$$

where a is the absorption coefficient of the sample. We can use the expression for the current in a time-of-flight experiment [49]

$$I\left(t\right) \propto \frac{\partial}{\partial t}\int_0^L \left(\frac{x}{L}-1\right) u\left(t,x\right)\mathrm{d}x, \tag{2.48}$$

to find the current directly from the number density solution of Eq. (2.1). For spatial consideration, we will make use of the centred finite difference approximations

$$\frac{\partial}{\partial x}u\left(t,x\right) = \frac{u_{j+1}^N - u_{j-1}^N}{2\Delta x} + O\left(\Delta x^2\right), \tag{2.49}$$

$$\frac{\partial^2}{\partial x^2}u\left(t,x\right) = \frac{u_{j+1}^N - 2u_j^N + u_{j-1}^N}{\Delta x^2} + O\left(\Delta x^2\right), \tag{2.50}$$

where $j = 0,\ldots,J$ is the spatial index, J is the total number of spatial nodes and subscripts have been used to denote spatial indexing $u_j^n \equiv u\left(n\Delta t, j\Delta x\right)$. Hence, we can enforce the boundary conditions by setting $u_0^n = 0 = u_J^n$ for all $n = 0,\ldots,N$. Applying these spatial derivative approximations, in conjunction with Eq. (2.20) for approximating the Caputo fractional derivative, results in the recurrence relationship for the number density solution to Eq. (2.1)

$$\mathbf{C}\mathbf{u}^N = \hat{w}_N\mathbf{u}^0 + \sum_{n=1}^{N-1}\left(\hat{w}_n - \hat{w}_{n+1}\right)\mathbf{u}^{N-n}, \tag{2.51}$$

where we have the tridiagonal matrix

$$\mathbf{C} \equiv \begin{bmatrix} 1-2r & r+s & 0 \\ r-s & 1-2r & \ddots \\ 0 & \ddots & \ddots \end{bmatrix}, \quad r \equiv -\frac{D\Delta t^\alpha}{w_1\Delta x^2}, \quad s \equiv \frac{W\Delta t^\alpha}{2w_1\Delta x}. \tag{2.52}$$

Figure 2.5 plots photocurrent data alongside the model (2.48) fitted using a trust-region-reflective non-linear least squares algorithm [84, 85], as implemented in the `lsqcurvefit` function [86] located in MATLAB's Curve Fitting Toolbox.

To explore the computational benefits of applying the solution mapping described in Section 2.4 and its truncation described in Section 2.5, we require the number density solution when $\alpha = 1$, corresponding to normal transport. Proceeding as before, this time using Eq. (2.22) for the approximation of the first derivative, yields the recurrence relationship for the integer order solution $v\left(t,x\right)$

$$\mathbf{C}\mathbf{v}^N = \mathbf{v}^{N-1}. \tag{2.53}$$

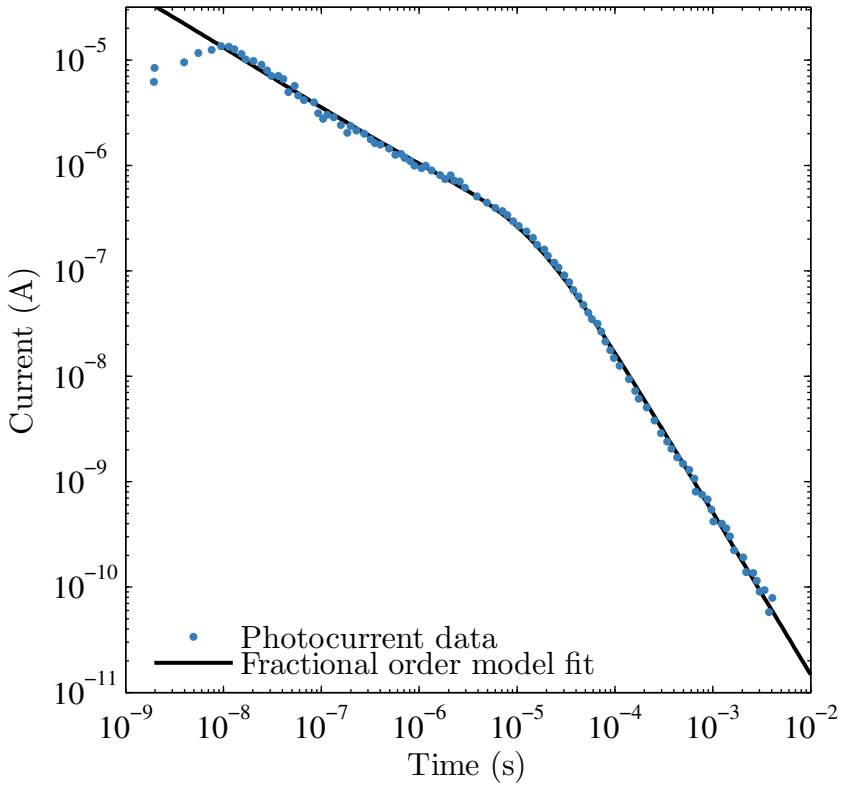

Figure 2.5: A least squares fit of the model (2.48) to the transient photocurrent in a sample of intrinsic hydrogenated amorphous silicon a-Si:H at 160K (adapted from Ref. [6]). To within a confidence interval of 95%, the fitting algorithm determined a severity of trapping of $\alpha = 0.535 \pm 2\%$, a generalised drift velocity of $Wt_{\mathrm{tr}}^{\alpha}/L = 2.89 \times 10^{-1} \pm 4\%$ and a generalised diffusion coefficient of $Dt_{\mathrm{tr}}^{\alpha}/L^2 = 6.07 \times 10^{-3} \pm 21\%$, where the "transit time" separating the current regimes has been taken as $t_{\mathrm{tr}} \equiv 10^{-5}$s.

As $\mathbf{C}$ is tridiagonal, we can step forward the fractional order solution recurrence relationship (2.51) in a time computational complexity of $O(J)$ [87]. As such, the total computational complexity to determine the fractional order solution in time and space becomes $O\left(N^2 J\right)$. Similarly, by applying the solution mapping we have a computational complexity of $O\left(N^2 J \ln N\right)$, which improves to $O\left(N^{1+\alpha} J \ln N\right)$ with truncation. The value of α present here can be estimated by noting the asymptotic form of the current in a time-of-flight experiment [12]

$$I(t) \sim \begin{cases} t^{-(1-\alpha)}, & \text{early times}, \\ t^{-(1+\alpha)}, & \text{late times}, \end{cases} \tag{2.54}$$

which provides a criterion for recognising dispersive transport by noting that the sum of the slopes of the asymptotic regions of a current versus time plot on logarithmic axes is -2. In this particular case, we can use this criterion to bound the severity of trapping to within the interval $0.5 < \alpha < 0.55$.

Figure 2.6 plots the computation time for fitting the model (2.48) to the photocurrent data considered in Figure 2.5 for an increasing number of time steps. The

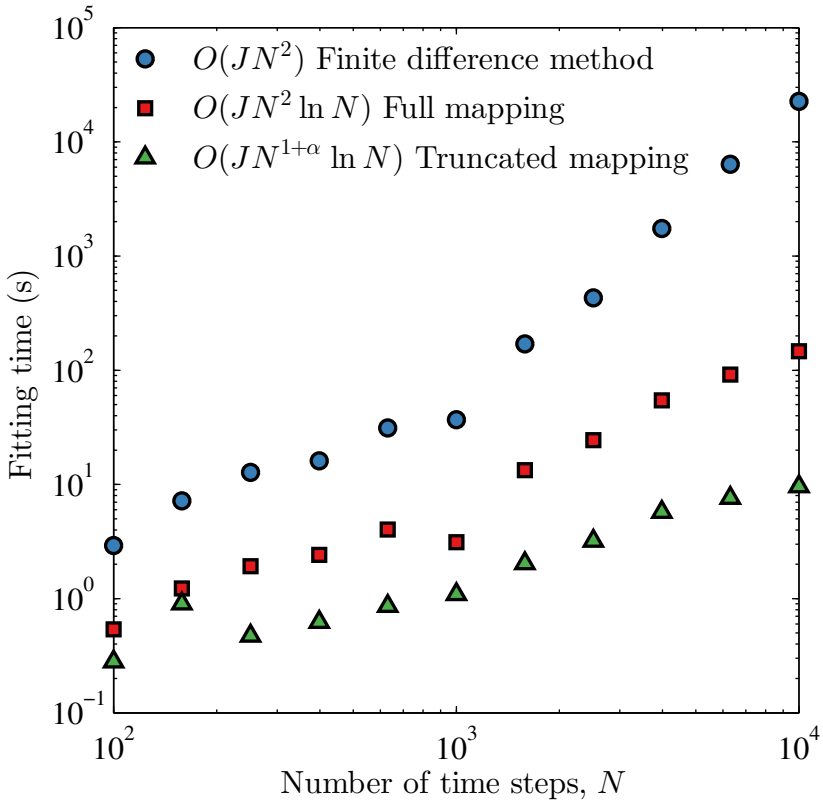

Figure 2.6: Comparison of computation time versus number of time steps for least squares fitting performed using the finite difference method (2.51), the accelerated solution mapping developed here (2.28) and the truncation thereof defined by Eq. (2.40). To maintain solution accuracy, the truncation tolerance ε was chosen to decrease in proportion to N and the spatial nodes J were chosen to increase in proportion to $\sqrt{N}$. It can be seen that the solution mapping without truncation is two orders of magnitude faster than the recursive approach for the largest problem size considered. With truncation, this improves to a three orders of magnitude speed up.

observed fitting times do not increase monotonically with N. This is due to the nature of the fast Fourier transform (FFT) algorithm. The FFT is very sensitive to the prime factorisation of the input size. For example, the FFT is fastest when N is a power of 2, and it is especially slow when N is prime. Additional variations in fitting time may be due to the curve fitting algorithm and the number of iterations it requires to perform the fit.

2.7 Concluding remarks and future work

Finite difference solutions to fractional differential equations are known to have a computation time that scales with the square of the number of time steps. This stems mathematically from the global nature of fractional differentiation, and physically can be interpreted as a consideration of memory effects. In this study, we have related the solution of the fractional diffusion equation (2.1) of order $0 < \alpha < 1$ to the solution of a the normal diffusion equation (2.14) using a linear mapping in time Eq.

(2.28). We have found that, for an N-point finite difference time discretisation, we can use this mapping to improve upon the $O\left(N^2\right)$ time computational complexity of the finite difference method and determine the solution at any instant in time in $O\left(N^{\alpha}\right)$, given a precomputation of $O\left(N^{1+\alpha}\ln N\right)$. This representation is especially useful in situations where the solution must be found repeatedly, as then the relatively expensive precomputation only has to be performed once. We have presented one such situation in Section 2.6 where we have successfully applied this approach to fit the fractional advection diffusion model (2.1) to experimental data for the current in a time-of-flight experiment. For this we achieved computational speed ups in the range of one to three orders of magnitude for the realistic problem sizes considered.

Although this chapter considered a fractional advection-diffusion model, the mapping approach described is applicable for any other linear spatial operator, including those of higher dimensions. For example, in Section 3.6 we apply this same technique to a different generalisation of the advection-diffusion equation. With modifications, this solution mapping can be generalised to consider both the inclusion of a source term as well as higher order fractional derivatives for which $\alpha > 1$.

3

Phase-space model for combined localised and delocalised transport

This chapter contains material that has been published in the following journal articles:

[2] Peter W. Stokes, Bronson Philippa, Daniel Cocks, and Ronald D. White. Solution of a generalized Boltzmann's equation for nonequilibrium charged-particle transport via localized and delocalized states. *Physical Review E*, **93**, 032119 (2016). doi:10.1103/PhysRevE.93.032119

[3] Peter W. Stokes, Bronson Philippa, Daniel Cocks, and Ronald D. White. Generalized balance equations for charged particle transport via localized and delocalized states: Mobility, generalized Einstein relations, and fractional transport. *Physical Review E*, **95**, 042119 (2017). doi:10.1103/PhysRevE.95.042119

3.1 Introduction

In the previous chapters, dispersive transport was modelled by replacing the the local time derivative in the diffusion equation with a global fractional time derivative of order α [41, 42]. Although the resulting fractional diffusion equation (2.1) satisfied the required sublinear scaling in mean squared displacement, it still has the same spatial operator as the standard diffusion equation which implies implicitly an assumption of small spatial gradients. At the same time, the memory of the initial condition can cause large spatial gradients to persist for all time, as seen in Figure 2.1. This inconsistency challenges the validity of fractional diffusion equations. This has been addressed

by using phase-space kinetic models for dispersive transport that make no such assumptions on the size of spatial gradients [32, 33]. Specifically, these approaches have made use of a Boltzmann equation with a generalisation of the Bhatnagar-Gross-Krook (BGK) collision operator [36], the standard collision operator in semiconductor physics. In the kinetic equation for dispersive transport, described in Section 1.3.3, trapping and detrapping is considered equivalent to a BGK collision scattering event occurring after a delay governed by a trapping time distribution. That model does not consider scattering as a separate process from trapping, thereby limiting it to situations where trapping dominates over scattering. However, scattering events are key to transport in delocalised states, such as in the conduction band of a semiconductor. The present chapter builds upon previous work by incorporating a genuine scattering model into a kinetic equation with memory of past trapping events. The new, proposed model also incorporates loss mechanisms such as charged carrier recombination.

In Section 3.2 of this chapter, we present a generalised Boltzmann equation with a BGK collision operator to describe transport via delocalised states, a delayed BGK operator to model trapping and detrapping associated with localised (trapped) states, and loss terms corresponding to free and trapped particle recombination. In Section 3.3, we determine an analytical Fourier-Laplace space solution of this model. This analytical solution is used, among other things, to determine analytical expressions for phase-space averaged moments of the generalised Boltzmann equation. Spatial moments provide transport coefficients describing the the motion of the centre of mass, while velocity moments are used in conjunction to describe the particle flux using flux transport coefficients. In Section 3.4, the model is explored in the weak-gradient hydrodynamic regime where it is shown to coincide with both a standard diffusion equation and a generalised diffusion equation with history dependence. In Section 3.5, the model is also shown to coincide with a Caputo fractional diffusion equation in the particular case where transport is dispersive. In Section 3.6, the solution of the generalised diffusion equation is expressed as a subordination transformation of the solution of a corresponding standard diffusion equation. We explore the signature impact of recombination loss processes in both the delocalised and localised states on the time-of-flight current transients in Section 3.7. Finally, in Section 3.8, we present conclusions and possible avenues for future work.

3.2 Generalised Boltzmann equation

We consider a generalised phase-space kinetic model describing the transport of free particles undergoing collisions, trapping, detrapping and recombination as illustrated in Figure 3.1. The free particles will be described by the phase-space distribution

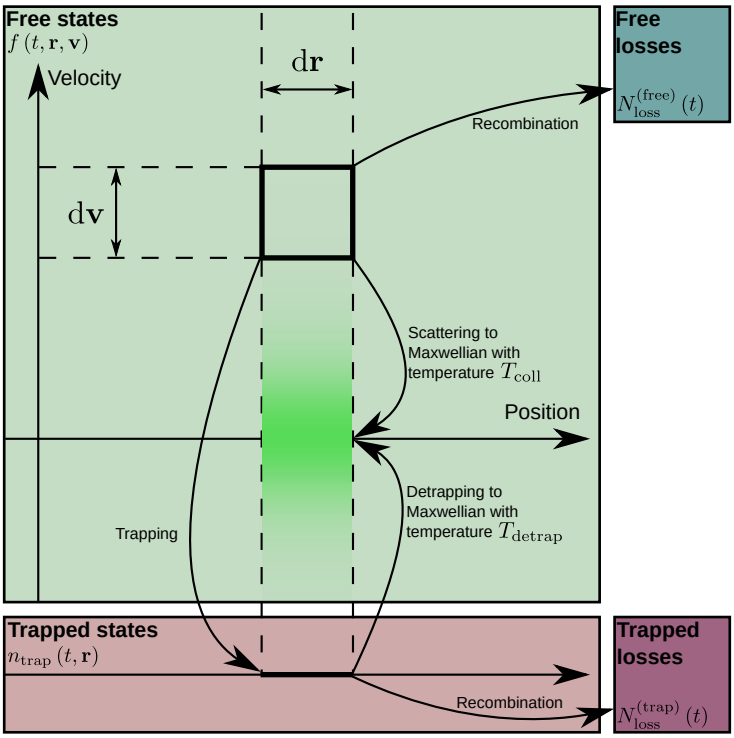

Figure 3.1: Phase-space diagram illustrating the collision, trapping, detrapping and recombination processes considered in the model defined by Eqs. (3.1)–(3.8).

function $f(t,\mathbf{r},\mathbf{v})$ which satisfies the Boltzmann equation

$$\left(\frac{\partial}{\partial t}+\mathbf{v}\cdot\frac{\partial}{\partial\mathbf{r}}+\mathbf{a}\cdot\frac{\partial}{\partial\mathbf{v}}\right)f(t,\mathbf{r},\mathbf{v})=-\nu_{\mathrm{coll}}\left[f(t,\mathbf{r},\mathbf{v})-n(t,\mathbf{r})\,w(\alpha_{\mathrm{coll}},v)\right]$$
$$-\nu_{\mathrm{trap}}\left[f(t,\mathbf{r},\mathbf{v})-\Phi(t)*n(t,\mathbf{r})\,w(\alpha_{\mathrm{detrap}},v)\right]-\nu_{\mathrm{loss}}^{(\mathrm{free})}f(t,\mathbf{r},\mathbf{v}), \quad (3.1)$$

where collision, trapping and free particle loss rates are respectively denoted ν_{coll}, ν_{trap} and $\nu_{\mathrm{loss}}^{(\mathrm{free})}$ and the free particle number density is defined $n(t,\mathbf{r})\equiv\int\mathrm{d}\mathbf{v}f(t,\mathbf{r},\mathbf{v})$. Collisions are described above by the Bhatnagar-Gross-Krook (BGK) collision operator [36]. Specifically, free particles are instantaneously scattered to a Maxwellian distribution of velocities of temperature T_{coll}. The Maxwellian velocity distribution is defined

$$w(\alpha,v) \equiv \left(\frac{\alpha^2}{2\pi}\right)^{\frac{3}{2}}\exp\left(-\frac{\alpha^2v^2}{2}\right), \quad (3.2)$$
$$\alpha^2 \equiv \frac{m}{k_{\mathrm{B}}T}, \quad (3.3)$$

where m is the free particle mass, k_{B} is the Boltzmann constant and T is the temperature of the scattered particles. Similarly, trapping and detrapping processes occur as described by a delayed BGK model (1.30) [33], according to an effective waiting time distribution $\Phi(t)$, with trapped particles eventually detrapping with a Maxwellian velocity distribution of temperature T_{detrap}. To define this waiting time distribution, consider the simple case of traps of fixed duration τ. Particles enter traps at the rate

$\nu_{\text{trap}} n(t, \mathbf{r})$ and so leave traps at this same rate τ units of time in the future. From the present perspective this rate of detrapping is $\nu_{\text{trap}} n(t-\tau, \mathbf{r})$. More generally, for a distribution of trapping times $\phi(t)$, the rate of detrapping is now written as the convolution

$$\nu_{\text{trap}} \phi(t) * n(t, \mathbf{r}) = \nu_{\text{trap}} \int_0^t \mathrm{d}\tau \phi(\tau) n(t-\tau, \mathbf{r}). \tag{3.4}$$

Here, the quantity $\mathrm{d}P \equiv \phi(\tau)\mathrm{d}\tau$ can be interpreted as an infinitesimal probability that particles will remain trapped for duration τ. Note that this expression does not take into account the possibility that particles may undergo trap-based losses instead of detrapping. As trapped particles are being lost exponentially at the rate $\nu_{\text{loss}}^{(\text{trap})}$, the probability of detrapping decays correspondingly, $\mathrm{d}P = \mathrm{e}^{-\nu_{\text{loss}}^{(\text{trap})}\tau}\phi(\tau)\mathrm{d}\tau$. That is, we have now the effective waiting time distribution

$$\Phi(t) \equiv \mathrm{e}^{-\nu_{\text{loss}}^{(\text{trap})}t}\phi(t). \tag{3.5}$$

Appendix D.1 contains an alternative derivation of this waiting time distribution. As trapped particles are localised in configuration space, we describe them with the number density $n_{\text{trap}}(t, \mathbf{r})$ that satisfies the continuity equation

$$\frac{\partial}{\partial t} n_{\text{trap}}(t, \mathbf{r}) = \nu_{\text{trap}}(1 - \Phi *) n(t, \mathbf{r}) - \nu_{\text{loss}}^{(\text{trap})} n_{\text{trap}}(t, \mathbf{r}), \tag{3.6}$$

where $\nu_{\text{loss}}^{(\text{trap})}$ is the loss rate of trapped particles. Although the loss processes of the free and trapped particles can occur through various mechanisms (e.g. recombination, attachment, ...), for simplicity we will refer to all losses as being due to recombination processes. The number of free and trapped particles that undergo recombination, $N_{\text{loss}}^{(\text{free})}(t)$ and $N_{\text{loss}}^{(\text{trap})}(t)$, can be counted accordingly

$$\frac{\mathrm{d}}{\mathrm{d}t} N_{\text{loss}}^{(\text{free})}(t) = \nu_{\text{loss}}^{(\text{free})} N(t), \tag{3.7}$$

$$\frac{\mathrm{d}}{\mathrm{d}t} N_{\text{loss}}^{(\text{trap})}(t) = \nu_{\text{loss}}^{(\text{trap})} N_{\text{trap}}(t), \tag{3.8}$$

in terms of the number of free and trapped particles, defined by $N(t) \equiv \int \mathrm{d}\mathbf{r} n(t, \mathbf{r})$ and $N_{\text{trap}}(t) \equiv \int \mathrm{d}\mathbf{r} n_{\text{trap}}(t, \mathbf{r})$.

The physical origin of the differences in the functional form of the waiting time distribution is dependent on the mechanism for trapping. For example, for amorphous/organic materials, trapping is into existing trapped states, and the waiting time distribution is calculated from the density of trapped states (see e.g. [33]). For dense gases/liquids, the trapped states are formed by the electron itself, and hence the waiting time distribution is dependent on the scattering, the fluctuation profiles and subsequent fluid bubble evolution (see e.g. [88]).

3.3 Analytical solution of the generalised Boltzmann equation

3.3.1 Solution in Fourier-Laplace-transformed phase space

The Boltzmann equation with the BGK collision operator has been solved analytically in Fourier-Laplace space [39]. This same solution technique can be applied to the generalised Boltzmann equation (3.1) with the additional processes of trapping, detrapping and recombination. Applying the Laplace transform in time, $t \to p$, and Fourier transform in phase-space, $(\mathbf{r}, \mathbf{v}) \to (\mathbf{k}, \mathbf{s})$, Eq. (3.1) transforms to

$$\left(\tilde{p} + \tilde{\nu} + \imath\frac{\partial}{\partial \mathbf{s}} \cdot \imath\mathbf{k} + \mathbf{a} \cdot \imath\mathbf{s}\right) f\left(p, \mathbf{k}, \mathbf{s}\right) = f\left(t = 0, \mathbf{k}, \mathbf{s}\right) + \nu_{\text{coll}} n\left(p, \mathbf{k}\right) w\left(\alpha_{\text{coll}}, s\right) + \nu_{\text{trap}} \Phi\left(p\right) n\left(p, \mathbf{k}\right) w\left(\alpha_{\text{detrap}}, s\right), \quad (3.9)$$

where the Fourier-Laplace transformed phase-space distribution function is

$$f\left(p, \mathbf{k}, \mathbf{s}\right) \equiv \int_0^\infty \mathrm{d}t \int \mathrm{d}\mathbf{r} \int \mathrm{d}\mathbf{v} \mathrm{e}^{-(pt + \imath\mathbf{k}\cdot\mathbf{r} + \imath\mathbf{s}\cdot\mathbf{v})} f\left(t, \mathbf{r}, \mathbf{v}\right), \quad (3.10)$$

the Fourier-transformed Maxwellian velocity distribution is

$$w\left(\alpha, s\right) \equiv \exp\left(-\frac{s^2}{2\alpha^2}\right), \quad (3.11)$$

and the following frequencies have been introduced

$$\tilde{p} \equiv p + \nu_{\text{trap}}\left[1 - \Phi\left(p\right)\right] + \nu_{\text{loss}}^{(\text{free})}, \quad (3.12)$$

$$\tilde{\nu} \equiv \nu_{\text{coll}} + \nu_{\text{trap}} \Phi\left(p\right). \quad (3.13)$$

By writing all vectors in terms of components parallel and perpendicular to the unit vector $\hat{\mathbf{k}} \equiv \mathbf{k}/k$

$$\mathbf{s}_\parallel = \left(\mathbf{s} \cdot \hat{\mathbf{k}}\right)\hat{\mathbf{k}}, \quad (3.14)$$

$$\mathbf{a}_\parallel = \left(\mathbf{a} \cdot \hat{\mathbf{k}}\right)\hat{\mathbf{k}}, \quad (3.15)$$

$$\mathbf{s}_\perp = \mathbf{s} - \mathbf{s}_\parallel, \quad (3.16)$$

$$\mathbf{a}_\perp = \mathbf{a} - \mathbf{a}_\parallel, \quad (3.17)$$

the Fourier-Laplace transformed Boltzmann equation (3.9) can be restated as a single first-order differential equation in the Fourier velocity space variable $s_\parallel$

$$\left[\frac{\partial}{\partial s_\parallel} - \frac{1}{k}\left(\tilde{p} + \tilde{\nu} + a_\parallel \imath s_\parallel + \mathbf{a}_\perp \cdot \imath\mathbf{s}_\perp\right)\right] f\left(p, \mathbf{k}, \mathbf{s}\right) = -\frac{f\left(t = 0, \mathbf{k}, \mathbf{s}\right)}{k} - \frac{\nu_{\text{coll}}}{k} n\left(p, \mathbf{k}\right) w\left(\alpha_{\text{coll}}, s\right) - \frac{\nu_{\text{trap}} \Phi\left(p\right)}{k} n\left(p, \mathbf{k}\right) w\left(\alpha_{\text{detrap}}, s\right). \quad (3.18)$$

Finally, solving Eq. (3.18) provides the Fourier-Laplace transformed solution of the generalised Boltzmann equation (3.1):

$$f(p,\mathbf{k},\mathbf{s}) = -\frac{1}{k\mu\left(s_{\parallel}\right)}\int_{-\infty}^{s_{\parallel}} \mathrm{d}\sigma\mu(\sigma)\Big\{f(t=0,\mathbf{k},\sigma,\mathbf{s}_{\perp}) + n(p,\mathbf{k})\left[\nu_{\mathrm{coll}}w(\alpha_{\mathrm{coll}},\sigma,s_{\perp}) + \nu_{\mathrm{trap}}\Phi(p)\,w(\alpha_{\mathrm{detrap}},\sigma,s_{\perp})\right]\Big\}, \quad (3.19)$$

written in terms of the integrating factor

$$\mu\left(s_{\parallel}\right) \equiv \exp\left[-\frac{s_{\parallel}}{k}\left(\tilde{p}+\tilde{\nu}+\frac{1}{2}a_{\parallel}\imath s_{\parallel}+\mathbf{a}_{\perp}\cdot\imath\mathbf{s}_{\perp}\right)\right]. \quad (3.20)$$

We will use the this analytical expression (3.19) to evaluate relevant spatial and velocity moments to obtain macroscopic transport properties.

3.3.2 Particle number and the existence of a steady state

Integration of the Boltzmann equation (3.1) throughout all phase-space provides the equation for the free particle number, $N(t)$:

$$\left[\frac{\mathrm{d}}{\mathrm{d}t}+\nu_{\mathrm{trap}}(1-\Phi*)+\nu_{\mathrm{loss}}^{(\mathrm{free})}\right]N(t)=0. \quad (3.21)$$

Similarly, integration over configuration space for the trapped continuity equation (3.6) provides an equation for the trapped particle number, $N_{\mathrm{trap}}(t)$:

$$\left[\frac{\mathrm{d}}{\mathrm{d}t}+\nu_{\mathrm{loss}}^{(\mathrm{trap})}\right]N_{\mathrm{trap}}(t)=\nu_{\mathrm{trap}}(1-\Phi(t)*)N(t). \quad (3.22)$$

In conjunction with Eqs. (3.7) and (3.8) for the respective number of recombined free and trapped particles, each particle number can be written explicitly in Laplace space

$$N(p) = \frac{N(0)}{p+\nu_{\mathrm{trap}}[1-\Phi(p)]+\nu_{\mathrm{loss}}^{(\mathrm{free})}}, \quad (3.23)$$

$$N_{\mathrm{trap}}(p) = \frac{\nu_{\mathrm{trap}}[1-\Phi(p)]}{p+\nu_{\mathrm{loss}}^{(\mathrm{trap})}}N(p), \quad (3.24)$$

$$N_{\mathrm{loss}}^{(\mathrm{free})}(p) = \frac{\nu_{\mathrm{loss}}^{(\mathrm{free})}}{p}N(p), \quad (3.25)$$

$$N_{\mathrm{loss}}^{(\mathrm{trap})}(p) = \frac{\nu_{\mathrm{loss}}^{(\mathrm{trap})}}{p}N_{\mathrm{trap}}(p), \quad (3.26)$$

allowing for steady state values to be determined using the final value theorem, $\lim_{t\to\infty}N(t)=\lim_{p\to 0}pN(p)$. Two possible situations arise in the long time limit. In the case of no recombination, $\nu_{\mathrm{loss}}^{(\mathrm{free})}=\nu_{\mathrm{loss}}^{(\mathrm{trap})}=0$, an equilibrium steady state is

reached between the free and trapped particle numbers

$$\lim_{t\to\infty}\frac{N(t)}{N(0)} = \frac{\nu_{\text{detrap}}}{\nu_{\text{detrap}}+\nu_{\text{trap}}}, \tag{3.27}$$

$$\lim_{t\to\infty}\frac{N_{\text{trap}}(t)}{N(0)} = \frac{\nu_{\text{trap}}}{\nu_{\text{detrap}}+\nu_{\text{trap}}}, \tag{3.28}$$

where the detrapping rate has been defined

$$\nu_{\text{detrap}}^{-1} \equiv \int_0^\infty \mathrm{d}t\phi(t)\, t. \tag{3.29}$$

Figure 3.2 plots the number of free and trapped particles, $N(t)$ and $N_{\text{trap}}(t)$, and their respective steady state values (3.27) and (3.28) for an exponential waiting time distribution $\phi(t) = \nu_{\text{detrap}}\mathrm{e}^{-\nu_{\text{detrap}}t}$.

In the case of *any* recombination, $\nu_{\text{loss}}^{(\text{free})} > 0$ or $\nu_{\text{loss}}^{(\text{trap})} > 0$, no free particle steady state is reached as all free and trapped particles are eventually lost in the proportions

$$\lim_{t\to\infty}\frac{N_{\text{loss}}^{(\text{free})}(t)}{N(0)} = \frac{\nu_{\text{loss}}^{(\text{free})}}{\nu_{\text{loss}}^{(\text{free})}+\nu_{\text{trap}}P_{\text{loss}}}, \tag{3.30}$$

$$\lim_{t\to\infty}\frac{N_{\text{loss}}^{(\text{trap})}(t)}{N(0)} = \frac{\nu_{\text{trap}}P_{\text{loss}}}{\nu_{\text{loss}}^{(\text{free})}+\nu_{\text{trap}}P_{\text{loss}}}, \tag{3.31}$$

where the probability that a trapped particle undergoes recombination instead of detrapping is

$$P_{\text{loss}} \equiv 1 - \int_0^\infty \mathrm{d}t\Phi(t). \tag{3.32}$$

Figure 3.3 plots the number of free, trapped and recombined particles in this case where recombination is present for the same exponential waiting time distribution used in Figure 3.2. It can be seen that, although there is an initial increase in the number of trapped particles, all free and trapped particles are eventually lost to recombination in the respective proportions (3.30) and (3.31).

3.3.3 Number density, moments and transient transport coefficients

In this and later sections we will be predominantly interested in steady state quantities, independent of the choice of initial condition. For simplicity, we will assume there are initially $N(0)$ free particles centred at the origin with a Maxwellian distribution of velocities of temperature $T_0 \equiv m/k_{\text{B}}\alpha_0^2$

$$f(t=0,\mathbf{r},\mathbf{v}) \equiv N(0)\,\delta(\mathbf{r})\,w(\alpha_0,v). \tag{3.33}$$

Velocity integration of the generalised Boltzmann equation (3.1) provides the continuity equation for the free particle number density

$$\left[\frac{\partial}{\partial t}+\nu_{\text{trap}}(1-\Phi(t)*)+\nu_{\text{loss}}^{(\text{free})}\right]n(t,\mathbf{r})+\frac{\partial}{\partial\mathbf{r}}\cdot\left[n(t,\mathbf{r})\langle\mathbf{v}\rangle(t,\mathbf{r})\right]=0. \tag{3.34}$$

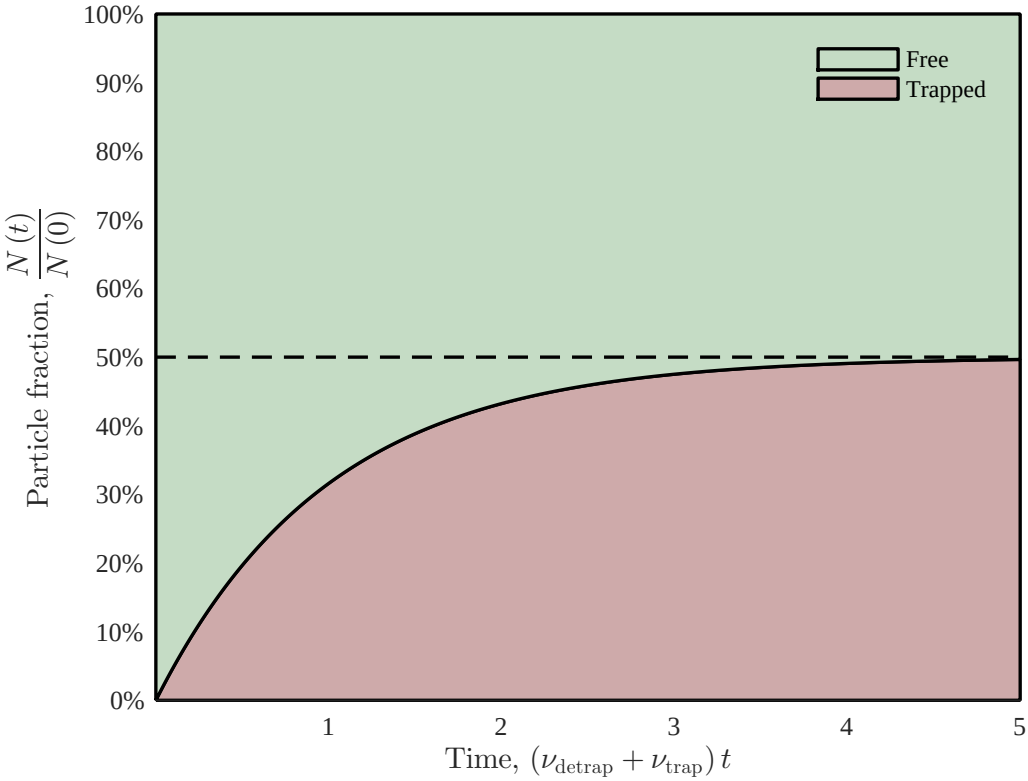

Figure 3.2: Free and trapped particle numbers for the exponential waiting time distribution $\phi(t) = \nu_{\text{detrap}} \mathrm{e}^{-\nu_{\text{detrap}} t}$. As no recombination is present, $\nu_{\text{loss}}^{(\text{free})} = \nu_{\text{loss}}^{(\text{trap})} = 0$, an equilibrium steady state is reached between the particles as described by Eqs. (3.27) and (3.28). Here, the detrapping and trapping rates are set equal, $\nu_{\text{detrap}} = \nu_{\text{trap}}$, resulting in the same number of free and trapped particles in the steady state.

This can be solved analytically using the generalised Boltzmann equation solution (3.19), yielding

$$n(p, \mathbf{k}) = \frac{N(0)\, \zeta_0(\mathbf{k})\, Z\left[-(\tilde{p} + \tilde{\nu})\, \zeta_0(\mathbf{k})\right]}{1 - \nu_{\text{coll}} \zeta_{\text{coll}}(\mathbf{k})\, Z\left[-(\tilde{p} + \tilde{\nu})\, \zeta_{\text{coll}}(\mathbf{k})\right] - \nu_{\text{trap}} \Phi(p)\, \zeta_{\text{detrap}}(\mathbf{k})\, Z\left[-(\tilde{p} + \tilde{\nu})\, \zeta_{\text{detrap}}(\mathbf{k})\right]}, \tag{3.35}$$

where the plasma dispersion function, $Z(\xi)$, is defined [89]

$$Z(\xi) \equiv \frac{1}{\sqrt{\pi}} \int_{-\infty}^{\infty} \mathrm{d}x \frac{\mathrm{e}^{-x^2}}{x - \xi}, \tag{3.36}$$

and each Maxwellian yields a term of the form

$$\zeta(\mathbf{k}) \equiv \left[2\imath \mathbf{k} \cdot \left(\frac{\imath \mathbf{k}}{\alpha^2} - \mathbf{a}\right)\right]^{-\frac{1}{2}}. \tag{3.37}$$

From this analytical solution, phase-space averaged moments of the generalised Boltzmann equation can be found exactly at all times. For example, we have the

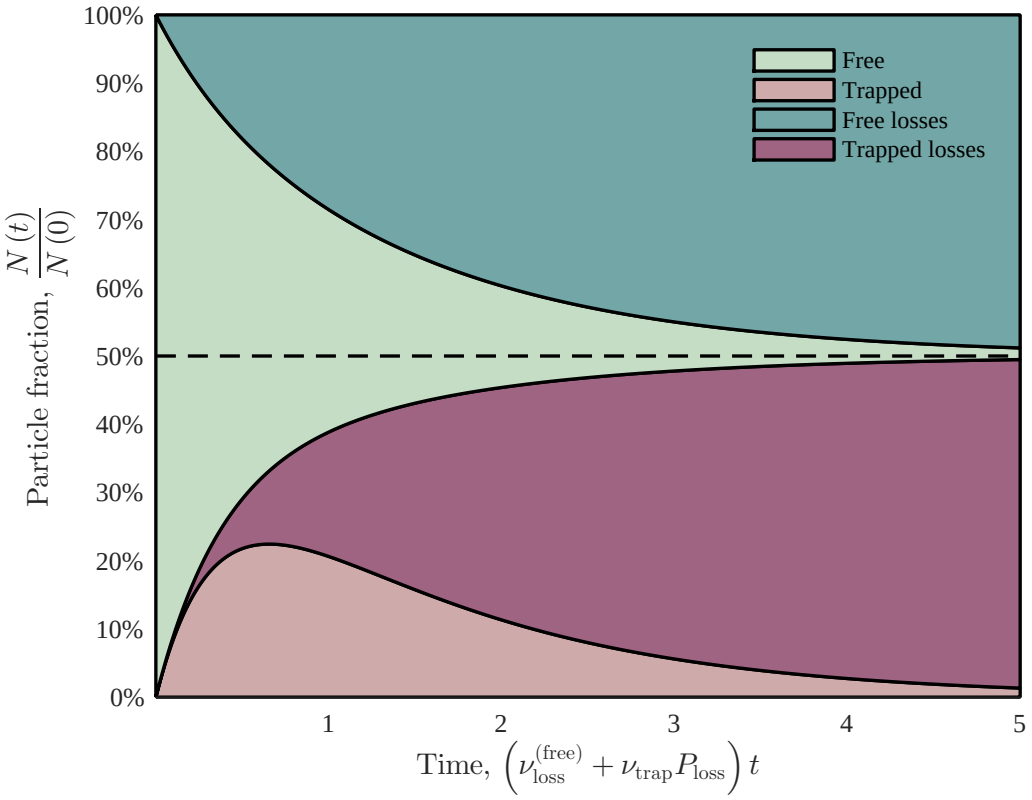

Figure 3.3: Free, trapped and recombined particle numbers for the exponential trapping time distribution $\phi(t) = \nu_{\text{detrap}} \mathrm{e}^{-\nu_{\text{detrap}} t}$. As recombination is present, all free and trapped particles are eventually lost in the proportions given by Eqs. (3.30) and (3.31). Transiently, however, there is an initial increase in the number of trapped particles. Here, we set equal the free particle recombination rate and the product of the trapping rate with the trapped particle recombination probability, $\nu_{\text{loss}}^{(\text{free})} = \nu_{\text{trap}} P_{\text{loss}}$. For this exponential distribution of waiting times this probability is $P_{\text{loss}} = \nu_{\text{loss}}^{(\text{trap})} / \left(\nu_{\text{detrap}} + \nu_{\text{loss}}^{(\text{trap})}\right)$. By making the aforementioned quantities equal, the number of recombined free and trapped particles also become equal in the long time limit. In this case, the detrapping and trapping rates are set to $\nu_{\text{detrap}} = \nu_{\text{trap}} = \nu_{\text{loss}}^{(\text{free})} + \nu_{\text{trap}} P_{\text{loss}}$, which consequently specifies the trapped particle recombination rate $\nu_{\text{loss}}^{(\text{trap})} = \nu_{\text{loss}}^{(\text{free})} + \nu_{\text{trap}} P_{\text{loss}}$.

spatial moments

$$\mathcal{L}\left\{\frac{N(t)}{N(0)}\langle\mathbf{r}\rangle(t)\right\} = \frac{\mathbf{a}}{\tilde{p}^2(\tilde{p}+\tilde{\nu})}, \tag{3.38}$$

$$\mathcal{L}\left\{\frac{N(t)}{N(0)}\langle\mathbf{rr}\rangle(t)\right\} = \frac{2\mathbf{I}}{\tilde{p}^2(\tilde{p}+\tilde{\nu})^2}\left[\frac{\tilde{p}}{\alpha_0^2}+\frac{\nu_{\text{coll}}}{\alpha_{\text{coll}}^2}+\frac{\nu_{\text{trap}}\Phi(p)}{\alpha_{\text{detrap}}^2}\right] + \frac{2\mathbf{aa}}{\tilde{p}^2(\tilde{p}+\tilde{\nu})^2}\left(\frac{1}{\tilde{p}}+\frac{2}{\tilde{p}+\tilde{\nu}}\right), \tag{3.39}$$

where the Laplace transform operator has been denoted explicitly here as $\mathcal{L}$. From these moments, the motion of the centre of mass (CM) can be described. The CM velocity is defined as the time rate of change of its position

$$\mathbf{W}_{\text{CM}}(t) \equiv \frac{\mathrm{d}}{\mathrm{d}t}\langle\mathbf{r}\rangle(t), \tag{3.40}$$

while the CM diffusivity is defined as being proportional to the rate of change of particle dispersion about it

$$\mathbf{D}_{\text{CM}}(t) \equiv \frac{1}{2}\frac{\mathrm{d}}{\mathrm{d}t}\left[\langle\mathbf{rr}\rangle(t) - \langle\mathbf{r}\rangle(t)\langle\mathbf{r}\rangle(t)\right]. \tag{3.41}$$

CM transport coefficients can be defined for the free, trapped and total particles. Although trapped particles are localised in space their CM still moves due to repeated trapping and detrapping.

The movement of the free particles can also be described by looking directly at velocity moments of the generalised Boltzmann equation (3.1)

$$\mathcal{L}\left\{\frac{N(t)}{N(0)}\langle\mathbf{v}\rangle(t)\right\} = \frac{\mathbf{a}}{\tilde{p}(\tilde{p}+\tilde{\nu})}, \tag{3.42}$$

$$\mathcal{L}\left\{\frac{N(t)}{N(0)}\langle\mathbf{rv}\rangle(t)\right\} = \frac{\mathbf{I}}{\tilde{p}(\tilde{p}+\tilde{\nu})^2}\left[\frac{\tilde{p}}{\alpha_0^2}+\frac{\nu_{\text{coll}}}{\alpha_{\text{coll}}^2}+\frac{\nu_{\text{trap}}\Phi(p)}{\alpha_{\text{detrap}}^2}\right] + \frac{\mathbf{aa}}{\tilde{p}(\tilde{p}+\tilde{\nu})^2}\left(\frac{1}{\tilde{p}}+\frac{2}{\tilde{p}+\tilde{\nu}}\right), \tag{3.43}$$

from which we define the average velocity

$$\mathbf{W}(t) \equiv \langle\mathbf{v}\rangle(t), \tag{3.44}$$

and average diffusivity

$$\mathbf{D}(t) \equiv \langle\mathbf{rv}\rangle(t) - \langle\mathbf{r}\rangle(t)\langle\mathbf{v}\rangle(t). \tag{3.45}$$

Figure 3.4 plots the CM velocity $\mathbf{W}_{\text{CM}}(t)$ for the free, trapped and total particles alongside the average velocity $\mathbf{W}(t)$ for the free particles. We see that all measures of velocity begin at zero due to the Maxwellian initial condition (3.33) being spherically symmetric in velocity space. All velocities then increase due to the applied field, with the free particle CM velocity $\mathbf{W}_{\text{CM}}^{(\text{free})}(t)$ and average velocity $\mathbf{W}(t)$ coinciding linearly

at early times

$$\mathbf{W}(t) \approx \mathbf{W}_{\mathrm{CM}}^{(\mathrm{free})}(t) \approx \mathbf{a}t. \tag{3.46}$$

A similar small time expansion can be written for the free particle diffusivites

$$\mathbf{D}(t) \approx \mathbf{D}_{\mathrm{CM}}^{(\mathrm{free})}(t) \approx \frac{\mathbf{I}}{\alpha_0^2}t + \frac{\mathbf{aa}}{12}\left[\nu_{\mathrm{coll}} + 6\left(\nu_{\mathrm{loss}}^{(\mathrm{free})} + \nu_{\mathrm{trap}}\right)\right]t^4. \tag{3.47}$$

This coincidence between the free particle CM and average velocities only lasts temporarily before the CM velocity decreases, becoming negative prior to reaching its positive steady state value. This movement of the free particle CM against the field is due to the processes of trapping and detrapping. Specifically, as all particles are initially free, an unusually large "pulse" of particles are trapped near the origin, which is later released, causing a bias of the distribution and shifting the CM towards the origin. Similarly, as the diffusivity of particles trapped early is initially small, the free particle CM diffusivity $\mathbf{D}_{\mathrm{CM}}^{(\mathrm{free})}(t)$ can also become transiently negative, as the distribution appears to "bunch up" near the origin as the initial pulse is released. Finally, we can see that all CM velocities approach the same steady state value, while the free particle average velocity approaches a separate steady state. Specifically, the CM transport coefficients, $\mathbf{W}_{\mathrm{CM}}(t)$ and $\mathbf{D}_{\mathrm{CM}}(t)$, approach the values given by Eqs. (3.84) and (3.85), while the average transport coefficients, $\mathbf{W}(t)$ and $\mathbf{D}(t)$, approach Eqs. (3.61) and (3.77).

3.4 Hydrodynamic regime and the generalised diffusion equation

3.4.1 Chapman-Enskog perturbative solution

The Chapman-Enskog perturbative solution technique [90] assumes that certain terms in the Boltzmann equation are small relative to others, allowing the solution to be written in the form of a Maclaurin series expansion. Traditionally, the Chapman-Enskog expansion assumes that both the explicit and implicit time derivatives in the Boltzmann equation are small. An implication of this is that the perturbative solution is valid only when the applied field is also small. We will relax this condition and instead use a generalisation of the Chapman-Enskog expansion that only considers small explicit time and space derivatives, known as a hydrodynamic expansion. We expect the resulting solution to be most accurate in the long distance steady state. Note, however, in Section 3.3.2 we determined that a steady state is not always attainable for our generalised Boltzmann equation (3.1). Specifically, if there is *any* recombination present, all free and trapped particles are eventually lost. For the purpose of performing a hydrodynamic expansion, we ensure that a steady state can always be reached by introducing a scaled phase-space distribution function with a constant particle number

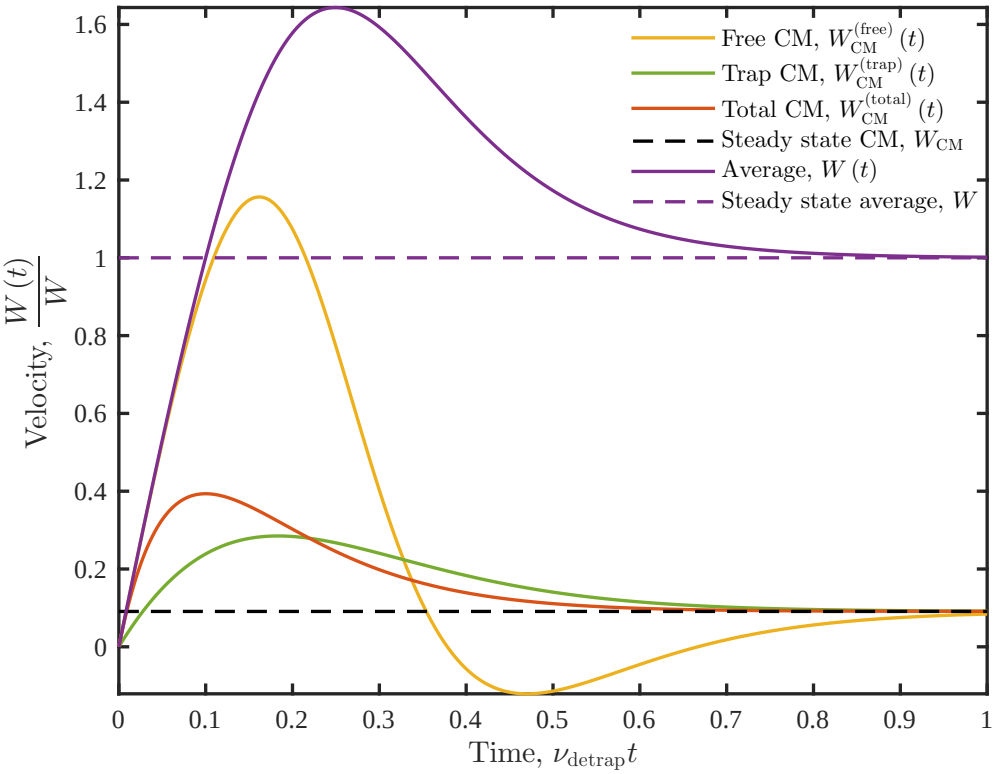

Figure 3.4: Plot of the centre of mass (CM) velocities for free, trapped and total particles, $\mathbf{W}_{\mathrm{CM}}^{(\mathrm{free})}(t)$, $\mathbf{W}_{\mathrm{CM}}^{(\mathrm{trap})}(t)$ and $\mathbf{W}_{\mathrm{CM}}^{(\mathrm{total})}(t)$, as well as the actual average velocity for the free particles, $\mathbf{W}(t)$, for the exponential waiting time distribution $\phi(t) = \nu_{\mathrm{detrap}} \mathrm{e}^{-\nu_{\mathrm{detrap}} t}$. The free particle CM velocity $\mathbf{W}_{\mathrm{CM}}^{(\mathrm{free})}(t)$ and average velocity $\mathbf{W}(t)$ coincide linearly at early times according to Eq. (3.46). The free particle CM velocity $\mathbf{W}_{\mathrm{CM}}(t)$ is seen to transiently become negative due to particles trapped early near the origin leaving their traps. In this case, there is no recombination present, $\nu_{\mathrm{loss}}^{(\mathrm{free})} = \nu_{\mathrm{loss}}^{(\mathrm{trap})} = 0$, the collision frequency is set to $\nu_{\mathrm{coll}}/\nu_{\mathrm{detrap}} = 1$ and the trapping rate is made sufficiently large so as the transient negative velocity manifests, with $\nu_{\mathrm{trap}}/\nu_{\mathrm{detrap}} = 10$. An additional consequence of this relatively large trapping rate is that almost all free particles become trapped early on, allowing the velocities to almost reach their steady state values after only a single trapping time $\nu_{\mathrm{detrap}} t = 1$.

$N(0)$

$$F(t,\mathbf{r},\mathbf{v}) \equiv \frac{N(0)}{N(t)} f(t,\mathbf{r},\mathbf{v}). \tag{3.48}$$

Substitution into the generalised Boltzmann equation (3.1) provides a corresponding equation for this scaled distribution

$$\left(\frac{\partial}{\partial t}+\mathbf{v}\cdot\frac{\partial}{\partial \mathbf{r}}+\mathbf{a}\cdot\frac{\partial}{\partial \mathbf{v}}\right)F(t,\mathbf{r},\mathbf{v}) = -\nu_{\text{coll}}\left[F(t,\mathbf{r},\mathbf{v}) - n_F(t,\mathbf{r})\, w(\alpha_{\text{coll}},v)\right] - \nu_{\text{trap}}\left[R(t)\,F(t,\mathbf{r},\mathbf{v}) - R(t,\mathbf{r})\, n_F(t,\mathbf{r})\, w(\alpha_{\text{detrap}},v)\right], \tag{3.49}$$

where $n_F(t,\mathbf{r}) \equiv \int \mathrm{d}\mathbf{v} F(t,\mathbf{r},\mathbf{v})$ and we have introduced the ratio of detrapping and trapping rates

$$R(t,\mathbf{r}) \equiv \frac{\Phi(t) * n(t,\mathbf{r})}{n(t,\mathbf{r})}, \tag{3.50}$$

and its spatially homogeneous form

$$R(t) \equiv \frac{\Phi(t) * N(t)}{N(t)}. \tag{3.51}$$

On the terms we wish to denote as small, we will temporarily introduce a multiplicative parameter δ

$$\delta\left(\frac{\partial}{\partial t}+\mathbf{v}\cdot\frac{\partial}{\partial \mathbf{r}}\right)F_\delta(t,\mathbf{r},\mathbf{v}) + \mathbf{a}\cdot\frac{\partial}{\partial \mathbf{v}}F_\delta(t,\mathbf{r},\mathbf{v}) = -\nu_{\text{coll}}\left[F_\delta(t,\mathbf{r},\mathbf{v}) - n_F(t,\mathbf{r})\, w(\alpha_{\text{coll}},v)\right] - \nu_{\text{trap}}\left[R(t)\,F_\delta(t,\mathbf{r},\mathbf{v}) - R(t,\mathbf{r})\, n_F(t,\mathbf{r})\, w(\alpha_{\text{detrap}},v)\right], \tag{3.52}$$

through which we can expand the solution in a power series

$$F_\delta(t,\mathbf{r},\mathbf{v}) = \sum_{n\geq 0} F^{(n)}(t,\mathbf{r},\mathbf{v})\,\delta^n. \tag{3.53}$$

This allows the actual solution to be recovered by setting $\delta = 1$ in the above series expansion [90]

$$F(t,\mathbf{r},\mathbf{v}) = \sum_{n\geq 0} F^{(n)}(t,\mathbf{r},\mathbf{v}). \tag{3.54}$$

The terms in this series solution can be found recursively by substituting the δ expansion (3.53) for $F_\delta(t,\mathbf{r},\mathbf{v})$ into the generalised Boltzmann equation (3.52) and equating powers of δ

$$\left[\nu_{\text{coll}} + \nu_{\text{trap}} R(t) + \mathbf{a}\cdot\frac{\partial}{\partial \mathbf{v}}\right]F^{(n)}(t,\mathbf{r},\mathbf{v}) = -\left(\frac{\partial}{\partial t}+\mathbf{v}\cdot\frac{\partial}{\partial \mathbf{r}}\right)F^{(n-1)}(t,\mathbf{r},\mathbf{v}). \tag{3.55}$$

This recurrence relationship is valid for $n \geq 1$, with the initial term given separately as

$$\left[1 + \langle \mathbf{v} \rangle^{(0)}(t) \cdot \frac{\partial}{\partial \mathbf{v}}\right] F^{(0)}(t, \mathbf{r}, \mathbf{v}) = \frac{\nu_{\text{coll}} w(\alpha_{\text{coll}}, v) + \nu_{\text{trap}} R(t, \mathbf{r}) w(\alpha_{\text{detrap}}, v)}{\nu_{\text{coll}} + \nu_{\text{trap}} R(t, \mathbf{r})} n_F(t, \mathbf{r}), \tag{3.56}$$

in terms of its corresponding average velocity

$$\langle \mathbf{v} \rangle^{(0)}(t) \equiv \frac{\mathbf{a}}{\nu_{\text{coll}} + \nu_{\text{trap}} R(t)}. \tag{3.57}$$

Note here we have enforced the normalisation condition

$$\int \mathrm{d}\mathbf{v} F^{(0)}(t, \mathbf{r}, \mathbf{v}) \equiv n_F(t, \mathbf{r}). \tag{3.58}$$

In Fourier-transformed velocity space we can write this initial term explicitly

$$F^{(0)}(t, \mathbf{r}, \mathbf{s}) = \tilde{w}(t, \mathbf{r}, \mathbf{s}) n_F(t, \mathbf{r}), \tag{3.59}$$

where

$$\tilde{w}(t, \mathbf{r}, \mathbf{s}) \equiv \frac{1}{1 + \langle \mathbf{v} \rangle^{(0)}(t) \cdot \imath \mathbf{s}} \frac{\nu_{\text{coll}} w(\alpha_{\text{coll}}, s) + \nu_{\text{trap}} R(t, \mathbf{r}) w(\alpha_{\text{detrap}}, s)}{\nu_{\text{coll}} + \nu_{\text{trap}} R(t, \mathbf{r})}. \tag{3.60}$$

We can confirm that this approximate hydrodynamic solution is most accurate in the steady state by noting that its average velocity coincides with the actual average velocity (3.44) at late times, $\lim_{t\to\infty} \langle \mathbf{v} \rangle^{(0)}(t) = \lim_{t\to\infty} \langle \mathbf{v} \rangle(t)$. We will denote this shared steady state velocity as

$$\mathbf{W} \equiv \frac{\mathbf{a}}{\nu_{\text{eff}}}, \tag{3.61}$$

where the separate collision and trapping processes contribute to the effective frequency

$$\nu_{\text{eff}} \equiv \nu_{\text{coll}} + R\nu_{\text{trap}}, \tag{3.62}$$

defined in terms of the spatially averaged limiting ratio of detrapping and trapping rates

$$R \equiv \lim_{t\to\infty} R(t) \equiv \lim_{t\to\infty} \frac{\Phi(t) * N(t)}{N(t)}. \tag{3.63}$$

This limit can be evaluated implicitly as satisfying

$$R \equiv \int_0^\infty \mathrm{d}t \Phi(t) \mathrm{e}^{\left[\nu_{\text{loss}}^{(\text{free})} + \nu_{\text{trap}}(1-R)\right]t}. \tag{3.64}$$

This implicit definition of R can be solved analytically only for certain choices of trapping time distribution $\phi(t)$. A table of such R values for a variety of corresponding $\phi(t)$ is presented in Appendix A.

In terms of this velocity, $\mathbf{W}$, we can write the steady state limit of Eq. (3.60) as

$$\tilde{w}(\mathbf{r},\mathbf{s}) = \frac{1}{1+\mathbf{W}\cdot\imath\mathbf{s}}\frac{\nu_{\text{coll}}w(\alpha_{\text{coll}},s)+\nu_{\text{trap}}R(\mathbf{r})\,w(\alpha_{\text{detrap}},s)}{\nu_{\text{coll}}+\nu_{\text{trap}}R(\mathbf{r})}, \tag{3.65}$$

where the limiting ratio of detrapping and trapping rates is

$$R(\mathbf{r}) \equiv \lim_{t\to\infty} R(t,\mathbf{r}). \tag{3.66}$$

In direct analogy with the implicit definition (3.64) of R we have the following implicit definition of $R(\mathbf{r})$

$$R(\mathbf{r}) \equiv \int_0^\infty \mathrm{d}t\Phi(t)\exp\left\{\left[\nu_{\text{loss}}^{(\text{free})}+\nu_{\text{trap}}(1-R(\mathbf{r}))+\frac{1}{n}\frac{\partial}{\partial\mathbf{r}}\cdot n\langle\mathbf{v}\rangle\right]t\right\}. \tag{3.67}$$

Finally, we can explore the spatial dependence of $\tilde{w}(\mathbf{r},\mathbf{s})$ by considering a perturbation from its spatially averaged state

$$\tilde{w}(\mathbf{s}) = \frac{\nu_{\text{coll}}w(\alpha_{\text{coll}},s)+\nu_{\text{trap}}Rw(\alpha_{\text{detrap}},s)}{\nu_{\text{coll}}+\nu_{\text{trap}}R+\mathbf{a}\cdot\imath\mathbf{s}}. \tag{3.68}$$

To spatially perturb $\tilde{w}(\mathbf{s})$, we must first spatially perturb R using the definition (3.67) of $R(\mathbf{r})$. Introducing the first order spatial perturbation δR and using the asymptotic velocity in the hydrodynamic regime, $\langle\mathbf{v}\rangle\sim\mathbf{W}$, provides the expression

$$R+\delta R = R\left\langle\exp\left[\left(\frac{1}{n}\frac{\partial n}{\partial\mathbf{r}}\cdot\mathbf{W}-\nu_{\text{trap}}\delta R\right)t\right]\right\rangle, \tag{3.69}$$

in terms of the time average defined by

$$\langle\eta(t)\rangle \equiv \frac{1}{R}\int_0^\infty \mathrm{d}t\Phi(t)\,\mathrm{e}^{\left[\nu_{\text{loss}}^{(\text{free})}+\nu_{\text{trap}}(1-R)\right]t}\eta(t). \tag{3.70}$$

Performing a power series expansion and truncating beyond first order gives the solution $R(\mathbf{r}) = R+\delta R$ as a density gradient expansion up to first order

$$R(\mathbf{r}) = R+\mathbf{R}^{(1)}\cdot\frac{1}{n}\frac{\partial n}{\partial\mathbf{r}}, \tag{3.71}$$

in terms of the vector coefficient

$$\mathbf{R}^{(1)} \equiv \frac{R\langle t\rangle}{1+\nu_{\text{trap}}R\langle t\rangle}\mathbf{W}. \tag{3.72}$$

Now the spatially averaged steady state velocity distribution $\tilde{w}(\mathbf{s})$ can be spatially perturbed using the density gradient expansion (3.71), resulting in, to first spatial order

$$\begin{aligned} F^{(0)}(t,\mathbf{r},\mathbf{s}) &= \tilde{w}(\mathbf{s})\,n_F(t,\mathbf{r}) \\ &\quad +\frac{w(\alpha_{\text{detrap}},s)-\tilde{w}(\mathbf{s})}{\nu_{\text{coll}}+\nu_{\text{trap}}R+\mathbf{a}\cdot\imath\mathbf{s}}\nu_{\text{trap}}\mathbf{R}^{(1)}\cdot\frac{\partial n_F}{\partial\mathbf{r}}. \end{aligned} \tag{3.73}$$

Using the recurrence relationship (3.55) and the continuity equation (3.34) to evaluate the explicit time derivative provides the next term, also to first spatial order

$$F^{(1)}(t,\mathbf{r},\mathbf{s}) = \frac{\mathbf{W}\tilde{w}(\mathbf{s}) - \imath\frac{\partial}{\partial\mathbf{s}}\tilde{w}(\mathbf{s})}{\nu_{\text{coll}} + \nu_{\text{trap}}R + \mathbf{a}\cdot\imath\mathbf{s}} \cdot \frac{\partial n_F}{\partial\mathbf{r}}. \tag{3.74}$$

Similarly, $F^{(2)}(t,\mathbf{r},\mathbf{v})$ can be found and shown to be of minimum second order in spatial gradients. In general, $F^{(n)}(t,\mathbf{r},\mathbf{v})$ is described by a full density gradient expansion of minimum spatial order n. Including all zeroth and first order contributions, the generalised Boltzmann equation solution is

$$f(t,\mathbf{r},\mathbf{s}) = \tilde{w}(\mathbf{s})\, n(t,\mathbf{r}) + \frac{\left[\mathbf{W} - \nu_{\text{trap}}\mathbf{R}^{(1)} - \imath\frac{\partial}{\partial\mathbf{s}}\right]\tilde{w}(\mathbf{s}) + \nu_{\text{trap}}\mathbf{R}^{(1)}w(\alpha_{\text{detrap}},s)}{\nu_{\text{coll}} + \nu_{\text{trap}}R + \mathbf{a}\cdot\imath\mathbf{s}} \cdot \frac{\partial n}{\partial\mathbf{r}}. \tag{3.75}$$

Velocity integration provides Fick's law for the free particle flux

$$n\langle\mathbf{v}\rangle = \mathbf{W}n - \mathbf{D}\cdot\frac{\partial n}{\partial\mathbf{r}}, \tag{3.76}$$

which implies that $\mathbf{W}$ is the flux drift velocity and defines the flux diffusion coefficient as

$$\mathbf{D} \equiv \frac{1}{\nu_{\text{eff}}}\left[\frac{\mathbf{I}}{\alpha_{\text{eff}}^2} + \left(\mathbf{W} + \nu_{\text{trap}}\mathbf{R}^{(1)}\right)\mathbf{W}\right], \tag{3.77}$$

written in terms of the effective frequency (3.62) and the effective temperature

$$T_{\text{eff}} \equiv \frac{\nu_{\text{coll}}}{\nu_{\text{coll}} + R\nu_{\text{trap}}}T_{\text{coll}} + \frac{R\nu_{\text{trap}}}{\nu_{\text{coll}} + R\nu_{\text{trap}}}T_{\text{detrap}}. \tag{3.78}$$

Similar to the flux drift velocity $\mathbf{W}$, the flux diffusion coefficient $\mathbf{D}$ could have also been derived as the long time limit of the average diffusivity (3.45)

$$\mathbf{D} \equiv \lim_{t\to\infty}\left[\langle\mathbf{rv}\rangle(t) - \langle\mathbf{r}\rangle(t)\langle\mathbf{v}\rangle(t)\right]. \tag{3.79}$$

The flux diffusion coefficient derived here differs slightly from what was derived in [33] for a similar phase-space kinetic model utilising the same operator for trapping and detrapping. It is likely they did not consider the spatial dependence in Eq. (3.50) for the ratio of detrapping and trapping rates $R(t,\mathbf{r})$, as their diffusion coefficient lacked the additional anisotropic component $\frac{\nu_{\text{trap}}}{\nu_{\text{eff}}}\mathbf{R}^{(1)}\mathbf{W}$. Subsequently, their diffusion coefficient is only valid in the isotropic case without an applied field, where $\mathbf{W} = 0$, or in the limit of instantaneous detrapping, where $\mathbf{R}^{(1)} = \mathbf{0}$.

3.4.2 Analytical correspondence of transport coefficients

Diffusion equations in the hydrodynamic regime

In the previous section we considered a perturbative solution of the generalised Boltzmann equation (3.1), written in the hydrodynamic regime as the density gradient

expansion (3.75). This solution directly provided the flux transport coefficients of velocity (3.61) and diffusion (3.77). In this section, we look to reconcile these results analytically using Eq. (3.35) for the number density. We can describe the asymptotics of the number density by looking at its poles in Laplace space, found by solving the dispersion relation [39]

$$1-\nu_{\mathrm{coll}}\zeta_{\mathrm{coll}}\left(\mathbf{k}\right)Z\left[-\left(\tilde{p}+\tilde{\nu}\right)\zeta_{\mathrm{coll}}\left(\mathbf{k}\right)\right]-\nu_{\mathrm{trap}}\Phi\left(p\right)\zeta_{\mathrm{detrap}}\left(\mathbf{k}\right)Z\left[-\left(\tilde{p}+\tilde{\nu}\right)\zeta_{\mathrm{detrap}}\left(\mathbf{k}\right)\right]=0. \tag{3.80}$$

Using the asymptotic series representation of the plasma dispersion function [89]

$$Z\left(\xi\right)=-\frac{1}{\xi}\sum_{n\geq 0}\frac{\left(2n-1\right)!!}{2^{n}}\xi^{-2n}=-\frac{1}{\xi}\left(1+\frac{1}{2}\xi^{-2}+\frac{3}{4}\xi^{-4}+\cdots\right), \tag{3.81}$$

we perform a small $\mathbf{k}$ expansion and find the root of the dispersion relation to second spatial order

$$p=-\nu_{\mathrm{trap}}\left(1-R\right)-\nu_{\mathrm{loss}}^{(\mathrm{free})}-\mathbf{W}_{\mathrm{CM}}\cdot\imath\mathbf{k}+\mathbf{D}_{\mathrm{CM}}\colon\imath\mathbf{k}\imath\mathbf{k}, \tag{3.82}$$

which corresponds to the diffusion equation

$$\left[\frac{\partial}{\partial t}+\nu_{\mathrm{trap}}\left(1-R\right)+\nu_{\mathrm{loss}}^{(\mathrm{free})}+\mathbf{W}_{\mathrm{CM}}\cdot\frac{\partial}{\partial\mathbf{r}}-\mathbf{D}_{\mathrm{CM}}\colon\frac{\partial^{2}}{\partial\mathbf{r}\partial\mathbf{r}}\right]n\left(t,\mathbf{r}\right)=0. \tag{3.83}$$

Here the steady state centre of mass (CM) transport coefficients are defined

$$\mathbf{W}_{\mathrm{CM}} \equiv \frac{\mathbf{R}^{(1)}}{R\left\langle t\right\rangle}, \tag{3.84}$$

$$\mathbf{D}_{\mathrm{CM}} \equiv \frac{\left\langle t^{2}\right\rangle}{2\left\langle t\right\rangle}\mathbf{W}_{\mathrm{CM}}\mathbf{W}_{\mathrm{CM}}-\frac{\mathbf{R}^{(2)}}{R\left\langle t\right\rangle}, \tag{3.85}$$

using the density gradient expansion of $R\left(\mathbf{r}\right)$

$$R\left(\mathbf{r}\right)=R+\mathbf{R}^{(1)}\cdot\frac{1}{n}\frac{\partial n}{\partial\mathbf{r}}+\mathbf{R}^{(2)}\colon\frac{1}{n}\frac{\partial^{2}n}{\partial\mathbf{r}\partial\mathbf{r}}, \tag{3.86}$$

written now to second order using the flux diffusion coefficient $\mathbf{D}$

$$\mathbf{R}^{(2)}\equiv\frac{R\left\langle t^{2}\right\rangle}{2\left(1+\nu_{\mathrm{trap}}R\left\langle t\right\rangle\right)^{3}}\mathbf{W}\mathbf{W}-\frac{R\left\langle t\right\rangle}{1+\nu_{\mathrm{trap}}R\left\langle t\right\rangle}\mathbf{D}, \tag{3.87}$$

where time averages are defined by Eq. (3.70). Substitution of the root of the dispersion relation into the time operator of the continuity equation yields, to second spatial order

$$p+\nu_{\mathrm{trap}}\left[1-\Phi\left(p\right)\right]+\nu_{\mathrm{loss}}^{(\mathrm{free})}=-\mathbf{W}\cdot\imath\mathbf{k}+\mathbf{D}\colon\imath\mathbf{k}\imath\mathbf{k}, \tag{3.88}$$

which corresponds to the generalised diffusion equation

$$\left[\frac{\partial}{\partial t}+\nu_{\mathrm{trap}}\left(1-\Phi\left(t\right)*\right)+\nu_{\mathrm{loss}}^{(\mathrm{free})}+\mathbf{W}\cdot\frac{\partial}{\partial\mathbf{r}}-\mathbf{D}\colon\frac{\partial^{2}}{\partial\mathbf{r}\partial\mathbf{r}}\right]n\left(t,\mathbf{r}\right)=0, \tag{3.89}$$

in terms of the flux transport coefficients $\mathbf{W}$ and $\mathbf{D}$. This could have alternatively been derived by approximating the flux in the continuity equation directly using its density gradient expansion (Fick's law) given by Eq. (3.76).

Approaching the steady state

Thus far we have considered the continuity equation in both the steady and near spatially homogeneous state. Using the analytical solution, it is possible to relax this steady state assumption. We can write the flux exactly by rearranging the continuity equation (3.34) in Fourier-Laplace space

$$\imath\mathbf{k}\cdot\mathcal{L}\left\{n\left(t,\mathbf{k}\right)\left\langle\mathbf{v}\right\rangle\left(t\right)\right\}=\left[\frac{N\left(0\right)}{n\left(p,\mathbf{k}\right)}-\tilde{p}\right]n\left(p,\mathbf{k}\right). \tag{3.90}$$

Performing a small $\mathbf{k}$ expansion of the above coefficient of $n\left(p,\mathbf{k}\right)$ gives an approximate continuity equation valid for large distances or near spatially homogeneous states

$$\left[p+\nu_{\mathrm{trap}}\left(1-\Phi\left(p\right)\right)+\nu_{\mathrm{loss}}^{(\mathrm{free})}+\mathfrak{W}\left(p\right)\cdot\imath\mathbf{k}-\mathfrak{D}\left(p\right):\imath\mathbf{k}\imath\mathbf{k}\right]n\left(p,\mathbf{k}\right)=N\left(0\right), \tag{3.91}$$

where the following p-dependent velocity and diffusivity are defined in Laplace space

$$\mathfrak{W}\left(p\right) \equiv \frac{\mathbf{a}}{\tilde{p}+\tilde{\nu}}, \tag{3.92}$$

$$\mathfrak{D}\left(p\right) \equiv \frac{\mathbf{I}}{\left(\tilde{p}+\tilde{\nu}\right)^{2}}\left[\frac{\tilde{p}}{\alpha_{0}^{2}}+\frac{\nu_{\mathrm{coll}}}{\alpha_{\mathrm{coll}}^{2}}+\frac{\nu_{\mathrm{trap}}\Phi\left(p\right)}{\alpha_{\mathrm{detrap}}^{2}}\right]+\frac{2\mathbf{aa}}{\left(\tilde{p}+\tilde{\nu}\right)^{3}}, \tag{3.93}$$

although in the time domain $\mathfrak{W}\left(t\right)$ and $\mathfrak{D}\left(t\right)$ have units of length and area respectively. Performing the inverse Fourier-Laplace transform yields

$$\left[\frac{\partial}{\partial t}+\nu_{\mathrm{trap}}\left(1-\Phi\left(t\right)*\right)+\nu_{\mathrm{loss}}^{(\mathrm{free})}+\mathfrak{W}\left(t\right)*\cdot\frac{\partial}{\partial\mathbf{r}}-\mathfrak{D}\left(t\right)*:\frac{\partial^{2}}{\partial\mathbf{r}\partial\mathbf{r}}\right]n\left(t,\mathbf{r}\right)=0, \tag{3.94}$$

which is of a similar form to the generalised diffusion equation, but now the "transport coefficients" are time convolved with the number density. It should be noted that, as the flux has been written to second spatial order, the first and second order spatial moments of this approximate continuity equation are exact for all times.

3.5 Connection with fractional transport

As described in Section 1.1, dispersive transport is physically characterised by long-lived traps. For the right choice of parameters, the generalised Boltzmann equation (3.1) is capable of modelling such trapped states. A necessary condition for dispersive transport is a waiting time distribution with a divergent mean [12]. One choice is a waiting time distribution with a heavy tail of the power law form

$$\phi\left(t\right)\sim t^{-(1+\alpha)}, \tag{3.95}$$

where $0 < \alpha < 1$. In Laplace space, this is equivalent to the small p approximation

$$\phi(p) \approx 1 - r_\alpha p^\alpha, \tag{3.96}$$

where r_α is a constant that is potentially dependent on α. Additionally, we must enforce that no trap-based recombination occurs, $\nu_{\text{loss}}^{(\text{trap})} = 0$, as this has the effect of causing particles to prematurely detrap, shortening the trapping time so that the mean trapping time no longer diverges. In this case, the effective waiting time distribution (3.5) is no longer weighted by an exponential decay term, $\Phi(t) \to \phi(t)$, and the continuity equation (3.34) becomes

$$\left[\frac{\partial}{\partial t} + \nu_{\text{trap}}\left(1 - \phi(t) *\right) + \nu_{\text{loss}}^{(\text{free})}\right] n(t, \mathbf{r}) + \frac{\partial}{\partial \mathbf{r}} \cdot \left[n(t, \mathbf{r}) \langle \mathbf{v} \rangle (t, \mathbf{r})\right] = 0. \tag{3.97}$$

We can separate the power law tail from the waiting time distribution as

$$\phi(t) * n(t, \mathbf{r}) = \psi(t) * n(t, \mathbf{r}) - r_\alpha \left[{}_0^{\text{C}}\mathcal{D}_t^\alpha n(t, \mathbf{r}) + \frac{t^{-\alpha}}{\Gamma(1-\alpha)} n(0, \mathbf{r})\right], \tag{3.98}$$

where $\psi(t)$ is a time distribution with well-defined moments and the operator of Caputo fractional differentiation of order α is defined

$${}_0^{\text{C}}\mathcal{D}_t^\alpha n(t, \mathbf{r}) \equiv \frac{1}{\Gamma(1-\alpha)} \int_0^t \mathrm{d}\tau \, (t-\tau)^{-\alpha} \frac{\partial}{\partial \tau} n(\tau, \mathbf{r}). \tag{3.99}$$

The continuity equation can now be written exactly as

$$\left[\frac{\partial}{\partial t} + r_\alpha \nu_{\text{trap}} {}_0^{\text{C}}\mathcal{D}_t^\alpha + \nu_{\text{trap}}\left(1 - \psi(t) *\right) + \nu_{\text{loss}}^{(\text{free})}\right] n(t, \mathbf{r}) + \frac{\partial}{\partial \mathbf{r}} \cdot \left[n(t, \mathbf{r}) \langle \mathbf{v} \rangle (t, \mathbf{r})\right] = -\frac{r_\alpha \nu_{\text{trap}}}{t^\alpha \Gamma(1-\alpha)} n(0, \mathbf{r}). \tag{3.100}$$

Performing a small p expansion in Laplace space and truncating yields a form of the continuity equation that is valid for long times

$$\left({}_0^{\text{C}}\mathcal{D}_t^\alpha + \frac{\nu_{\text{loss}}^{(\text{free})}}{r_\alpha \nu_{\text{trap}}}\right) n(t, \mathbf{r}) + \frac{\partial}{\partial \mathbf{r}} \cdot \left[n(t, \mathbf{r}) \frac{\langle \mathbf{v} \rangle (t, \mathbf{r})}{r_\alpha \nu_{\text{trap}}}\right] = \left[\delta(r_\alpha \nu_{\text{trap}} t) - \frac{t^{-\alpha}}{\Gamma(1-\alpha)}\right] n(0, \mathbf{r}), \tag{3.101}$$

written now solely in terms of the time operator of fractional differentiation. Finally, performing a small $\mathbf{k}$ approximation in Fourier space provides the Caputo time-fractional advection-diffusion equation

$$\left({}_0^{\text{C}}\mathcal{D}_t^\alpha + \frac{\nu_{\text{loss}}^{(\text{free})}}{r_\alpha \nu_{\text{trap}}} + \mathbf{W}_\alpha \cdot \frac{\partial}{\partial \mathbf{r}} - \mathbf{D}_\alpha \cdot \frac{\partial^2}{\partial \mathbf{r} \partial \mathbf{r}}\right) n(t, \mathbf{r}) = \left[\delta(r_\alpha \nu_{\text{trap}} t) - \frac{t^{-\alpha}}{\Gamma(1-\alpha)}\right] n(0, \mathbf{r}), \tag{3.102}$$

with fractional transport coefficients defined as

$$\mathbf{W}_\alpha \equiv \frac{\mathbf{W}}{\nu_{\text{trap}} r_\alpha}, \tag{3.103}$$

$$\mathbf{D}_\alpha \equiv \frac{\mathbf{D}}{\nu_{\text{trap}} r_\alpha}, \tag{3.104}$$

in terms of the flux drift velocity (3.61) and diffusion coefficient (3.77), respectively. Note that, as the waiting time distribution $\phi(t)$ has a divergent mean, the flux diffusion coefficient now takes the particular form

$$\mathbf{D} \equiv \frac{1}{\nu_{\text{eff}}} \left(\frac{\mathbf{I}}{\alpha_{\text{eff}}^2} + 2\mathbf{W}\mathbf{W} \right). \tag{3.105}$$

In addition, the quantity R, which affects the transport coefficients through its presence in Eq. (3.62) for the effective frequency ν_{eff}, can no longer be defined by the integral in Eq. (3.64) as this integral now diverges due to the asymptotic power law form (3.95) of the waiting time distribution. In the case of fractional transport, we have instead

$$R \equiv 1 + \frac{\nu_{\text{loss}}^{(\text{free})} - \nu_{\text{loss}}^{(\text{trap})}}{\nu_{\text{trap}}}, \tag{3.106}$$

valid irrespective of the chosen heavy-tailed trapping time distribution.

It should be noted that performing a similar asymptotic approximation of the generalised Boltzmann equation (3.1) does not result in a fractional time operator that acts on the phase-space distribution function $f(t, \mathbf{r}, \mathbf{v})$. That is, it does not seem possible to derive a similar "fractional Boltzmann equation" from our model. This conclusion differs from [32] who used a similar kinetic model to successfully derive a fractional Boltzmann equation. However, their model was inconsistent as it simultaneously described trapping while also maintaining a constant number of free particles.

There also exist generalisations of time-fractional diffusion equations, like Eq. (3.102), where spatial derivatives are also taken to be of non-integer order [91]. Physically, these fractional space derivatives arise when particles undergo long jumps in space [92]. This is analogous to the above situation where a time-fractional diffusion equation arose from particles experiencing traps of long duration. As our model currently only allows for variation in the trapping time, we conclude that to similarly derive a space-fractional diffusion equation would require adjustments to the kinetic theory.

3.6 Mapping between normal and generalised diffusion

As shown in the previous section, the generalised diffusion equation is capable of describing dispersive transport in the same way the Caputo fractional diffusion equation

does. A general feature shared by both of these diffusion equations is the history dependence of their solutions. This is physically due to the existence of trapped states and delayed detrapping. Mathematically, this manifests as a global time operator, be it a fractional derivative or, in the case of the generalised diffusion equation (3.89), a convolution with the effective waiting time distribution $\Phi(t)$.

As described in Chapter 2, the nature of global operators introduces additional complexity when it comes to solving problems numerically. For example, in finite difference schemes with only local time operators the computation time scales linearly with the number of time steps chosen. When a global time operator is present, however, the computation time scales *quadratically* with the number of time steps. Although this increased computational complexity is inherent to these systems, a number of techniques have been suggested to improve upon it for fractional differential equations [1, 63–65]. One approach, explored in Section 2.4, involves first solving a standard diffusion equation and then performing a subordination integral transformation [1, 41] to find the desired solution of the fractional diffusion equation. We will generalise this approach to solve the generalised diffusion equation for the free particle number density $n(t, \mathbf{r})$.

Replacing the time operator in the generalised diffusion equation with an explicit time derivative yields a standard diffusion equation with the same linear spatial operator

$$\left(\frac{\partial}{\partial \tau} + \mathbf{W} \cdot \frac{\partial}{\partial \mathbf{r}} - \mathbf{D} \colon \frac{\partial^2}{\partial \mathbf{r} \partial \mathbf{r}}\right) u(\tau, \mathbf{r}) = 0. \tag{3.107}$$

For the same initial conditions, $u(0, \mathbf{r}) \equiv n(0, \mathbf{r})$, we can relate both solutions directly in Laplace space

$$n(p, \mathbf{r}) = u\left(p + \nu_{\text{loss}}^{(\text{free})} + \nu_{\text{trap}}\left[1 - \Phi(p)\right], \mathbf{r}\right), \tag{3.108}$$

which in the time domain corresponds to the subordination integral transform, denoted by $\mathcal{A}$:

$$\begin{aligned} n(t, \mathbf{r}) &\equiv \mathcal{A} u(t, \mathbf{r}) \\ &\equiv \int_0^t \mathrm{d}\tau A(\tau, t - \tau)\, u(\tau, \mathbf{r}), \end{aligned} \tag{3.109}$$

where the kernel is defined in terms of the inverse Laplace transform $\mathcal{L}^{-1}$

$$A(\tau, t) \equiv \mathrm{e}^{-\left(\nu_{\text{loss}}^{(\text{free})} + \nu_{\text{trap}}\right)\tau} \mathrm{e}^{-\nu_{\text{loss}}^{(\text{trap})} t} \mathcal{L}^{-1}\left\{e^{\nu_{\text{trap}} \phi(p) \tau}\right\}. \tag{3.110}$$

Appendix B contains kernels corresponding to various choices of the waiting time distribution $\phi(t)$.

As a simple example, consider the case of a shifted Dirac delta waiting time distribution

$$\phi(t) = \delta\left(t - \nu_{\text{detrap}}^{-1}\right), \tag{3.111}$$

corresponding to traps of fixed duration ν_{detrap}^{-1}. In this case, the subordination transformation (3.109) simply becomes the summation

$$n\left(t,\mathbf{r}\right)=\sum_{k\geq 0}n^{(k)}\left(t-k\nu_{\text{detrap}}^{-1},\mathbf{r}\right), \tag{3.112}$$

the terms of which can be physically interpreted as those free particles which have been trapped k times in the past

$$n^{(k)}\left(\tau,\mathbf{r}\right)\equiv H\left(\tau\right)\frac{\left(\mathrm{e}^{-\frac{\nu_{\text{loss}}^{(\text{trap})}}{\nu_{\text{detrap}}}\nu_{\text{trap}}\tau}\right)^{k}}{k!}\mathrm{e}^{-\left(\nu_{\text{loss}}^{(\text{free})}+\nu_{\text{trap}}\right)\tau}u\left(\tau,\mathbf{r}\right), \tag{3.113}$$

where $H\left(\tau\right)$ is the Heaviside step function. Figure 3.5 plots this solution on a one-dimensional unbounded domain $z\in\left(-\infty,\infty\right)$ for the impulse initial condition $n\left(0,z\right)\equiv N\left(0\right)\delta\left(z\right)$, and shows its construction in terms of the corresponding Gaussian solution of the standard diffusion equation (3.107)

$$u\left(t,z\right)=\frac{N\left(0\right)}{2\sqrt{\pi Dt}}\exp\left[-\left(\frac{z-Wt}{2\sqrt{Dt}}\right)^{2}\right]. \tag{3.114}$$

Note that, as the subordination transformation acts on time alone, the same mapping operator $\mathcal{A}$ can be used to map between spatial moments of the normal and generalised diffusion equations

$$\left\langle\mathbf{r}\right\rangle^{(\text{GDE})}\left(t\right)=\mathcal{A}\left\langle\mathbf{r}\right\rangle^{(\text{SDE})}\left(t\right), \tag{3.115}$$

$$\left\langle\mathbf{rr}\right\rangle^{(\text{GDE})}\left(t\right)=\mathcal{A}\left\langle\mathbf{rr}\right\rangle^{(\text{SDE})}\left(t\right), \tag{3.116}$$

where the superscript "(GDE)" denotes the generalised diffusion equation (3.89) and "(SDE)" denotes the standard diffusion equation (3.107). Additionally, the commutation relationship

$$\left[\mathcal{A},\frac{\mathrm{d}}{\mathrm{d}t}\right]\equiv\left[\nu_{\text{loss}}^{(\text{free})}+\nu_{\text{trap}}\left(1-\Phi\left(t\right)*\right)\right]\mathcal{A}, \tag{3.117}$$

also allows the centre of mass (CM) transport coefficients for each diffusion equation to be related through the subordination transformation $\mathcal{A}$

$$\mathbf{W}_{\text{CM}}^{(\text{GDE})}\left(t\right)=\mathcal{A}\mathbf{W}_{\text{CM}}^{(\text{SDE})}\left(t\right)-\left[\nu_{\text{loss}}^{(\text{free})}+\nu_{\text{trap}}\left(1-\Phi\left(t\right)*\right)\right]\mathcal{A}\left\langle\mathbf{r}\right\rangle^{(\text{SDE})}\left(t\right), \tag{3.118}$$

$$\begin{aligned}\mathbf{D}_{\text{CM}}^{(\text{GDE})}\left(t\right)&=\mathcal{A}\mathbf{D}_{\text{CM}}^{(\text{SDE})}\left(t\right)\\&-\frac{1}{2}\left[\nu_{\text{loss}}^{(\text{free})}+\nu_{\text{trap}}\left(1-\Phi\left(t\right)*\right)\right]\mathcal{A}\left[\left\langle\mathbf{rr}\right\rangle^{(\text{SDE})}\left(t\right)-\left\langle\mathbf{r}\right\rangle^{(\text{SDE})}\left(t\right)\left\langle\mathbf{r}\right\rangle^{(\text{SDE})}\left(t\right)\right],\end{aligned} \tag{3.119}$$

where the CM transport coefficients are defined in terms of spatial moments according to Eqs. (3.40) and (3.41).

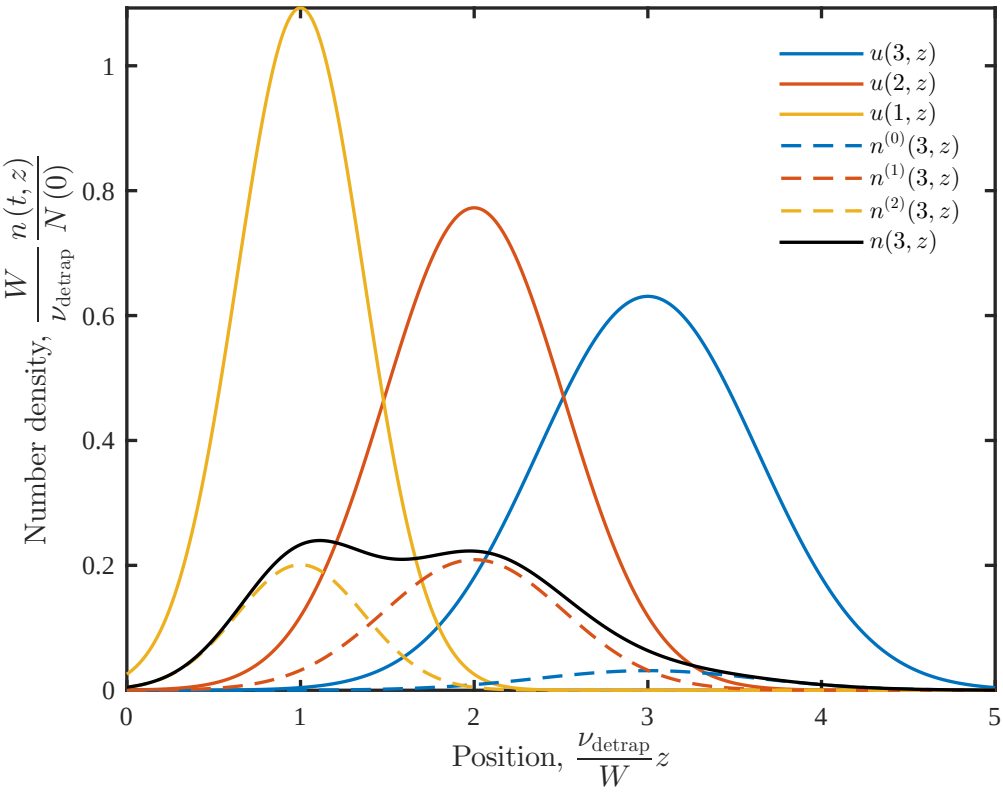

Figure 3.5: The solution $n(t,z)$ of the generalised diffusion equation (3.89) is written by sampling from the Gaussian solution $u(t,z)$ of the standard diffusion equation (3.107) at multiple points in time. This is achieved using the subordination transformation (3.109). Here, traps are of fixed duration, $\nu_{\text{detrap}}t = 1$, as described by the waiting time distribution $\phi(t)/\nu_{\text{detrap}} = \delta(\nu_{\text{detrap}}t - 1)$. In this case, the subordination transformation becomes the summation (3.112) whose individual terms $n^{(k)}(t,z)$ correspond to those free particles which have been trapped k times in the past. Here, there is no recombination, $\nu_{\text{loss}}^{(\text{free})} = \nu_{\text{loss}}^{(\text{trap})} = 0$, the trapping rate is set to $\nu_{\text{trap}}/\nu_{\text{detrap}} = 1$ and the diffusion coefficient is made small so as to emphasise each individual Gaussian's contribution to the solution, $D\nu_{\text{detrap}}/W^2 = 1/15$.

3.7 Time-of-flight current transients

In practice, charged particle transport properties can be quantified using a time-of-flight experiment, where the transit time through a material for a pulse of charge carriers is found by measuring the corresponding current. In this section, we explore the impact that recombination losses of both delocalised and localised particles has on time-of-flight current transients. We consider the analytical current in a time-of-flight experiment for a material of thickness L situated between two plane-parallel electrodes. As this geometry is one-dimensional, the charge carrier number density $n(t,x)$ is defined by the generalised diffusion equation (3.89) in one dimension:

$$\left[\frac{\partial}{\partial t} + \nu_{\text{trap}}\left(1 - \Phi(t)*\right) + \nu_{\text{loss}}^{(\text{free})}\right] n + W\frac{\partial n}{\partial x} - D\frac{\partial^2 n}{\partial x^2} = 0, \tag{3.120}$$

where W is a scalar drift velocity and D is a scalar diffusion coefficient. From the number density, the current in a time-of-flight experiment can be found as the spatially averaged flux [49]:

$$j(t) = e\frac{\partial}{\partial t}\int_0^L \left(\frac{x}{L} - 1\right) n(t,x)\,\mathrm{d}x. \tag{3.121}$$

For an impulse initial condition, $n(0,x) = N(0)\,\delta(x - x_0)$, and perfectly absorbing boundaries, $n(t,0) = n(t,L) = 0$, we can proceed as in [33] to write this current explicitly in Laplace space:

$$j(p) = eN(0)\,\frac{W}{L\tilde{p}}\left\{1 - \mathrm{e}^{-\lambda x_0}\left[\mathrm{e}^{-\beta x_0} + \frac{\sinh(\beta x_0)}{\sinh(\beta L)}\left(\mathrm{e}^{\lambda L} - \mathrm{e}^{-\beta L}\right)\right]\right\}, \tag{3.122}$$

where

$$\tilde{p} \equiv p + \nu_{\mathrm{trap}}\left[1 - \Phi(p)\right] + \nu_{\mathrm{loss}}^{(\mathrm{free})}, \tag{3.123}$$

$$\lambda \equiv \frac{W}{2D}, \tag{3.124}$$

$$\beta \equiv \sqrt{\frac{\tilde{p}}{D} + \lambda^2}. \tag{3.125}$$

Note that the trapped carrier recombination rate is present here in the term $\Phi(p) \equiv \phi\left(p + \nu_{\mathrm{loss}}^{(\mathrm{trap})}\right)$.

3.7.1 Normal transport

We consider the explicit effect that free and trapped particle recombination rates have on the current transient in a time-of-flight experiment in Figure 3.6 by plotting Eq. (3.122) for the current, keeping the effects of mobility (drift velocity) and diffusion constant. A system of units is chosen that uses the material thickness L and the trap-free transit time, defined as $t_{\mathrm{tr}} \equiv L/W$. In this system of units, the drift velocity is equal to unity. We specify the diffusion coefficient to be $Dt_{\mathrm{tr}}/L^2 = 0.02$, the initial impulse is set to occur at $x_0/L = 1/3$ and the trapping rate is made large so as trap-based effects can occur within the transit time, $\nu_{\mathrm{trap}}t_{\mathrm{tr}} = 10^2$. For trapping times, an exponential distribution is considered, $\phi(t) = \nu_{\mathrm{detrap}}\mathrm{e}^{-\nu_{\mathrm{detrap}}t}$, with a mean trapping time of $(\nu_{\mathrm{detrap}}t_{\mathrm{tr}})^{-1} = 0.03$.

In Figure 3.6, the recombination-free current transient is included in black as a reference. This transient has a number of notable regimes. At early times, the current is still close to unity as no processes have had a chance to affect it greatly. What then follows is a decrease in current as free charge carriers enter traps. This decrease is temporary, however, and eventually the current plateaus as a transient equilibrium arises between free and trapped particles. The value of the current at this plateau is numerically equal to the proportion of free particles at the equilibrium, $\nu_{\mathrm{detrap}}/(\nu_{\mathrm{detrap}} + \nu_{\mathrm{trap}}) = 0.25 \approx 10^{-0.6}$. Finally, the last of the free particles extract causing the remaining filled traps to gradually exhaust and the system to leave equilibrium.

Figure 3.6a) considers an increasing free particle recombination rate, $\nu_{\text{loss}}^{(\text{free})}$, without any trapped particle recombination, $\nu_{\text{loss}}^{(\text{trap})} = 0$. It can be seen that the free particle losses start decreasing the current at roughly the characteristic time for free particle recombination, $\left(\nu_{\text{loss}}^{(\text{free})} t_{\text{tr}}\right)^{-1}$. Because free particles are being lost, an equilibrium is not established as in the recombination-free case. However, detrapping events do still cause a slowing in the descent of the current.

Figure 3.6b) considers an increasing trapped particle recombination rate, $\nu_{\text{loss}}^{(\text{trap})}$, without any free particle recombination, $\nu_{\text{loss}}^{(\text{free})} = 0$. Trap-based recombination can only affect the current via detrapping events and so we do not see a decrease in the current until at least the characteristic time for trapping, $(\nu_{\text{trap}} t_{\text{tr}})^{-1} = 10^{-2}$. Similar to Figure 3.6a), an equilibrium cannot be established here due to the constant loss of trapped particles. Unlike Figure 3.6a), however, detrapping events have a diminishing contribution to the current as increasing trap-based recombination also increases the probability that trapped particles recombine instead of detrapping.

In practice, time-of-flight current transients will be measured in experiments. These current traces will be fitted to solutions of the generalised diffusion equation (3.120), which enable the transport coefficients (drift velocity W, diffusion coefficient D), various rates ν and the trapping time distribution $\phi(t)$ to be determined empirically.

3.7.2 Fractional transport

Plotting the current in a time-of-flight experiment versus time takes on a signature form when transport is dispersive. That is, two power-law regimes arise whose exponents sum to -2. Specifically, for a trapping time distribution of the asymptotic form of Eq. (3.95), these exponents are $-(1-\alpha)$ and $-(1+\alpha)$ [12]. This signature has been observed experimentally in a variety of physical systems, including charge-carrier transport in amorphous semiconductors [6, 12] and electron transport in liquid neon [20].

As was done in Figure 3.6 for normal transport, Figure 3.7 explores the effect that varying free and trapped particle recombination rates has on time-of-flight current transients by plotting the current given by Eq. (3.122) for dispersive transport. For this, we have chosen to use the heavy-tailed trapping time distribution (1.31), as derived in [33]:

$$\phi(t) = \alpha \nu_0 (\nu_0 t)^{-\alpha-1} \gamma(\alpha+1, \nu_0 t), \tag{3.126}$$

where $\gamma(a,z) \equiv \int_0^z \mathrm{d}\zeta\, \zeta^{a-1} \mathrm{e}^{-\zeta}$ is the lower incomplete Gamma function and ν_0 is a frequency characterising the rate of escape from traps. In this case, the trap severity has a physical interpretation as the ratio $\alpha \equiv T/T_{\text{c}}$, where T is the temperature and T_{c} is a characteristic temperature that describes the width of the density of states. In Figure 3.7 we use the same system of units as Figure 3.6 and all the same relevant parameters, except for the trapping frequency which we increase to $\nu_{\text{trap}} t_{\text{tr}} = 10^4$. The new parameters that we must specify here are chosen as $\alpha = 1/2$ and $\nu_0 t_{\text{tr}} = 5 \times 10^5$.

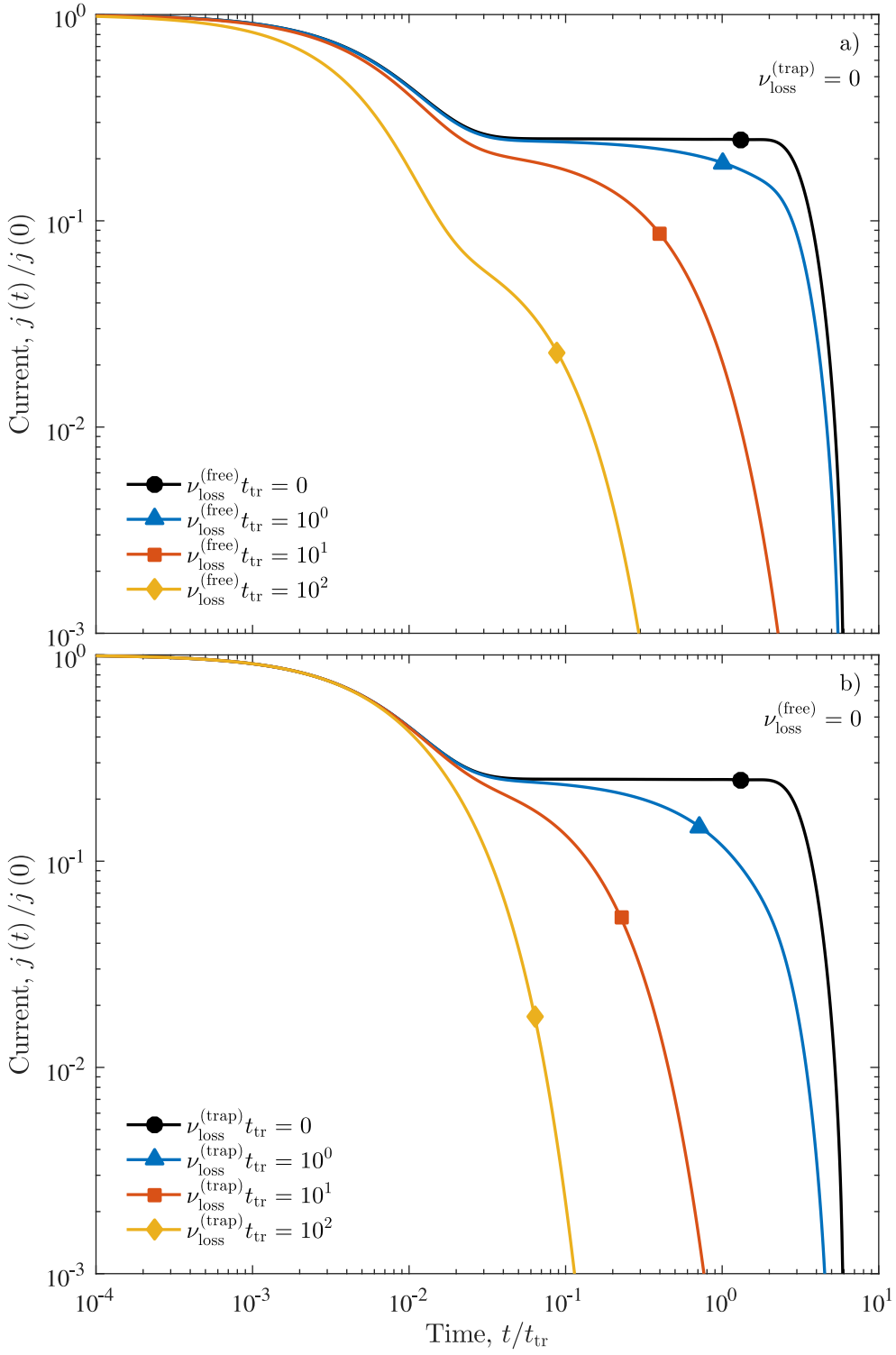

Figure 3.6: The impact of free and trapped particle recombination on current transients for an ideal time-of-flight experiment as modelled by Eq. (3.122). Nondimensionalisation has been performed using the material thickness L, trap-free transit time, $t_{\text{tr}} \equiv L/W$, and the initial current $j(0) = eN(0)/t_{\text{tr}}$. For these plots we define the diffusion coefficient, $Dt_{\text{tr}}/L^2 = 0.02$, the initial impulse location, $x_0/L = 1/3$, and the trapping rate, $\nu_{\text{trap}} t_{\text{tr}} = 10^2$. We choose an exponential distribution of trapping times, $\phi(t) = \nu_{\text{detrap}} \mathrm{e}^{-\nu_{\text{detrap}} t}$, with the mean trapping time chosen as $(\nu_{\text{detrap}} t_{\text{tr}})^{-1} = 0.03$.

In Figure 3.7, the recombination-free current transient is included in black as a reference. The most notable aspect of this curve are the two power-law regimes indicative of dispersive transport. The first power-law regime is analogous to the plateau in Figure 3.6, as we have trapping and detrapping simultaneously and contrarily affecting the current. However, unlike Figure 3.6, detrapping is such a rare event that we never reach a transient equilibrium and the current decreases overall. The second power-law regime is analogous to the rapid drop in current seen in Figure 3.6 after almost all free particles have been extracted. Here we actually have a slower decrease in current as, unlike Figure 3.6, traps are so long-lived that detrapping events continue to contribute to the current, even at very late times.

Figure 3.7a) considers an increasing free particle recombination rate, $\nu_{\text{loss}}^{(\text{free})}$. Notably, as the free particle recombination rate increases, the first power-law regime vanishes. In effect, the large recombination rate of free particles causes an earlier emergence of the second power-law regime that occurs when most free particles have been extracted. Thus, it is also possible to conclude the existence of dispersive transport from a time-of-flight current transient with a single power-law regime at late times.

Figure 3.7b) considers an increasing trapped particle recombination rate, $\nu_{\text{loss}}^{(\text{trap})}$. This subplot illustrates the necessity that there to be no trap-based recombination for transport to be dispersive, as even a small amount of trapped particle losses causes the second power-law regime to vanish. We observe that the first power-law regime does not always vanish completely and so it is important to note that the presence of a single power-law regime at intermediate times does *not* imply dispersive transport.

3.8 Conclusion

We have considered a general phase-space kinetic equation (3.1) which considers transport of charged particles via both delocalised and localised states, including collisional trapping, detrapping and recombination processes. The solution of this model was found analytically in Fourier-Laplace space which in turn provided analytical expressions for phase-space averaged spatial and velocity moments. These moments provided determination of both centre of mass (CM) and flux transport coefficients. As consequence of the processes of trapping and detrapping, the free particle CM transport coefficients were found to be transiently negative for high trapping rates. We have also shown that, in the hydrodynamic regime, a number of diffusion equations accurately describe the generalised Boltzmann equation (3.1). These include the standard diffusion equation (3.83), the generalised diffusion equation (3.89) and, when transport is dispersive, the Caputo fractional diffusion equation (3.102). Finally, we have written the solution of the generalised diffusion equation (3.89) as a subordination transformation (3.109) from the corresponding solution of a standard diffusion equation (3.107).

The model of focus in this work, Eqs. (3.1)–(3.8), was considered only for constant process rates, independent of particle energy. Extension to higher order balance equations (e.g. momentum and energy) including energy dependent rates represents

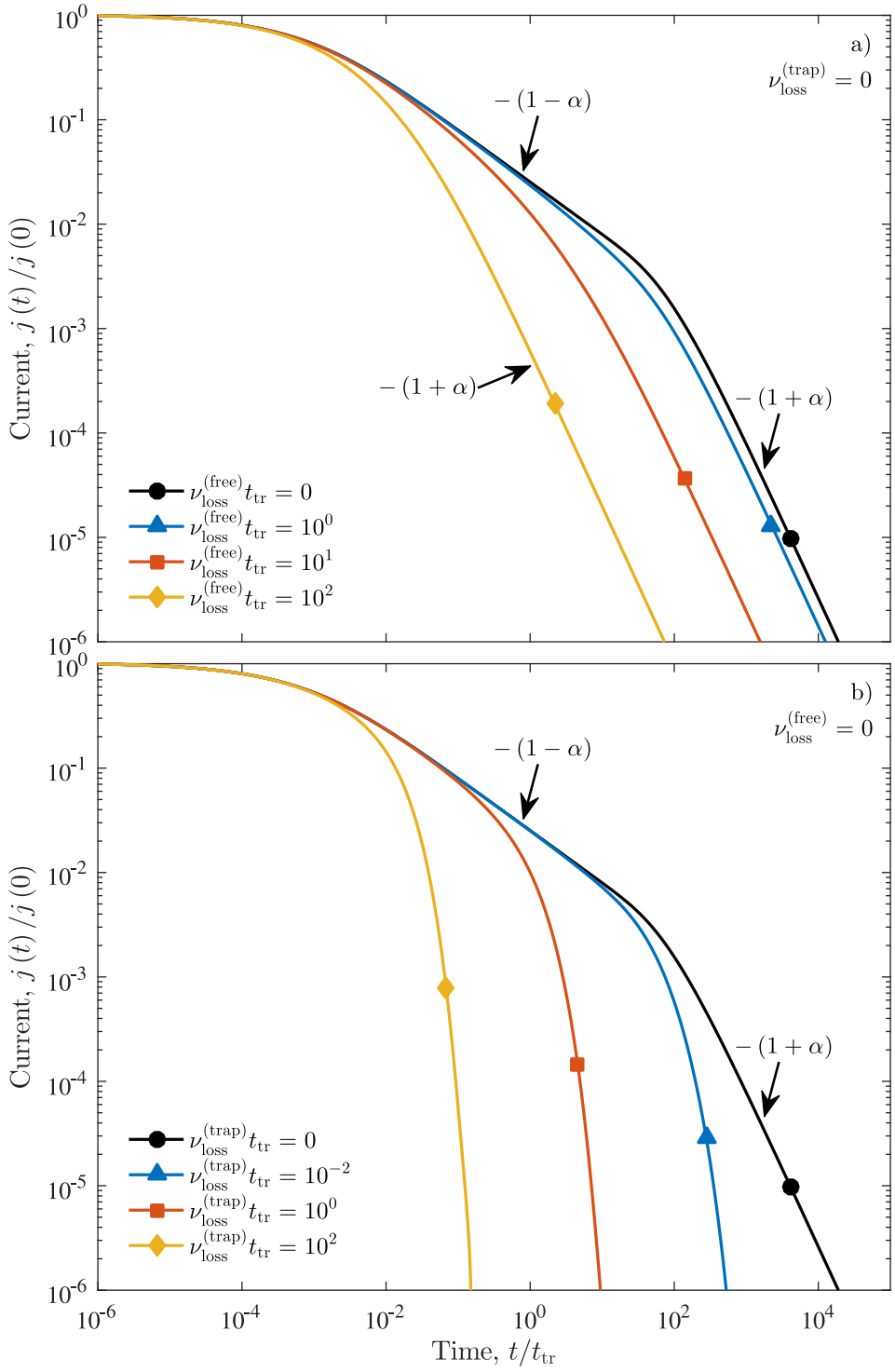

Figure 3.7: The impact of free and trapped particle recombination on current transients for an ideal time-of-flight experiment as modelled by Eq. (3.122) for the case of dispersive transport. Nondimensionalisation has been performed using the material thickness L, trap-free transit time, $t_{\text{tr}} \equiv L/W$, and the initial current $j(0) = eN(0)/t_{\text{tr}}$. For these plots we define the diffusion coefficient, $Dt_{\text{tr}}/L^2 = 0.02$, the initial impulse location, $x_0/L = 1/3$, and the trapping rate, $\nu_{\text{trap}} t_{\text{tr}} = 10^4$. For dispersive transport to occur we have chosen to describe trapping times by the heavy-tailed distribution (1.31) with a trap severity of $\alpha = 1/2$. This corresponds specifically to the distribution $\phi(t) = \frac{1}{2t}\left(\frac{\sqrt{\pi}}{2}\frac{\text{erf}\sqrt{\nu_0 t}}{\sqrt{\nu_0 t}} - \text{e}^{-\nu_0 t}\right)$, where we have chosen $\nu_0 t_{\text{tr}} = 5 \times 10^5$. The exponents of the power-law regimes are indicated with arrows. Such regimes, especially at late times, can be indicative of dispersive transport.

the next step in extending this model and is the focus of Chapter 5. This will facilitate the generalisation of well known empirical relationships (e.g. Generalised Einstein relations, Wannier energy relation, mobility expressions) to include combined localised/delocalised transport systems. Additionally, for our model to be applied to transport in dense fluids, it is necessary to have reasonable inputs ν_{trap} and $\phi(t)$. Although there are many investigations of the trapping, for example light-particle solvation in the literature [93–95], including free-energy changes and solvation time-scales, none of these directly produce an energy-dependent trapping frequency or waiting time distribution. The *ab initio* calculation of such capture collision frequencies and waiting time distributions in liquids and dense gases remains the focus of our current attention.

4

Third-order transport coefficients for localised/delocalised transport

This chapter contains material that has been published in the following journal article:

[4] Peter W. Stokes, Ilija Simonović, Bronson Philippa, Daniel Cocks, Saša Dujko, and Ronald D. White. Third-order transport coefficients for localised and delocalised charged-particle transport. *Scientific Reports*, **8**, 2226 (2018). doi:10.1038/s41598-018-19711-5

4.1 Introduction

Very little data regarding third-order transport coefficients (the skewness tensor) can be found in the literature. This is understandable, since they have not been included in the interpretations of traditional swarm experiments. There is, however, a growing interest regarding these transport coefficients, partially due to estimations that third-order transport coefficients could be measured in the present or near future [96,97]. It is also considered that third-order transport coefficients would be very useful, in combination with transport coefficients of a lower order, for determination of cross section sets, by means of inverse swarm procedure [96,97]. Third-order transport coefficients are also required for the conversion of the hydrodynamic transport coefficients into transport data measured in steady state Townsend and arrival time spectra experiments [98,99]. The skewness tensor can also be employed in fluid models of discharges, by pairing a generalised diffusion equation, which includes the contributions of the third-order transport coefficients, with Poisson's equation. This could be particularly important for discharges where ions play an important role [100], or in situations where the

hydrodynamic approximation is at the limit of applicability, as in the presence of sources and sinks of particles or in the close vicinity of physical boundaries.

In this chapter, we are concerned with the form of the skewness tensor for charged-particle transport in the presence of trapped (localised) states. In particular, we are interested in the scenario where transport is dispersive, with a mean squared displacement that increases sublinearly with time. Third-order transport coefficients are expected to be more sensitive to the influence of non-conservative collisions than those of lower order, suggesting that the presence of such trapped states would significantly influence the skewness tensor. Indeed, skewness and other higher order transport coefficients have been used to characterise fractional transport in a variety of contexts, including transport in biological cells [101–104]. Consider also Figure 4.1, which plots the solution of the Caputo fractional advection-diffusion equation (2.1). Notice that this solution exhibits a large skewness in comparison to the accompanying Gaussian solution of the corresponding classical advection-diffusion equation.

In the following, we describe charged particle transport using a full phase-space kinetic model as defined by a generalised Boltzmann equation with a corresponding trapping and detrapping operator. In the previous chapter, we introduced and studied such a generalised Boltzmann equation (3.1), deriving lower-order transport coefficients (up to diffusion) and corresponding generalisations of the Einstein relation. We will extend these results to determine the skewness tensor. Calculations of the skewness tensor for the Boltzmann equation have been performed previously by a number of authors [39, 97, 105–107]. We will use these earlier studies to confirm the structure of the skewness tensor and to benchmark our results in the trap-free case.

In Section 4.2 of this chapter, we derive the flux transport coefficients up to third order for the for the phase-space model introduced in the previous chapter. Section 4.3 explores the structure of these transport coefficients and their symmetries under parity transformation. The transport coefficients are used to extend Fick's law, which leads to a generalised advection-diffusion-skewness equation, presented in Section 4.4. In this section, we also provide a physical interpretation of trap-induced skewness. By analogy with Einstein's relation, Section 4.5 provides a relation between skewness, diffusion, mobility and temperature. Section 4.6 looks at the case of fractional transport and its effects on the flux transport coefficients. Finally, Section 4.7 lists conclusions along with possible avenues for future work.

4.2 Skewness

In Section 3.4, we confirmed that the flux of free particles described by the generalised Boltzmann equation (3.1) could be written as a density gradient expansion in the weak-gradient hydrodynamic regime. In Eq. (3.76) we wrote such an expansion to first spatial order and introduced the transport coefficients of drift velocity $\mathbf{W}$, given by Eq. (3.61), and diffusion $\mathbf{D}$, given by Eq. (3.77).

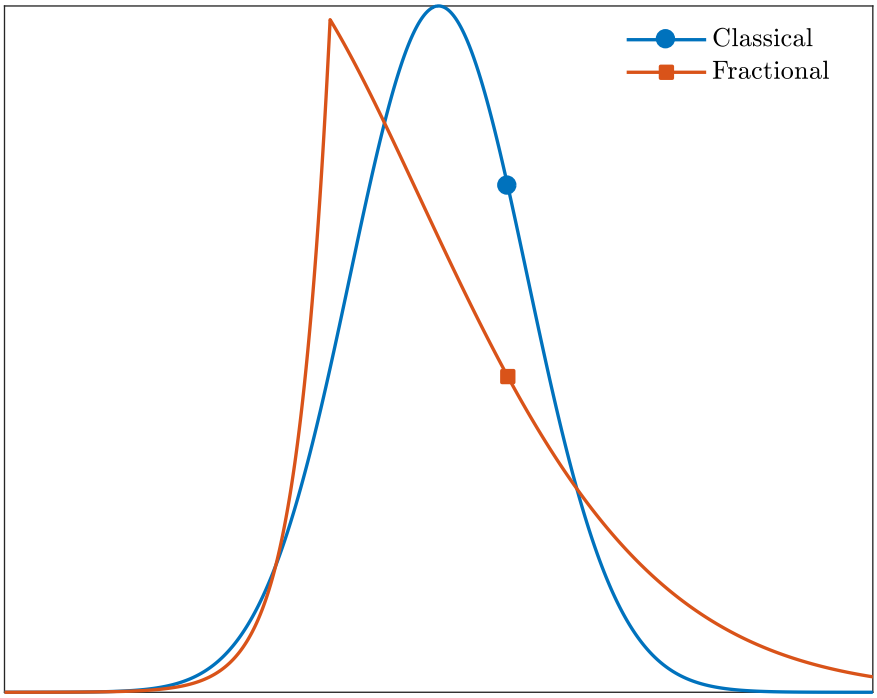

Figure 4.1: Skewed solution of the Caputo fractional advection-diffusion equation alongside the corresponding Gaussian solution of the classical advection-diffusion equation. Both pulses have evolved from an impulse initial condition. The cusp in the fractional solution denotes the location of this initial impulse.

In this section, we consider the transport coefficient beyond diffusion, known as skewness and denoted as the rank-3 tensor $\mathbf{Q}$. Extending the expression for the flux in Eq. (3.76) to also include skewness yields the following generalisation of Fick's law:

$$n\left\langle \mathbf{v}\right\rangle =\mathbf{W}n-\mathbf{D}\cdot\frac{\partial n}{\partial\mathbf{r}}+\mathbf{Q}\colon\frac{\partial^{2}n}{\partial\mathbf{r}\partial\mathbf{r}}-\cdots. \tag{4.1}$$

The above flux transport coefficients can be determined by performing a similar expansion of the phase-space distribution function $f\left(t,\mathbf{r},\mathbf{v}\right)$. Extending the first-order expansion in Eq. (3.75) to second spatial order yields

$$f\left(t,\mathbf{r},\mathbf{v}\right)=f^{(0)}\left(\mathbf{v}\right)n+\mathbf{f}^{(1)}\left(\mathbf{v}\right)\cdot\frac{\partial n}{\partial\mathbf{r}}+\mathbf{f}^{(2)}\left(\mathbf{v}\right):\frac{\partial^{2}n}{\partial\mathbf{r}\partial\mathbf{r}}+\cdots, \tag{4.2}$$

where, in Fourier-transformed velocity space:

$$f^{(0)}\left(\mathbf{s}\right)=\frac{\nu_{\mathrm{coll}}w\left(\alpha_{\mathrm{coll}},s\right)+R\nu_{\mathrm{trap}}w\left(\alpha_{\mathrm{detrap}},s\right)}{\nu_{\mathrm{coll}}+R\nu_{\mathrm{trap}}+\mathbf{a}\cdot\imath\mathbf{s}}, \tag{4.3}$$

$$\mathbf{f}^{(1)}\left(\mathbf{s}\right)=\frac{\nu_{\mathrm{trap}}\mathbf{R}^{(1)}w\left(\alpha_{\mathrm{detrap}},s\right)+f^{(0)}\left(\mathbf{s}\right)\left(\mathbf{W}-\nu_{\mathrm{trap}}\mathbf{R}^{(1)}\right)-\imath\frac{\partial f^{(0)}}{\partial\mathbf{s}}}{\nu_{\mathrm{coll}}+R\nu_{\mathrm{trap}}+\mathbf{a}\cdot\imath\mathbf{s}}, \tag{4.4}$$

$$\mathbf{f}^{(2)}\left(\mathbf{s}\right)=\frac{\nu_{\mathrm{trap}}\mathbf{R}^{(2)}w\left(\alpha_{\mathrm{detrap}},s\right)-f^{(0)}\left(\mathbf{s}\right)\left(\mathbf{D}+\nu_{\mathrm{trap}}\mathbf{R}^{(2)}\right)+\mathbf{f}^{(1)}\left(\mathbf{s}\right)\left(\mathbf{W}-\nu_{\mathrm{trap}}\mathbf{R}^{(1)}\right)-\imath\frac{\partial\mathbf{f}^{(1)}}{\partial\mathbf{s}}}{\nu_{\mathrm{coll}}+R\nu_{\mathrm{trap}}+\mathbf{a}\cdot\imath\mathbf{s}}. \tag{4.5}$$

Using the above expansion to evaluate the flux term-wise, results in the following expressions for the transport coefficients

$$\mathbf{W} \equiv \int \mathrm{d}\mathbf{v}\, \mathbf{v} f^{(0)}(\mathbf{v}), \tag{4.6}$$

$$\mathbf{D} \equiv \int \mathrm{d}\mathbf{v}\, \mathbf{v}\mathbf{f}^{(1)}(\mathbf{v}), \tag{4.7}$$

$$\mathbf{Q} \equiv \int \mathrm{d}\mathbf{v}\, \mathbf{v}\mathbf{f}^{(2)}(\mathbf{v}), \tag{4.8}$$

which when evaluated yields

$$\mathbf{W} \equiv \frac{\mathbf{a}}{\nu_{\mathrm{eff}}}, \tag{4.9}$$

$$\mathbf{D} \equiv \frac{1}{\nu_{\mathrm{eff}}}\left(\frac{k_{\mathrm{B}}T_{\mathrm{eff}}}{m}\mathbf{I} + \frac{1+2\nu_{\mathrm{trap}}R\langle t\rangle}{1+\nu_{\mathrm{trap}}R\langle t\rangle}\mathbf{W}\mathbf{W}\right), \tag{4.10}$$

$$\begin{aligned}\mathbf{Q} \equiv &\left[1+\left(\frac{1+2\nu_{\mathrm{trap}}R\langle t\rangle}{1+\nu_{\mathrm{trap}}R\langle t\rangle}\right)^2 - \frac{\nu_{\mathrm{trap}}R\langle t^2\rangle}{4\left(1+\nu_{\mathrm{trap}}R\langle t\rangle\right)^3}\nu_{\mathrm{eff}}\right]\frac{2\mathbf{W}\mathbf{W}\mathbf{W}}{\nu_{\mathrm{eff}}^2} \\ &+ \frac{1+2\nu_{\mathrm{trap}}R\langle t\rangle}{1+\nu_{\mathrm{trap}}R\langle t\rangle}\frac{k_{\mathrm{B}}T_{\mathrm{eff}}}{m\nu_{\mathrm{eff}}^2}\left(\mathbf{I}\mathbf{W}+\mathbf{e}_1\mathbf{W}\mathbf{e}_1+\mathbf{e}_2\mathbf{W}\mathbf{e}_2+\mathbf{e}_3\mathbf{W}\mathbf{e}_3\right) \\ &+ \frac{\nu_{\mathrm{trap}}R\langle t\rangle}{1+\nu_{\mathrm{trap}}R\langle t\rangle}\frac{\nu_{\mathrm{coll}}}{\nu_{\mathrm{eff}}}\frac{k_{\mathrm{B}}\left(T_{\mathrm{coll}}-T_{\mathrm{detrap}}\right)}{m\nu_{\mathrm{eff}}}\frac{\mathbf{W}\mathbf{I}}{\nu_{\mathrm{eff}}},\end{aligned} \tag{4.11}$$

where $\mathbf{e}_1$, $\mathbf{e}_2$ and $\mathbf{e}_3$ are standard orthonormal basis vectors. As is expected, the transport coefficients for drift velocity $\mathbf{W}$ and diffusion $\mathbf{D}$, found previously in Eqs. (3.61) and (3.77), are also recovered in addition to the skewness $\mathbf{Q}$.

We confirm that when there are no traps present, $\nu_{\mathrm{trap}} = 0$, the transport coefficients agree with those of the BGK collision model, previously found by Robson [39]:

$$\mathbf{W} \equiv \frac{\mathbf{a}}{\nu_{\mathrm{coll}}}, \tag{4.12}$$

$$\mathbf{D} \equiv \frac{1}{\nu_{\mathrm{coll}}}\left(\frac{k_{\mathrm{B}}T_{\mathrm{coll}}}{m}\mathbf{I} + \mathbf{W}\mathbf{W}\right), \tag{4.13}$$

$$\mathbf{Q} \equiv \frac{1}{\nu_{\mathrm{coll}}^2}\left[\frac{k_{\mathrm{B}}T_{\mathrm{coll}}}{m}\left(\mathbf{I}\mathbf{W}+\mathbf{e}_1\mathbf{W}\mathbf{e}_1+\mathbf{e}_2\mathbf{W}\mathbf{e}_2+\mathbf{e}_3\mathbf{W}\mathbf{e}_3\right)+4\mathbf{W}\mathbf{W}\mathbf{W}\right]. \tag{4.14}$$

4.3 Structure and symmetry of transport coefficients

In this section, we consider an applied electric field $\mathbf{E}$, corresponding to the acceleration

$$\mathbf{a} \equiv \frac{e\mathbf{E}}{m}. \tag{4.15}$$

If we align the basis vector $\mathbf{e}_3$ parallel to the applied electric field $\mathbf{E}$, the transport coefficients (4.9)–(4.11) take on the known tensor structure [37, 97, 105, 107, 108]:

$$\mathbf{W} \equiv \begin{bmatrix} 0 \\ 0 \\ W \end{bmatrix}, \tag{4.16}$$

$$\mathbf{D} \equiv \begin{bmatrix} D_\perp & 0 & 0 \\ 0 & D_\perp & 0 \\ 0 & 0 & D_\parallel \end{bmatrix} \tag{4.17}$$

$$\mathbf{Q}_{xab} \equiv \begin{bmatrix} 0 & 0 & Q_1 \\ 0 & 0 & 0 \\ Q_1 & 0 & 0 \end{bmatrix}, \tag{4.18}$$

$$\mathbf{Q}_{yab} \equiv \begin{bmatrix} 0 & 0 & 0 \\ 0 & 0 & Q_1 \\ 0 & Q_1 & 0 \end{bmatrix}, \tag{4.19}$$

$$\mathbf{Q}_{zab} \equiv \begin{bmatrix} Q_2 & 0 & 0 \\ 0 & Q_2 & 0 \\ 0 & 0 & 2Q_1 + Q_2 + Q_3 \end{bmatrix}, \tag{4.20}$$

where $a, b \in \{x, y, z\}$. Here, the drift velocity is defined by the speed

$$W \equiv \frac{eE}{m\nu_{\text{eff}}}, \tag{4.21}$$

the diffusion coefficient is defined by two components perpendicular and parallel to the field

$$D_\perp \equiv \frac{k_{\text{B}} T_{\text{eff}}}{m\nu_{\text{eff}}}, \tag{4.22}$$

$$D_\parallel \equiv D_\perp + \frac{1 + 2\nu_{\text{trap}} R \langle t \rangle}{1 + \nu_{\text{trap}} R \langle t \rangle} \frac{W^2}{\nu_{\text{eff}}}, \tag{4.23}$$

and the skewness is defined by the three independent components

$$Q_1 \equiv \frac{1 + 2\nu_{\text{trap}} R \langle t \rangle}{1 + \nu_{\text{trap}} R \langle t \rangle} \frac{k_{\text{B}} T_{\text{eff}}}{m\nu_{\text{eff}}} \frac{W}{\nu_{\text{eff}}}, \tag{4.24}$$

$$Q_2 \equiv \frac{\nu_{\text{trap}} R \langle t \rangle}{1 + \nu_{\text{trap}} R \langle t \rangle} \frac{\nu_{\text{coll}}}{\nu_{\text{eff}}} \frac{k_{\text{B}} \left(T_{\text{coll}} - T_{\text{detrap}} \right)}{m\nu_{\text{eff}}} \frac{W}{\nu_{\text{eff}}}, \tag{4.25}$$

$$Q_3 \equiv \left[1 + \left(\frac{1 + 2\nu_{\text{trap}} R \langle t \rangle}{1 + \nu_{\text{trap}} R \langle t \rangle} \right)^2 - \frac{\nu_{\text{trap}} R \langle t^2 \rangle}{4 \left(1 + \nu_{\text{trap}} R \langle t \rangle \right)^3} \nu_{\text{eff}} \right] \frac{2W^3}{\nu_{\text{eff}}^2}. \tag{4.26}$$

Although this is the case in general, there are situations where the skewness can be defined using fewer than three components. Indeed, this is the case for the BGK model as studied by Robson [39] where the skewness given by Eq. (4.14) is defined using only the components Q_1 and Q_3, with $Q_2 = 0$. The component Q_2 vanishes in this case due to the simple Maxwellian source term used to describe scattered particles. For Q_2

to arise, it is necessary that this source term has some spatial dependence, as occurs for our model through the concentration of particles leaving traps, $\Phi(t) * n(t, \mathbf{r})$, and its density gradient expansion (3.86).

Lastly, we also confirm that the symmetry of transport coefficients with respect to the parity transformation $\mathbf{E} \to -\mathbf{E}$ depends on the parity of the order of each transport coefficient [105, 109]:

$$\mathbf{W} \to -\mathbf{W}, \tag{4.27}$$

$$\mathbf{D} \to \mathbf{D}, \tag{4.28}$$

$$\mathbf{Q} \to -\mathbf{Q}. \tag{4.29}$$

4.4 Generalised advection-diffusion-skewness equation

Using the density gradient expansion (4.1) for the flux $\mathbf{\Gamma}(t, \mathbf{r})$ up to second spatial order in conjunction with the continuity equation 3.34 results in the generalised advection-diffusion-skewness equation

$$\left[\frac{\partial}{\partial t} + \nu_{\text{trap}}\left(1 - \Phi(t) *\right) + \nu_{\text{loss}}^{(\text{free})}\right] n(t, \mathbf{r}) + \mathbf{W} \cdot \frac{\partial n}{\partial \mathbf{r}} - \mathbf{D} : \frac{\partial^2 n}{\partial \mathbf{r} \partial \mathbf{r}} + \mathbf{Q} \vdots \frac{\partial^3 n}{\partial \mathbf{r} \partial \mathbf{r} \partial \mathbf{r}} = 0, \tag{4.30}$$

valid in the weak-gradient hydrodynamic regime. In Cartesian coordinates (x, y, z) with the electric field $\mathbf{E}$ aligned in the z-direction, the transport coefficients take the form of Eqs. (4.16)–(4.20) and the advection-diffusion-skewness equation becomes

$$\left[\frac{\partial}{\partial t} + \nu_{\text{trap}}\left(1 - \Phi(t) *\right) + \nu_{\text{loss}}^{(\text{free})}\right] n(t, x, y, z) + W \frac{\partial n}{\partial z} - D_{\perp}\left(\frac{\partial^2 n}{\partial x^2} + \frac{\partial^2 n}{\partial y^2}\right) - D_{\parallel} \frac{\partial^2 n}{\partial z^2} + 3 Q_{\perp}\left(\frac{\partial^2}{\partial x^2} + \frac{\partial^2}{\partial y^2}\right) \frac{\partial n}{\partial z} + Q_{\parallel} \frac{\partial^3 n}{\partial z^3} = 0, \tag{4.31}$$

where the skewness manifests as components perpendicular and parallel to the applied field [97, 100, 107]:

$$Q_{\perp} \equiv \frac{Q_{zxx} + Q_{xzx} + Q_{xxz}}{3}, \tag{4.32}$$

$$Q_{\parallel} \equiv Q_{zzz}, \tag{4.33}$$

which in terms of the independent components (4.24)–(4.26) are

$$Q_{\perp} = \frac{2Q_1 + Q_2}{3}, \tag{4.34}$$

$$Q_{\parallel} = 2Q_1 + Q_2 + Q_3. \tag{4.35}$$

Written in full, the perpendicular and parallel skewnesses are

$$Q_\perp = \frac{2D_\perp W}{3\nu_{\text{eff}}} + \frac{\nu_{\text{trap}} R\langle t\rangle}{1+\nu_{\text{trap}} R\langle t\rangle}\left(D_\perp - \frac{k_{\text{B}}T_{\text{detrap}}}{3m\nu_{\text{eff}}}\right)\frac{W}{\nu_{\text{eff}}}, \tag{4.36}$$

$$Q_\parallel = 3Q_\perp + \frac{4W^3}{\nu_{\text{eff}}^2} + \frac{\nu_{\text{trap}} R\langle t\rangle}{1+\nu_{\text{trap}} R\langle t\rangle}\left[6 - \frac{2}{1+\nu_{\text{trap}} R\langle t\rangle} - \frac{\nu_{\text{eff}}\langle t^2\rangle}{2\langle t\rangle\left(1+\nu_{\text{trap}} R\langle t\rangle\right)^2}\right]\frac{W^3}{\nu_{\text{eff}}^2}, \tag{4.37}$$

where terms present due to trapping have been grouped separately and the lower-order transport coefficients (4.21)–(4.23) have been used to simplify. An alternative form of the skewness tensor that makes use of these components explicitly is

$$\tilde{\mathbf{Q}}_{xab} \equiv \begin{bmatrix} 0 & 0 & 0 \\ 0 & 0 & 0 \\ 0 & 0 & 0 \end{bmatrix}, \tag{4.38}$$

$$\tilde{\mathbf{Q}}_{yab} \equiv \begin{bmatrix} 0 & 0 & 0 \\ 0 & 0 & 0 \\ 0 & 0 & 0 \end{bmatrix}, \tag{4.39}$$

$$\tilde{\mathbf{Q}}_{zab} \equiv \begin{bmatrix} 3Q_\perp & 0 & 0 \\ 0 & 3Q_\perp & 0 \\ 0 & 0 & Q_\parallel \end{bmatrix}, \tag{4.40}$$

where $a, b \in \{x, y, z\}$. This form was used by Robson [39] when expressing the BGK model skewness (4.14) and is valid only when the skewness is triple-contracted with a symmetric tensor, as occurs in the advection-diffusion-skewness equation (4.30).

To provide some physical intuition regarding the perpendicular and parallel skewness coefficients, $Q_\perp$ and $Q_\parallel$, we solve the advection-diffusion-skewness equation (4.31) for an impulse initial condition and perform contour plots of the resulting pulse in Figure 4.2. Figure 4.2 a) considers the case of no skewness, $Q_\perp = Q_\parallel = 0$, and displays the expected Gaussian solution with elliptical contours due to anisotropic diffusion. Figure 4.2 b) and c) consider positive perpendicular and parallel skewnesses, respectively. In both cases, it can be seen that skewness introduces asymmetry in the pulse in the direction of the field. In general, positive skewness can be seen to reduce the spread of particles behind the pulse, while enhancing the spread toward the front of the pulse. In Figure 4.2 b) for positive perpendicular skewness, this change in particle spread primarily occurs transverse to the field, resulting in a vaguely triangular pulse profile. In Figure 4.2 c) for positive parallel skewness, this change in particle spread occurs longitudinally which, in the language of statistics, results in a distribution with positive skew.

In the previous chapter, we interpreted the trap-induced anisotropic diffusion present in Eq. (4.23) as a consequence of the physical separation between trapped

particles and free particles moving with the field. In a similar fashion, we can interpret the trap-induced skewness present in the perpendicular and parallel skewness coefficients (4.36) and (4.37). To achieve this, we plot the skewness against the detrapping temperature T_{detrap} for various mean trapping times in Figure 4.3. The resulting plots are linear with gradients that characterise of the type of skewness caused by traps. That is, positive or negative gradients correspond respectively to positive or negative trap-based skewness.

When the mean trapping time is zero, the gradients in Figure 4.3 are positive and traps cause positive skewness. This is to be expected as, in this case, trapping and detrapping simply act as an elastic scattering process with a positive skewness akin to Eq. (4.14) for the BGK collision model. As the mean trapping time increases, the nature of the skewness caused by traps changes, ultimately becoming negative for the parameters considered in Figure 4.3. As illustrated in Figure 4.2, negative skewness corresponds to an increased spread of particles behind the pulse. We interpret the increased spread here as being due to particles returning from traps. This interpretation implies that the skewness coefficients could become overall negative if particles remain trapped for a sufficient length of time before returning with a sufficiently large temperature. Indeed, these are the conditions for which the skewness coefficients become negative in Figure 4.3.

This phenomenon of negative skewness has been observed previously by Petrović *et al.* [100] in the calculation of the perpendicular skewness of electrons in methane. Only collisions were considered in this study and so trapping is evidently not a necessary condition for negative skewness to occur. However, it should be emphasised that the skewness is strictly positive when collisions are described by the simple BGK collision operator, as is seen in Eq. (4.14).

4.5 Relating skewness, mobility and temperature

The classical Einstein relation between diffusion, mobility and temperature is [110]

$$\frac{\mathbf{D}}{K} = \frac{k_{\text{B}}\mathbf{T}}{e}, \tag{4.41}$$

where K is the mobility defined as satisfying $\mathbf{W} \equiv K\mathbf{E}$ and $\mathbf{T}$ is the rank-2 temperature tensor. As seen by Eq. (4.10) for the diffusion coefficient, the phase-space model described by Eq. 3.1 has an enhanced diffusivity in the direction of the field due to trapping and detrapping. This enhancement manifests as the following generalised Einstein relation [3]

$$\frac{\mathbf{D}}{K} = \frac{k_{\text{B}}\mathbf{T}}{e} + \frac{\nu_{\text{trap}} R \langle t \rangle}{1 + \nu_{\text{trap}} R \langle t \rangle} \frac{m\mathbf{W}\mathbf{W}}{e}. \tag{4.42}$$

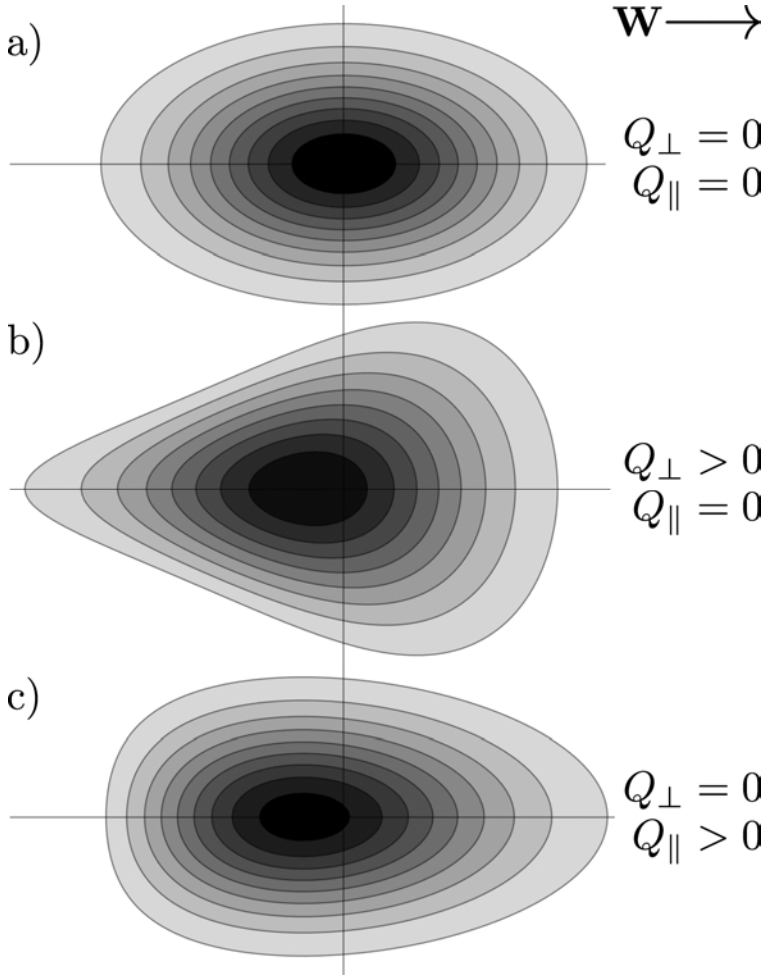

Figure 4.2: Contours of constant number density as defined by the advection-diffusion-skewness equation (4.31) with drift velocity $\mathbf{W}$ and anisotropic diffusion $D_\parallel > D_\perp > 0$ for no skewness, a), positive perpendicular skewness, b), and positive parallel skewness, c). Each profile has evolved from an impulse initial condition. As the skewness tensor is odd under parity transformation, Eq. (4.29), the case of negative skewness can be considered by reflecting the above profiles horizontally across the vertical axis.

By relating the skewness to the temperature tensor though this diffusion coefficient, we find a skewness analogue to the Einstein relation:

$$\begin{aligned}\mathbf{Q} \equiv & \left[1 - \frac{\nu_{\text{trap}} R \left\langle t^2 \right\rangle}{4 \left(1 + \nu_{\text{trap}} R \left\langle t \right\rangle\right)^3} \nu_{\text{eff}}\right] \frac{2\mathbf{WWW}}{\nu_{\text{eff}}^2} \\ & + \frac{1 + 2\nu_{\text{trap}} R \left\langle t \right\rangle}{1 + \nu_{\text{trap}} R \left\langle t \right\rangle} \frac{\mathbf{DW} + D_\perp \mathbf{e}_1 \mathbf{We}_1 + D_\perp \mathbf{e}_2 \mathbf{We}_2 + D_\parallel \mathbf{e}_3 \mathbf{We}_3}{\nu_{\text{eff}}} \\ & + \frac{\nu_{\text{trap}} R \left\langle t \right\rangle}{1 + \nu_{\text{trap}} R \left\langle t \right\rangle} \frac{\nu_{\text{coll}}}{\nu_{\text{eff}}} \frac{k_{\text{B}} \left(T_{\text{coll}} - T_{\text{detrap}}\right)}{m \nu_{\text{eff}}} \frac{\mathbf{WI}}{\nu_{\text{eff}}}.\end{aligned} \tag{4.43}$$

Koutselos [111] has presented a similar relationship between the skewness tensor and lower-order transport coefficients for the case of the classical Boltzmann equation.

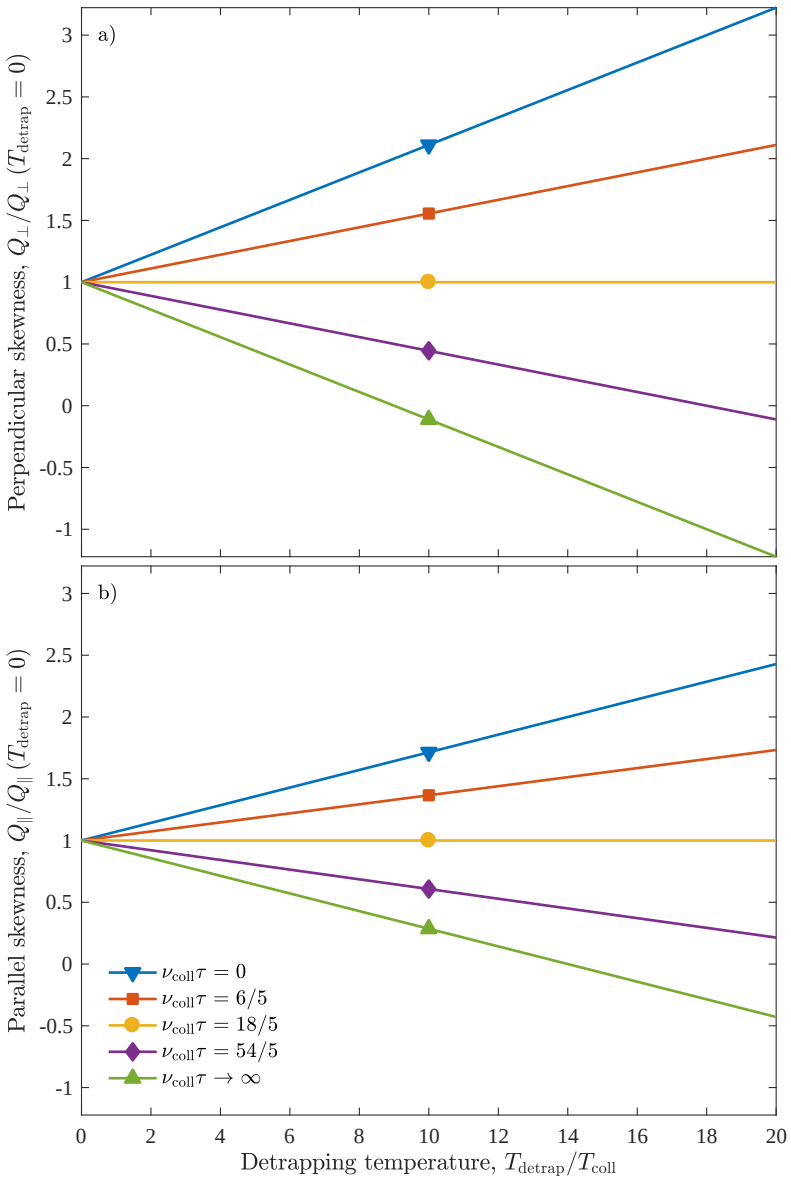

Figure 4.3: Linear plots of perpendicular and parallel skewness coefficients, $Q_\perp$ and $Q_\parallel$, versus the detrapping temperature $T_{\rm detrap}$. Here, traps are described by an exponential distribution of trapping times $\phi(t) = \frac{1}{\tau}\exp\left(-\frac{t}{\tau}\right)$, and no recombination is considered, $\nu_{\rm loss}^{\rm (free)} = \nu_{\rm loss}^{\rm (trap)} = 0$. To perform these plots, we choose a trapping frequency of $\nu_{\rm trap}/\nu_{\rm coll} = 1/9$, while b) also requires that we specify a drift velocity $\mathbf{W}$, which we choose such that $mW^2/k_{\rm B}T_{\rm coll} = 1/4$. The gradients in b) are of smaller magnitude than a) due to the greater dependence of the parallel skewness (4.37) on the drift speed W as compared to the perpendicular skewness (4.36). Thus, as the drift speed decreases, the plots in b) coincide with those in a). When detrapping is instantaneous, $\tau = 0$, the skewness gradients are positive, implying that the skewness caused by traps is also positive. As the mean trapping time τ increases, the skewness gradients decrease, becoming negative and implying a corresponding negative skewness due to traps. The limiting case of an infinite mean trapping time, $\tau \to \infty$, corresponds to fractional transport, which is the subject of Section 4.6. We observe from this figure that the skewness coefficients become overall negative when particles leave traps with a sufficiently large temperature $T_{\rm detrap}$ after a sufficiently long amount of time τ. This observation coincides with the illustration of skewness in Figure 4.2 where negative skewness is characterised by an increased particle spread behind the pulse, which we attribute here to particles returning from traps.

4.6 The case of fractional transport

For the phase-space kinetic model described by Eq. 3.1, fractional transport can occur when the distribution of trapping times has a heavy power-law tail of the form [2]

$$\phi(t) \sim t^{-(1+\alpha)}. \tag{4.44}$$

Note that, as transport here is dispersive in nature, the mean trapping time diverges:

$$\int_0^\infty \mathrm{d}t \phi(t)\, t \to \infty. \tag{4.45}$$

Consequently, the time averages defined by Eq. (5.87) also diverge, correspondingly affecting the transport coefficients. Thus, for fractional transport, the transport coefficients (4.9)–(4.11) take on the simpler form [2]

$$\mathbf{W} = \frac{e\mathbf{E}}{m\nu_{\mathrm{eff}}}, \tag{4.46}$$

$$\mathbf{D} = \frac{1}{\nu_{\mathrm{eff}}}\left(\frac{k_{\mathrm{B}}T_{\mathrm{eff}}}{m}\mathbf{I} + 2\mathbf{W}\mathbf{W}\right), \tag{4.47}$$

$$\begin{aligned}\mathbf{Q} = {} & \frac{2\mathbf{W}\mathbf{W}\mathbf{W}}{\nu_{\mathrm{eff}}^2} \\ & + \frac{2\left(\mathbf{D}\mathbf{W} + D_\perp \mathbf{e}_1\mathbf{W}\mathbf{e}_1 + D_\perp \mathbf{e}_2\mathbf{W}\mathbf{e}_2 + D_\parallel \mathbf{e}_3\mathbf{W}\mathbf{e}_3\right)}{\nu_{\mathrm{eff}}} \\ & + \frac{\nu_{\mathrm{coll}}}{\nu_{\mathrm{eff}}}\frac{k_{\mathrm{B}}\left(T_{\mathrm{coll}} - T_{\mathrm{detrap}}\right)}{m\nu_{\mathrm{eff}}}\frac{\mathbf{W}\mathbf{I}}{\nu_{\mathrm{eff}}},\end{aligned} \tag{4.48}$$

where the effective frequency is now defined

$$\nu_{\mathrm{eff}} \equiv \nu_{\mathrm{coll}} + \nu_{\mathrm{trap}} + \nu_{\mathrm{loss}}^{(\mathrm{free})}. \tag{4.49}$$

Note that transport coefficients are now independent of the specific choice of the trapping time distribution $\phi(t)$, so long as the condition (4.44) for fractional transport is satisfied.

Knowledge of the skewness coefficient (4.48), as well as other higher-order transport coefficients, is useful for characterising fractional transport. For example, Norregaard *et al.* [101] use higher-order moments to analyse the motion of biological particles.

4.7 Conclusion

We have explored the transport coefficients of a phase-space kinetic model 3.1 for both localised and delocalised transport. In particular, we have considered up to the third-order transport coefficient of skewness $\mathbf{Q}$, which takes the form of a rank-3 tensor. The structure of the skewness tensor and its symmetry under parity transformation was found to be in agreement with previous studies. These transport coefficients provide

an extension to Fick's law, Eq. (4.1), which we used to form a generalised advection-diffusion-skewness equation (4.30) with a non-local time operator. We observed trap-induced negative skewness and provided a corresponding physical interpretation. In addition, by analogy with Einstein's relation, the skewness was related to the mobility and temperature through Eq. (4.43). Lastly, the form of the transport coefficients for the particular case of fractional transport were outlined in Eqs. (4.46)–(4.48).

There exist a number of possibilities for future work. The focus of this chapter was on constant transport coefficients that define the flux in the hydrodynamic regime as the density gradient expansion (4.1). Transient transport coefficients and transport coefficients of the bulk were not considered. Section 3.3 outlines an analytical solution of the kinetic model 3.1 that could be used to compute such transport coefficients through time-varying velocity and spatial moments of the phase-space distribution function $f(t, \mathbf{r}, \mathbf{v})$.

Another extension to this work could be to explore what consequences energy-dependent collision, trapping and recombination frequencies have on the skewness. Such a generalisation for Eq. 3.1 is the focus of Chapter 5, although the nature of skewness is not explored there. This would allow for the derivation of a skewness analogue of Einstein's relation that would also take into account the field dependence of mobility [3]. This may also shed light on the recent results of Petrović *et al.* [100], that suggest a correlation between the energy-dependent phenomenon of negative differential conductivity and skewness.

Lastly, it is important to note that the extension to Fick's law described in this chapter is only useful when an electric field is present. Without an applied field, the drift velocity, skewness and all other odd-ordered transport coefficients would vanish. If we wish to extend Fick's law in such a situation, we must also consider the kurtosis coefficient, the next even-ordered transport coefficient beyond diffusion. The kurtosis can be found in a straightforward fashion from the rank-3 tensorial coefficient $\mathbf{f}^{(3)}(\mathbf{v})$ in the density gradient expansion (4.2) of the phase-space distribution function $f(t, \mathbf{r}, \mathbf{v})$, in the same way drift velocity, diffusion and skewness were found using Eqs. (4.6)–(4.8).

5

Energy-dependent localised and delocalised transport phenomena

This chapter contains material that has been published in the following journal article:

[3] Peter W. Stokes, Bronson Philippa, Daniel Cocks, and Ronald D. White. Generalized balance equations for charged particle transport via localized and delocalized states: Mobility, generalized Einstein relations, and fractional transport. *Physical Review E*, **95**, 042119 (2017). doi:10.1103/PhysRevE.95.042119

5.1 Introduction

In Chapters 3 and 4, we explored a generalised phase-space kinetic model for charged particle transport that considered separate collisional, trapping/detrapping and recombination loss processes. This model takes the form of a generalised Boltzmann equation (3.1) with corresponding operators for each aforementioned process. Rather than performing a direct solution of this Boltzmann equation, as is considered in Section 3.3, in this chapter we embrace a more physical insight and explore the relationships between the measured macroscopic transport properties and the underlying microscopic processes (as determined by the appropriate collision frequencies). This is a philosophy that has been adopted in swarm physics, and now is routinely applied in a variety of fields including low-temperature plasma physics [32, 112–115], positron physics [116–118], liquid particle detectors [119, 120] and radiation damage [121–123].

For gaseous systems, or those where transport occurs through delocalised states, there exists a wealth of literature that explores relationships between experimentally measurable transport properties, and links the underlying microscopic physics to the

macroscopic through simple analytic expressions. In fact, transport properties were initially used as the means to indirectly measure scattering cross-sections and their energy dependence. In this chapter, we aim to generalise many existing results for such systems and explore the impact of localised (trapped) states and loss/recombinations on (i) the mobility, (ii) the Wannier energy relation [124], which relates the mean energy of the charged particles to the mobility, and (iii) the Einstein relations [125, 126] which relate the mobility to the diffusivity and enable the quantification of the anisotropic nature of diffusion. Using these we postulate the existence of a number of new phenomena, including trap-induced particle heating/cooling and trap-induced negative differential conductivity (NDC), the origin of which differs significantly from that in which transport is delocalised. Criteria on the various collision, trapping and loss frequencies are presented for the occurrence of such phenomena.

In Section 5.2 of this chapter we present a generalised Boltzmann equation with energy-dependent process rates for collisions, trapping and recombination. In Section 5.3, balance equations are formed for particle continuity, momentum and energy, via the appropriate moments of the generalised Boltzmann equation, which are also used to develop expressions for mobility, mean energy and diffusivity. Phenomena such as heating/cooling, NDC, and generalised Einstein relations (GER) are explored in Sections 5.4–5.5. In Section 3.5, the fractional transport equivalents of the above are considered including fractional GER, while in Section 5.6, we present conclusions and outline some possible avenues for future work.

5.2 Extended phase-space model

In this section, we consider a generalisation of the kinetic model defined by Eq. (3.1) of Chapter 4 that describes the processes of collisions, trapping and recombination, as depicted by Figure 3.1. Specifically, we consider processes that are selective of particle energy $\epsilon \equiv \frac{1}{2}mv^2$. This results in a free particle phase-space distribution function $f(t, \mathbf{r}, \mathbf{v})$, defined by the generalised Boltzmann equation

$$\begin{aligned}\left(\frac{\partial}{\partial t} + \mathbf{v}\cdot\frac{\partial}{\partial \mathbf{r}} + \frac{e\mathbf{E}}{m}\cdot\frac{\partial}{\partial \mathbf{v}}\right) f(t,\mathbf{r},\mathbf{v}) = &-\nu_{\text{coll}}(\epsilon)\, f(t,\mathbf{r},\mathbf{v}) + n(t,\mathbf{r})\,\langle\nu_{\text{coll}}(\epsilon)\rangle\,\tilde{w}_{\text{coll}}(v) \\ &- \nu_{\text{trap}}(\epsilon)\, f(t,\mathbf{r},\mathbf{v}) + \Phi(t) * [n(t,\mathbf{r})\,\langle\nu_{\text{trap}}(\epsilon)\rangle]\,\tilde{w}_{\text{detrap}}(v) \\ &- \nu_{\text{loss}}^{(\text{free})}(\epsilon)\, f(t,\mathbf{r},\mathbf{v}), \end{aligned} \tag{5.1}$$

which describes particles of charge e and mass m in the presence of an applied electric field $\mathbf{E}$. Here, the energy-dependent process rates for collisions, trapping and recombination losses are respectively denoted $\nu_{\text{coll}}(\epsilon)$, $\nu_{\text{trap}}(\epsilon)$, $\nu_{\text{loss}}^{(\text{free})}(\epsilon)$, $*$ denotes a time convolution and $\langle\cdot\rangle$ denotes an average over velocity space:

$$\langle\psi(\mathbf{v})\rangle \equiv \frac{1}{n(t,\mathbf{r})}\int \mathrm{d}\mathbf{v}\, f(t,\mathbf{r},\mathbf{v})\,\psi(\mathbf{v}), \tag{5.2}$$

where the free particle number density is defined $n(t,\mathbf{r}) \equiv \int \mathrm{d}\mathbf{v} f(t,\mathbf{r},\mathbf{v})$.

Note that, unlike the free particle process rates, the recombination rate of trapped particles $\nu_{\text{loss}}^{(\text{trap})}$, which is present in the effective trapping time distribution $\Phi(t) \equiv \mathrm{e}^{-\nu_{\text{loss}}^{(\text{trap})} t}\phi(t)$, is *not* a function of energy as trapped particles are localised in space.

The processes of scattering and detrapping are taken to be isotropic and to occur according to Maxwellian velocity distributions. Specifically, we introduce

$$\tilde{w}_{\text{coll}}(v) \equiv \frac{\nu_{\text{coll}}(\epsilon)\, w(\alpha_{\text{coll}}, v)}{\int \mathrm{d}\mathbf{v}\nu_{\text{coll}}(\epsilon)\, w(\alpha_{\text{coll}}, v)}, \tag{5.3}$$

$$\tilde{w}_{\text{detrap}}(v) \equiv \frac{\nu_{\text{trap}}(\epsilon)\, w(\alpha_{\text{detrap}}, v)}{\int \mathrm{d}\mathbf{v}\nu_{\text{trap}}(\epsilon)\, w(\alpha_{\text{detrap}}, v)}, \tag{5.4}$$

where the Maxwellian velocity distribution of temperature T is defined

$$w(\alpha, v) \equiv \left(\frac{\alpha^2}{2\pi}\right)^{\frac{3}{2}} \exp\left(-\frac{\alpha^2 v^2}{2}\right), \tag{5.5}$$

$$\alpha^2 \equiv \frac{m}{k_{\text{B}} T}, \tag{5.6}$$

where k_{B} is the Boltzmann constant.

As stated, this model is very general and requires the precise specification of atomic and molecular details to properly define the process frequencies. In practice, this is usually achieved by using cross-section data in the relationship $\nu(\epsilon) \equiv n_0 v \sigma(\epsilon)$, where n_0 is the number density of the background medium and $\sigma(\epsilon)$ is the cross-section corresponding to the process of frequency $\nu(\epsilon)$.

Similar to the description of free particles by Eq. (5.1), trapped particles can be described by a distribution function in configuration space $n_{\text{trap}}(t, \mathbf{r})$, defined by the continuity equation

$$\begin{aligned}\frac{\partial}{\partial t} n_{\text{trap}}(t, \mathbf{r}) = (1 - \Phi(t) *) \left[n(t, \mathbf{r}) \left\langle \nu_{\text{trap}}(\epsilon) \right\rangle\right] \\ - \nu_{\text{loss}}^{(\text{trap})} n_{\text{trap}}(t, \mathbf{r}).\end{aligned} \tag{5.7}$$

Lastly, the number of particles lost to recombination can also be counted

$$\frac{\mathrm{d}}{\mathrm{d}t} N_{\text{loss}}^{(\text{free})}(t) = \left\langle\left\langle \nu_{\text{loss}}^{(\text{free})}(\epsilon) \right\rangle\right\rangle N(t), \tag{5.8}$$

$$\frac{\mathrm{d}}{\mathrm{d}t} N_{\text{loss}}^{(\text{trap})}(t) = \nu_{\text{loss}}^{(\text{trap})} N_{\text{trap}}(t), \tag{5.9}$$

where $\langle\langle\cdot\rangle\rangle$ denotes an average over phase-space

$$\langle\langle\psi\rangle\rangle \equiv \frac{1}{N(t)} \int \mathrm{d}\mathbf{r} \int \mathrm{d}\mathbf{v}\, f(t, \mathbf{r}, \mathbf{v})\, \psi, \tag{5.10}$$

and free and trapped particle numbers are respectively defined

$$N(t) \equiv \int \mathrm{d}\mathbf{r}\, n(t, \mathbf{r}), \tag{5.11}$$

$$N_{\mathrm{trap}}(t) \equiv \int \mathrm{d}\mathbf{r}\, n_{\mathrm{trap}}(t, \mathbf{r}). \tag{5.12}$$

5.3 Balance equations

A knowledge of the full free particle phase-space distribution, $f(t, \mathbf{r}, \mathbf{v})$, defined by the generalised Boltzmann equation (5.1), is often not required to analyse and interpret experiment. A computationally economical and more physically appealing alternative is to solve for average quantities directly, through solution of the appropriate fluid or velocity moment equations. In what follows, we form these moment equations by evaluating velocity averages of the phase-space distribution function, thus grounding them physically through the generalised Boltzmann equation.

From the Boltzmann equation (5.1), we show most generally that the average of a velocity functional $\psi(\mathbf{v})$ satisfies the differential equation

$$\begin{aligned}\frac{\partial}{\partial t} n \langle \psi \rangle + \frac{\partial}{\partial \mathbf{r}} \cdot n \langle \mathbf{v} \psi \rangle - \frac{e\mathbf{E}}{m} \cdot n \left\langle \frac{\partial \psi}{\partial \mathbf{v}} \right\rangle = & - n \langle \psi \nu_{\mathrm{coll}}(\epsilon) \rangle + n \langle \nu_{\mathrm{coll}}(\epsilon) \rangle \langle \psi \rangle_{\mathrm{coll}} \\ & - n \langle \psi \nu_{\mathrm{trap}}(\epsilon) \rangle + \Phi(t) * (n \langle \nu_{\mathrm{trap}}(\epsilon) \rangle) \langle \psi \rangle_{\mathrm{detrap}} \\ & - n \left\langle \psi \nu_{\mathrm{loss}}^{(\mathrm{free})}(\epsilon) \right\rangle, \end{aligned} \tag{5.13}$$

where the velocity average $\langle \cdot \rangle$ is defined by Eq. (5.2), while $\langle \cdot \rangle_{\mathrm{coll}}$ and $\langle \cdot \rangle_{\mathrm{detrap}}$ are defined as

$$\langle \psi(\mathbf{v}) \rangle_{\mathrm{coll}} \equiv \int \mathrm{d}\mathbf{v} \psi(\mathbf{v}) \tilde{w}_{\mathrm{coll}}(v), \tag{5.14}$$

$$\langle \psi(\mathbf{v}) \rangle_{\mathrm{detrap}} \equiv \int \mathrm{d}\mathbf{v} \psi(\mathbf{v}) \tilde{w}_{\mathrm{detrap}}(v). \tag{5.15}$$

By choosing $\psi(\mathbf{v}) = 1$, $\psi(\mathbf{v}) = m\mathbf{v}$ and $\psi(\mathbf{v}) = \epsilon \equiv \frac{1}{2}mv^2$, respective balance equations for free particle continuity, momentum and energy result:

$$\begin{aligned}\frac{\partial}{\partial t}n + \frac{\partial}{\partial \mathbf{r}}\cdot n\langle\mathbf{v}\rangle =& -n\langle\nu_{\text{trap}}(\epsilon)\rangle + \Phi(t) * (n\langle\nu_{\text{trap}}(\epsilon)\rangle) \\ & - n\left\langle\nu_{\text{loss}}^{(\text{free})}(\epsilon)\right\rangle, \qquad (5.16)\\ \frac{\partial}{\partial t}n\langle m\mathbf{v}\rangle + \frac{\partial}{\partial \mathbf{r}}\cdot n\langle m\mathbf{v}\mathbf{v}\rangle - e\mathbf{E}n =& -n\langle m\mathbf{v}\nu_{\text{coll}}(\epsilon)\rangle \\ & - n\langle m\mathbf{v}\nu_{\text{trap}}(\epsilon)\rangle \\ & - n\left\langle m\mathbf{v}\nu_{\text{loss}}^{(\text{free})}(\epsilon)\right\rangle, \qquad (5.17)\\ \frac{\partial}{\partial t}n\langle\epsilon\rangle + \frac{\partial}{\partial \mathbf{r}}\cdot n\langle\epsilon\mathbf{v}\rangle - e\mathbf{E}\cdot n\langle\mathbf{v}\rangle =& -n\langle\epsilon\nu_{\text{coll}}(\epsilon)\rangle + n\langle\nu_{\text{coll}}(\epsilon)\rangle\langle\epsilon\rangle_{\text{coll}} \\ & - n\langle\epsilon\nu_{\text{trap}}(\epsilon)\rangle + \Phi(t) * (n\langle\nu_{\text{trap}}(\epsilon)\rangle)\langle\epsilon\rangle_{\text{detrap}} \\ & - n\left\langle\epsilon\nu_{\text{loss}}^{(\text{free})}(\epsilon)\right\rangle. \qquad (5.18)\end{aligned}$$

The latter two equations can be written explicitly as differential equations in the average momentum and energy by expanding time derivatives and applying the continuity equation (5.16):

$$\begin{aligned}n\frac{\partial\langle m\mathbf{v}\rangle}{\partial t} + \frac{\partial}{\partial \mathbf{r}}\cdot n\langle m\mathbf{v}\mathbf{v}\rangle - \langle m\mathbf{v}\rangle\frac{\partial}{\partial \mathbf{r}}\cdot n\langle\mathbf{v}\rangle - e\mathbf{E}n =& -n\langle m\mathbf{v}\nu_{\text{coll}}(\epsilon)\rangle \\ & - n\langle m\mathbf{v}\nu_{\text{trap}}(\epsilon)\rangle + n\langle m\mathbf{v}\rangle\langle\nu_{\text{trap}}(\epsilon)\rangle \\ & - \langle m\mathbf{v}\rangle\Phi(t) * (n\langle\nu_{\text{trap}}(\epsilon)\rangle) \\ & - n\left\langle m\mathbf{v}\nu_{\text{loss}}^{(\text{free})}(\epsilon)\right\rangle + n\langle m\mathbf{v}\rangle\left\langle\nu_{\text{loss}}^{(\text{free})}(\epsilon)\right\rangle, \qquad (5.19)\\ n\frac{\partial\langle\epsilon\rangle}{\partial t} + \frac{\partial}{\partial \mathbf{r}}\cdot n\langle\epsilon\mathbf{v}\rangle - \langle\epsilon\rangle\frac{\partial}{\partial \mathbf{r}}\cdot n\langle\mathbf{v}\rangle - e\mathbf{E}\cdot n\langle\mathbf{v}\rangle =& -n\langle\epsilon\nu_{\text{coll}}(\epsilon)\rangle + n\langle\nu_{\text{coll}}(\epsilon)\rangle\langle\epsilon\rangle_{\text{coll}} \\ & - n\langle\epsilon\nu_{\text{trap}}(\epsilon)\rangle + n\langle\epsilon\rangle\langle\nu_{\text{trap}}(\epsilon)\rangle \\ & - \left(\langle\epsilon\rangle - \langle\epsilon\rangle_{\text{detrap}}\right)\Phi(t) * (n\langle\nu_{\text{trap}}(\epsilon)\rangle) \\ & - n\left\langle\epsilon\nu_{\text{loss}}^{(\text{free})}(\epsilon)\right\rangle + n\langle\epsilon\rangle\left\langle\nu_{\text{loss}}^{(\text{free})}(\epsilon)\right\rangle. \qquad (5.20)\end{aligned}$$

Solution of these balance equations requires some approximation in the evaluation of the averages of the collision frequencies. In what follows we solve these balance equations using momentum transfer theory [126] to develop expressions for the mobility, diffusion and the mean energy in terms of the underlying microscopic frequencies for collisions, trapping and losses. Application of these relationships yield some interesting phenomenon including negative differential conductivity (NDC) and heating/cooling, as well as conditions on the relevant frequencies for such phenomena to occur.

5.4 Mobility and the Wannier energy relation: heating/cooling and NDC

In this section, we are interested in physical properties in the weak-gradient hydrodynamic regime. In this limit, properties that are intensive (independent of particle number) become time invariant and spatial gradients vanish [113], resulting in simplified momentum and energy balance equations that provide expressions for the applied acceleration and power input by the field:

$$\begin{aligned}\frac{e\mathbf{E}}{m} &= \langle \mathbf{v}\nu_{\text{coll}}(\epsilon)\rangle^{(0)} \\ &\quad + \langle \mathbf{v}\nu_{\text{trap}}(\epsilon)\rangle^{(0)} - (1-R)\,\mathbf{W}\langle \nu_{\text{trap}}(\epsilon)\rangle^{(0)} \\ &\quad + \left\langle \mathbf{v}\nu_{\text{loss}}^{(\text{free})}(\epsilon)\right\rangle^{(0)} - \mathbf{W}\left\langle \nu_{\text{loss}}^{(\text{free})}(\epsilon)\right\rangle^{(0)}, \end{aligned} \tag{5.21}$$

$$\begin{aligned}e\mathbf{E}\cdot\mathbf{W} &= \langle \epsilon\nu_{\text{coll}}(\epsilon)\rangle^{(0)} - \langle \nu_{\text{coll}}(\epsilon)\rangle^{(0)}\langle\epsilon\rangle_{\text{coll}} \\ &\quad + \langle \epsilon\nu_{\text{trap}}(\epsilon)\rangle^{(0)} - \varepsilon\langle \nu_{\text{trap}}(\epsilon)\rangle^{(0)} + R\langle \nu_{\text{trap}}(\epsilon)\rangle^{(0)}\left(\varepsilon - \langle\epsilon\rangle_{\text{detrap}}\right) \\ &\quad + \left\langle \epsilon\nu_{\text{loss}}^{(\text{free})}(\epsilon)\right\rangle^{(0)} - \varepsilon\left\langle \nu_{\text{loss}}^{(\text{free})}(\epsilon)\right\rangle^{(0)}. \end{aligned} \tag{5.22}$$

where the superscript "(0)" denotes that quantities are in the steady, spatially uniform state. Here, the moments of drift velocity and mean energy have been respectively defined

$$\mathbf{W} \equiv \langle \mathbf{v}\rangle^{(0)}, \tag{5.23}$$

$$\varepsilon \equiv \langle \epsilon\rangle^{(0)}, \tag{5.24}$$

and we have reintroduced the steady-state ratio R defined previously by Eq. (3.63):

$$R \equiv \left(\frac{\Phi(t) * n(t,\mathbf{r})}{n(t,\mathbf{r})}\right)^{(0)} \equiv \lim_{t\to\infty}\frac{\Phi(t) * N(t)}{N(t)}. \tag{5.25}$$

In the following sections, we make these balance equations more useful by using momentum transfer theory to approximate the velocity averages of the form $\langle \nu(\epsilon)\rangle$, $\langle \mathbf{v}\nu(\epsilon)\rangle$ and $\langle \epsilon\nu(\epsilon)\rangle$. The simplified balance equations that result provide expressions for particle mobility and mean energy which in turn can be used to quantify heating/cooling and to explore NDC.

5.4.1 Momentum transfer theory

Momentum-transfer theory [126] enables a systematic procedure for evaluating the average rates detailed above. In this procedure, process rates, $\nu(\epsilon)$, are expanded about some representative energy, which we take to be the mean energy, ε:

$$\nu(\epsilon) = \sum_{i\geq 0}\frac{\nu^{(i)}(\varepsilon)}{i!}(\epsilon-\varepsilon)^i, \tag{5.26}$$

where the superscript "(i)" denotes the i-th energy derivative. This expansion can then be truncated to the desired order of accuracy. By truncating to just the initial constant term, we have zeroth-order momentum transfer theory, which provides a mobility and a Wannier energy relation that is sufficient for exploring NDC and energy-independent heating/cooling. For heating/cooling that varies with energy, we must use first-order momentum transfer theory by truncating the above expansion linearly.

Zeroth-order momentum transfer theory

Truncating the energy expansion, Eq. (5.26), to the constant term gives the zeroth-order momentum transfer theory approximation

$$\langle \psi(\mathbf{v}) \nu(\epsilon) \rangle \approx \langle \psi(\mathbf{v}) \rangle \nu(\varepsilon). \tag{5.27}$$

This approximation yields results that are functionally equivalent to what arises for the case of constant process rates, as considered in Chapter 4, but with some functional dependence on the representative energy ε. Substituting this approximation into the momentum and energy balance equations (5.17) and (5.18) yields

$$\frac{e\mathbf{E}}{m} = \mathbf{W}\nu_{\text{eff}}(\varepsilon), \tag{5.28}$$

$$e\mathbf{E}\cdot\mathbf{W} = \left[\varepsilon - \frac{3}{2}k_{\text{B}}T_{\text{eff}}(\varepsilon)\right]\nu_{\text{eff}}(\varepsilon), \tag{5.29}$$

where we have introduced an effective frequency

$$\nu_{\text{eff}}(\varepsilon) \equiv \nu_{\text{coll}}(\varepsilon) + R\nu_{\text{trap}}(\varepsilon), \tag{5.30}$$

and an effective temperature, written as a weighted sum of the two Maxwellian source temperatures

$$T_{\text{eff}}(\varepsilon) \equiv \omega_{\text{coll}}(\varepsilon) T_{\text{coll}} + \omega_{\text{detrap}}(\varepsilon) T_{\text{detrap}}, \tag{5.31}$$

with energy-dependent weights defined

$$\omega_{\text{coll}}(\varepsilon) \equiv \frac{\nu_{\text{coll}}(\varepsilon)}{\nu_{\text{coll}}(\varepsilon) + R\nu_{\text{trap}}(\varepsilon)}, \tag{5.32}$$

$$\omega_{\text{trap}}(\varepsilon) \equiv \frac{R\nu_{\text{trap}}(\varepsilon)}{\nu_{\text{coll}}(\varepsilon) + R\nu_{\text{trap}}(\varepsilon)}. \tag{5.33}$$

These effective quantities, $\nu_{\text{eff}}(\varepsilon)$ and $T_{\text{eff}}(\varepsilon)$, arose previously in Eqs. (3.62) and (3.78), without any dependence on energy. Similarly, the quantity R is now also energy-dependent, as evident by its implicit definition in Eq. (3.64), which now takes the form

$$R \equiv \int_0^\infty \mathrm{d}t\, \Phi(t)\, \mathrm{e}^{\left[\nu_{\text{loss}}^{(\text{free})}(\varepsilon) + \nu_{\text{trap}}(\varepsilon)(1-R)\right]t}. \tag{5.34}$$

The zeroth-order momentum balance equation (5.28) provides the drift velocity in terms of the electric field **E**:

$$\mathbf{W} \equiv K\mathbf{E}, \tag{5.35}$$

where the constant of proportionality K defines the charged particle mobility

$$K \equiv \frac{e}{m\nu_{\text{eff}}(\varepsilon)}. \tag{5.36}$$

We observe that the mobility is inversely proportional to both collision and trapping process rates through the effective frequency defined in Eq. (5.30). This result is expected as both the scattering and detrapping processes occur isotropically. Evidently, precisely how mobility varies with energy depends entirely on the energy dependence of the process frequencies.

Using both the momentum and energy balance equations (5.28) and (5.29), we can also find the Wannier energy relation for the average energy

$$\varepsilon = \frac{3}{2}k_{\text{B}}T_{\text{eff}}(\varepsilon) + mW^2. \tag{5.37}$$

We can confirm that when there is no trapping, $\nu_{\text{trap}}(\varepsilon) = 0$, the mobility and Wannier energy relation reduce to the classical results valid for dilute gaseous systems [113]:

$$K = \frac{e}{m\nu_{\text{coll}}(\varepsilon)}, \tag{5.38}$$

$$\varepsilon = \frac{3}{2}k_{\text{B}}T_{\text{coll}} + mW^2. \tag{5.39}$$

The zeroth-order mobility and Wannier energy relation derived here are used to describe energy-independent heating/cooling in Sections 5.4.2 and 5.4.2 as well as NDC in Section 5.4.3.

First-order momentum transfer theory

Including an additional term in the energy expansion, Eq. (5.26), gives the first-order momentum transfer theory approximation

$$\langle\psi(\mathbf{v})\nu(\epsilon)\rangle \approx \langle\psi(\mathbf{v})\rangle\nu(\varepsilon) + \langle\psi(\mathbf{v})(\epsilon-\varepsilon)\rangle\nu'(\varepsilon), \tag{5.40}$$

where $\nu'(\varepsilon)$ denotes the energy derivative of $\nu(\varepsilon)$. Substitution into the momentum and energy balance equations (5.17) and (5.18) yields

$$\frac{e\mathbf{E}}{m} = \mathbf{W}\nu_{\text{eff}}(\varepsilon) + \text{cov}(\mathbf{v},\epsilon)\,\nu'_{\text{total}}(\varepsilon), \tag{5.41}$$

$$\begin{aligned} e\mathbf{E}\cdot\mathbf{W} = {} & \left[\varepsilon - \frac{3}{2}k_{\text{B}}T_{\text{eff}}(\varepsilon)\right]\nu_{\text{eff}}(\varepsilon) + \text{var}(\epsilon)\,\nu'_{\text{total}}(\varepsilon) \\ & - \frac{\frac{3}{2}(k_{\text{B}}T_{\text{coll}})^2\,\nu'_{\text{coll}}(\varepsilon)}{1+\left(\frac{3}{2}k_{\text{B}}T_{\text{coll}}-\varepsilon\right)\frac{\nu'_{\text{coll}}(\varepsilon)}{\nu_{\text{coll}}(\varepsilon)}} - \frac{\frac{3}{2}(k_{\text{B}}T_{\text{detrap}})^2\,R\nu'_{\text{trap}}(\varepsilon)}{1+\left(\frac{3}{2}k_{\text{B}}T_{\text{detrap}}-\varepsilon\right)\frac{\nu'_{\text{trap}}(\varepsilon)}{\nu_{\text{trap}}(\varepsilon)}}, \end{aligned} \tag{5.42}$$

where we define $\nu_{\text{total}}(\varepsilon) \equiv \nu_{\text{coll}}(\varepsilon) + \nu_{\text{trap}}(\varepsilon) + \nu_{\text{loss}}^{(\text{free})}(\varepsilon)$, and higher-order velocity moments have been introduced in the form of the velocity-energy covariance

$$\text{cov}(\mathbf{v}, \epsilon) \equiv \langle (\mathbf{v} - \mathbf{W})(\epsilon - \varepsilon) \rangle^{(0)} \equiv \boldsymbol{\xi} - \varepsilon \mathbf{W}, \tag{5.43}$$

where $\boldsymbol{\xi} \equiv \langle \epsilon \mathbf{v} \rangle^{(0)}$ is the energy flux, and the energy variance

$$\text{var}(\epsilon) \equiv \left\langle (\epsilon - \varepsilon)^2 \right\rangle^{(0)} \equiv \langle \epsilon^2 \rangle^{(0)} - \varepsilon^2. \tag{5.44}$$

These higher-order velocity moments can be approximated using zeroth-order momentum transfer theory, as is done in Appendix C, to yield approximations expressed solely in terms of the lower-order velocity moments $\mathbf{W}$ and ε. For example, the velocity-energy covariance can be approximated with

$$\text{cov}(\mathbf{v}, \epsilon) \approx \frac{2}{3}\left(\varepsilon + 2mW^2\right)\mathbf{W}. \tag{5.45}$$

Using this approximation in conjunction with the first-order momentum balance equation (5.41), we find the mobility, as defined by Eq. (3.61):

$$K \approx \frac{e}{m\left[\nu_{\text{eff}}(\varepsilon) + \frac{2}{3}(\varepsilon + 2mW^2)\,\nu'_{\text{total}}(\varepsilon)\right]}. \tag{5.46}$$

This is of the same functional form as the zeroth-order mobility, Eq. (5.36), but with a modification to the effective frequency in the denominator. Note that the mobility now depends explicitly on the drift velocity, through the $2mW^2$ term. Terms such as this are sometimes omitted in the literature as their contribution is minimal when light particles are being considered [113].

As in zeroth-order momentum transfer theory, a Wannier energy relation can be formed by combining both momentum and energy balance equations (5.41) and (5.42):

$$\begin{aligned}\varepsilon = {} & \frac{3}{2}k_{\text{B}}T_{\text{eff}}(\varepsilon) + mW^2 \\ & - \frac{\nu'_{\text{total}}(\varepsilon)}{\nu_{\text{eff}}(\varepsilon)}\text{cov}(\epsilon, \epsilon - m\mathbf{W}\cdot\mathbf{v}) + \frac{\frac{3}{2}(k_{\text{B}}T_{\text{coll}})^2 \frac{\nu'_{\text{coll}}(\varepsilon)}{\nu_{\text{eff}}(\varepsilon)}}{1 + \left(\frac{3}{2}k_{\text{B}}T_{\text{coll}} - \varepsilon\right)\frac{\nu'_{\text{coll}}(\varepsilon)}{\nu_{\text{coll}}(\varepsilon)}} + \frac{\frac{3}{2}(k_{\text{B}}T_{\text{detrap}})^2 \frac{R\nu'_{\text{trap}}(\varepsilon)}{\nu_{\text{eff}}(\varepsilon)}}{1 + \left(\frac{3}{2}k_{\text{B}}T_{\text{detrap}} - \varepsilon\right)\frac{\nu'_{\text{trap}}(\varepsilon)}{\nu_{\text{trap}}(\varepsilon)}}.\end{aligned} \tag{5.47}$$

This first-order Wannier energy relation is written in terms of higher-order velocity moments via the covariance

$$\text{cov}(\epsilon, \epsilon - m\mathbf{W}\cdot\mathbf{v}) \equiv \text{var}(\epsilon) - m\mathbf{W}\cdot\text{cov}(\mathbf{v}, \epsilon). \tag{5.48}$$

As before, the results in Appendix C allow for this covariance to also be written approximately in terms of lower-order velocity moments:

$$\begin{aligned}\operatorname{cov}(\epsilon, \epsilon - m\mathbf{W}\cdot\mathbf{v}) \approx \frac{2}{3}\left(\varepsilon - \frac{1}{2}mW^2\right)^2 + \frac{17}{6}\left(mW^2\right)^2 \\ + \frac{5}{3}\omega_{\mathrm{coll}}(\varepsilon)\,\omega_{\mathrm{trap}}(\varepsilon)\left[\frac{3}{2}k_{\mathrm{B}}\left(T_{\mathrm{coll}} - T_{\mathrm{detrap}}\right)\right]^2.\end{aligned} \tag{5.49}$$

This expression can be used to write the first-order Wannier energy relation (5.47) in an approximate closed form, independent of higher-order velocity moments.

Comparing the above first-order momentum transfer theory results for mobility and average energy, Eqs. (5.46) and (5.47), to their zeroth-order counterparts, Eqs. (5.36) and (5.37), provides an estimate of the error incurred by the zeroth-order momentum transfer theory approximation.

In Section 5.4.2, we use the first-order mobility and Wannier energy relation derived here to describe heating/cooling that is due to the energy dependence of physical processes.

5.4.2 Heating and cooling

In this section, we determine the effect that each of the physical processes described by the generalised Boltzmann equation (5.1) have on the average particle energy. That is, whether there is an increase or decrease in the average energy corresponding to a respective heating or cooling of the particles as a result of collisions, trapping or recombination.

Collisional and trap-based heating/cooling

To consider the effect of collisions on the average energy, we consider the case of constant process rates where the average energy is given by the zeroth-order Wannier energy relation (5.37). For collisions that are infrequent relative to trapping, i.e. $\nu_{\mathrm{coll}} < R\nu_{\mathrm{trap}}$, the average energy can be written approximately to first order in $\nu_{\mathrm{coll}}/R\nu_{\mathrm{trap}}$:

$$\varepsilon \approx \varepsilon_0 + 2\left(\frac{3}{2}k_{\mathrm{B}}T_{\mathrm{HC}} - \varepsilon_0\right)\frac{\nu_{\mathrm{coll}}}{R\nu_{\mathrm{trap}}}, \tag{5.50}$$

where the subscript "0" denotes the collisionless case, i.e. $\nu_{\mathrm{coll}} = 0$:

$$\varepsilon_0 = \frac{3}{2}k_{\mathrm{B}}T_{\mathrm{detrap}} + mW_0^2, \tag{5.51}$$

$$\mathbf{W}_0 = \frac{e\mathbf{E}}{mR\nu_{\mathrm{trap}}}, \tag{5.52}$$

and T_{HC} is a threshold temperature which defines the transition between collisional heating and cooling:

$$T_{\mathrm{HC}} \equiv \frac{T_{\mathrm{coll}} + T_{\mathrm{detrap}}}{2}. \tag{5.53}$$

In the event that $\varepsilon_0 = \frac{3}{2}k_\mathrm{B}T_\mathrm{HC}$, the first-order term in the expansion above vanishes and we must instead consider the second-order approximation:

$$\varepsilon \approx \varepsilon_0 + mW_0^2 \left(\frac{\nu_\mathrm{coll}}{R\nu_\mathrm{trap}}\right)^2. \tag{5.54}$$

The expansions (5.50) and (5.54) show that the introduction of collisions cause cooling only if the initial average energy ε_0 exceeds the threshold energy proportional to the temperature T_HC:

$$\varepsilon_0 > \frac{3}{2}k_\mathrm{B}T_\mathrm{HC}, \tag{5.55}$$

with collisional heating occurring otherwise.

These conditions can also be shown to be applicable to trap-based heating/cooling, in which case ε_0 would denote the trap-free mean energy with $\nu_\mathrm{trap} = 0$.

Energy-indiscriminate recombination heating/cooling

We now explore the possibility of recombination heating/cooling by once again considering constant process rates. It is usually expected that constant loss rates, which act indiscriminate of energy, result in a decrease in particle number that affects extensive properties but leaves intensive properties, like the average energy, unchanged [113]. Although it is true that the recombination considered here is not selective of particle energy, the separate recombination rates for free and trapped particles means that recombination *is* selective of whether particles are trapped or not. Indeed, the average energy can be shown to be a function of the difference in these recombination rates, $\Delta\nu_\mathrm{loss} \equiv \nu_\mathrm{loss}^{(\mathrm{free})} - \nu_\mathrm{loss}^{(\mathrm{trap})}$, only becoming independent when recombination acts uniformly across all particles, i.e. $\nu_\mathrm{loss}^{(\mathrm{free})} = \nu_\mathrm{loss}^{(\mathrm{trap})}$. The recombination dependence appears in the average energy through the quantity R, whose definition in Eq. (5.34) is rewritten here explicitly in terms of $\Delta\nu_\mathrm{loss}$:

$$R \equiv \int_0^\infty \mathrm{d}t\, \phi\,(t)\, \mathrm{e}^{[\Delta\nu_\mathrm{loss} + \nu_\mathrm{trap}(1-R)]t}. \tag{5.56}$$

The original definition of R was given by Eq. (3.63) as the steady-state ratio between the number of particles leaving and entering traps. Without recombination, this ratio is unity as an equilibrium arises between free and trapped particles, Eqs. (3.27) and (3.27). Even with recombination, this ratio should remain at unity so long as the number of free and trapped particles decrease equally due to recombination, $\Delta\nu_\mathrm{loss} = 0$.

We explore the effect of R on heating/cooling by performing a small $\Delta\nu_\mathrm{loss}$ expansion:

$$R \approx 1 + \frac{\Delta\nu_\mathrm{loss}}{\nu_\mathrm{detrap} + \nu_\mathrm{trap}}, \tag{5.57}$$

where the detrapping rate has been introduced

$$\nu_\mathrm{detrap}^{-1} \equiv \int_0^\infty \mathrm{d}t\, \phi\,(t)\, t. \tag{5.58}$$

Proceeding to perform a small $\Delta\nu_{\text{loss}}$ expansion of the average energy, in part by using the above expansion of R, gives the average energy to first order:

$$\varepsilon \approx \varepsilon_0 + 2\left(\frac{3}{2}k_{\text{B}}T_{\text{HC}} - \varepsilon_0\right)\frac{\nu_{\text{trap}}}{\nu_{\text{coll}}+\nu_{\text{trap}}}\frac{\Delta\nu_{\text{loss}}}{\nu_{\text{detrap}}+\nu_{\text{trap}}}, \tag{5.59}$$

where the subscript "0" denotes the case of uniform recombination, $\Delta\nu_{\text{loss}} = 0$:

$$\varepsilon_0 = \frac{3}{2}k_{\text{B}}T_{\text{eff},0} + mW_0^2, \tag{5.60}$$

$$\mathbf{W}_0 = \frac{e\mathbf{E}}{m\left(\nu_{\text{coll}}+\nu_{\text{trap}}\right)}, \tag{5.61}$$

$$T_{\text{eff},0} = \frac{\nu_{\text{coll}}T_{\text{coll}} + \nu_{\text{trap}}T_{\text{detrap}}}{\nu_{\text{coll}}+\nu_{\text{trap}}}, \tag{5.62}$$

and the threshold temperature in this case is defined as

$$T_{\text{HC}} \equiv \frac{T_{\text{eff},0} + T_{\text{detrap}}}{2}. \tag{5.63}$$

In the event that $\varepsilon_0 = \frac{3}{2}k_{\text{B}}T_{\text{HC}}$, we have instead the second-order approximation for average energy:

$$\varepsilon \approx \varepsilon_0 + mW_0^2\left(\frac{\nu_{\text{trap}}}{\nu_{\text{coll}}+\nu_{\text{trap}}}\frac{\Delta\nu_{\text{loss}}}{\nu_{\text{detrap}}+\nu_{\text{trap}}}\right)^2, \tag{5.64}$$

From the small $\Delta\nu_{\text{loss}}$ expansions (5.59) and (5.64), we see that if there is a relative loss of free particles, $\nu_{\text{loss}}^{(\text{free})} > \nu_{\text{loss}}^{(\text{trap})}$, then recombination cooling can occur if those free particles are sufficiently energetic prior to being lost:

$$\varepsilon_0 > \frac{3}{2}k_{\text{B}}T_{\text{HC}}. \tag{5.65}$$

Conversely, if there is a relative gain of free particles, $\nu_{\text{loss}}^{(\text{free})} < \nu_{\text{loss}}^{(\text{trap})}$, then recombination cooling can occur if those free particles are sufficiently cold to begin with:

$$\varepsilon_0 < \frac{3}{2}k_{\text{B}}T_{\text{HC}}. \tag{5.66}$$

Overall, for distinct free and trapped particle recombination rates such that $\nu_{\text{loss}}^{(\text{free})} \neq \nu_{\text{loss}}^{(\text{trap})}$, the condition for recombination cooling can be summarised as

$$\left(\varepsilon_0 - \frac{3}{2}k_{\text{B}}T_{\text{HC}}\right)\Delta\nu_{\text{loss}} > 0, \tag{5.67}$$

with recombination heating occurring otherwise.

Energy-selective recombination heating/cooling

In the event that no traps are present, $\nu_{\text{trap}} = 0$, or where recombination acts uniformly across all free and trapped particles, $\nu_{\text{loss}}^{(\text{free})} = \nu_{\text{loss}}^{(\text{trap})}$, heating and cooling can not occur

due to the trap-selective recombination described previously. In this case, heating or cooling can only occur if recombination acts selectively based on the energy of the free particles. To show this, we will consider the first-order Wannier energy relation (5.47) with constant collision and trapping rates and constant free particle recombination rate energy derivative $\nu_{\text{loss}}^{(\text{free})\prime}$. Performing a small $\nu_{\text{loss}}^{(\text{free})\prime}/\nu_{\text{eff}}$ expansion of this average energy gives, to first order:

$$\varepsilon \approx \varepsilon_0 - \left\{ \frac{2}{3}\left(\varepsilon_0 + \frac{1}{2}mW_0^2\right)^2 + \frac{11}{2}\left(mW_0^2\right)^2 + \frac{5}{3}\omega_{\text{coll}}\omega_{\text{trap}}\left[\frac{3}{2}k_{\text{B}}\left(T_{\text{coll}} - T_{\text{detrap}}\right)\right]^2 \right\} \frac{\nu_{\text{loss}}^{(\text{free})\prime}}{\nu_{\text{eff}}}, \tag{5.68}$$

where the subscript "0" denotes no energy dependence in the free particle recombination rate, $\nu_{\text{loss}}^{(\text{free})\prime} = 0$:

$$\varepsilon_0 = \frac{3}{2}k_{\text{B}}T_{\text{eff}} + mW_0^2, \tag{5.69}$$

$$\mathbf{W}_0 = \frac{e\mathbf{E}}{m\nu_{\text{eff}}}. \tag{5.70}$$

As is expected, the expansion (5.68) suggests that recombination cooling occurs when recombination is selective of higher energy particles,

$$\nu_{\text{loss}}^{(\text{free})\prime} > 0, \tag{5.71}$$

with recombination heating occurring when it is selective of lower energy particles. This confirms for this model the well known phenomena of attachment heating/cooling [113].

5.4.3 Negative differential conductivity

Negative differential conductivity (NDC) occurs when an *increase* in field strength causes a *decrease* in the drift velocity [126]:

$$\frac{\mathrm{d}W}{\mathrm{d}E} < 0. \tag{5.72}$$

The field rate of change of drift velocity can be found directly from the zeroth-order Wannier energy relation (5.37) as

$$\frac{\mathrm{d}W}{\mathrm{d}E} = \frac{1}{2mW}\left[1 - \frac{3}{2}k_{\text{B}}T_{\text{eff}}'\left(\varepsilon\right)\right]\frac{\mathrm{d}\varepsilon}{\mathrm{d}E}, \tag{5.73}$$

which provides the condition for the occurrence of NDC:

$$\frac{3}{2}k_{\text{B}}T_{\text{eff}}'\left(\varepsilon\right) > 1. \tag{5.74}$$

The NDC condition assumes that the mean energy increases monotonically with the field

$$\frac{\mathrm{d}\varepsilon}{\mathrm{d}E} > 0. \tag{5.75}$$

This is equivalent to restricting the effective frequency $\nu_{\text{eff}}(\varepsilon)$ so as to avoid runaway and ensure that an equilibrium is reached [127]:

$$\frac{\mathrm{d}}{\mathrm{d}\varepsilon}\left(\nu_{\text{eff}}(\varepsilon)\sqrt{\varepsilon-\frac{3}{2}k_{\text{B}}T_{\text{eff}}(\varepsilon)}\right)>0. \tag{5.76}$$

Note that the occurrence of NDC depends solely on how the effective temperature varies with energy. This energy rate of change is proportional to the difference in Maxwellian temperatures:

$$T'_{\text{eff}}(\varepsilon)=(T_{\text{coll}}-T_{\text{detrap}})\,\omega'_{\text{coll}}(\varepsilon)=(T_{\text{detrap}}-T_{\text{coll}})\,\omega'_{\text{trap}}(\varepsilon)\,. \tag{5.77}$$

Hence, in comparison with Eq. (5.74), we see that NDC here cannot occur when both scattering and detrapping sources are of equal temperature or when the relative collision or trapping rates, $\omega_{\text{coll}}(\varepsilon)$ and $\omega_{\text{trap}}(\varepsilon)$, do not vary rapidly enough with mean energy.

Figure 5.1 plots both the drift velocity W and mean energy ε as functions of the applied electric field E for a situation in which NDC arises. Previous studies [126, 128] found that, for inelastic processes, the signature of NDC is a rapidly-increasing mean energy. Interestingly, the opposite is true in the example considered for our model, with the mean energy plateauing when NDC occurs. This contrast can be understood by considering the frequency that defines the mobility in each case. For NDC to occur, this frequency must increase sufficiently quickly with applied field. In the referenced studies this frequency increases over a range of energies, causing the mean energy to increase rapidly through this range when NDC occurs. However, in our example in Figure 5.1, the effective frequency increases rapidly at a particular energy, causing the mean energy to plateau at this energy during the NDC regime.

5.5 Generalised Einstein relation

In this section, we form a generalisation of the classical Einstein relation between diffusivity $\mathbf{D}$ and temperature $\mathbf{T}$ tensors [110]:

$$\frac{\mathbf{D}}{K}=\frac{k_{\text{B}}\mathbf{T}}{e}, \tag{5.78}$$

for the phase-space model described by Eq. (5.1). To do this, we make use of Fick's law:

$$\langle\mathbf{v}\rangle\approx\mathbf{W}-\mathbf{D}\cdot\frac{1}{n}\frac{\partial n}{\partial\mathbf{r}}. \tag{5.79}$$

The use of Fick's law here is justified in Section 3.4 where it is shown that velocity averages can be written in the weak-gradient hydrodynamic regime as a density gradient expansion

$$\langle\psi\rangle=\langle\psi\rangle^{(0)}+\langle\psi\rangle^{(1)}\cdot\frac{1}{n}\frac{\partial n}{\partial\mathbf{r}}+\langle\psi\rangle^{(2)}:\frac{1}{n}\frac{\partial^2 n}{\partial\mathbf{r}\partial\mathbf{r}}+\cdots. \tag{5.80}$$

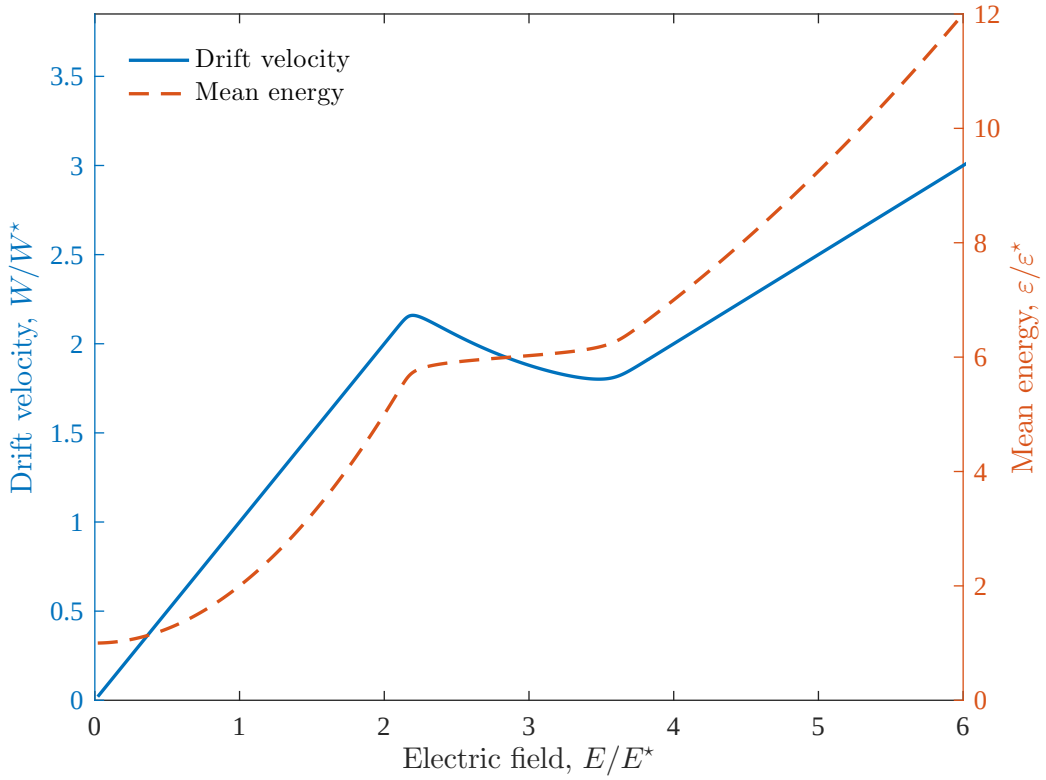

Figure 5.1: Plots of drift velocity, Eq. (3.61), and mean energy, Eq. (5.37), against electric field for a situation in which negative differential conductivity arises. All quantities have been nondimensionalised with respect to the mean energy without a field applied, $\varepsilon^\star \equiv \frac{3}{2}k_\mathrm{B}T_\mathrm{eff}\left(\varepsilon^\star\right)$. Specifically, we have chosen to nondimensionalise using $W^\star \equiv \sqrt{\frac{\varepsilon^\star}{m}}$ and $E^\star \equiv \frac{m\nu_\mathrm{eff}(\varepsilon^\star)}{e}W^\star$. For this figure, we consider a constant collision frequency, $\nu_\mathrm{coll}\left(\varepsilon\right) = 1$, and a trapping frequency that approximates a step function, $R\nu_\mathrm{trap}\left(\varepsilon\right) = \frac{1}{2}\left\{1+\tanh\left[5\left(\varepsilon-\varepsilon_\mathrm{thresh}\right)\right]\right\} \approx H\left(\varepsilon-\varepsilon_\mathrm{thresh}\right)$, turning on at the threshold energy $\varepsilon_\mathrm{thresh} = 6$. In addition, Maxwellian temperatures have been chosen such that $k_\mathrm{B}T_\mathrm{coll} = 1$ and $k_\mathrm{B}T_\mathrm{detrap} = 5$.

To find an expression for the diffusion coefficient, we must apply density gradient expansions to all average quantities in the momentum and energy balance equations (5.17) and (5.18). For the mean energy we have, to first spatial order

$$\left\langle\epsilon\right\rangle \approx \varepsilon + \boldsymbol{\gamma}\cdot\frac{1}{n}\frac{\partial n}{\partial\mathbf{r}}, \tag{5.81}$$

where $\boldsymbol{\gamma}$ is the energy gradient parameter. Using the density gradient expansions of average velocity and energy, Eqs. (5.79) and (5.81), we can determine the following density gradient expansions valid for an arbitrary frequency $\nu\left(\epsilon\right)$:

$$\left\langle\nu\left(\epsilon\right)\right\rangle \approx \nu\left(\varepsilon\right) + \nu'\left(\varepsilon\right)\boldsymbol{\gamma}\cdot\frac{1}{n}\frac{\partial n}{\partial\mathbf{r}}, \tag{5.82}$$

$$\left\langle\mathbf{v}\nu\left(\epsilon\right)\right\rangle \approx \mathbf{W}\nu\left(\varepsilon\right) + \left[\nu'\left(\varepsilon\right)\boldsymbol{\gamma}\mathbf{W} - \nu\left(\varepsilon\right)\mathbf{D}\right]\cdot\frac{1}{n}\frac{\partial n}{\partial\mathbf{r}}, \tag{5.83}$$

$$\left\langle\epsilon\nu\left(\epsilon\right)\right\rangle \approx \varepsilon\nu\left(\varepsilon\right) + \left[\nu\left(\varepsilon\right) + \varepsilon\nu'\left(\varepsilon\right)\right]\boldsymbol{\gamma}\cdot\frac{1}{n}\frac{\partial n}{\partial\mathbf{r}}. \tag{5.84}$$

Lastly, we also perform the density gradient expansion of the concentration of particles leaving traps

$$\Phi(t) * n(t, \mathbf{r}) \approx Rn + \mathbf{R}^{(1)} \cdot \frac{\partial n}{\partial \mathbf{r}}, \tag{5.85}$$

where R is defined by Eq. (5.34) as the steady-state ratio between the number of particles leaving and entering traps, and $\mathbf{R}^{(1)}$ is a vector that has a component due to the energy dependence of R and an intrinsic component present even for constant process rates, as was found in Eq. (3.72):

$$\mathbf{R}^{(1)} \equiv R'(\varepsilon)\boldsymbol{\gamma} + \frac{R\tau}{1 + \nu_{\text{trap}}(\varepsilon) R\tau}\mathbf{W}, \tag{5.86}$$

where we have introduced the average time

$$\tau \equiv \frac{1}{R}\int_0^\infty \mathrm{d}t\, \Phi(t)\, \mathrm{e}^{\left[\nu_{\text{loss}}^{(\text{free})}(\varepsilon) + \nu_{\text{trap}}(\varepsilon)(1-R)\right]t} t, \tag{5.87}$$

which coincides with the mean trapping time when the free and trapped particle recombination rates coincide, $\nu_{\text{loss}}^{(\text{free})}(\varepsilon) = \nu_{\text{loss}}^{(\text{trap})}$.

The weak-gradient hydrodynamic regime balance equations can now be considered to first spatial order by applying all of the above density gradient expansions. Doing so and equating first-order terms yields

$$\frac{k_{\text{B}}\mathbf{T}}{m} = \nu_{\text{eff}}(\varepsilon)\mathbf{D} - \nu'_{\text{eff}}(\varepsilon)\boldsymbol{\gamma}\mathbf{W} - \frac{\nu_{\text{trap}}(\varepsilon) R\tau}{1 + \nu_{\text{trap}}(\varepsilon) R\tau}\mathbf{W}\mathbf{W}, \tag{5.88}$$

$$\begin{aligned} -\frac{\mathbf{Q}_{\text{heat}}}{\nu_{\text{eff}}(\varepsilon)} &= \left[1 - \frac{3}{2}k_{\text{B}}T'_{\text{eff}}(\varepsilon)\right]\boldsymbol{\gamma} + 2m\mathbf{W}\cdot\mathbf{D} \\ &\quad + \frac{3}{2}k_{\text{B}}\left(T_{\text{coll}} - T_{\text{detrap}}\right)\omega_{\text{coll}}(\varepsilon)\,\omega_{\text{detrap}}(\varepsilon)\,\frac{R\tau}{1 + \nu_{\text{trap}}(\varepsilon) R\tau}\mathbf{W}, \end{aligned} \tag{5.89}$$

where the temperature $\mathbf{T}$ and heat flux $\mathbf{Q}_{\text{heat}}$ are defined in terms of the peculiar velocity $\mathbf{V} \equiv \mathbf{v} - \mathbf{W}$ as

$$k_{\text{B}}\mathbf{T} \equiv m\left\langle \mathbf{V}\mathbf{V}\right\rangle^{(0)}, \tag{5.90}$$

$$\mathbf{Q}_{\text{heat}} \equiv \frac{1}{2}m\left\langle V^2\mathbf{V}\right\rangle^{(0)}. \tag{5.91}$$

By writing the above system of equations in terms of components of diffusivity and temperature perpendicular and parallel to the field:

$$\mathbf{D} \equiv D_\perp\left(\mathbf{I} - \hat{\mathbf{E}}\hat{\mathbf{E}}\right) + D_\parallel\hat{\mathbf{E}}\hat{\mathbf{E}}, \tag{5.92}$$

$$\mathbf{T} \equiv T_\perp\left(\mathbf{I} - \hat{\mathbf{E}}\hat{\mathbf{E}}\right) + T_\parallel\hat{\mathbf{E}}\hat{\mathbf{E}}, \tag{5.93}$$

and solving for each component of diffusivity separately yields the generalised Einstein relations

$$D_{\perp} = \frac{k_{\mathrm{B}} T_{\perp}}{m \nu_{\mathrm{eff}}(\varepsilon)}, \tag{5.94}$$

$$D_{\parallel} = \frac{k_{\mathrm{B}} T_{\parallel} + mW^2 \frac{\nu_{\mathrm{trap}}(\varepsilon) R\tau}{1+\nu_{\mathrm{trap}}(\varepsilon) R\tau} - \left[\frac{Q}{W} + \frac{3}{2} k_{\mathrm{B}} \left(T_{\mathrm{coll}} - T_{\mathrm{detrap}}\right) \frac{\nu_{\mathrm{coll}}(\varepsilon)}{\nu_{\mathrm{eff}}(\varepsilon)} \frac{\nu_{\mathrm{trap}}(\varepsilon) R\tau}{1+\nu_{\mathrm{trap}}(\varepsilon) R\tau}\right] \frac{mW^2}{1-\frac{3}{2} k_{\mathrm{B}} T'_{\mathrm{eff}}(\varepsilon)} \frac{\nu'_{\mathrm{eff}}(\varepsilon)}{\nu_{\mathrm{eff}}(\varepsilon)}}{m \nu_{\mathrm{eff}}(\varepsilon) \left(1 + \frac{2mW^2}{1-\frac{3}{2} k_{\mathrm{B}} T'_{\mathrm{eff}}(\varepsilon)} \frac{\nu'_{\mathrm{eff}}(\varepsilon)}{\nu_{\mathrm{eff}}(\varepsilon)}\right)}. \tag{5.95}$$

Using the zeroth-order mobility and Wannier energy relation derived in Section 5.4.1, we find the identity:

$$\frac{\frac{\mathrm{d} \ln K}{\mathrm{d} \ln E}}{1 + \frac{\mathrm{d} \ln K}{\mathrm{d} \ln E}} \equiv -\frac{2mW^2}{1 - \frac{3}{2} k_{\mathrm{B}} T'_{\mathrm{eff}}(\varepsilon)} \frac{\nu'_{\mathrm{eff}}(\varepsilon)}{\nu_{\mathrm{eff}}(\varepsilon)}, \tag{5.96}$$

which allows the above generalised Einstein relations to be written in terms of the field-dependence of the mobility K:

$$\frac{D_{\perp}}{K} = \frac{k_{\mathrm{B}} T_{\perp}}{e}, \tag{5.97}$$

$$\frac{D_{\parallel}}{K} = \frac{k_{\mathrm{B}} T_{\parallel} + mW^2 \frac{\nu_{\mathrm{trap}}(\varepsilon) R\tau}{1+\nu_{\mathrm{trap}}(\varepsilon) R\tau}}{e} \left[1 + (1+\Delta) \frac{\mathrm{d} \ln K}{\mathrm{d} \ln E}\right], \tag{5.98}$$

where

$$\Delta \equiv \frac{Q + \frac{3}{2} k_{\mathrm{B}} \left(T_{\mathrm{coll}} - T_{\mathrm{detrap}}\right) W \frac{\nu_{\mathrm{coll}}(\varepsilon)}{\nu_{\mathrm{eff}}(\varepsilon)} \frac{\nu_{\mathrm{trap}}(\varepsilon) R\tau}{1+\nu_{\mathrm{trap}}(\varepsilon) R\tau}}{2 k_{\mathrm{B}} T_{\parallel} W + 2mW^3 \frac{\nu_{\mathrm{trap}}(\varepsilon) R\tau}{1+\nu_{\mathrm{trap}}(\varepsilon) R\tau}}. \tag{5.99}$$

We can see that the perpendicular generalised Einstein relation coincides with the classical Einstein relation (5.78) and that the parallel one deviates from it, highlighting the anisotropic nature of diffusion. In the case where there is no trapping, $\nu_{\mathrm{trap}}(\varepsilon) = 0$, the above parallel Einstein relation reduces to

$$\frac{D_{\parallel}}{K} = \frac{k_{\mathrm{B}} T_{\parallel}}{e} \left[1 + (1+\Delta) \frac{\mathrm{d} \ln K}{\mathrm{d} \ln E}\right], \tag{5.100}$$

with

$$\Delta \equiv \frac{Q}{2 k_{\mathrm{B}} T_{\parallel} W}, \tag{5.101}$$

which coincides with the well-known gas-phase results [125,126]. The deviation of this collision-only generalised Einstein relation (5.100) from the classical Einstein relation (5.78) is due entirely to the energy dependence of the process rates. Interestingly, this is not the case when trapping is considered, as choosing constant process rates for the generalised Einstein relation (5.98) results in a parallel diffusion coefficient that still has some enhancement:

$$\frac{D_{\parallel}}{K} = \frac{k_{\mathrm{B}} T_{\parallel} + mW^2 \frac{\nu_{\mathrm{trap}} R\tau}{1+\nu_{\mathrm{trap}} R\tau}}{e}, \tag{5.102}$$

as observed previously in Chapter 4 where anisotropic diffusion was quantified for

constant process rates in Eq. (5.102). This anisotropy is to be expected as, rather than moving with the applied field, some particles become localised in traps only to detrap later to contribute to the spread of free particles.

5.6 Conclusion

We have explored a generalised phase-space model that considers collision, trapping, detrapping and recombination processes, all of which act selectively according to particle energy. We form balance equations (5.16)–(5.18) describing the conservation and transport of particle number, momentum and energy, and use these balance equations to form expressions for the particle mobility, Eqs. (5.36) and (5.46), and for the average particle energy in the form of Wannier energy relations (5.37) and (5.47). These Wannier energy relations were then used to provide conditions for particle heating or cooling due to collisions or trapping, Eq. (5.55), and recombination, Eqs. (5.67) and (5.71). Notably, recombination heating and cooling was found to occur even when particles recombined indiscriminate of energy, in contrast to the case where recombination occurs only in the delocalised states. Transport via combined localised/delocalised states was shown to produce negative differential conductivity under certain conditions (5.74), and the impact of scattering, trapping/detrapping and recombination on the anisotropic nature of diffusion was expressed through the development of the generalised Einstein relations (5.97) and (5.98). Lastly, fractional transport analogues of the aforementioned results were explored by using a trapping time distribution with a heavy tail of the form of Eq. (3.95).

For direct application of this model, it is necessary to have reasonable inputs for the trapping frequency, ν_{trap}, and the trapping time distribution, $\phi(t)$. Some progress has been made already for organic materials where the trapping time distribution can be calculated from the density of existing trapped states [33]. Also for dense gases/liquids, where trapped states are formed by the electron itself and the trapping time distribution is dependent on the scattering, fluctuation profiles and subsequent fluid bubble evolution [88]. Other investigations of trapping also exist in the literature [93–95], including free energy changes and solvation time scales, but none of these directly produces an energy-dependent trapping frequency or trapping time distribution. Presently, the focus of our attention is on the *ab initio* calculation of energy-dependent trapping frequencies and waiting time distributions in liquids and dense gases, as well as the simulation of charge carrier transport in 2D organic devices, including those with long-lived traps where transport is dispersive. The latter is the subject of Chapter 6.

6

Planar organic semiconductor device simulation

This chapter outlines a simulation for charge carrier transport in planar organic semiconductors. The model takes the form of a two-dimensional generalised drift-diffusion-Poisson system that accounts for charge carrier trapping and detrapping, as well as recombination of both free and trapped carriers. We begin by describing each component of this model separately, before presenting the model in its entirety. Numerical details regarding the implementation of the model in the Julia programming language are then presented. The resulting model implementation is then benchmarked against known results for one-dimensional plane-parallel systems. Finally, we apply the model to a parameter exploration of a planar TOF experiment. In the process, we explore a potential experimental technique for the characterisation of the recombination coefficient. Finally, we explore what effects traps may have on the measured current in various charge transport experiments in planar geometry, including TOF, Photo-CELIV and RPV.

This chapter forms the basis of a forthcoming publication:

[129] Peter W. Stokes, Bronson Philippa, Almantas Pivrikas, and Ronald D. White. Localised and delocalised charge transport in planar organic semiconducting devices (2018)

6.1 Outline of planar device model

6.1.1 Charge-carrier transport

We describe the transport of free and trapped electrons and holes using the generalised continuity equations (3.34) and (3.6):

$$\left[\frac{\partial}{\partial t} + \nu_{\text{trap},n}\left(1 - R_n\left(t,\mathbf{r}\right)\right)\right] n + \frac{\partial}{\partial \mathbf{r}} \cdot \mathbf{\Gamma}_n\left(t,\mathbf{r}\right) = -\nu_{\text{loss},n}^{(\text{free})} n, \tag{6.1}$$

$$\left[\frac{\partial}{\partial t} + \nu_{\text{trap},p}\left(1 - R_p\left(t,\mathbf{r}\right)\right)\right] p + \frac{\partial}{\partial \mathbf{r}} \cdot \mathbf{\Gamma}_p\left(t,\mathbf{r}\right) = -\nu_{\text{loss},p}^{(\text{free})} p, \tag{6.2}$$

$$\frac{\partial n_{\text{trap}}}{\partial t} = \nu_{\text{trap},n}\left(1 - R_n\left(t,\mathbf{r}\right)\right) n - \nu_{\text{loss},n}^{(\text{trap})} n_{\text{trap}}, \tag{6.3}$$

$$\frac{\partial p_{\text{trap}}}{\partial t} = \nu_{\text{trap},p}\left(1 - R_p\left(t,\mathbf{r}\right)\right) p - \nu_{\text{loss},p}^{(\text{trap})} p_{\text{trap}}, \tag{6.4}$$

where $n\left(t,\mathbf{r}\right)$ and $p\left(t,\mathbf{r}\right)$ are free electron and hole number densities, $n_{\text{trap}}\left(t,\mathbf{r}\right)$ and $p_{\text{trap}}\left(t,\mathbf{r}\right)$ are trapped electron and hole number densities and quantities are subscripted with "n" or "p" when they pertain to electrons or holes, respectively, including the carrier flux $\mathbf{\Gamma}\left(t,\mathbf{r}\right)$, free and trapped carrier recombination rates, $\nu_{\text{loss}}^{(\text{free})}$ and $\nu_{\text{loss}}^{(\text{trap})}$, and the ratio between carriers leaving and entering traps, $R\left(t,\mathbf{r}\right)$, specified in terms of the distribution of carrier trapping times $\phi\left(t\right)$:

$$R_n\left(t,\mathbf{r}\right) = \frac{\left(\mathrm{e}^{-\nu_{\text{loss},n}^{(\text{trap})} t}\phi_n\left(t\right)\right) * n\left(t,\mathbf{r}\right)}{n\left(t,\mathbf{r}\right)}, \tag{6.5}$$

$$R_p\left(t,\mathbf{r}\right) = \frac{\left(\mathrm{e}^{-\nu_{\text{loss},p}^{(\text{trap})} t}\phi_p\left(t\right)\right) * p\left(t,\mathbf{r}\right)}{p\left(t,\mathbf{r}\right)}. \tag{6.6}$$

As stated, the above continuity equations consider time-invariant recombination rates for both free and trapped particles. However, in the context of a semiconductor device simulation, we can be more specific regarding the recombination process. In particular, we consider bimolecular recombination where the recombination rate of one carrier is proportional to the number density of the other [130–132]:

$$\left(\frac{\partial n}{\partial t}\right)_{\text{recomb with } p} = \left(\frac{\partial p}{\partial t}\right)_{\text{recomb with } n} = -\beta n\left(t,\mathbf{r}\right) p\left(t,\mathbf{r}\right), \tag{6.7}$$

where β is the bimolecular recombination coefficient. In a similar way, we also account for trap-assisted bimolecular recombination between free and trapped carriers. We consider such recombination as being transport-limited, where the recombination rate between free and trapped carriers decreases by a factor proportional to the relative mobility of the free carrier [133]. For electron and hole mobilities, μ_n and μ_p, we thus

have the following recombination rates:

$$\left(\frac{\partial n}{\partial t}\right)_{\text{recomb with } p_{\text{trap}}} = \left(\frac{\partial p_{\text{trap}}}{\partial t}\right)_{\text{recomb with } n} = -\frac{\mu_n}{\mu_p + \mu_n}\beta n\left(t, \mathbf{r}\right) p_{\text{trap}}\left(t, \mathbf{r}\right), \quad (6.8)$$

$$\left(\frac{\partial p}{\partial t}\right)_{\text{recomb with } n_{\text{trap}}} = \left(\frac{\partial n_{\text{trap}}}{\partial t}\right)_{\text{recomb with } p} = -\frac{\mu_p}{\mu_p + \mu_n}\beta n_{\text{trap}}\left(t, \mathbf{r}\right) p\left(t, \mathbf{r}\right). \quad (6.9)$$

Given each of the above recombination rates, the resulting coupled continuity equations for free and trapped electrons and holes become

$$\left[\frac{\partial}{\partial t} + \nu_{\text{trap},n}\left(1 - R_n\left(t, \mathbf{r}\right)\right)\right] n + \frac{\partial}{\partial \mathbf{r}} \cdot \mathbf{\Gamma}_n\left(t, \mathbf{r}\right) = -\beta np - \frac{\mu_n}{\mu_p + \mu_n}\beta np_{\text{trap}}, \quad (6.10)$$

$$\left[\frac{\partial}{\partial t} + \nu_{\text{trap},p}\left(1 - R_p\left(t, \mathbf{r}\right)\right)\right] p + \frac{\partial}{\partial \mathbf{r}} \cdot \mathbf{\Gamma}_p\left(t, \mathbf{r}\right) = -\beta np - \frac{\mu_p}{\mu_p + \mu_n}\beta n_{\text{trap}} p, \quad (6.11)$$

$$\frac{\partial n_{\text{trap}}}{\partial t} = \nu_{\text{trap},n}\left(1 - R_n\left(t, \mathbf{r}\right)\right) n - \frac{\mu_p}{\mu_p + \mu_n}\beta n_{\text{trap}} p, \quad (6.12)$$

$$\frac{\partial p_{\text{trap}}}{\partial t} = \nu_{\text{trap},p}\left(1 - R_p\left(t, \mathbf{r}\right)\right) p - \frac{\mu_n}{\mu_p + \mu_n}\beta np_{\text{trap}}, \quad (6.13)$$

where $\mathbf{\Gamma}_n\left(t, \mathbf{r}\right)$ and $\mathbf{\Gamma}_p\left(t, \mathbf{r}\right)$ are electron and hole fluxes, and $R_n\left(t, \mathbf{r}\right)$ and $R_p\left(t, \mathbf{r}\right)$ are ratios between electrons and holes leaving and entering traps. These ratios now take on the following form to account for the decrease in particles leaving traps due to trap-based bimolecular recombination:

$$R_n\left(t, \mathbf{r}\right) \equiv \frac{\phi_n\left(t\right) * \left[n\left(t, \mathbf{r}\right) \exp\left(\frac{\mu_p}{\mu_p + \mu_n}\beta \int_0^t \mathrm{d}\tau p\left(\tau, \mathbf{r}\right)\right)\right]}{n\left(t, \mathbf{r}\right) \exp\left(\frac{\mu_p}{\mu_p + \mu_n}\beta \int_0^t \mathrm{d}\tau p\left(\tau, \mathbf{r}\right)\right)}, \quad (6.14)$$

$$R_p\left(t, \mathbf{r}\right) \equiv \frac{\phi_p\left(t\right) * \left[p\left(t, \mathbf{r}\right) \exp\left(\frac{\mu_n}{\mu_p + \mu_n}\beta \int_0^t \mathrm{d}\tau n\left(\tau, \mathbf{r}\right)\right)\right]}{p\left(t, \mathbf{r}\right) \exp\left(\frac{\mu_n}{\mu_p + \mu_n}\beta \int_0^t \mathrm{d}\tau n\left(\tau, \mathbf{r}\right)\right)}, \quad (6.15)$$

where $\phi_n\left(t\right)$ and $\phi_p\left(t\right)$ are distributions of trapping times for electrons and holes. Details regarding the derivation of these ratios are presented in Appendix D.2. Finally, as was justified in Section 3.4, we can use Fick's law to evaluate the fluxes approximately:

$$\mathbf{\Gamma}_n\left(t, \mathbf{r}\right) = \mathbf{W}_n n\left(t, \mathbf{r}\right) - \mathbf{D}_n \cdot \frac{\partial n}{\partial \mathbf{r}}, \quad (6.16)$$

$$\mathbf{\Gamma}_p\left(t, \mathbf{r}\right) = \mathbf{W}_p p\left(t, \mathbf{r}\right) - \mathbf{D}_p \cdot \frac{\partial p}{\partial \mathbf{r}}. \quad (6.17)$$

Thus, transport of each carrier is described by a generalised drift-diffusion equation, similar to Eq. (3.89). Using Einstein's relation (4.41), along with the mobility μ, which satisfies the definition $\mathbf{W} \equiv \mu\mathbf{E}$, we can express the above fluxes as

$$\mathbf{\Gamma}_n\left(t, \mathbf{r}\right) = -\mu_n \mathbf{E}\left(t, \mathbf{r}\right) n\left(t, \mathbf{r}\right) - \frac{\mu_n k_{\text{B}} T}{e}\frac{\partial n}{\partial \mathbf{r}}, \quad (6.18)$$

$$\mathbf{\Gamma}_p\left(t, \mathbf{r}\right) = \mu_p \mathbf{E}\left(t, \mathbf{r}\right) p\left(t, \mathbf{r}\right) - \frac{\mu_p k_{\text{B}} T}{e}\frac{\partial p}{\partial \mathbf{r}}, \quad (6.19)$$

where T is the temperature of the material and $\mathbf{E}(t, \mathbf{r})$ is the local electric field. Although the classical Einstein relation has been used here to relate diffusion and temperature, any of the more sophisticated Einstein relations, Eqs. (5.98) and (5.102), could also have be used, allowing for the consideration of anisotropic diffusion.

Finally, we specify the various boundary conditions for the particle fluxes:

Blocking boundary condition — At interfaces between the semiconductor and an insulator, such as the surrounding air, we set the fluxes to zero:

$$\mathbf{\Gamma}_n(t, \mathbf{r}) = 0, \tag{6.20}$$

$$\mathbf{\Gamma}_p(t, \mathbf{r}) = 0. \tag{6.21}$$

Outflow boundary condition — At interfaces between the semiconductor and the metal electrodes, when charge extraction occurs, we set the fluxes proportional to the field strength at the interface:

$$\mathbf{\Gamma}_n(t, \mathbf{r}) = -\mu_n \mathbf{E}(t, \mathbf{r})\, n(t, \mathbf{r}), \tag{6.22}$$

$$\mathbf{\Gamma}_p(t, \mathbf{r}) = \mu_p \mathbf{E}(t, \mathbf{r})\, p(t, \mathbf{r}). \tag{6.23}$$

This guarantees that charges will leave the device if there is a field there to drive them. This boundary condition has been used previously in both numerical simulations [134, 135] and analytical solutions [136].

Ohmic boundary condition — At interfaces between the semiconductor and the metal electrodes, when charge injection occurs, the number density within the injecting electrode is held fixed at an effective density of states n_{EDOS} [137]:

$$\mathbf{\Gamma}_n(t, \mathbf{r}) = \mu_n \mathbf{E}(t, \mathbf{r})\, n_{\mathrm{EDOS}}, \tag{6.24}$$

$$\mathbf{\Gamma}_p(t, \mathbf{r}) = -\mu_p \mathbf{E}(t, \mathbf{r})\, n_{\mathrm{EDOS}}. \tag{6.25}$$

In practice, n_{EDOS} is an additional parameter that must be fit using experimental data.

6.1.2 Electric potential and field

To fully define the carrier fluxes in Eqs. (6.18) and (6.19), the electric field $\mathbf{E}(t, \mathbf{r})$ must be known throughout the device. In terms of the electric potential $V(t, \mathbf{r})$, the electric field is

$$\mathbf{E}(t, \mathbf{r}) = -\frac{\partial}{\partial \mathbf{r}} V(t, \mathbf{r}). \tag{6.26}$$

In turn, the electric potential $V(t, \mathbf{r})$ can be found by solving Poisson's equation:

$$\frac{\partial}{\partial \mathbf{r}} \cdot \left[\varepsilon(\mathbf{r}) \frac{\partial V}{\partial \mathbf{r}} \right] = -\rho(t, \mathbf{r}), \tag{6.27}$$

where $\varepsilon(\mathbf{r})$ is the electric permittivity and

$$\rho(t, \mathbf{r}) \equiv e\left[p(t, \mathbf{r}) - n(t, \mathbf{r}) + p_{\mathrm{trap}}(t, \mathbf{r}) - n_{\mathrm{trap}}(t, \mathbf{r}) \right], \tag{6.28}$$

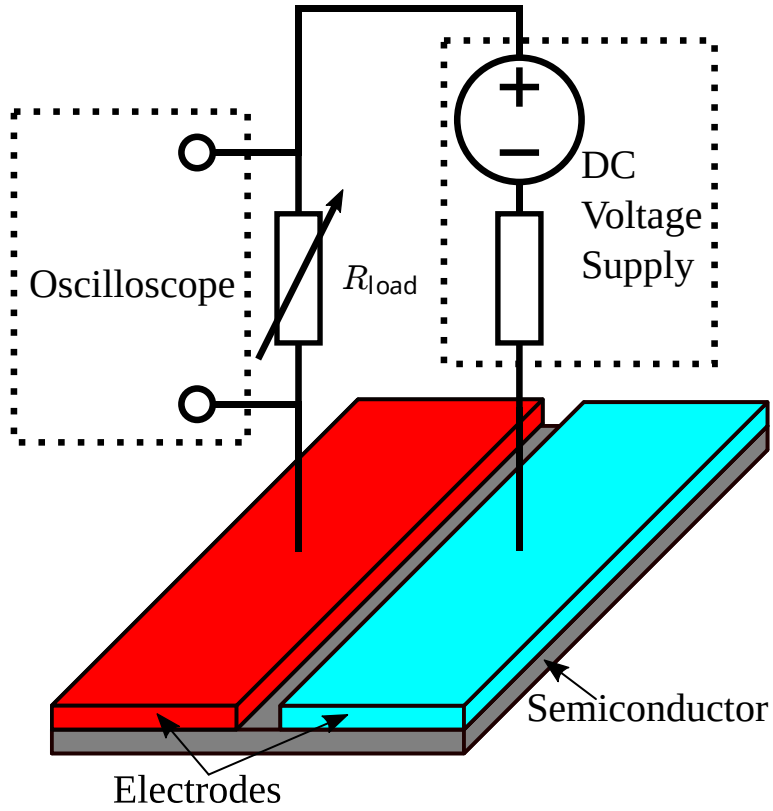

Figure 6.1: Planar semiconductor and accompanying measurement circuitry.

is the net charge density. The voltages of the metal electrodes provide Dirichlet boundary conditions for Poisson's equation. Specifically, we define one electrode to have a voltage equal to the potential difference between both electrodes, $U(t)$:

$$V(t, \mathbf{r}) = U(t), \quad \forall \mathbf{r} \in \text{positive electrode}, \tag{6.29}$$

with the other electrode consequently having a zero voltage:

$$V(t, \mathbf{r}) = 0, \quad \forall \mathbf{r} \in \text{negative electrode}. \tag{6.30}$$

Lastly, as the problem domain is unbounded, a zero-field Neumann boundary condition is applied at a radial distance from the device. This approximates the actual zero-field condition at infinity:

$$\lim_{\|\mathbf{r}\| \to \infty} \mathbf{E}(t, \mathbf{r}) = 0. \tag{6.31}$$

6.1.3 External measurement circuitry

As described in the previous section, in order to solve Poisson's equation (6.27) we require knowledge of the electrode potential difference $U(t)$. An expression containing $U(t)$ can be found by applying Kirchhoff's voltage law to the circuit depicted in Figure 6.1:

$$V_{\text{psu}}(t) = U(t) + i(t) R, \tag{6.32}$$

where $i(t)$ is the current in the external circuit. This current can in turn be found using Kirchhoff's current law:

$$\oiint_{\mathcal{S}} \mathrm{d}\mathbf{S} \cdot \mathbf{i}(t, \mathbf{r}) = \begin{cases} i(t), & \mathcal{S} \text{ encloses positive electrode,} \\ -i(t), & \mathcal{S} \text{ encloses negative electrode,} \\ 0, & \text{otherwise,} \end{cases} \tag{6.33}$$

where $\mathrm{d}\mathbf{S}$ is a differential of the surface $\mathcal{S}$. Here, $\mathbf{i}(t, \mathbf{r})$ is the current density, which is a sum of conduction and displacement current densities:

$$\mathbf{i}(t, \mathbf{r}) = \mathbf{j}_{\mathrm{c}}(t, \mathbf{r}) + \frac{\partial \mathbf{D}(t, \mathbf{r})}{\partial t}, \tag{6.34}$$

where $\mathbf{j}_{\mathrm{c}}(t, \mathbf{r}) \equiv e[\mathbf{\Gamma}_p(t, \mathbf{r}) - \mathbf{\Gamma}_n(t, \mathbf{r})]$ is the conduction current density and $\mathbf{D}(t, \mathbf{r}) \equiv \varepsilon(\mathbf{r})\mathbf{E}(t, \mathbf{r})$ is the electric displacement field. Taking the surface $\mathcal{S}$ to lie on the surface of the positive electrode yields the following expression for the current:

$$i(t) = i_{\mathrm{c}}(t) + \frac{\partial Q}{\partial t}, \tag{6.35}$$

where the conduction current being injected by the positive electrode is

$$i_{\mathrm{c}}(t) \equiv \oiint_{\mathcal{S}} \mathrm{d}\mathbf{S} \cdot \mathbf{j}_{\mathrm{c}}(t, \mathbf{r}), \tag{6.36}$$

and the charge on the positive electrode is given by Gauss's law:

$$Q(t) \equiv \oiint_{\mathcal{S}} \mathrm{d}\mathbf{S} \cdot \mathbf{D}(t, \mathbf{r}). \tag{6.37}$$

Substituting Eq. (6.35) for the current into Eq. (6.32) yields an ordinary differential equation for the charge $Q(t)$ on the positive electrode:

$$\frac{\partial Q}{\partial t} = \frac{V_{\mathrm{psu}}(t) - U(t)}{R} - i_{\mathrm{c}}(t). \tag{6.38}$$

Notice that writing Eq. (6.37) for the charge $Q(t)$ out in full suggests that $Q(t)$ is linearly related to $U(t)$:

$$Q(t) \equiv \oiint_{\mathcal{S}} \mathrm{d}\mathbf{S} \cdot \mathbf{D}(t, \mathbf{r}) = \oiint_{\mathcal{S}} \mathrm{d}\mathbf{S} \cdot \varepsilon(\mathbf{r})\mathbf{E}(t, \mathbf{r}) = -\oiint_{\mathcal{S}} \mathrm{d}\mathbf{S} \cdot \varepsilon(\mathbf{r}) \frac{\partial V(t, \mathbf{r})}{\partial \mathbf{r}}. \tag{6.39}$$

Thus, the above differential equation (6.38) for $Q(t)$ is also a differential equation for $U(t)$ and we can find $U(t)$ in practice by quantifying the linear relationship between $Q(t)$ and $U(t)$. To do this, we use the principle of superposition to write the electric potential $V(t, \mathbf{r})$ as a linear function of $U(t)$:

$$V(t, \mathbf{r}) \equiv \tilde{V}(t, \mathbf{r})U(t) + V_{U=0}(t, \mathbf{r}), \tag{6.40}$$

where $\tilde{V}(t, \mathbf{r})$ is a dimensionless potential characterising purely the geometric effect of the electrodes on the electric potential and $V_{U=0}(t, \mathbf{r})$ is simply what the electric potential would be if both electrodes had equal potentials, i.e. $U(t) = 0$. Corresponding expressions follow for both the electric field $\mathbf{E}(t, \mathbf{r})$ and the electric displacement field $\mathbf{D}(t, \mathbf{r})$:

$$\mathbf{E}(t, \mathbf{r}) \equiv \tilde{\mathbf{E}}(t, \mathbf{r}) U(t) + \mathbf{E}_{U=0}(t, \mathbf{r}), \tag{6.41}$$

$$\mathbf{D}(t, \mathbf{r}) \equiv \tilde{\mathbf{D}}(t, \mathbf{r}) U(t) + \mathbf{D}_{U=0}(t, \mathbf{r}). \tag{6.42}$$

Finally, performing the surface integral in Eq. (6.37) yields an expression for the charge on the positive conductor $Q(t)$ in terms of the electrode potential difference $U(t)$:

$$Q(t) = CU(t) + Q_{U=0}(t), \tag{6.43}$$

where the geometric capacitance is defined as

$$C \equiv \oiint_{\mathcal{S}} \mathrm{d}\mathbf{S} \cdot \varepsilon(\mathbf{r}) \tilde{\mathbf{E}}(t, \mathbf{r})(t, \mathbf{r}), \tag{6.44}$$

and the charge on the positive conductor solely due to space charge is

$$Q_{U=0}(t) = \oiint_{\mathcal{S}} \mathrm{d}\mathbf{S} \cdot \varepsilon(\mathbf{r}) \mathbf{E}_{U=0}(t, \mathbf{r}). \tag{6.45}$$

In practice, the differential equation (6.38) can be solved for the charge $Q(t)$, which in turn can be used to find the potential difference $U(t)$ via Eq. (6.43):

$$U(t) = \frac{Q(t) - Q_{U=0}(t)}{C}. \tag{6.46}$$

6.1.4 Photogeneration of charge carriers

To model charge transport experiments that photogenerate charge carriers with an initial flash of light, we set the free electron and hole number densities to be initially equal to

$$n(0, \mathbf{r}) = p(0, \mathbf{r}) = Q_{\mathrm{ph}} Q_1(\mathbf{r}), \tag{6.47}$$

where $Q_1(\mathbf{r})$ is normalised to unity within the semiconductor and describes the initial distribution of charge due to photogeneration and Q_{ph} is the total charge generated, which increases with the intensity of the light. The precise form of $Q_1(\mathbf{r})$ depends on the device geometry, where the light is directed, whether the light is focused or not and also on the optical absorption model used. For example, in the case of the Beer-Lambert law in one spatial dimension x, we have an exponential decay in light intensity:

$$Q_1(x) \propto \mathrm{e}^{-\alpha_{\mathrm{BL}} x}, \tag{6.48}$$

where α_{BL} is the optical absorption coefficient of the semiconductor.

6.1.5 Model summary and implementation

Collating Eqs. (6.10)–(6.15), (6.18), (6.19), (6.26), (6.27), (6.38), (6.36), (6.45) and (6.46) yields the following complete description of the general planar semiconductor model:

$$\left[\frac{\partial}{\partial t}+\nu_{\mathrm{trap},p}\left(1-R_p\left(t,\mathbf{r}\right)\right)\right]p+\frac{\partial}{\partial\mathbf{r}}\cdot\mathbf{\Gamma}_p\left(t,\mathbf{r}\right)=-\beta np-\frac{\mu_p}{\mu_p+\mu_n}\beta n_{\mathrm{trap}}p, \tag{6.49}$$

$$\left[\frac{\partial}{\partial t}+\nu_{\mathrm{trap},n}\left(1-R_n\left(t,\mathbf{r}\right)\right)\right]n+\frac{\partial}{\partial\mathbf{r}}\cdot\mathbf{\Gamma}_n\left(t,\mathbf{r}\right)=-\beta np-\frac{\mu_n}{\mu_p+\mu_n}\beta np_{\mathrm{trap}}, \tag{6.50}$$

$$\frac{\partial p_{\mathrm{trap}}}{\partial t}=\nu_{\mathrm{trap},p}\left(1-R_p\left(t,\mathbf{r}\right)\right)p-\frac{\mu_n}{\mu_p+\mu_n}\beta np_{\mathrm{trap}}, \tag{6.51}$$

$$\frac{\partial n_{\mathrm{trap}}}{\partial t}=\nu_{\mathrm{trap},n}\left(1-R_n\left(t,\mathbf{r}\right)\right)n-\frac{\mu_p}{\mu_p+\mu_n}\beta n_{\mathrm{trap}}p, \tag{6.52}$$

$$\frac{\partial Q}{\partial t}=\frac{V_{\mathrm{psu}}\left(t\right)-U\left(t\right)}{R\left(t\right)}-i_{\mathrm{c}}\left(t\right), \tag{6.53}$$

$$\frac{\partial}{\partial\mathbf{r}}\cdot\left[\varepsilon\left(\mathbf{r}\right)\frac{\partial V}{\partial\mathbf{r}}\right]=e\left(n-p+n_{\mathrm{trap}}-p_{\mathrm{trap}}\right), \tag{6.54}$$

$$R_p\left(t,\mathbf{r}\right)=\frac{\phi_p\left(t\right)*\left[p\left(t,\mathbf{r}\right)\exp\left(\frac{\mu_n}{\mu_p+\mu_n}\beta\int_0^t\mathrm{d}\tau n\left(\tau,\mathbf{r}\right)\right)\right]}{p\left(t,\mathbf{r}\right)\exp\left(\frac{\mu_n}{\mu_p+\mu_n}\beta\int_0^t\mathrm{d}\tau n\left(\tau,\mathbf{r}\right)\right)}, \tag{6.55}$$

$$R_n\left(t,\mathbf{r}\right)=\frac{\phi_n\left(t\right)*\left[n\left(t,\mathbf{r}\right)\exp\left(\frac{\mu_p}{\mu_p+\mu_n}\beta\int_0^t\mathrm{d}\tau p\left(\tau,\mathbf{r}\right)\right)\right]}{n\left(t,\mathbf{r}\right)\exp\left(\frac{\mu_p}{\mu_p+\mu_n}\beta\int_0^t\mathrm{d}\tau p\left(\tau,\mathbf{r}\right)\right)}, \tag{6.56}$$

$$\mathbf{\Gamma}_p\left(t,\mathbf{r}\right)=\mu_p\mathbf{E}\left(t,\mathbf{r}\right)p\left(t,\mathbf{r}\right)-\frac{\mu_p k_{\mathrm{B}}T}{e}\frac{\partial p}{\partial\mathbf{r}}, \tag{6.57}$$

$$\mathbf{\Gamma}_n\left(t,\mathbf{r}\right)=-\mu_n\mathbf{E}\left(t,\mathbf{r}\right)n\left(t,\mathbf{r}\right)-\frac{\mu_n k_{\mathrm{B}}T}{e}\frac{\partial n}{\partial\mathbf{r}}, \tag{6.58}$$

$$\mathbf{E}\left(t,\mathbf{r}\right)=-\frac{\partial V}{\partial\mathbf{r}}, \tag{6.59}$$

$$U\left(t\right)=\frac{Q\left(t\right)-Q_{U=0}\left(t\right)}{C}, \tag{6.60}$$

$$i_{\mathrm{c}}\left(t\right)=\oiint_{\mathcal{S}}\mathrm{d}\mathbf{S}\cdot e\left[\mathbf{\Gamma}_p\left(t,\mathbf{r}\right)-\mathbf{\Gamma}_n\left(t,\mathbf{r}\right)\right], \tag{6.61}$$

$$Q_{U=0}\left(t\right)=\oiint_{\mathcal{S}}\mathrm{d}\mathbf{S}\cdot\varepsilon\left(\mathbf{r}\right)\mathbf{E}_{U=0}\left(t,\mathbf{r}\right). \tag{6.62}$$

To simplify the resulting device simulation and to aid the interpretation of results, we nondimensionalise each physical quantity using a system of units similar to those used for one-dimensional systems by Juška [135, 138] and Philippa [134]. In this system of units, we make use of a reference voltage U_{ref} that depends on the experiment being performed. For the TOF experiment, this is simply the applied voltage, U_{applied}. For CELIV, this is the maximum of the voltage ramp, U_{max}. Similarly, the time scale is also chosen depending on the experiment. For the CELIV experiment, the most natural scale is the pulse time t_{pulse} of the voltage ramp. For other experiments, we

Table 6.1: System of units used in simulation.

Variable	Reference value
Voltage	$U_{\mathrm{ref}} = \begin{cases} U_{\mathrm{max}}, & \text{CELIV,} \\ U_{\mathrm{applied}}, & \text{TOF.} \end{cases}$
Length	d
Time	$t_{\mathrm{scale}} = \begin{cases} t_{\mathrm{pulse}}, & \text{CELIV,} \\ t_{\mathrm{tr}} = \frac{d^2}{\mu_{\mathrm{fast}} U_{\mathrm{ref}}}, & \text{other.} \end{cases}$
Permittivity	Cd/S
Bimolecular recombination coefficient	$\beta_{\mathrm{L}} = \frac{e(\mu_{\mathrm{n}}+\mu_{\mathrm{p}})}{\varepsilon_{\mathrm{s}}}$
Charge	CU_{ref}
Charge density	CU_{ref}/Sd
Number density	$CU_{\mathrm{ref}}/eSd = \varepsilon_{\mathrm{ref}} U_{\mathrm{ref}}/ed^2$
Particle flux	$CU_{\mathrm{ref}}/eSt_{\mathrm{scale}} = \varepsilon_{\mathrm{ref}} U_{\mathrm{ref}}/edt_{\mathrm{scale}}$
Mobility	$d^2/t_{\mathrm{scale}} U_{\mathrm{ref}}$
Electric field	U_{ref}/d
Current	$CU_{\mathrm{ref}}/t_{\mathrm{scale}}$
Resistance	t_{scale}/C
Temperature	$eU_{\mathrm{ref}}/k_{\mathrm{B}}$

choose to use the "transit time" of the faster carrier:

$$t_{\mathrm{tr}} = \frac{d^2}{\mu_{\mathrm{fast}} U_{\mathrm{ref}}}, \tag{6.63}$$

where d is our chosen length scale, the inter-electrode spacing. In analogy to a one-dimensional plane-parallel geometry, we also make use of the surface area S of the positive electrode to define the reference permittivity:

$$\varepsilon_{\mathrm{ref}} = \frac{Cd}{S}. \tag{6.64}$$

For the bimolecular recombination coefficient β, we normalise using the case of Langevin recombination [139–141]:

$$\beta_{\mathrm{L}} = \frac{e\left(\mu_{\mathrm{n}} + \mu_{\mathrm{p}}\right)}{\varepsilon_{\mathrm{s}}}, \tag{6.65}$$

where ε_{s} is the permittivity of the semiconductor.

The full system of units is listed in Table 6.1. In this system, we have the full dimensionless model:

$$\left[\frac{\partial}{\partial t}+\nu_{\mathrm{trap},p}\left(1-R_p\left(t,\mathbf{r}\right)\right)\right]p+\frac{\partial}{\partial\mathbf{r}}\cdot\mathbf{\Gamma}_p\left(t,\mathbf{r}\right)=-\frac{\mu_n+\mu_p}{\varepsilon_\mathrm{s}}\beta np-\frac{\mu_p}{\varepsilon_\mathrm{s}}\beta n_\mathrm{trap}p, \tag{6.66}$$

$$\left[\frac{\partial}{\partial t}+\nu_{\mathrm{trap},n}\left(1-R_n\left(t,\mathbf{r}\right)\right)\right]n+\frac{\partial}{\partial\mathbf{r}}\cdot\mathbf{\Gamma}_n\left(t,\mathbf{r}\right)=-\frac{\mu_n+\mu_p}{\varepsilon_\mathrm{s}}\beta np-\frac{\mu_n}{\varepsilon_\mathrm{s}}\beta np_\mathrm{trap}, \tag{6.67}$$

$$\frac{\partial p_\mathrm{trap}}{\partial t}=\nu_{\mathrm{trap},p}\left(1-R_p\left(t,\mathbf{r}\right)\right)p-\frac{\mu_n}{\varepsilon_\mathrm{s}}\beta np_\mathrm{trap}, \tag{6.68}$$

$$\frac{\partial n_\mathrm{trap}}{\partial t}=\nu_{\mathrm{trap},n}\left(1-R_n\left(t,\mathbf{r}\right)\right)n-\frac{\mu_p}{\varepsilon_\mathrm{s}}\beta n_\mathrm{trap}p, \tag{6.69}$$

$$\frac{\partial Q}{\partial t}=\frac{V_\mathrm{psu}\left(t\right)-U\left(t\right)}{R\left(t\right)}-i_\mathrm{c}\left(t\right), \tag{6.70}$$

$$\frac{\partial}{\partial\mathbf{r}}\cdot\left[\varepsilon\left(\mathbf{r}\right)\frac{\partial V}{\partial\mathbf{r}}\right]=n-p+n_\mathrm{trap}-p_\mathrm{trap}, \tag{6.71}$$

$$R_p\left(t,\mathbf{r}\right)=\frac{\phi_p\left(t\right)*\left[p\left(t,\mathbf{r}\right)\exp\left(\frac{\mu_n}{\varepsilon_\mathrm{s}}\beta\int_0^t\mathrm{d}\tau n\left(\tau,\mathbf{r}\right)\right)\right]}{p\left(t,\mathbf{r}\right)\exp\left(\frac{\mu_n}{\varepsilon_\mathrm{s}}\beta\int_0^t\mathrm{d}\tau n\left(\tau,\mathbf{r}\right)\right)}, \tag{6.72}$$

$$R_n\left(t,\mathbf{r}\right)=\frac{\phi_n\left(t\right)*\left[n\left(t,\mathbf{r}\right)\exp\left(\frac{\mu_p}{\varepsilon_\mathrm{s}}\beta\int_0^t\mathrm{d}\tau p\left(\tau,\mathbf{r}\right)\right)\right]}{n\left(t,\mathbf{r}\right)\exp\left(\frac{\mu_p}{\varepsilon_\mathrm{s}}\beta\int_0^t\mathrm{d}\tau p\left(\tau,\mathbf{r}\right)\right)}, \tag{6.73}$$

$$\mathbf{\Gamma}_p\left(t,\mathbf{r}\right)=\mu_p\mathbf{E}\left(t,\mathbf{r}\right)p\left(t,\mathbf{r}\right)-\mu_pT\frac{\partial p}{\partial\mathbf{r}}, \tag{6.74}$$

$$\mathbf{\Gamma}_n\left(t,\mathbf{r}\right)=-\mu_n\mathbf{E}\left(t,\mathbf{r}\right)n\left(t,\mathbf{r}\right)-\mu_nT\frac{\partial n}{\partial\mathbf{r}}, \tag{6.75}$$

$$\mathbf{E}\left(t,\mathbf{r}\right)=-\frac{\partial V}{\partial\mathbf{r}}, \tag{6.76}$$

$$U\left(t\right)=Q\left(t\right)-Q_{U=0}\left(t\right), \tag{6.77}$$

$$i_\mathrm{c}\left(t\right)=\oiint_{\mathcal{S}}\mathrm{d}\mathbf{S}\cdot\left[\mathbf{\Gamma}_p\left(t,\mathbf{r}\right)-\mathbf{\Gamma}_n\left(t,\mathbf{r}\right)\right], \tag{6.78}$$

$$Q_{U=0}\left(t\right)=\oiint_{\mathcal{S}}\mathrm{d}\mathbf{S}\cdot\varepsilon\left(\mathbf{r}\right)\mathbf{E}_{U=0}\left(t,\mathbf{r}\right). \tag{6.79}$$

We use the Julia programming language [142–144] to implement this model in a planar semiconductor device simulation. To solve the charged-particle continuity equations (6.66)–(6.69), we apply a finite volume spatial discretisation as described in Appendix E.1. To accurately evaluate the carrier fluxes (6.74) and (6.75), we make use of a third-order WENO method [145], detailed in Appendix E.2. Poisson's equation (6.71) is solved implicitly using a centred second-order finite difference scheme, outlined in Appendix E.3. This Poisson solution is found strictly within the domain of the semiconductor where it is required. This is achieved using the Schur complement method, as described in Appendix E.4. Finally, to perform the time integration, we make use of the Julia package ecosystem for solving differential equations, *DifferentialEquations.jl* [146]. In the trap-free case, we perform explicit time integration using the $(2,3)$ Runge-Kutta pair of Bogacki and Shampine [147], implemented as the `BS3` function in the *OrdinaryDiffEq.jl* package [148]. When traps are present, we first use Gauss-Lobatto quadrature to discretise the convolution integrals in Eqs. (6.72) and (6.73)

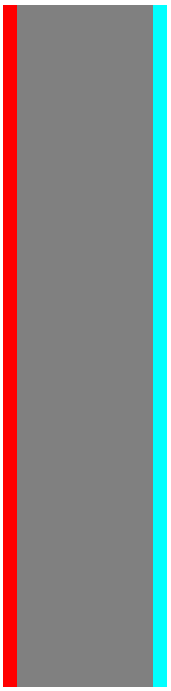

Figure 6.2: Considered plane-parallel device geometry. Grey denotes the semiconductor, while red and cyan denote the positive and negative electrodes, respectively. The electrodes have a thickness of $d/10$ and a length of $5d$, where d is the inter-electrode distance.

and then solve the resulting system of delay differential equations using the method of steps alongside the aforementioned explicit-in-time scheme. This is achieved simply by using the `MethodOfSteps` function provided by the *DelayDiffEq.jl* package [149] in conjunction with the `BS3` function.

6.2 Simulation benchmarks: Two-dimensional treatment of a plane-parallel device geometry

In this section, we benchmark the two-dimensional simulation described in the previous section against known results for one-dimensional plane-parallel systems. We do this using the plane-parallel geometry illustrated in Figure 6.2.

6.2.1 Single carrier injection and extraction

To begin with, we confirm the steady-state current for single charge-carrier injection and extraction in a one-dimensional plane-parallel system free of traps [150]:

$$\lim_{t\to\infty} i\left(t\right) = \frac{9\varepsilon_{\mathrm{s}}\mu A U_{\mathrm{ref}}^{2}}{8d^{3}}, \tag{6.80}$$

where A is the cross-sectional area of the device. We can approximate this system using the two-dimensional geometry illustrated in Figure 6.2. For this particular geometry,

we apply the system of units in Table 6.1 to find the dimensionless steady state current:

$$\lim_{t\to\infty} i\left(t\right) = \frac{75\varepsilon_{\mathrm{s}}\mu}{136}, \tag{6.81}$$

in terms of the dimensionless mobility and permittivity. We numerically determine the dimensionless semiconductor permittivity to be

$$\varepsilon_{\mathrm{s}} \approx 2.0575. \tag{6.82}$$

At first glance, this dimensionless permittivity appears to be roughly double what one would expect from a dimensionless plane-parallel system. This is discrepancy is simply an artefact of the system of units used (outlined in Table 6.1). In this system, the reference permittivity is defined in terms of the total surface area S of the positive electrode, rather than the cross-sectional area of the device A, which is conventionally used. The factor of two thus arises from the ratio of these areas, which in this case is $S/A = 51/25 \approx 2$.

Substituting the dimensionless permittivity (6.82), in conjunction with a dimensionless mobility of $\mu = 1$, into Eq. (6.81), results in the following dimensionless current in the steady state:

$$\lim_{t\to\infty} i\left(t\right) \approx 1.1347. \tag{6.83}$$

Indeed, this limiting value agrees well with the the corresponding simulated current trace, plotted in Figure 6.3.

6.2.2 Scher-Montroll behaviour

Here, we benchmark the trapping aspect of the simulation by performing a TOF experiment in the presence of long-lived traps. We consider an initial Beer-Lambert photogeneration of charge carriers due to light shone through the positive electrode, as depicted in Figure 6.4. To describe traps, we make use of the multiple trapping model trapping time distribution function (1.31). By varying the trap severity α, we observe the expected late-time Scher-Montroll power-law regime [12] with exponent $-\left(1+\alpha\right)$ in the TOF current traces plotted in Figure 6.5.

6.3 Planar time of flight experiment: Exploration of the parameter space

In this section, we simulate TOF experiments for the planar device geometry depicted in Figure 6.6 where charge is photogenerated initially by light masked by the electrodes, as depicted in Figure 6.7. Our aim here is to determine the effects that each simulation parameter has on the current trace in a planar-device TOF experiment, while highlighting any features that arise that are unique to the planar geometry.

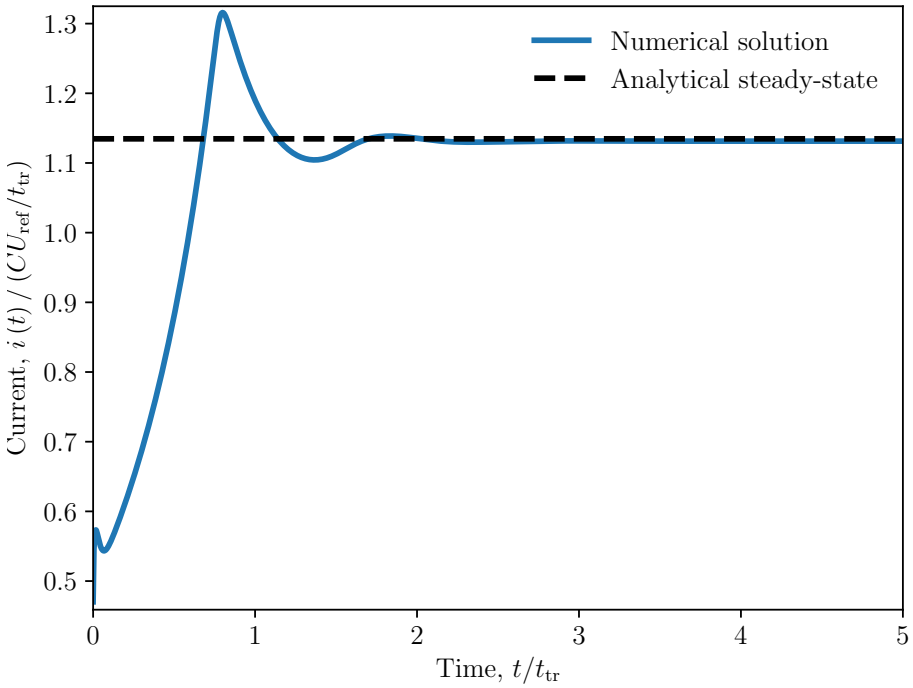

Figure 6.3: Current transient for single carrier injection and extraction for the plane-parallel geometry depicted in Figure 6.2. The device is initially devoid of carriers and the carrier mobility is set equal to $\mu = d^2/t_{\mathrm{tr}}U_{\mathrm{ref}}$. No traps, temperature or external circuit resistances are considered. The numerical steady-state current agrees well with the theoretical value, given by Eq. (6.83). The slight discrepancy is likely due to edge effects of the two-dimensional geometry, which are not accounted for in the derivation of the analytical current expression (6.80).

Unless stated otherwise, we consider a system with equal charge carrier mobilities $\mu_p = \mu_n = d^2/t_{\mathrm{tr}}U_{\mathrm{ref}}$, a relative semiconductor permittivity of $\varepsilon_{\mathrm{s}} = 3\varepsilon_0$, a Langevin recombination coefficient of $\beta = \beta_{\mathrm{L}}$, and an initial light intensity such that the initial photogenerated charge is $Q_{\mathrm{ph}} = 10^3 CU_{\mathrm{ref}}$. For simplicity, the temperature, T, external resistance R and the trapping frequencies, $\nu_{\mathrm{trap},p}$ and $\nu_{\mathrm{trap},n}$, will all be set equal to zero in this section. Figure 6.8 illustrates the planar TOF experiment for the aforementioned system by plotting the charge carrier number densities and the electric field at five instances in time. In this figure, we see the expected separation of charge carriers consistent with a stronger electric field closer to the electrodes. The specified Langevin bimolecular recombination is also seen to have an effect on the carrier number densities. The transient effect of space charge is also seen in the electric field shortly after the carriers begin to separate.

6.3.1 Light intensity

Figure 6.9 considers light of different intensities by varying the initial amount of photogenerated charge Q_{ph}. As expected, an increase in Q_{ph} causes a proportional increase in the initial current. After this initial plateau, the current begins to drop according to a power law. This only becomes obvious for large intensities, with $Q_{\mathrm{ph}} \geq 10^2 CU_{\mathrm{ref}}$, and occurs an order of magnitude earlier for every order of magnitude increase in Q_{ph}.

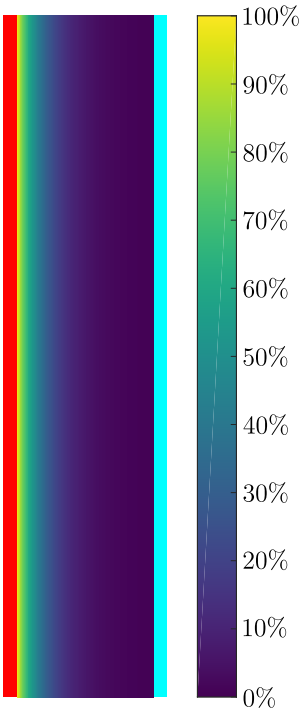

Figure 6.4: Intensity of light shone through the positive electrode of the plane-parallel device depicted in Figure 6.2. Here, optical absorption is described by the Beer-Lambert law with an absorption coefficient of $\alpha_{\mathrm{BL}} = 10d^{-1}$, where d is the inter-electrode distance. The light intensity has been normalised to its peak at the semiconductor surface. Charge carriers are photogenerated in pairs in direct proportion to this intensity.

These observations suggest that this drop in current is due to bimolecular recombination, which is expected to dominate in the large intensity, early time regime. Indeed, this can be confirmed by considering the following very simple zero-dimensional model for charge carrier number density that considers bimolecular recombination as the dominant process:

$$\frac{\mathrm{d}n}{\mathrm{d}t} = -\beta n\left(t\right)^2, \tag{6.84}$$

where we have assumed that electron and hole number densities remain equal. Assuming also that the current is proportional to this number density, we find that

$$i\left(t\right) \propto n\left(t\right) = \frac{n\left(0\right)}{1 + n\left(0\right)\beta t}. \tag{6.85}$$

Figure 6.10 plots this analytical expression for the current, which agrees qualitatively with Figure 6.9 at early times. Thus, up until the transit time $t = t_{\mathrm{tr}}$, charge is extracted from the inter-electrode channel along the surface of the device, while also undergoing substantial recombination. After $t = t_{\mathrm{tr}}$, the current does not drop instantaneously, as there are still charge carriers that were generated deeper within the device that are arriving later due both to their distance from the electrodes and the weaker electric field within the device. There is, finally, a sharp drop at $t \approx 15t_{\mathrm{tr}}$, corresponding to the maximum transit time from the opposite end of the device.

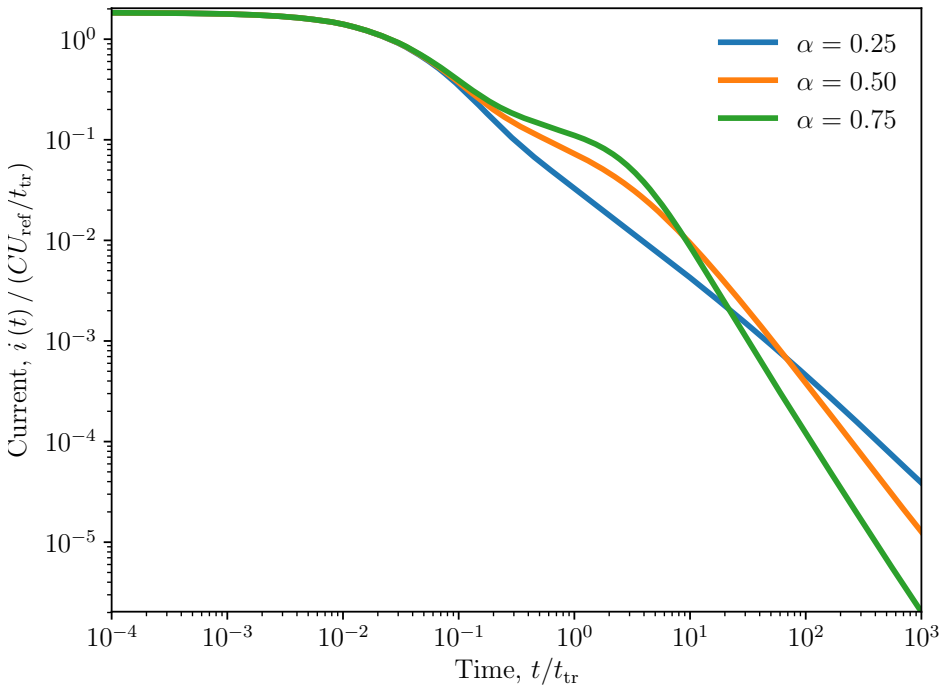

Figure 6.5: TOF current transients for the plane-parallel device depicted in Figure 6.2. An initial pulse of light is shone through the positive electrode and is absorbed according to the Beer-Lambert law with an absorption coefficient $\alpha_{\mathrm{BL}} = 10d^{-1}$, as shown in Figure 6.4. This results in the photogeneration of an initial $Q_{\mathrm{ph}} = CU_{\mathrm{ref}}$ of positive and negative charge carriers. Carrier mobilities are set equal to $\mu_p = \mu_n = d^2/t_{\mathrm{tr}}U_{\mathrm{ref}}$. No temperature or external circuit resistance is considered. Traps are considered with equal hole and electron trapping frequencies $\nu_{\mathrm{trap},p} = \nu_{\mathrm{trap},n} = 10t_{\mathrm{tr}}^{-1}$. Transport is dispersive as traps are described by a multiple trapping model trapping time distribution function, $\phi\,(t) = \alpha\nu_0\,(\nu_0 t)^{-\alpha-1}\,\gamma\,(\alpha+1, \nu_0 t)$ with $\nu_0 = 10t_{\mathrm{tr}}^{-1}$. As the trap severity α is varied, the decay of the current during the late-time Scher-Montroll power-law regime is seen to vary accordingly.

Figure 6.6: Considered planar device geometry. Grey denotes the semiconductor, while red and cyan denote the positive and negative electrodes, respectively. The semiconductor has a thickness equal to the length of the inter-electrode gap d and a width equal to $4d$. The electrodes have an equal thickness of $d/10$.

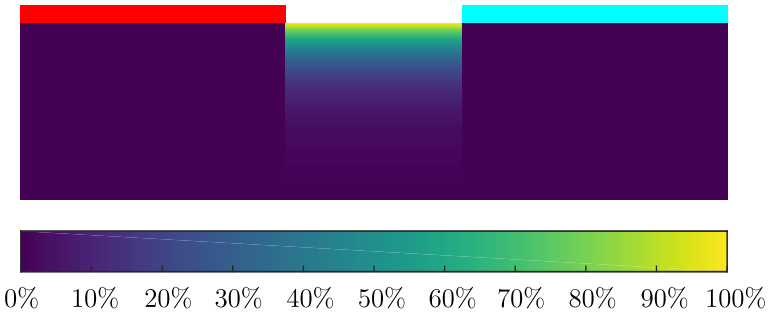

Figure 6.7: Intensity of light shone between the electrodes of the planar device depicted in Figure 6.6. Here, optical absorption is described by the Beer-Lambert law, with absorption coefficient $\alpha_{\mathrm{BL}} = 10d^{-1}$, where d is the inter-electrode distance. The light intensity has been normalised to its peak at the semiconductor surface. Charge carriers are photogenerated in pairs in direct proportion to this intensity.

6.3.2 Bimolecular recombination coefficient

Figure 6.11 varies the bimolecular recombination coefficient β. Evidently, as less recombination occurs, a greater amount of charge is able to extract and contribute to the current. In addition to this overall increase in current, a smaller β also delays the final drop in the current. This can be attributed to the restoring field that is formed when carriers separate, slowing further separation and delaying carrier extraction from the device. When the recombination coefficient β is high, more carriers undergo recombination, weakening this delaying space charge effect and resulting in an earlier extraction.

6.3.3 Absorption coefficient

Figure 6.12 varies the optical absorption coefficient of the semiconductor, α_{BL}. As α_{BL} is increased, more charge is photogenerated near the surface of the device, adjacent to the electrodes, resulting in an increase in the initial current, $i\,(0)$. The most notable feature of this plot, however, occurs at late times where both the rate and time of extraction are seen to vary with α_{BL}. These features arise due to the later arrival of charge carriers that were photogenerated deep within the device. There are very few such carriers when α_{BL} is large, resulting in an earlier and sharper drop in current after the inter-electrode channel is vacated.

6.3.4 Carrier mobility

Figure 6.13 varies the mobility ratio between charge carriers, $\mu_{\mathrm{fast}}/\mu_{\mathrm{slow}}$. As expected, increasing this ratio slows the transport of carriers, resulting in a decrease in the current initially. At intermediate times, recombination causes all current traces to decay in unison. Finally, at late times, the total extraction of charge is dictated by the mobility of the slower carrier, μ_{slow}, occurring at a time proportional to the mobility ratio, $\mu_{\mathrm{fast}}/\mu_{\mathrm{slow}}$.

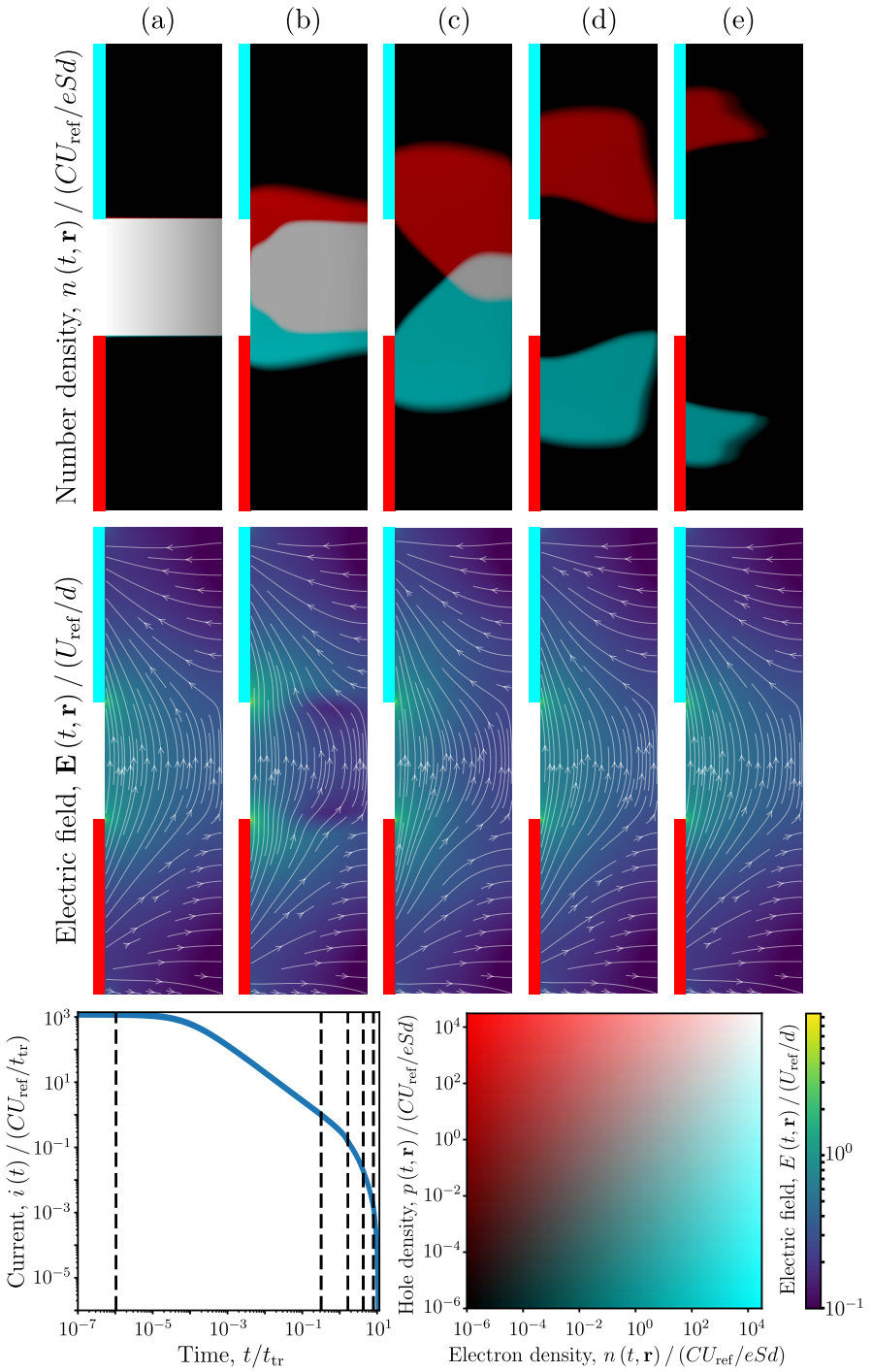

Figure 6.8: Plots of number density and electric field at five instances in time (a)–(e) for a TOF experiment in the planar geometry depicted in Figure 6.6. These instances are denoted on the accompanying current plot using dashed vertical lines. Charge carriers are photogenerated as depicted in Figure 6.7 by light masked by the electrodes that is absorbed according to the Beer-Lambert law with optical absorption coefficient $\alpha_{\mathrm{BL}} = 10d^{-1}$. Here we have the charge carrier mobilities $\mu_p = \mu_n = d^2/t_{\mathrm{tr}}U_{\mathrm{ref}}$, a relative semiconductor permittivity of $\varepsilon_{\mathrm{s}} = 3\varepsilon_0$, a Langevin recombination coefficient $\beta = \beta_{\mathrm{L}}$, and an initial light intensity such that the initial photogenerated charge is $Q_{\mathrm{ph}} = 10^3 CU_{\mathrm{ref}}$. For simplicity, the temperature, T, external resistance, R, and the trapping frequencies, $\nu_{\mathrm{trap},p}$ and $\nu_{\mathrm{trap},n}$, are all set equal to zero. Due to the specified Langevin bimolecular recombination, we observe an overall decrease in number density with time that is most prominent between (a) and (b). Also, due to the equal mobilities of the charge carriers, we observe a symmetric separation of charge carriers that occurs quicker adjacent to the electrodes, as expected from the increased field strength there. Transient space charge effects are seen most clearly in the electric field in (b), shortly after carrier separation has begun.

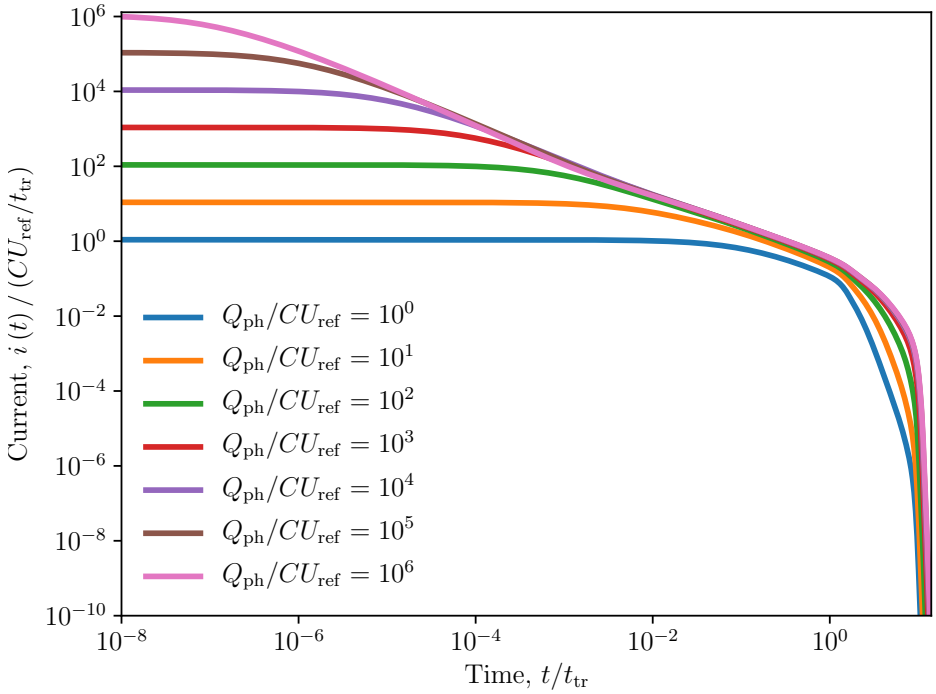

Figure 6.9: TOF current transients for various photogenerated charges, Q_{ph}, for the planar geometry depicted in Figure 6.6. Charge carriers are photogenerated as depicted in Figure 6.7 by light masked by the electrodes that is absorbed according to the Beer-Lambert law with optical absorption coefficient $\alpha_{\mathrm{BL}} = 10d^{-1}$. Here we have the charge carrier mobilities $\mu_p = \mu_n = d^2/t_{\mathrm{tr}}U_{\mathrm{ref}}$, a relative semiconductor permittivity of $\varepsilon_{\mathrm{s}} = 3\varepsilon_0$ and a Langevin recombination coefficient $\beta = \beta_{\mathrm{L}}$. For simplicity, the temperature, T, external resistance, R, and the trapping frequencies, $\nu_{\mathrm{trap},p}$ and $\nu_{\mathrm{trap},n}$, are all set equal to zero. Increasing the total amount of photogenerated charge Q_{ph} increases the current up until a point, after which the resulting substantial recombination limits any further current increase.

6.4 Planar time of flight characterisation of the recombination coefficient

In this section, we explore a potential experimental technique for quantifying the recombination coefficient β, based upon the simple zero-dimensional model (6.84) for charge transport used in Section 6.3.1 to describe the qualitative features of the recombination-dominant regimes of the TOF current transients in Figure 6.9:

$$\frac{\mathrm{d}n}{\mathrm{d}t} = -\beta n\left(t\right)^2 . \tag{6.86}$$

We assume that the current $i\left(t\right)$ measured in a TOF experiment is proportional to the above number density $n\left(t\right)$. Specifically, for electrons and holes extracting due to an effective electric field E through electrode-semiconductor interfaces of cumulative area A, we have

$$i\left(t\right) = e\left(\mu_n + \mu_p\right) EAn\left(t\right) . \tag{6.87}$$

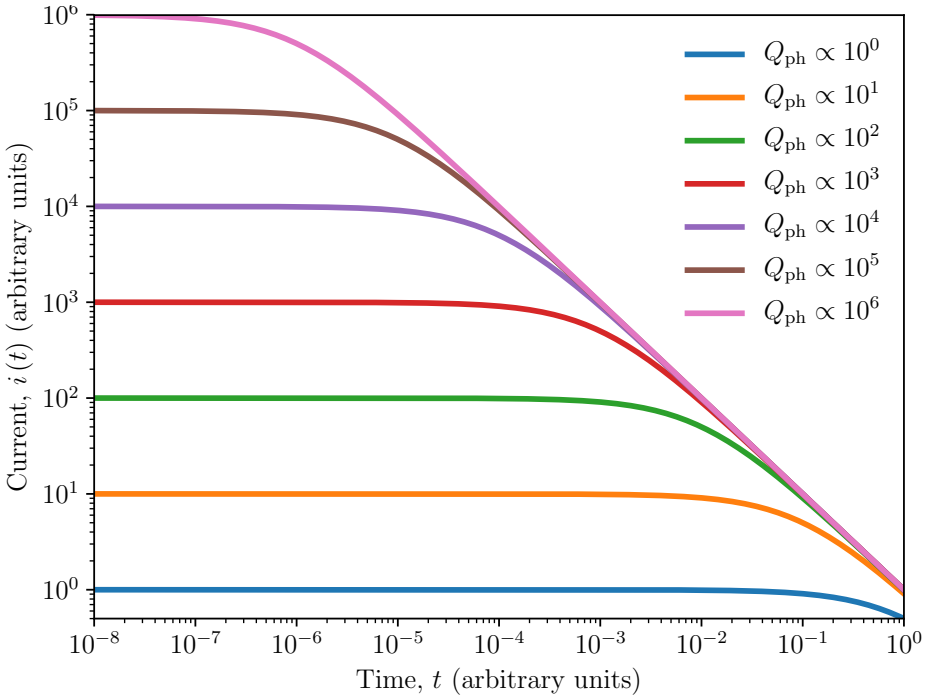

Figure 6.10: TOF current transients for a simple analytical model (6.85) as light intensity is varied through the initial photogenerated charge, Q_{ph}. This plot is qualitatively similar to the simulated Figure 6.9, over the same time domain.

Using this relationship, the number density solution (6.85) of Eq. (6.86) provides the following expression for the current:

$$i\,(t) = \left[\frac{1}{i\,(0)} + \frac{\beta t}{e\,(\mu_n + \mu_p)\,EA}\right]^{-1}, \tag{6.88}$$

which, after nondimensionalisation using Table 6.1, becomes

$$i\,(t) = \left[\frac{1}{i\,(0)} + \frac{S\beta}{EA\varepsilon_{\mathrm{s}}}t\right]^{-1}, \tag{6.89}$$

where S is the surface area of the positive electrode and ε_{s} is the dimensionless permittivity of the semiconductor. To quantify the recombination coefficient β, we consider the time required for the current to decay to half of its initial value, $t_{\frac{1}{2}}$, satisfying $i\left(t_{\frac{1}{2}}\right) = i\,(0)\,/2$. This results in the following expression for the recombination coefficient in terms of the half-decay time $t_{\frac{1}{2}}$:

$$\beta = \frac{EA\varepsilon_{\mathrm{s}}}{Si\,(0)\,t_{\frac{1}{2}}}. \tag{6.90}$$

This equation provides a way to determine the recombination coefficient experimentally, given knowledge of the material geometry, permittivity, and charge carrier mobilities. Using the planar device simulation presented in this chapter, we would like to determine when the above equation may be a valid representation for β. Notice that, for it to be valid, the following product must remain constant for different light intensities and

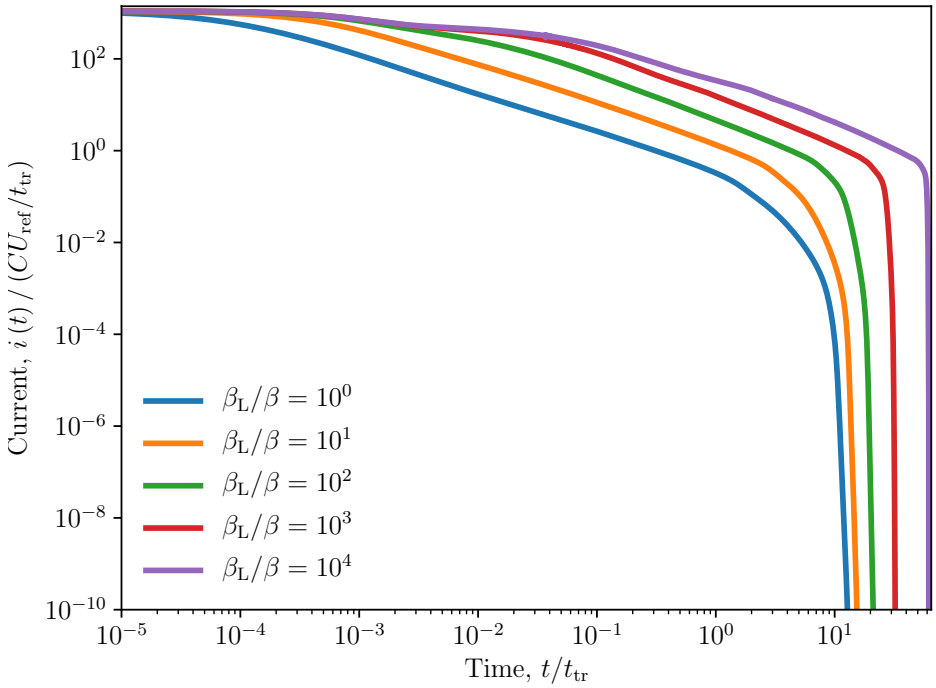

Figure 6.11: TOF current transients for various recombination coefficients, β, for the planar geometry depicted in Figure 6.6. Charge carriers are photogenerated as depicted in Figure 6.7 by light masked by the electrodes that is absorbed according to the Beer-Lambert law with optical absorption coefficient $\alpha_{\mathrm{BL}} = 10d^{-1}$. Here we have the charge carrier mobilities $\mu_p = \mu_n = d^2/t_{\mathrm{tr}}U_{\mathrm{ref}}$, a relative semiconductor permittivity of $\varepsilon_{\mathrm{s}} = 3\varepsilon_0$, and an initial light intensity such that the initial photogenerated charge is $Q_{\mathrm{ph}} = 10^3 CU_{\mathrm{ref}}$. For simplicity, the temperature, T, external resistance, R, and the trapping frequencies, $\nu_{\mathrm{trap},p}$ and $\nu_{\mathrm{trap},n}$, are all set equal to zero. At early times, very little recombination has occurred and all plots coincide. For smaller recombination coefficients β/β_{L}(larger β_{L}/β), a substantial amount of oppositely charged carriers remain to be attracted to one another via space charge effects, as seen by the resulting extraction delays.

across different materials with different recombination coefficients:

$$i\,(0)\,\beta t_{\frac{1}{2}} = \frac{EA\varepsilon_{\mathrm{s}}}{S} = \text{constant}. \tag{6.91}$$

We plot this product in Figure 6.14 against the initial photogenerated charge Q_{ph} for a variety of recombination coefficients β. As expected, each plot is seen to become constant in the regime where recombination dominates (beyond roughly $Q_{\mathrm{ph}} = 10^3 CU_{\mathrm{ref}}$ for the cases considered). Importantly, even as Q_{ph} becomes very large, each plot remains constant, suggesting that space-charge effects do not compromise the validity of the recombination coefficient expression (6.90). Unfortunately, while the product $i\,(0)\,\beta t_{\frac{1}{2}}$ does approach a constant as Q_{ph} increases, the value of this constant changes depending on the recombination coefficient β considered. This is contrary to what is concluded by Eq. (6.91). This suggests that, if Eq. (6.90) is to be used in practice to compute the recombination coefficient, then it needs to be corrected in some way to improve its accurate in this case.

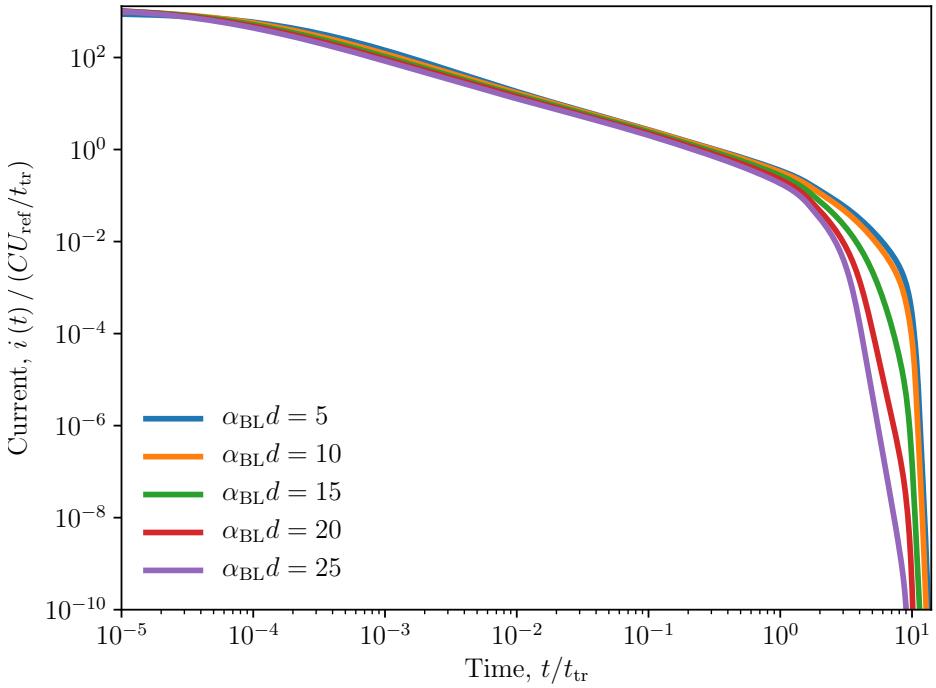

Figure 6.12: TOF current transients for various optical absorption coefficients, α_{BL}, for the planar geometry depicted in Figure 6.6. Charge carriers are photogenerated as depicted in Figure 6.7 by light masked by the electrodes that is absorbed according to the Beer-Lambert law. Here we have the charge carrier mobilities $\mu_p = \mu_n = d^2/t_{\mathrm{tr}}U_{\mathrm{ref}}$, a relative semiconductor permittivity of $\varepsilon_{\mathrm{s}} = 3\varepsilon_0$, a Langevin recombination coefficient $\beta = \beta_{\mathrm{L}}$, and an initial light intensity such that the initial photogenerated charge is $Q_{\mathrm{ph}} = 10^3 CU_{\mathrm{ref}}$. For simplicity, the temperature, T, external resistance, R, and the trapping frequencies, $\nu_{\mathrm{trap},p}$ and $\nu_{\mathrm{trap},n}$, are all set equal to zero. At early times, a large absorption coefficient α_{BL} causes more carriers to photogenerate near the electrodes, increasing the initial current. This consequently means that fewer such carriers extract at later times. Indeed, for smaller values of α_{BL}, where more charge is photogenerated deeper within the device, extraction is seen to occur at a later time.

6.5 Effects of trapping in planar charge transport experiments

In this section, we explore what effects traps have on the current measured in charge transport experiments for the planar geometry in Figure 6.6, with the Beer-Lambert initial condition as depicted in Figure 6.7. We choose a planar device geometry as its comparatively large transit times to thin film devices provide many more opportunities for charge carriers to become trapped within the device before extraction. Thus, potentially allowing for easier experimental characterisation of disordered semiconductors containing traps.

We begin by considering the TOF experiment, continuing the parameter exploration started in Section 6.3, and then move on to also consider the Photo-CELIV experiment, described in Section 1.2.2. Unless stated otherwise, we consider a system with equal charge carrier mobilities $\mu_p = \mu_n = d^2/t_{\mathrm{tr}}U_{\mathrm{ref}}$, a relative semiconductor

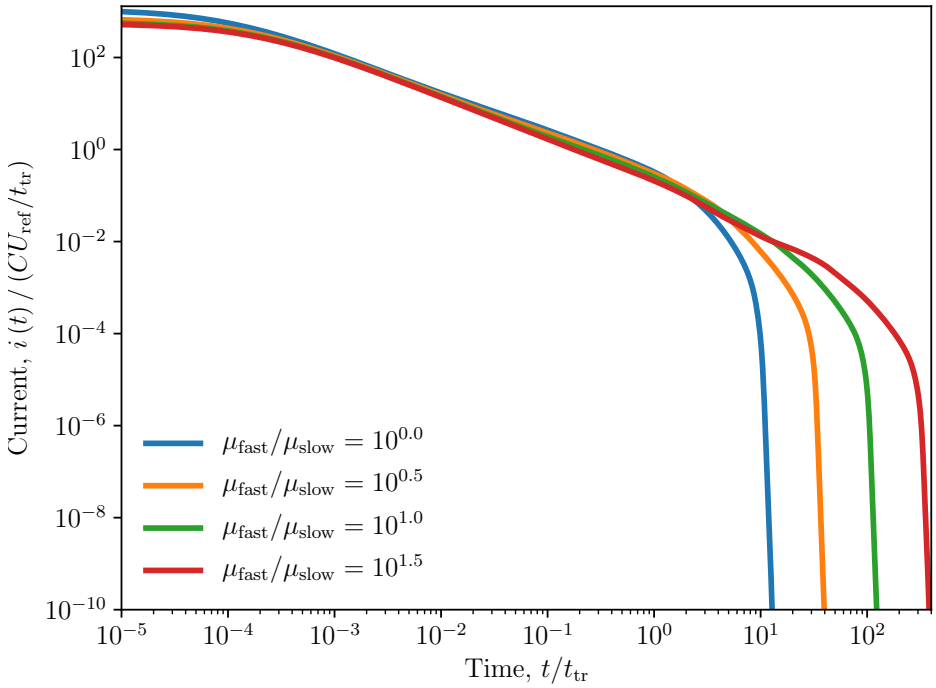

Figure 6.13: TOF current transients for various charge carrier mobility ratios, $\mu_{\mathrm{fast}}/\mu_{\mathrm{slow}}$, for the planar geometry depicted in Figure 6.6. Charge carriers are photogenerated as depicted in Figure 6.7 by light masked by the electrodes that is absorbed according to the Beer-Lambert law with optical absorption coefficient $\alpha_{\mathrm{BL}} = 10d^{-1}$. Here we have a relative semiconductor permittivity of $\varepsilon_{\mathrm{s}} = 3\varepsilon_0$, a Langevin recombination coefficient $\beta = \beta_{\mathrm{L}}$, and an initial light intensity such that the initial photogenerated charge is $Q_{\mathrm{ph}} = 10^3 CU_{\mathrm{ref}}$. For simplicity, the temperature, T, external resistance, R, and the trapping frequencies, $\nu_{\mathrm{trap},p}$ and $\nu_{\mathrm{trap},n}$, are all set equal to zero. At early times, large mobility ratios $\mu_{\mathrm{fast}}/\mu_{\mathrm{slow}}$ have lower initial currents due to the introduction of slower carriers. At late times, these slower carriers are observed to extract at a time proportional to the ratio of mobilities.

permittivity of $\varepsilon_{\mathrm{s}} = 3\varepsilon_0$, a Langevin recombination coefficient of $\beta = \beta_{\mathrm{L}}$, and an initial light intensity such that the initial photogenerated charge is $Q_{\mathrm{ph}} = 10^3 CU_{\mathrm{ref}}$. For simplicity, the temperature, T, and the external resistance R will be set equal to zero. In order for multiple trapping events to occur within the reference time t_{ref}, we consider a system with $\nu_{\mathrm{trap},p} = \nu_{\mathrm{trap},n} = 10t_{\mathrm{ref}}^{-1}$. We again consider a multiple trapping model trapping time distribution $\phi(t) = \alpha\nu_0 (\nu_0 t)^{-\alpha-1} \gamma(\alpha+1, \nu_0 t)$, here with $\alpha = 0.5$ and $\nu_0 = 100t_{\mathrm{ref}}^{-1}$. Figure 6.15 illustrates the TOF experiment for the aforementioned system by plotting the charge carrier number densities and the electric field at five instances in time. This figure depicts what Figure 6.8 would look like if it considered the presence of traps. Unlike Figure 6.8, in this figure there is no clear separation of electrons and holes. In fact, memory of the initial condition in the form of trapped carriers persists through later and later times. In addition, the trapping of charge carriers is seen to extend the duration of the transient space charge effects observed in Figure 6.8.

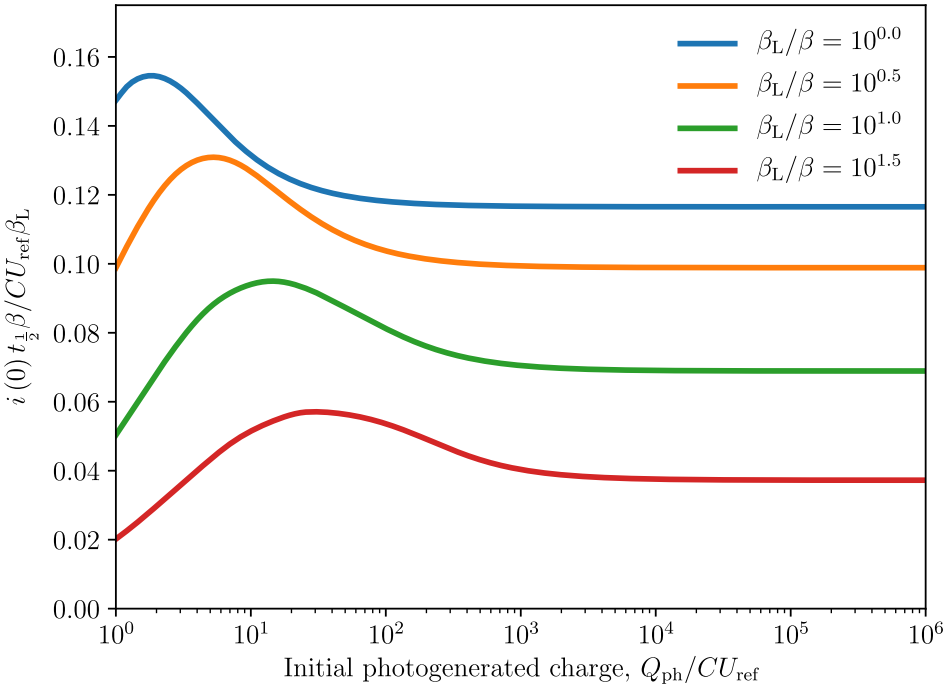

Figure 6.14: Plots of the product of the initial current, $i(0)$, the bimolecular recombination coefficient, β, and the half-decay time for the current, $t_{\frac{1}{2}}$, versus the initial photogenerated charge, Q_{ph}, for different values of the recombination coefficient, β, in a planar TOF experiment. The planar geometry considered is depicted in Figure 6.6, with charge carriers photogenerated as depicted in Figure 6.7 by light masked by the electrodes that decays according to the Beer-Lambert law with optical absorption coefficient $\alpha_{BL} = 10d^{-1}$. Here we have a relative semiconductor permittivity of $\varepsilon_s = 3\varepsilon_0$ and for simplicity, the temperature, T, external resistance, R, and the trapping frequencies, $\nu_{trap,p}$ and $\nu_{trap,n}$, are all set equal to zero. According to the zero-dimensional model (6.86) this plotted product $i(0)\,\beta t_{\frac{1}{2}}$ should be equal to a constant (6.91) independent of the recombination coefficient and initial laser light intensity. If this is true, then the recombination coefficient β can be computed from experimental measurements using Eq. 6.90. Promisingly, at large light intensities (large Q_{ph}), we indeed see $i(0)\,\beta t_{\frac{1}{2}}$ approach a constant. Unfortunately, the constant changes depending on the recombination coefficient β, suggesting that the zero-dimensional model (6.86) needs to be corrected in some fashion before Eq. 6.90 becomes a practical representation of the recombination coefficient.

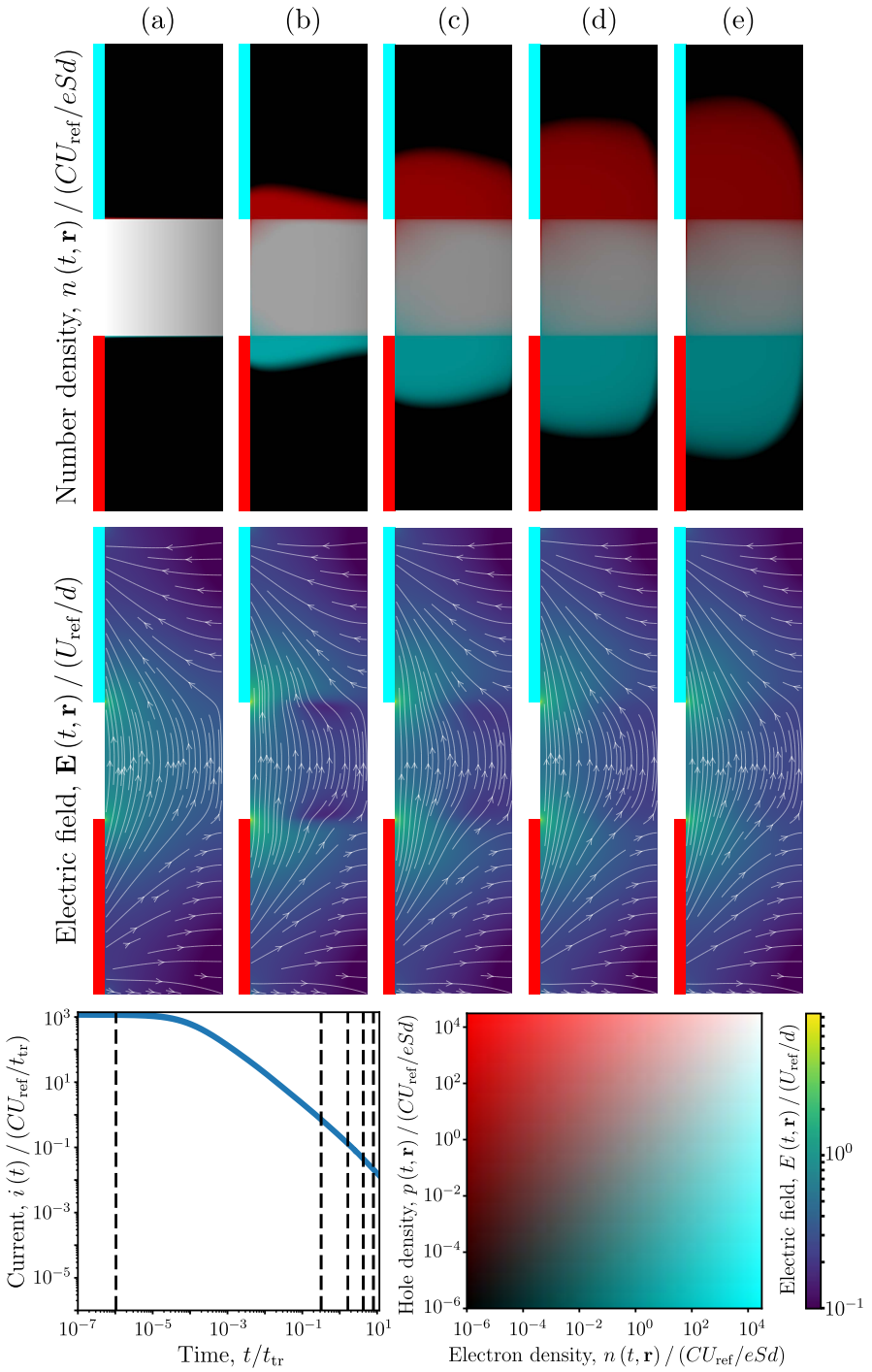

Figure 6.15: Plots of number density and electric field at five instances in time (a)–(e) for a TOF experiment in the planar geometry depicted in Figure 6.6. These instances are denoted on the accompanying current plot using dashed vertical lines. Charge carriers are photogenerated as depicted in Figure 6.7 by light masked by the electrodes that is absorbed according to the Beer-Lambert law with optical absorption coefficient $\alpha_{\text{BL}} = 10d^{-1}$. Here we have the charge carrier mobilities $\mu_p = \mu_n = d^2/t_{\text{tr}}U_{\text{ref}}$, a relative semiconductor permittivity of $\varepsilon_{\text{s}} = 3\varepsilon_0$, a Langevin recombination coefficient $\beta = \beta_{\text{L}}$, and an initial light intensity such that the initial photogenerated charge is $Q_{\text{ph}} = 10^3 CU_{\text{ref}}$. For simplicity, the temperature, T, and external resistance, R, are set equal to zero. Trapping occurs at equal frequencies for both holes and electrons, $\nu_{\text{trap},p} = \nu_{\text{trap},n} = 10t_{\text{tr}}^{-1}$, and traps are described by a multiple trapping model trapping time distribution function, $\phi(t) = \alpha\nu_0 (\nu_0 t)^{-\alpha-1} \gamma(\alpha+1, \nu_0 t)$ with $\alpha = 0.5$ and $\nu_0 = 100t_{\text{tr}}^{-1}$. Unlike Figure 6.8, which lacks traps, there is no clear separation of electrons and holes here. In fact, memory of the initial condition in the form of trapped carriers persists through (a)–(e). In addition, the trapping of charge carriers is seen to extend the transient space charge effects observed in Figure 6.8 (b), which here persist through (b)–(e).

6.5.1 Planar TOF experiment

We consider here the effects of traps on the current measured in a TOF experiment in planar geometry.

Figure 6.16 varies the trap severity α and compares the resulting current transients to the case without traps. At very early times all curves coincide as very few trapping events have yet occurred. Then, at the expected time of $t \approx \nu_{\mathrm{trap},p}^{-1} = \nu_{\mathrm{trap},n}^{-1} = 10^{-1} t_{\mathrm{tr}}$, carriers begin to enter traps, causing a corresponding drop in the relevant current traces. This drop is greater for traps of greater severity (smaller α). Finally, at late times, the current consists entirely of previously-trapped particles. This means the current is actually higher here in cases of more severe traps. As expected, in this late-time regime we observe the same Scher-Montroll asymptotic power-law behaviour that was seen with the plane-parallel system in Figure 6.5.

In addition to α, which determines how long-lived traps are, in Figure 6.17 we also vary the frequencies at which carriers enter traps, $\nu_{\mathrm{trap},p}$ and $\nu_{\mathrm{trap},n}$. As before, at early times, very few trapping events have occurred and all curves coincide. Then, one after another, starting with the case of most frequent trapping, we have a drop in the current due to charge carriers entering traps. These drops in current are accompanied by proportional increases in the current at late times due to said carriers leaving traps. Although there are differences in the precise amount of current at late times, the power law decay is consistent across all cases for the considered trap severity of $\alpha = 0.5$.

6.5.2 Planar Photo-CELIV experiment

We consider here the effects of traps on the current measured in a Photo-CELIV experiment in planar geometry.

Figures 6.18 and 6.19 vary the trap severity α and the trapping frequencies, $\nu_{\mathrm{trap},p}$ and $\nu_{\mathrm{trap},n}$, respectively, for plots of the CELIV current trace. As in the previous section, we find that increasing either the duration or frequency of traps results in a decrease in current at early times and a corresponding increase in current at late times. This has the effect of broadening the Photo-CELIV current transient, resulting in current traces that are qualitatively similar to those presented by Philippa [134] for a plane-parallel system with a related multiple trapping model.

6.5.3 Planar RPV experiment

We consider here what effects traps have on the transit times determined from an RPV experiment in planar geometry.

In order to probe transit times while minimising charge carrier recombination, we consider low light intensities with photogenerated charge $Q_{\mathrm{ph}} \ll CU_{\mathrm{ref}}$. Figures 6.20 and 6.21 vary the trap severity α and the trapping frequencies, $\nu_{\mathrm{trap},p}$ and $\nu_{\mathrm{trap},n}$, respectively, for plots of the RPV voltage trace. Each figure plots the trap-free case (in black), where the transit times appear as clear "shoulders" in the voltage transient at roughly $t \approx t_{\mathrm{tr}}$ and $t \approx 10 t_{\mathrm{tr}}$, as expected from the chosen charge carrier mobility

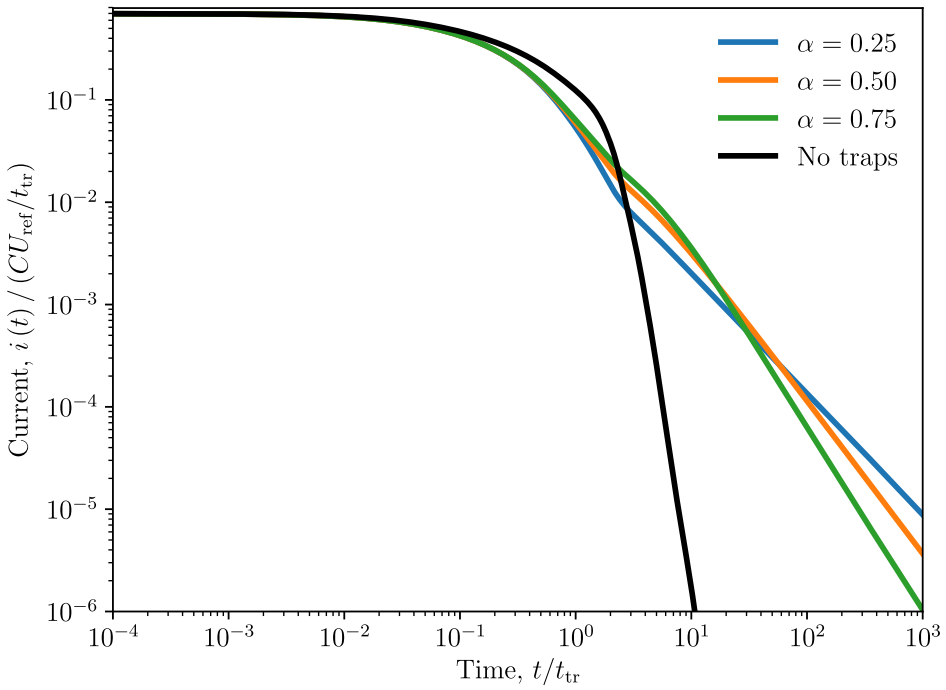

Figure 6.16: TOF current transients for various trap severities, α, alongside the trap-free case for the planar geometry depicted in Figure 6.6. Charge carriers are photogenerated as depicted in Figure 6.7 by light masked by the electrodes that is absorbed according to the Beer-Lambert law with optical absorption coefficient $\alpha_{\mathrm{BL}} = 10d^{-1}$. Here we have the charge carrier mobilities $\mu_p = \mu_n = d^2/t_{\mathrm{tr}}U_{\mathrm{ref}}$, a relative semiconductor permittivity of $\varepsilon_{\mathrm{s}} = 3\varepsilon_0$, a Langevin recombination coefficient $\beta = \beta_{\mathrm{L}}$, and an initial light intensity such that the initial photogenerated charge is $Q_{\mathrm{ph}} = CU_{\mathrm{ref}}$. For simplicity, the temperature, T, external resistance, R are set equal to zero. Trapping occurs at equal frequencies for both holes and electrons, $\nu_{\mathrm{trap},p} = \nu_{\mathrm{trap},n} = 1t_{\mathrm{tr}}^{-1}$, and traps are described by a multiple trapping model trapping time distribution function, $\phi\,(t) = \alpha\nu_0\,(\nu_0 t)^{-\alpha-1}\,\gamma\,(\alpha+1, \nu_0 t)$ with $\nu_0 = 100t_{\mathrm{tr}}^{-1}$. At early times, few trapping events have occurred and all plots coincide. At intermediate times, prior to the carrier transit time, the case of largest trap severity α (blue curve) has the lowest current, due to particles remaining trapped for a longer duration. At late times, these trapped particles exit the system, resulting in the blue curve exceeding all the others. In each case, the late time asymptotic slope of $-(1+\alpha)$ is observed, indicative of dispersive transport.

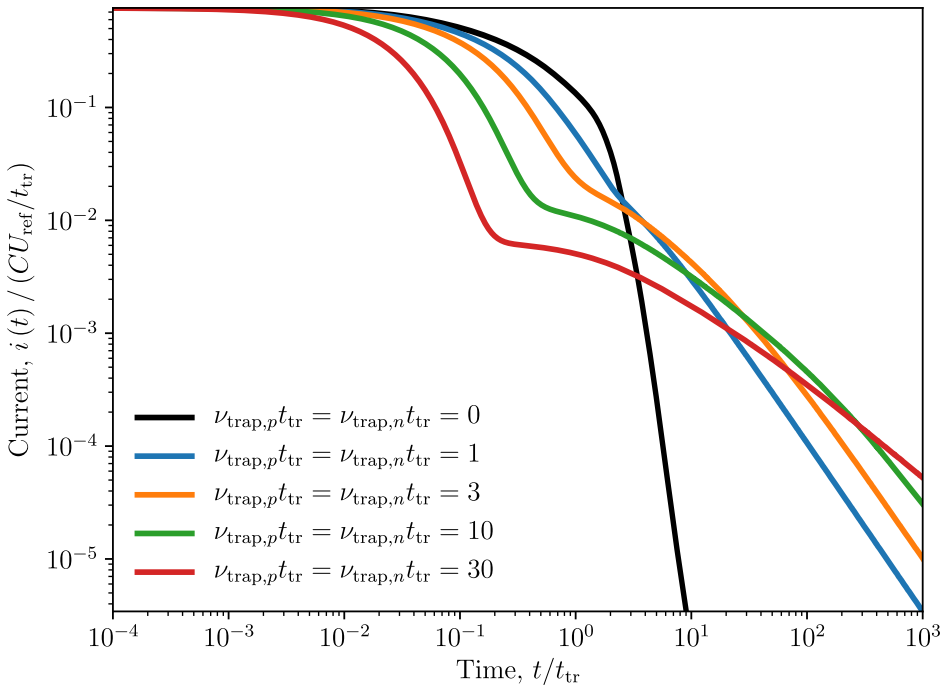

Figure 6.17: TOF current transients for various trapping frequencies, $\nu_{\mathrm{trap},p}$ and $\nu_{\mathrm{trap},n}$, for the planar geometry depicted in Figure 6.6. Charge carriers are photogenerated as depicted in Figure 6.7 by light masked by the electrodes that is absorbed according to the Beer-Lambert law with optical absorption coefficient $\alpha_{\mathrm{BL}} = 10d^{-1}$. Here we have the charge carrier mobilities $\mu_p = \mu_n = d^2/t_{\mathrm{tr}}U_{\mathrm{ref}}$, a relative semiconductor permittivity of $\varepsilon_{\mathrm{s}} = 3\varepsilon_0$, a Langevin recombination coefficient $\beta = \beta_{\mathrm{L}}$, and an initial light intensity such that the initial photogenerated charge is $Q_{\mathrm{ph}} = CU_{\mathrm{ref}}$. For simplicity, the temperature, T, external resistance, R are set equal to zero. Traps are described by a multiple trapping model trapping time distribution function, $\phi\,(t) = \alpha\nu_0\,(\nu_0 t)^{-\alpha-1}\,\gamma\,(\alpha+1, \nu_0 t)$ with $\alpha = 0.5$ and $\nu_0 = 100t_{\mathrm{tr}}^{-1}$. At early times, few trapping events have occurred and all plots coincide. At intermediate times, prior to the carrier transit time, the case of largest trapping frequencies $\nu_{\mathrm{trap},p}$ and $\nu_{\mathrm{trap},n}$ (red curve) has the lowest current, due to having more particles entering traps. At late times, these trapped particles exit the system, resulting in the red curve exceeding all the others. In each case, the same late time asymptotic slope of $-\,(1+\alpha) = -1.5$ is observed, indicating dispersive transport.

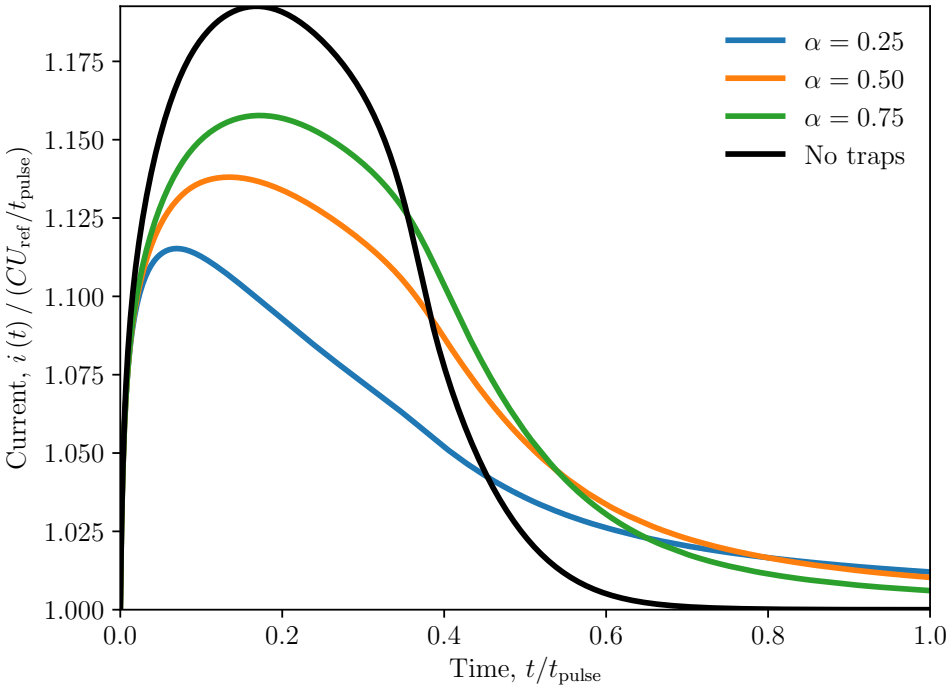

Figure 6.18: Photo-CELIV current transients for various trap severities, α, alongside the trap-free case for the planar geometry depicted in Figure 6.6. Charge carriers are photogenerated as depicted in Figure 6.7 by light masked by the electrodes that is absorbed according to the Beer-Lambert law with optical absorption coefficient $\alpha_{\mathrm{BL}} = 10d^{-1}$. Here we have the charge carrier mobilities $\mu_p = \mu_n = 20d^2/t_{\mathrm{pulse}}U_{\mathrm{ref}}$, a relative semiconductor permittivity of $\varepsilon_{\mathrm{s}} = 3\varepsilon_0$, a Langevin recombination coefficient $\beta = \beta_{\mathrm{L}}$, and an initial light intensity such that the initial photogenerated charge is $Q_{\mathrm{ph}} = CU_{\mathrm{ref}}$. For simplicity, the temperature, T, external resistance, R are set equal to zero. Trapping occurs at equal frequencies for both holes and electrons, $\nu_{\mathrm{trap},p} = \nu_{\mathrm{trap},n} = 10t_{\mathrm{pulse}}^{-1}$, and traps are described by a multiple trapping model trapping time distribution function, $\phi\,(t) = \alpha\nu_0\,(\nu_0 t)^{-\alpha-1}\,\gamma\,(\alpha+1, \nu_0 t)$ with $\nu_0 = 100t_{\mathrm{pulse}}^{-1}$. Increasing the trap severity α is seen to broaden the CELIV current transient.

ratio $\mu_{\mathrm{fast}}/\mu_{\mathrm{slow}} = 10$. At early times, very few trapping events have a chance to occur and all curves in both figures coincide with this trap-free case. At later times, the curves separate due to trapping. By increasing the frequency or severity of traps, we find that the shoulders become less well-defined, due to the distribution of arrival times of previously-trapped carriers. Specifically, the slower carrier shoulder is most affected, as it occurs later in time. Overall, we find the RPV method is resilient at characterising the carrier transit times even in many cases where traps are present. It is only when trapping is very severe or frequent, that the shoulders are seen to vanish completely.

6.6 Conclusion

In this chapter, we developed a model for charge carrier transport in planar organic semiconductors that accounts for drift, diffusion, trapping, detrapping, recombination and space-charge effects. We then used this model to implement a Julia-based

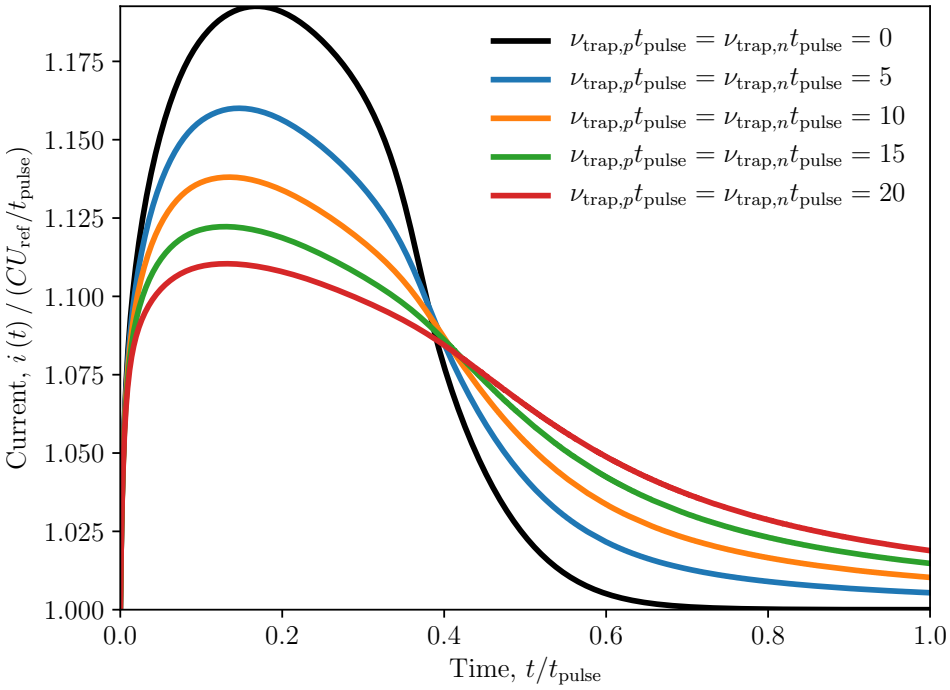

Figure 6.19: Photo-CELIV current transients for various trapping frequencies, $\nu_{\mathrm{trap},p}$ and $\nu_{\mathrm{trap},n}$, for the planar geometry depicted in Figure 6.6. Charge carriers are photogenerated as depicted in Figure 6.7 by light masked by the electrodes that is absorbed according to the Beer-Lambert law with optical absorption coefficient $\alpha_{\mathrm{BL}} = 10d^{-1}$. Here we have the charge carrier mobilities $\mu_p = \mu_n = 20d^2/t_{\mathrm{pulse}}U_{\mathrm{ref}}$, a relative semiconductor permittivity of $\varepsilon_{\mathrm{s}} = 3\varepsilon_0$, a Langevin recombination coefficient $\beta = \beta_{\mathrm{L}}$, and an initial light intensity such that the initial photogenerated charge is $Q_{\mathrm{ph}} = CU_{\mathrm{ref}}$. For simplicity, the temperature, T, external resistance, R are set equal to zero. Traps are described by a multiple trapping model trapping time distribution function, $\phi\,(t) = \alpha\nu_0\,(\nu_0 t)^{-\alpha-1}\,\gamma\,(\alpha+1, \nu_0 t)$ with $\alpha = 0.5$ and $\nu_0 = 100t_{\mathrm{pulse}}^{-1}$. Increasing the trapping frequencies $\nu_{\mathrm{trap},p}$ and $\nu_{\mathrm{trap},n}$ is seen to broaden the CELIV current transient.

simulation of planar organic semiconductor devices. The simulation was successfully benchmarked against known results for plane-parallel systems. We then proceeded to simulate a TOF experiment in a planar device free of traps. By varying each simulation parameter we were able to discern what effect each would have on the measured current. Using the simulation, we also investigated a potential experimental technique for the characterisation of the recombination coefficient β. We found that the resulting expression for the recombination coefficient was most valid when recombination was near-Langevin. Future work is required for this technique to be applied accurately across all systems. Finally, traps were introduced into the device and their effects in TOF, Photo-CELIV and RPV experiments in a planar geometry were explored.

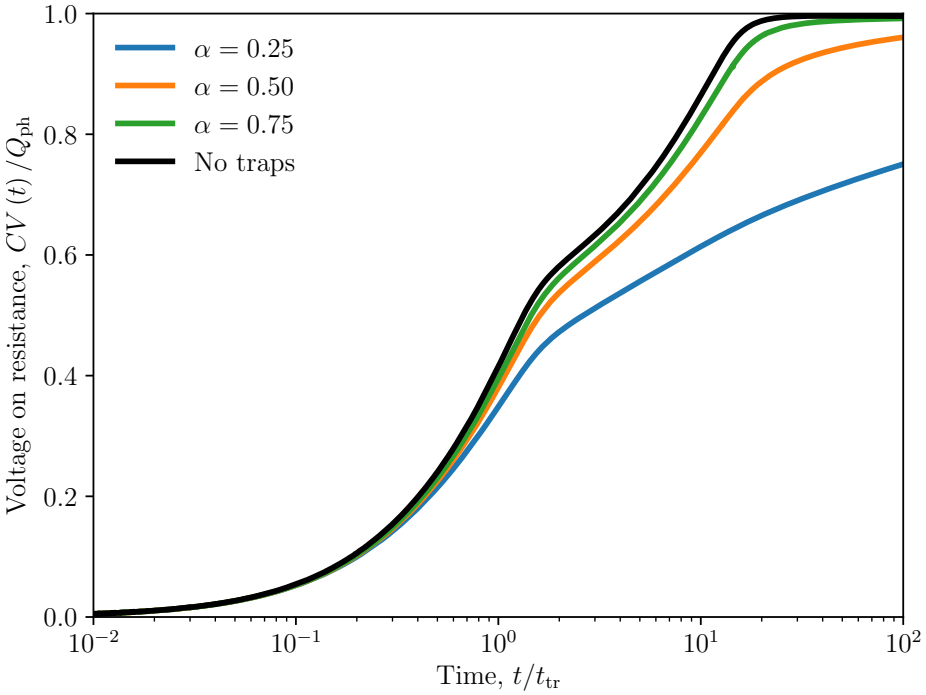

Figure 6.20: RPV current transients for various trap severities, α, alongside the trap-free case for the planar geometry depicted in Figure 6.6. Charge carriers are photogenerated as depicted in Figure 6.7 by light masked by the electrodes that is absorbed according to the Beer-Lambert law with optical absorption coefficient $\alpha_{\mathrm{BL}} = 10d^{-1}$. Here we have specified a charge carrier mobility ratio of $\mu_{\mathrm{fast}}/\mu_{\mathrm{slow}} = 10$, a relative semiconductor permittivity of $\varepsilon_{\mathrm{s}} = 3\varepsilon_0$, and an initial light intensity such that the initial photogenerated charge is $Q_{\mathrm{ph}} = 10^{-3}CU_{\mathrm{ref}} \ll CU_{\mathrm{ref}}$, so as to minimise recombination losses. We set the load resistance $R = 10^5 t_{\mathrm{tr}}/C$ to reveal both "shoulders" corresponding to the transit times of each carrier. For simplicity, the temperature, T is set equal to zero. Trapping occurs at equal frequencies for both holes and electrons, $\nu_{\mathrm{trap},p} = \nu_{\mathrm{trap},n} = t_{\mathrm{tr}}^{-1}$, and traps are described by a multiple trapping model trapping time distribution function, $\phi(t) = \alpha\nu_0 (\nu_0 t)^{-\alpha-1} \gamma(\alpha+1, \nu_0 t)$ with $\nu_0 = 100 t_{\mathrm{pulse}}^{-1}$. At early times, few trapping events have occurred and all plots coincide. At later times, trapping causes each plot to separate. Increasing the severity of traps α is seen to decrease the definition of each transient shoulder. In fact, for the smallest value of α considered, the slower-carrier shoulder is seen to vanish entirely. The faster carrier shoulder is seen to be much more resilient to trapping, retaining much of its definition even for very severe traps.

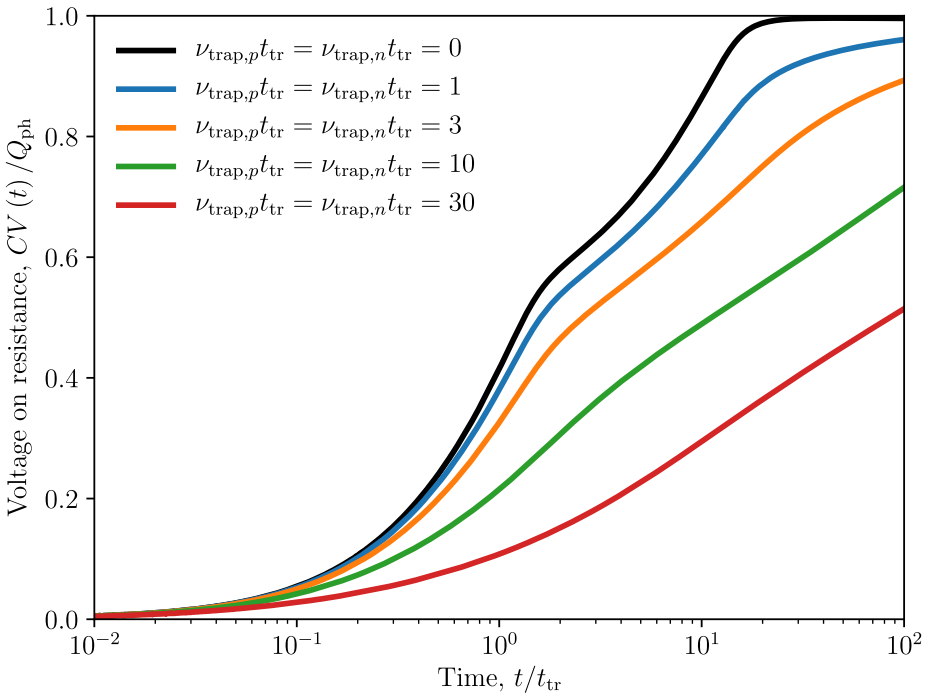

Figure 6.21: RPV current transients for various trapping frequencies, $\nu_{\mathrm{trap},p}$ and $\nu_{\mathrm{trap},n}$, for the planar geometry depicted in Figure 6.6. Charge carriers are photogenerated as depicted in Figure 6.7 by light masked by the electrodes that is absorbed according to the Beer-Lambert law with optical absorption coefficient $\alpha_{\mathrm{BL}} = 10d^{-1}$. Here we have specified a charge carrier mobility ratio of $\mu_{\mathrm{fast}}/\mu_{\mathrm{slow}} = 10$, a relative semiconductor permittivity of $\varepsilon_{\mathrm{s}} = 3\varepsilon_0$, and an initial light intensity such that the initial photogenerated charge is $Q_{\mathrm{ph}} = 10^{-3}CU_{\mathrm{ref}} \ll CU_{\mathrm{ref}}$, so as to minimise recombination losses. We set the load resistance $R = 10^5 t_{\mathrm{tr}}/C$ to reveal both "shoulders" corresponding to the transit times of each carrier. For simplicity, the temperature, T is set equal to zero. Traps are described by a multiple trapping model trapping time distribution function, $\phi\,(t) = \alpha\nu_0\,(\nu_0 t)^{-\alpha-1}\,\gamma\,(\alpha+1, \nu_0 t)$ with $\alpha = 0.5$ and $\nu_0 = 100t_{\mathrm{pulse}}^{-1}$. At early times, few trapping events have occurred and all plots coincide. At later times, trapping causes each plot to separate. Increasing the trapping frequencies $\nu_{\mathrm{trap},p}$ and $\nu_{\mathrm{trap},n}$ is seen to make this plot separation due to trapping effects occur at earlier times. In addition, an increased trapping frequency is seen to decrease the definition of the transient shoulders. For large trapping frequencies the shoulders vanish entirely, suggesting that other techniques should be used to characterise carrier transport in this case.

7 Conclusion

7.1 Summary

We began by introducing the mathematics of fractional calculus and described its application toward modelling dispersive transport due to traps using a fractional generalisation of the diffusion equation. The numerical solution of this so-called Caputo time-fractional diffusion equation was explored using finite differences. It was noted that the time computational complexity of this approach was observed to have quadratic scaling in the number of time steps (contrary to the linear scaling observed for the classical diffusion equation). This difference stems mathematically from the global nature of fractional differentiation, and can be interpreted physically as accounting for the memory of previous trapping events. By using a subordination transformation in time (2.28), we were able to relate the solution of a fractional diffusion equation (2.1) of order $0 < \alpha < 1$ directly to the solution of a the normal diffusion equation (2.14). This meant that, for an N-point finite-difference time discretisation, the mapping could be used to improve upon the $O\left(N^2\right)$ time computational complexity usually required to solve the fractional diffusion equation, allowing for the solution to be found at any instant in time in only $O\left(N^\alpha\right)$, given a precomputation of $O\left(N^{1+\alpha} \ln N\right)$. We applied this representation in Section 2.6 to perform the fitting of the fractional advection diffusion model (2.1) to experimental data for the current in a time-of-flight experiment. Here, the mapping approach was found to be exceptionally useful as the relatively expensive precomputation only had to be performed once before it could be used to solve the model repeatedly for each instance the current was measured. We achieved subsequent computational speed ups in the range of one to three orders of magnitude for this problem.

Next, we introduced a general phase-space kinetic equation (3.1) which generalises Boltzmann's equation by considering charged-particle transport via both delocalised and localised states, accounting for collisional, trapping/detrapping and recombination loss processes. Using Fourier and Laplace transforms, we determine analytical expressions for the phase-space distribution function $f(t, \mathbf{r}, \mathbf{v})$ defined by this model, as well as for its spatial and velocity moments. In turn, these moments provide expressions for centre of mass (CM) and flux transport coefficients, which allow the effects of trapping and detrapping on transport to be quantified. In the hydrodynamic regime, the generalised Boltzmann equation (3.1) can be described by a generalised diffusion equation (3.89) with a unique global time operator. This generalisation was shown to reduce to either the classical diffusion equation (3.83) or the Caputo fractional diffusion equation (3.102), depending on whether transport is dispersive or not. Utilising this link to the fractional calculus literature, we show that the solution of the generalised diffusion equation (3.89) can be written as a subordination transformation (3.109) of the corresponding solution of a standard diffusion equation (3.107).

In what followed, we generalised Fick's law for the aforementioned phase-space kinetic model 3.1 by including terms up to the third-order transport coefficient of skewness $\mathbf{Q}$. We derived this rank-3 skewness tensor and confirmed that its structure and symmetries were in agreement with previous studies. This extension to Fick's law, Eq. (4.1), was used to form a generalised advection-diffusion-skewness equation (4.30). This equation was observed to exhibit a negative skewness, which we were able to attribute to traps. We were able to relate the skewness to the mobility and temperature through Eq. (4.43), in analogy with Einstein's relation. In Eqs. (4.46)–(4.48), we explored the form of the transport coefficients up to skewness in the particular case of fractional transport.

As described thus far, the phase-space kinetic model (3.1) considered constant process frequencies that are independent of particle energy. We proceeded to relax this restriction by considering collision, trapping/detrapping and recombination loss processes that all act selectively according to the energy of the free particles. This generalisation made finding a direct analytical solution for the model challenging. Instead, we formed balance equations (5.16)–(5.18) describing the conservation and transport of particle number, momentum and energy. These were then used to find expressions for the particle mobility, Eqs. (5.36) and (5.46), and energy in the form of Wannier energy relations (5.37) and (5.47). A variety of physical phenomena were shown to arise due to the consideration of particle energy in this generalised model. For example, the Wannier energy relations were use to show the presence of particle heating or cooling due to collisions or trapping, Eq. (5.55), and recombination, Eqs. (5.67) and (5.71). Additionally, transport via combined localised/delocalised states was shown to produce negative differential conductivity under certain conditions (5.74), and the impact of scattering, trapping/detrapping and recombination on the anisotropic nature of diffusion was expressed through the development of generalised Einstein relations (5.97) and (5.98). Lastly, fractional transport analogues of the aforementioned results

were explored by using a trapping time distribution with a heavy tail of the form of Eq. (3.95).

Finally, we applied our generalised phase-space kinetic model toward the development of a model for the transport of charge carriers in planar organic semiconductors. In addition to the processes of drift, diffusion, trapping, detrapping and recombination, we also used Poisson's equation to account for space-charge effects and Kirchoff's laws to account for circuit effects due to the external measurement circuitry used in charge transport experiments. We then used this model to implement a simulation of planar organic semiconductor devices in the Julia programming language. We were able to successfully benchmark this simulation against known results for plane-parallel systems. We then proceeded to simulate a TOF experiment in a trap-free planar device, varying each simulation parameter to discern what effect each would have on the measured current. A potential experimental technique for the characterisation of the recombination coefficient was presented and we used the simulation to investigate its regime of validity. Finally, traps were introduced into the device and their effects in TOF, Photo-CELIV and RPV experiments were explored.

7.2 Future work recommendations

There exist a number of avenues for future work.

Probing trapping using time-varying electric and magnetic fields — In Chapter 3, we introduce a phase-space kinetic model for charged-particle transport that takes the form of a generalised Boltzmann equation. In Chapter 5, we generalise this model further to account for the energy-dependence of collision, trapping and recombination loss processes. In every instance of the model, however, it is assumed simply that charged particles undergo a constant acceleration due to a uniform time-invariant electric field. Relaxing this assumption and considering arbitrary time-varying electric and magnetic fields may provide a way to characterise the nature of trapping within a system. For example, oscillating applied fields should cause measurable quantities like transport coefficients to vary with both the amplitude and frequency of oscillation. The corresponding analytical expressions for these quantities could then be used to shed light on the trapping process.

Kurtosis coefficient — In Chapter 4, we derive the third-order transport coefficient of skewness for the phase-space model introduced in Chapter 3. This provides an extension to Fick's law for this model that ultimately results in an advection-diffusion-skewness equation (4.30). However, it is important to note that this extension is only useful when an electric field is present. Without an applied electric field, all odd-ordered transport coefficients vanish, including the skewness coefficient. In this situation, to extend Fick's law, we must rely upon the kurtosis coefficient, the next even-ordered transport coefficient beyond diffusion. The kurtosis can be found using the density gradient expansion (4.2), in the same way that the drift velocity, diffusion and skewness were found using Eqs. (4.6)–(4.8).

Energy-dependent skewness analogue to Einstein's relation — As the skewness coefficient was derived in Chapter 4, before energy dependence was introduced into the phase-space model in Chapter 5, it remains to be seen what consequences energy-dependent collision, trapping and recombination frequencies have on the skewness. This would allow for the derivation of a skewness analogue of Einstein's relation that would also take into account the field dependence of mobility [3]. This may also shed light on the recent results of Petrović *et al.* [100], that suggest a correlation between the energy-dependent phenomenon of negative differential conductivity and skewness.

ab initio calculation of the trapping frequency ν_{trap} and waiting time distribution $\phi(t)$ in liquids and dense gases — For the general phase-space model in Chapter 5 to be applied in practice to a particular system, both the trapping frequency ν_{trap} and the waiting time distribution function $\phi(t)$ must be specified accordingly. For example, in organic materials it is known that the waiting time distribution can be calculated from the density of existing trapped states [33]. In the case of liquids and dense gases, trapped states are formed by the electron itself and the waiting time distribution is dependent on the scattering, fluctuation profiles and subsequent fluid bubble evolution [88]. Although both free-energy changes and solvation time-scales have been investigated in the literature on light-particle solvation [93–95], none of these results directly produce an energy-dependent trapping frequency or waiting time distribution. It is recommended that the *ab initio* calculation of energy-dependent trapping frequencies and waiting time distributions in liquids and dense gases be pursued. For progress in this regard, see Ref. [88].

Consideration for device doping — In the planar semiconductor device simulation presented in Chapter 6, the device is assumed to be free of impurities. Thus, in its current form the simulation cannot be applied to model n-type or p-type doped semiconductors. Accounting for doping would be a simple matter of including the concentrations of dopants in Poisson's equation 6.27. This proposed extension would require additional simulation parameters to specify the concentration and distribution of donor and acceptor ions.

Improved experimental technique for characterisation of the recombination coefficient β — In Chapter 6, we investigated an experimental technique for the characterisation of the recombination coefficient β. We found that the resulting expression for the recombination coefficient was most valid when recombination was near-Langevin. Future work is required for this technique to be usefully applied to systems, independent of their recombination coefficient.

Effects of inhomogeneous permittivity — The device simulation in Chapter 6 assumes the planar semiconductor is uniform with a constant permittivity ε_{s}. To account for the dependence of the permittivity on device morphology, the simulation must be generalised to allow for the permittivity to vary spatially. This would result in a non-zero permittivity gradient term in Poisson's equation. It remains to be seen what effects an inhomogeneous permittivity would have, especially near discontinuous interfaces between regions of different permittivities.

References

[1] Peter W. Stokes, Bronson Philippa, Wayne Read, and Ronald D. White. Efficient numerical solution of the time fractional diffusion equation by mapping from its Brownian counterpart. *Journal of Computational Physics*, **282**, 334 (2015). doi:10.1016/j.jcp.2014.11.023.

[2] Peter W. Stokes, Bronson Philippa, Daniel Cocks, and Ronald D. White. Solution of a generalized Boltzmann's equation for nonequilibrium charged-particle transport via localized and delocalized states. *Physical Review E*, **93**, 032119 (2016). doi:10.1103/PhysRevE.93.032119.

[3] Peter W. Stokes, Bronson Philippa, Daniel Cocks, and Ronald D. White. Generalized balance equations for charged particle transport via localized and delocalized states: Mobility, generalized Einstein relations, and fractional transport. *Physical Review E*, **95**, 042119 (2017). doi:10.1103/PhysRevE.95.042119.

[4] Peter W. Stokes, Ilija Simonović, Bronson Philippa, Daniel Cocks, Saša Dujko, and Ronald D. White. Third-order transport coefficients for localised and delocalised charged-particle transport. *Scientific Reports*, **8**, 2226 (2018). doi:10.1038/s41598-018-19711-5.

[5] R. D. White, D. G. Cocks, G. Boyle, M. Casey, N. A. Garland, D. Konovalov, B. Philippa, P. Stokes, J. de Urquijo, O. González-Magaña, R. P McEachran, S. J. Buckman, M. J. Brunger, G. Garcia, S. Dujko, and Z. L. Petrovic. Electron transport in biomolecular gaseous and liquid systems: Theory, experiment and self-consistent cross-sections. *Plasma Sources Science and Technology* (2018). doi:10.1088/1361-6595/aabdd7.

[6] Harvey Scher. Time scale invariance in transport and relaxation. *AIP Conference Proceedings*, **256**, 485 (1992). doi:10.1063/1.42416.

[7] Yasuhiko Shirota and Hiroshi Kageyama. Charge Carrier Transporting Molecular Materials and Their Applications in Devices Charge Carrier Transporting Molecular Materials and Their Applications in Devices. *Chemical reviews*, **107**, 953 (2007). doi:10.1021/cr050143.

[8] Matthew S. White, Martin Kaltenbrunner, Eric D. Głowacki, Kateryna Gutnichenko, Gerald Kettlgruber, Ingrid Graz, Safae Aazou, Christoph Ulbricht,

Daniel A M Egbe, Matei C. Miron, Zoltan Major, Markus C. Scharber, Tsuyoshi Sekitani, Takao Someya, Siegfried Bauer, and Niyazi Serdar Sariciftci. Ultrathin, highly flexible and stretchable PLEDs. *Nature Photonics*, **7**, 811 (2013). doi:10.1038/nphoton.2013.188.

[9] Stephen R. Forrest. The path to ubiquitous and low-cost organic electronic appliances on plastic. *Nature*, **428**, 911 (2004). doi:10.1038/nature02498.

[10] Stephen R Forrest and Mark E Thompson. Introduction: Organic Electronics and Optoelectronics. *Chem. Rev.*, **107**, 923 (2007). doi:doi:10.1021/cr0501590.

[11] Ralf Metzler and Joseph Klafter. The random walk's guide to anomalous diffusion: a fractional dynamics approach. *Physics Reports*, **339**, 1 (2000). doi:10.1016/S0370-1573(00)00070-3.

[12] Harvey Scher and Elliott W. Montroll. Anomalous transit-time dispersion in amorphous solids. *Physical Review B*, **12**, 2455 (1975). doi:10.1103/PhysRevB.12.2455.

[13] R. T. Sibatov and V. V. Uchaikin. Fractional differential kinetics of charge transport in unordered semiconductors. *Semiconductors*, **41**, 335 (2007). doi:10.1134/S1063782607030177.

[14] Marcel Schubert, Eduard Preis, James C. Blakesley, Patrick Pingel, Ullrich Scherf, and Dieter Neher. Mobility relaxation and electron trapping in a donor/acceptor copolymer. *Physical Review B - Condensed Matter and Materials Physics*, **87**, 024203 (2013). doi:10.1103/PhysRevB.87.024203.

[15] Henning Krüsemann, Aljaž Godec, and Ralf Metzler. First-passage statistics for aging diffusion in systems with annealed and quenched disorder. *Physical Review E - Statistical, Nonlinear, and Soft Matter Physics*, **89**, 040101 (2014). doi:10.1103/PhysRevE.89.040101.

[16] Henning Krüsemann, Richard Schwarzl, and Ralf Metzler. Ageing Scher–Montroll Transport. *Transport in Porous Media*, **115**, 327 (2016). doi:10.1007/s11242-016-0686-y.

[17] Gert Jan A.H. Wetzelaer, Max Scheepers, Araceli Miquel Sempere, Cristina Momblona, Jorge Ávila, and Henk J. Bolink. Trap-Assisted Non-Radiative Recombination in Organic-Inorganic Perovskite Solar Cells. *Advanced Materials*, **27**, 1837 (2015). doi:10.1002/adma.201405372.

[18] Andreas Mauracher, Matthias Daxner, Johannes Postler, Stefan E. Huber, Stephan Denifl, Paul Scheier, and J. Peter Toennies. Detection of negative charge carriers in superfluid helium droplets: The metastable anions He*- and He2*-. *Journal of Physical Chemistry Letters*, **5**, 2444 (2014). doi:10.1021/jz500917z.

[19] A. F. Borghesani, M. Folegani, P. L. Frabetti, and L. Piemontese. Effect of CH4 addition on excess electron mobility in liquid Kr. *Journal of Chemical Physics*, **117**, 5794 (2002). doi:10.1063/1.1502251.

[20] Yosuke Sakai, Werner F. Schmidt, and Alexei Khrapak. High- and low-mobility electrons in liquid neon. *Chemical Physics*, **164**, 139 (1992). doi:10.1016/0301-0104(92)87138-Y.

[21] Sergey V. Stepanov, Vsevolod M. Byakov, Dmitrii S. Zvezhinskiy, Gilles Duplâtre, Roman R. Nurmukhametov, and Petr S. Stepanov. Positronium in a liquid phase: Formation, bubble state and chemical reactions. *Advances in Physical Chemistry*, **2012** (2012). doi:10.1155/2012/431962.

[22] Sergey V. Stepanov, Vsevolod M. Byakov, Bichitra Nandi Ganguly, Debarshi Gangopadhyay, Tapas Mukherjee, and Binayak Dutta-Roy. A molecular basis of the bubble model of positronium annihilation in liquids. *Physica B: Condensed Matter*, **322**, 68 (2002). doi:10.1016/S0921-4526(02)00601-4.

[23] M. Charlton and J. W. Humberston. *Positron Physics*. Cambridge University Press, Cambridge (2000). ISBN 9780511535208. doi:10.1017/CBO9780511535208.

[24] M G Colucci, D P van der Werf, and M Charlton. The temperature and density dependence of positron annihilation in CO 2 and SF 6. *Journal of Physics B: Atomic, Molecular and Optical Physics*, **44**, 175204 (2011). doi:10.1088/0953-4075/44/17/175204.

[25] W E Spear. Transit Time Measurements of Charge Carriers in Amorphous Selenium Films. *Proceedings of the Physical Society. Section B*, **70**, 669 (1957). doi:10.1088/0370-1301/70/7/304.

[26] Sanjay Tiwari and N. C. Greenham. Charge mobility measurement techniques in organic semiconductors. *Optical and Quantum Electronics*, **41**, 69 (2009). doi:10.1007/s11082-009-9323-0.

[27] G. Juška, K. Arlauskas, M. Viliūnas, and J. Kočka. Extraction Current Transients: New Method of Study of Charge Transport in Microcrystalline Silicon. *Physical Review Letters*, **84**, 4946 (2000). doi:10.1103/PhysRevLett.84.4946.

[28] Bronson Philippa, Martin Stolterfoht, Paul L. Burn, Gytis Juška, Paul Meredith, Ronald D. White, and Almantas Pivrikas. The impact of hot charge carrier mobility on photocurrent losses in polymer-based solar cells. *Scientific Reports*, **4**, 5695 (2014). doi:10.1038/srep05695.

[29] Loukas Vlahos, Heinz Isliker, Yannis Kominis, and Kyriakos Hizanidis. Normal and Anomalous Diffusion: A Tutorial. *ArXiv e-prints* (2008).

[30] Elliott W. Montroll and George H. Weiss. Random Walks on Lattices. II. *Journal of Mathematical Physics*, **6**, 167 (1965). doi:10.1063/1.1704269.

[31] J. Klafter, A. Blumen, and M. F. Shlesinger. Stochastic pathway to anomalous diffusion. *Physical Review A*, **35**, 3081 (1987). doi:10.1103/PhysRevA.35.3081.

[32] R. E. Robson and A. Blumen. Analytically solvable model in fractional kinetic theory. *Physical Review E - Statistical, Nonlinear, and Soft Matter Physics*, **71**, 061104 (2005). doi:10.1103/PhysRevE.71.061104.

[33] Bronson Philippa, R. E. Robson, and R. D. White. Generalized phase-space kinetic and diffusion equations for classical and dispersive transport. *New Journal of Physics*, **16**, 073040 (2014). doi:10.1088/1367-2630/16/7/073040.

[34] L Boltzmann. Weitere Studien über das Wärmegleichgewicht unter Gasmolekülen. *Sitz. Math.-Naturwiss. Cl.~Akad. Wiss.~Wien*, **66**, 275 (1872).

[35] H Goldstein. *Classical mechanics*. Addison-Wesley (1964).

[36] P. L. Bhatnagar, E. P. Gross, and M. Krook. A model for collision processes in gases. I. Small amplitude processes in charged and neutral one-component systems. *Physical Review*, **94**, 511 (1954). doi:10.1103/PhysRev.94.511.

[37] Robert Robson, Ronald White, and Malte Hildebrandt. *Fundamentals of Charged Particle Transport in Gases and Condensed Matter*. CRC Press (2017). ISBN 9781498736367.

[38] R E Robson and B V Paranjape. Interaction of plasma and lattice waves in piezoelectric semiconductors. *Physica Status Solidi (b)*, **59**, 641 (1973). doi:10.1002/pssb.2220590232.

[39] R E Robson. Nonlinear Diffusion of Ions in a Gas. *North*, **28**, 523 (1975). doi:10.1071/PH750523.

[40] T. Tiedje and A. Rose. A physical interpretation of dispersive transport in disordered semiconductors. *Solid State Communications*, **37**, 49 (1981). doi:10.1016/0038-1098(81)90886-3.

[41] E. Barkai. Fractional Fokker-Planck equation, solution, and application. *Physical Review E*, **63**, 046118 (2001). doi:10.1103/PhysRevE.63.046118.

[42] Ralf Metzler, Eli Barkai, and Joseph Klafter. Anomalous diffusion and relaxation close to thermal equilibrium: A fractional fokker-planck equation approach. *Physical Review Letters*, **82**, 3563 (1999). doi:10.1103/PhysRevLett.82.3563.

[43] Enrico Scalas, Rudolf Gorenflo, and Francesco Mainardi. Fractional calculus and continuous-time finance. *Physica A: Statistical Mechanics and its Applications*, **284**, 376 (2000). doi:10.1016/S0378-4371(00)00255-7.

[44] Tomáš Škovránek, Igor Podlubny, and Ivo Petráš. Modeling of the national economies in state-space: A fractional calculus approach. *Economic Modelling*, **29**, 1322 (2012). doi:10.1016/j.econmod.2012.03.019.

[45] Marko Janev, Stevan Pilipović, Teodor Atanacković, Radovan Obradović, and Nebojša Ralević. Fully fractional anisotropic diffusion for image denoising. *Mathematical and Computer Modelling*, **54**, 729 (2011). doi:10.1016/j.mcm.2011.03.017.

[46] Jing-Nuo Wu, Hsin-Chien Huang, Szu-Cheng Cheng, and Wen-Feng Hsieh. Fractional Langevin Equation in Quantum Systems with Memory Effect. *Applied Mathematics*, **5**, 1741 (2014). doi:10.4236/am.2014.512167.

[47] Igor M. Sokolov, Joseph Klafter, and Alexander Blumen. Fractional Kinetics. *Physics Today*, **55**, 48 (2002). doi:10.1063/1.1535007.

[48] Gianni Pagnini. Short note on the emergence of fractional kinetics. *Physica A: Statistical Mechanics and its Applications*, **409**, 29 (2014). doi:10.1016/j.physa.2014.03.079.

[49] B. W. Philippa, R. D. White, and R. E. Robson. Analytic solution of the fractional advection-diffusion equation for the time-of-flight experiment in a finite geometry. *Physical Review E - Statistical, Nonlinear, and Soft Matter Physics*, **84**, 041138 (2011). doi:10.1103/PhysRevE.84.041138.

[50] Yoav Sagi, Miri Brook, Ido Almog, and Nir Davidson. Observation of anomalous diffusion and fractional self-similarity in one dimension. *Physical Review Letters*, **108**, 93002 (2012). doi:10.1103/PhysRevLett.108.093002.

[51] Rasiel Toledo-Hernandez, Vicente Rico-Ramirez, Gustavo A. Iglesias-Silva, and Urmila M. Diwekar. A fractional calculus approach to the dynamic optimization of biological reactive systems. Part I: Fractional models for biological reactions. *Chemical Engineering Science*, **117**, 217 (2014). doi:10.1016/j.ces.2014.06.034.

[52] Vladimir V. Uchaikin and Renat T. Sibatov. Fractional theory for transport in disordered semiconductors. *Communications in Nonlinear Science and Numerical Simulation*, **13**, 715 (2008). doi:10.1016/j.cnsns.2006.07.008.

[53] Trifce Sandev, Ralf Metzler, and Živorad Tomovski. Fractional diffusion equation with a generalized Riemann-Liouville time fractional derivative. *Journal of Physics A: Mathematical and Theoretical*, **44**, 255203 (2011). doi:10.1088/1751-8113/44/25/255203.

[54] F. Mainardi. The fundamental solutions for the fractional diffusion-wave equation. *Applied Mathematics Letters*, **9**, 23 (1996). doi:10.1016/0893-9659(96)00089-4.

[55] Michele Caputo. Linear Models of Dissipation whose Q is almost Frequency Independent-II. *Geophysical Journal of the Royal Astronomical Society*, **13**, 529 (1967). doi:10.1111/j.1365-246X.1967.tb02303.x.

[56] Guang Hua Gao and Zhi Zhong Sun. A compact finite difference scheme for the fractional sub-diffusion equations. *Journal of Computational Physics*, **230**, 586 (2011). doi:10.1016/j.jcp.2010.10.007.

[57] Guang hua Gao, Zhi zhong Sun, and Hong wei Zhang. A new fractional numerical differentiation formula to approximate the Caputo fractional derivative and its applications. *Journal of Computational Physics*, **259**, 33 (2014). doi:10.1016/j.jcp.2013.11.017.

[58] Ya-nan Zhang, Zhi-zhong Sun, and Hong-lin Liao. Finite difference methods for the time fractional diffusion equation on non-uniform meshes. *Journal of Computational Physics*, **265**, 195 (2014). doi:10.1016/j.jcp.2014.02.008.

[59] Xuehua Yang, Haixiang Zhang, and Da Xu. Orthogonal spline collocation method for the two-dimensional fractional sub-diffusion equation. *Journal of Computational Physics*, **256**, 824 (2014). doi:10.1016/j.jcp.2013.09.016.

[60] A. H. Bhrawy, E. H. Doha, D. Baleanu, and S. S. Ezz-Eldien. A spectral tau algorithm based on Jacobi operational matrix for numerical solution of time fractional diffusion-wave equations. *Journal of Computational Physics*, **293**, 142 (2015). doi:10.1016/j.jcp.2014.03.039.

[61] Zhuo Jia Fu, Wen Chen, and Hai Tian Yang. Boundary particle method for Laplace transformed time fractional diffusion equations. *Journal of Computational Physics*, **235**, 52 (2013). doi:10.1016/j.jcp.2012.10.018.

[62] Guo-cheng Wu. A Fractional Lie Group Method For Anomalous Diffusion Equations. *Communications in Fractional Calculus*, **1**, 27 (2010).

[63] Igor Podlubny. *List of Figures*, volume 198. Academic Press (1999). ISBN 978-0-12-558840-9. doi:10.1016/S0076-5392(99)80017-4.

[64] Neville J. Ford and A. Charles Simpson. The numerical solution of fractional differential equations: Speed versus accuracy. *Numerical Algorithms*, **26**, 333 (2001). doi:10.1023/A:1016601312158.

[65] Masataka Fukunaga and Nobuyuki Shimizu. High Speed Algorithm for Computation of Fractional Differentiation and Integration. In *ASME 2011 International Design Engineering Technical Conferences and Computers and Information in Engineering Conference*, 169–178. American Society of Mechanical Engineers (2011). ISBN 9780791854808. doi:10.1115/DETC2011-47408.

[66] Kai Diethelm. An efficient parallel algorithm for the numerical solution of fractional differential equations. *Fractional Calculus and Applied Analysis*, **14**, 475 (2011). doi:10.2478/s13540-011-0029-1.

[67] Chunye Gong, Weimin Bao, Guojian Tang, Bo Yang, and Jie Liu. An efficient parallel solution for Caputo fractional reaction-diffusion equation. *Journal of Supercomputing*, **68**, 1521 (2014). doi:10.1007/s11227-014-1123-z.

[68] Gottfried Wilhelm Leibniz and Von. Leibnizens mathematische Schriften. *Zweite Abth*, **1**, 442 (1849).

[69] G W Leibniz. Nova methodus pro maximis et minimis, itemque tangentibus, quae nec fractas, nec irrationales quantitates moratur, et singulare pro illis calculi genus. *Acta Eruditorum*, 467–473 (1684).

[70] Rudolf Hilfer. Threefold Introduction to Fractional Derivatives. *Anomalous Transport: Foundations and Applications*, 17–73 (2008). doi:10.1002/9783527622979.ch2.

[71] W. R. Schneider and W. Wyss. Fractional diffusion and wave equations. *Journal of Mathematical Physics*, **30**, 134 (1989). doi:10.1063/1.528578.

[72] Jean Philippe Bouchaud and Antoine Georges. Anomalous diffusion in disordered media: Statistical mechanisms, models and physical applications. *Physics Reports*, **195**, 127 (1990). doi:10.1016/0370-1573(90)90099-N.

[73] J. Klafter and G. Zumofen. Probability distributions for continuous-time random walks with long tails. *Journal of Physical Chemistry*, **98**, 7366 (1994). doi:10.1021/j100081a022.

[74] Alexander I. Saichev and George M. Zaslavsky. Fractional kinetic equations: Solutions and applications. *Chaos*, **7**, 753 (1997). doi:10.1063/1.166272.

[75] Eli Barkai and R J Silbey. Fractional Kramers Equation. *The Journal of Physical Chemistry B*, **104**, 3866 (2000). doi:10.1021/jp993491m.

[76] Salomon Bochner. *Harmonic analysis and the theory of probability*. University of California Press (1955). ISBN 0486446204.

[77] Oldham K B and Spanier J. *The Fractional Calculus*, volume 111. Academic Press, New York (1974). ISBN 9780125255509.

[78] Yumin Lin and Chuanju Xu. Finite difference/spectral approximations for the time-fractional diffusion equation. *Journal of Computational Physics*, **225**, 1533 (2007). doi:10.1016/j.jcp.2007.02.001.

[79] Diego A. Murio. Implicit finite difference approximation for time fractional diffusion equations. *Computers and Mathematics with Applications*, **56**, 1138 (2008). doi:10.1016/j.camwa.2008.02.015.

[80] Xuan Zhao and Zhi zhong Sun. A box-type scheme for fractional sub-diffusion equation with Neumann boundary conditions. *Journal of Computational Physics*, **230**, 6061 (2011). doi:10.1016/j.jcp.2011.04.013.

[81] J. W. Thomas. *Numerical Partial Differential Equations: Finite Difference Methods*, volume 22. Springer (1995). ISBN 1489972781.

[82] Tom M. Apostol. *Modular Functions and Dirichlet Series in Number Theory*, volume 41. Springer-Verlag, New York (1990). ISBN 978-1-4612-6978-6. doi:10.1007/978-1-4612-0999-7.

[83] H. J. Haubold, A. M. Mathai, and R. K. Saxena. Mittag-leffler functions and their applications. *Journal of Applied Mathematics*, **2011** (2011). doi:10.1155/2011/298628.

[84] Thomas F. Coleman and Yuying Li. On the convergence of interior-reflective Newton methods for nonlinear minimization subject to bounds. *Mathematical Programming*, **67**, 189 (1994). doi:10.1007/BF01582221.

[85] Thomas F. Coleman and Yuying Li. An Interior Trust Region Approach for Nonlinear Minimization Subject to Bounds. *SIAM Journal on Optimization*, **6**, 418 (1996). doi:10.1137/0806023.

[86] *MATLAB 8.3 and Curve Fitting Toolbox 3.4.1*. The MathWorks, Inc., Natick, Massachusetts (2014).

[87] W Press, S Teukolsky, W Vetterling, and B Flannery. *Numerical Recipes 3rd Edition: The Art of Scientific Computing*. Cambridge University Press (2007). ISBN 0521880688, 9780521880688.

[88] D. G. Cocks and R. D. White. Fluctuation capture in non-polar gases and liquids (2016).

[89] S. Peter Gary. *The plasma dispersion function*. Academic Press, New York (1961). ISBN 9780511551512. doi:10.1017/CBO9780511551512.010.

[90] Michael I Cotterell, Bernard J Mason, Antonia E Carruthers, Jim S Walker, Andrew J Orr-Ewing, and Jonathan P Reid. *Measurements of the evaporation and hygroscopic response of single fine-mode aerosol particles using a Bessel beam optical trap.*, volume 16. Cambridge University Press (2014). ISBN 1463-9076; 1463-9084. doi:10.1039/c3cp54368d.

[91] Francesco Mainardi, Yuri Luchko, and Gianni Pagnini. The fundamental solution of the space-time fractional diffusion equation. *Fractional Calculus and Applied Analysis*, **4**, 153 (2007). doi:10.1142/9789812776273_0020.

[92] Ralf Metzler and Joseph Klafter. The restaurant at the end of the random walk: Recent developments in the description of anomalous transport by fractional dynamics. *Journal of Physics A: Mathematical and General*, **37**, R161 (2004). doi:10.1088/0305-4470/37/31/R01.

[93] D. M. Ceperley and B. J. Alder. Ground state of the electron gas by a stochastic method. *Physical Review Letters*, **45**, 566 (1980). doi:10.1103/PhysRevLett.45.566.

[94] Bruce N. Miller and Terrence L. Reese. Self-trapping at the liquid-vapor critical point: A path-integral study. *Physical Review E - Statistical, Nonlinear, and Soft Matter Physics*, **78**, 061123 (2008). doi:10.1103/PhysRevE.78.061123.

[95] J. Cao and B. J. Berne. A Born–Oppenheimer approximation for path integrals with an application to electron solvation in polarizable fluids. *The Journal of Chemical Physics*, **99**, 2902 (1993). doi:10.1063/1.465198.

[96] K Kondo and H Tagashira. *Nonequilibrium Effects in Ion and Electron Transport*, volume 23. Springer US, Boston, MA (1990). ISBN 978-1-4612-7915-0. doi:10.1007/978-1-4613-0661-0.

[97] Slobodan B. Vrhovac, Zoran Lj Petrović, Larry A. Viehland, and Thalanayar S. Santhanam. Third-order transport coefficients for charged particle swarms. *Journal of Chemical Physics*, **110**, 2423 (1999). doi:10.1063/1.477948.

[98] S. Dujko, R. D. White, and Z. Lj Petrović. Monte Carlo studies of non-conservative electron transport in the steady-state Townsend experiment. *Journal of Physics D: Applied Physics*, **41**, 245205 (2008). doi:10.1088/0022-3727/41/24/245205.

[99] K Kondo and H Tagashira. *Nonequilibrium Effects in Ion and Electron Transport*, volume 23. Springer US, Boston, MA (1990). ISBN 978-1-4612-7915-0. doi:10.1007/978-1-4613-0661-0.

[100] Z. Lj Petrović, I. Simonović, S. Marjanović, D. Bošnjaković, D. Marić, G. Malović, and S. Dujko. Non-equilibrium of charged particles in swarms and plasmas - From binary collisions to plasma effects. *Plasma Physics and Controlled Fusion*, **59**, 014026 (2017). doi:10.1088/0741-3335/59/1/014026.

[101] Kamilla Norregaard, Ralf Metzler, Christine M. Ritter, Kirstine Berg-Sørensen, and Lene B. Oddershede. Manipulation and Motion of Organelles and Single Molecules in Living Cells. *Chemical Reviews*, **117**, 4342 (2017). doi:10.1021/acs.chemrev.6b00638.

[102] Maria Schwarzl, Aljaž Godec, and Ralf Metzler. Quantifying non-ergodicity of anomalous diffusion with higher order moments. *Scientific Reports*, **7**, 3878 (2017). doi:10.1038/s41598-017-03712-x.

[103] Felix Höfling and Thomas Franosch. Anomalous transport in the crowded world of biological cells. *Reports on Progress in Physics*, **76**, 046602 (2013). doi:10.1088/0034-4885/76/4/046602.

[104] Marcin Magdziarz, Aleksander Weron, Krzysztof Burnecki, and Joseph Klafter. Fractional brownian motion versus the continuous-time random walk: A simple test for subdiffusive dynamics. *Physical Review Letters*, **103**, 180602 (2009). doi:10.1103/PhysRevLett.103.180602.

[105] J H Whealton and E A Mason. Transport coefficients of gaseous ions in an electric field. *Chemical Physics*, **206**, 9 (1974). doi:10.1016/0003-4916(74)90293-0.

[106] P. H. Larsen, H. R. Skullerud, T. H. Lovaas, and T. Stefansson. Transport coefficients and interaction potentials for lithium ions in helium and argon. *Journal of Physics B: Atomic, Molecular and Optical Physics*, **21**, 2519 (1988). doi:10.1088/0953-4075/21/13/018.

[107] Andreas D. Koutselos. Third-order transport properties of ions in electrostatic fields. *Chemical Physics*, **270**, 165 (2001). doi:10.1016/S0301-0104(01)00395-0.

[108] Robert E. Robson. *Introductory Transport Theory for Charged Particles in Gases*. WORLD SCIENTIFIC (2006). ISBN 978-981-270-011-7. doi:10.1142/6225.

[109] R D White, R E Robson, K F Ness, and B Li. Charged-particle transport in gases in electric and magnetic fields crossed at arbitrary angles: Multiterm solution of Boltzmann's equation. *Phys. Rev. E*, **27**, 1249 (1999). doi:10.1103/PhysRevE.60.2231.

[110] A. Einstein. Über die von der molekularkinetischen Theorie der Wärme geforderte Bewegung von in ruhenden Flüssigkeiten suspendierten Teilchen. *Annalen der Physik*, **322**, 549 (1905). doi:10.1002/andp.19053220806.

[111] Andreas D. Koutselos. Third-order transport properties of ion-swarms from mobility and diffusion coefficients. *Chemical Physics*, **315**, 193 (2005). doi:10.1016/j.chemphys.2005.03.026.

[112] Edward A. Mason and Earl W. McDaniel. *Transport Properties of Ions in Gases*. Wiley, New York (1988). ISBN 9783527602858. doi:10.1002/3527602852.

[113] R.E. Robson. Physics of reacting particle swarms in gases. *The Journal of Chemical Physics*, **85**, 4486 (1986). doi:10.1063/1.451769.

[114] S. Dujko, A. H. Markosyan, R. D. White, and U. Ebert. High-order fluid model for streamer discharges: I. Derivation of model and transport data. *Journal of Physics D: Applied Physics*, **46**, 475202 (2013). doi:10.1088/0022-3727/46/47/475202.

[115] S. Dujko, D. Bošnjaković, R. D. White, and Z. Lj Petrović. Heating mechanisms for electron swarms in radio-frequency electric and magnetic fields. *Plasma Sources Science and Technology*, **24**, 054006 (2015). doi:10.1088/0963-0252/24/5/054006.

[116] R. D. White and R. E. Robson. Multiterm solution of a generalized Boltzmann kinetic equation for electron and positron transport in structured and soft condensed matter. *Physical Review E - Statistical, Nonlinear, and Soft Matter Physics*, **84**, 031125 (2011). doi:10.1103/PhysRevE.84.031125.

[117] G. J. Boyle, R. D. White, R. E. Robson, S. Dujko, and Z. Lj Petrovic. On the approximation of transport properties in structured materials using momentum-transfer theory. *New Journal of Physics*, **14**, 045011 (2012). doi:10.1088/1367-2630/14/4/045011.

[118] R. E. Robson, M. J. Brunger, S. J. Buckman, G. Garcia, Z. Lj Petrovic, and R. D. White. Positron kinetics in an idealized PET environment. *Scientific Reports*, **5**, 12674 (2015). doi:10.1038/srep12674.

[119] G. J. Boyle, R. P. McEachran, D. G. Cocks, and R. D. White. Electron scattering and transport in liquid argon. *Journal of Chemical Physics*, **142**, 154507 (2015). doi:10.1063/1.4917258.

[120] G. J. Boyle, R. P. McEachran, D. G. Cocks, M. J. Brunger, S. J. Buckman, S. Dujko, and R. D. White. Ab initio electron scattering cross-sections and transport in liquid xenon. *Journal of Physics D: Applied Physics*, **49**, 355201 (2016). doi:10.1088/0022-3727/49/35/355201.

[121] K. F. Ness, R. E. Robson, M. J. Brunger, and R. D. White. Transport coefficients and cross sections for electrons in water vapour: Comparison of cross section sets using an improved Boltzmann equation solution. *Journal of Chemical Physics*, **136**, 024318 (2012). doi:10.1063/1.3675921.

[122] Ronald D. White, Michael J. Brunger, Nathan A. Garland, Robert E. Robson, Kevin F. Ness, Gustavo Garcia, Jaime De Urquijo, Sasa Dujko, and Zoran Lj Petrović. Electron swarm transport in THF and water mixtures. *European Physical Journal D*, **68**, 125 (2014). doi:10.1140/epjd/e2014-50085-7.

[123] J. De Urquijo, E. Basurto, A. M. Juárez, K. F. Ness, R. E. Robson, M. J. Brunger, and R. D. White. Electron drift velocities in He and water mixtures: Measurements and an assessment of the water vapour cross-section sets. *Journal of Chemical Physics*, **141**, 14308 (2014). doi:10.1063/1.4885357.

[124] Gregory H. Wannier. Motion of Gaseous Ions in Strong Electric Fields. *Bell System Technical Journal*, **32**, 170 (1953). doi:10.1002/j.1538-7305.1953.tb01426.x.

[125] R. E. Robson. On the generalized Einstein relation for gaseous ions in an electrostatic field. *Journal of Physics B: Atomic and Molecular Physics*, **9**, L337 (1976). doi:10.1088/0022-3700/9/11/009.

[126] RE Robson. Generalized Einstein Relation and Negative Differential Conductivity in Gases. *Australian Journal of Physics*, **37**, 35 (1984). doi:10.1071/PH840035.

[127] H. R. Skullerud and L. R. Forsth. Perturbation treatment of thermal motions in gaseous ion-transport theory. *Journal of Physics B: Atomic and Molecular Physics*, **12**, 1881 (1979). doi:10.1088/0022-3700/12/11/014.

[128] Z. Lj. Petrović, R. W. Crompton, and G. N. Haddad. Model Calculations of Negative Differential Conductivity in Gases. *Aust. J. Phys.*, **37**, 23 (1984). doi:10.1071/PH840023.

[129] Peter W. Stokes, Bronson Philippa, Almantas Pivrikas, and Ronald D. White. Localised and delocalised charge transport in planar organic semiconducting devices (2018).

[130] L. J.A. Koster, V. D. Mihailetchi, and P. W.M. Blom. Bimolecular recombination in polymer/fullerene bulk heterojunction solar cells. *Applied Physics Letters*, **88**, 1 (2006). doi:10.1063/1.2170424.

[131] Girish Lakhwani, Akshay Rao, and Richard H. Friend. Bimolecular Recombination in Organic Photovoltaics. *Annual Review of Physical Chemistry*, **65**, 557 (2014). doi:10.1146/annurev-physchem-040513-103615.

[132] Daniel Rauh, Carsten Deibel, and Vladimir Dyakonov. Charge density dependent nongeminate recombination in organic bulk heterojunction solar cells. *Advanced Functional Materials*, **22**, 3371 (2012). doi:10.1002/adfm.201103118.

[133] M. Kuik, L. J. A. Koster, G. A. H. Wetzelaer, and P. W. M. Blom. Trap-Assisted Recombination in Disordered Organic Semiconductors. *Physical Review Letters*, **107**, 256805 (2011). doi:10.1103/PhysRevLett.107.256805.

[134] Condensed Matter and Materials Physics. *Modelling charge transport in organic solar cells*. Phd thesis, James Cook University (2014).

[135] G. Juka, M. Viliunas, K. Arlauskas, and J. Kočka. Space-charge-limited photocurrent transients: The influence of bimolecular recombination. *Physical Review B*, **51**, 16668 (1995). doi:10.1103/PhysRevB.51.16668.

[136] G. Juška, K. Genevičius, G. Sliaužys, A. Pivrikas, M. Scharber, and R. Österbacka. Double-injection current transients as a way of measuring transport in insulating organic films. *Journal of Applied Physics*, **101**, 114505 (2007). doi:10.1063/1.2736791.

[137] L. J. A. Koster, E. C. P. Smits, V. D. Mihailetchi, and P. W. M. Blom. Device model for the operation of polymer/fullerene bulk heterojunction solar cells. *Physical Review B*, **72**, 085205 (2005). doi:10.1103/PhysRevB.72.085205.

[138] G. Juška, M. Viliunas, O. Klíma, E. Šipek, and J. Kocka. New features in space-charge-limited-photocurrent transients. *Philosophical Magazine B: Physics of Condensed Matter; Statistical Mechanics, Electronic, Optical and Magnetic Properties*, **69**, 277 (1994). doi:10.1080/01418639408240109.

[139] Carsten Deibel and Vladimir Dyakonov. Polymer-fullerene bulk heterojunction solar cells. *Reports on Progress in Physics*, **73**, 1 (2010). doi:10.1088/0034-4885/73/9/096401.

[140] A. Pivrikas, N. S. Sariciftci, G. Juška, and R. Österbacka. A review of charge transport and recombination in polymer/fullerene organic solar cells. *Progress in Photovoltaics: Research and Applications*, **15**, 677 (2007). doi:10.1002/pip.791.

[141] J. J.M. Van Der Holst, F. W.A. Van Oost, R. Coehoorn, and P. A. Bobbert. Electron-hole recombination in disordered organic semiconductors: Validity of the Langevin formula. *Physical Review B - Condensed Matter and Materials Physics*, **80**, 235202 (2009). doi:10.1103/PhysRevB.80.235202.

[142] The Julia Language. `https://julialang.org/`.

[143] Jeff Bezanson, Alan Edelman, Stefan Karpinski, and Viral B. Shah. Julia: A Fresh Approach to Numerical Computing. *SIAM Review*, **59**, 65 (2014). doi:10.1137/141000671.

[144] Yi Wang, Meilin Liu, Huiping Li, Shu Liang, and Qunsheng Cao. Implementation of DG-fem with dynamic Julia language for accurate em simulation. *IEEE Antennas and Propagation Society, AP-S International Symposium (Digest)*, **2015-Octob**, 1850 (2015). doi:10.1109/APS.2015.7305314.

[145] Chi-Wang Shu. High Order ENO and WENO Schemes for Computational Fluid Dynamics. 439–582 (1999). doi:10.1007/978-3-662-03882-6_5.

[146] Christopher Rackauckas and Qing Nie. DifferentialEquations.jl – A Performant and Feature-Rich Ecosystem for Solving Differential Equations in Julia. *Journal of Open Research Software*, **5**, 15 (2017). doi:doi.org/10.5334/jors.151.

[147] P. Bogacki and L. F. Shampine. A 3(2) pair of Runge - Kutta formulas. *Applied Mathematics Letters*, **2**, 321 (1989). doi:10.1016/0893-9659(89)90079-7.

[148] OrdinaryDiffEq.jl. `https://github.com/JuliaDiffEq/OrdinaryDiffEq.jl`.

[149] DelayDiffEq.jl. `https://github.com/JuliaDiffEq/DelayDiffEq.jl`.

[150] MURRAY A. LAMPERT MARK. and PETER. *Current Injection in Solids*, volume 170. Academic Press (1970). ISBN 0124353509. doi:10.1038/139352d0.

[151] Xu Dong Liu. Weighted essentially non-oscillatory schemes. *Journal of Computational Physics*, **115**, 200 (1994). doi:10.1006/jcph.1994.1187.

[152] Guang Shan Jiang and Chi Wang Shu. Efficient implementation of weighted ENO schemes. *Journal of Computational Physics*, **126**, 202 (1996). doi:10.1006/jcph.1996.0130.

A

List of ratios, R, between particles leaving and entering traps

Table A.1: Specific cases of the dimensionless quantity R that is defined in Eq. (3.63) as the limiting ratio of particle detrapping and trapping rates. From its alternate definition (3.64), it can be seen that R is a function of the difference in recombination loss rates $\Delta\nu_{\text{loss}} \equiv \nu_{\text{loss}}^{(\text{free})} - \nu_{\text{loss}}^{(\text{trap})}$.

Trap type	Trapping time distribution $\phi(t)$	Limiting ratio of detrapping and trapping rates R
Instantaneous	$\delta(t)$	1
Fixed delay	$\delta\left(t-\nu_{\text{detrap}}^{-1}\right)$	$\frac{\nu_{\text{detrap}}}{\nu_{\text{trap}}} W_{\text{Lambert}}\left[\frac{\nu_{\text{trap}}}{\nu_{\text{detrap}}}\exp\left(\frac{\Delta\nu_{\text{loss}}+\nu_{\text{trap}}}{\nu_{\text{detrap}}}\right)\right]$ †
Poisson process	$\nu_{\text{detrap}} \mathrm{e}^{-\nu_{\text{detrap}} t}$	$\frac{\Delta\nu_{\text{loss}}+\nu_{\text{trap}}-\nu_{\text{detrap}}+\sqrt{\left(\Delta\nu_{\text{loss}}+\nu_{\text{trap}}+\nu_{\text{detrap}}\right)^2-4\nu_{\text{detrap}}\Delta\nu_{\text{loss}}}}{2\nu_{\text{trap}}}$
Multiple trapping model	$\alpha\nu_0\left(\nu_0 t\right)^{-\alpha-1}\gamma\left(\alpha+1,\nu_0 t\right)$	‡

† The Lambert W-function is defined as satisfying

$$W_{\text{Lambert}}(z)\,\mathrm{e}^{W_{\text{Lambert}}(z)} \equiv z. \tag{A.1}$$

‡ R is the positive solution of the transcendental equation

$$R = -\frac{\alpha\pi}{\sin\alpha\pi}\left(-\frac{\Delta\nu_{\text{loss}}+\nu_{\text{trap}}(1-R)}{\nu_0}\right)^{\alpha} - \alpha\Phi_{\text{Lerch}}\left(\frac{\Delta\nu_{\text{loss}}+\nu_{\text{trap}}(1-R)}{\nu_0}, 1, -\alpha\right), \tag{A.2}$$

where the Lerch transcendent is defined

$$\Phi_{\text{Lerch}}(z,s,a) \equiv \sum_{n\geq 0}\frac{z^n}{(n+a)^s}. \tag{A.3}$$

In the event that a real solution to this equation does not exist, we have instead

$$R = 1 + \frac{\Delta\nu_{\text{loss}}}{\nu_{\text{trap}}}. \tag{A.4}$$

B

List of subordination kernels, $A(\tau, t)$

Table B.1: Specific cases of the integral kernel (3.110), $A(\tau, t)$, used in the subordination transformation (3.109) that maps from the solution of the standard diffusion equation (3.107) to that of the generalised diffusion equation (3.89).

Trap type	Trapping time distribution $\phi(t)$	Scaled subordination kernel $\mathrm{e}^{\left(\nu_{\mathrm{loss}}^{(\mathrm{free})}+\nu_{\mathrm{trap}}\right)\tau} A(\tau, t)$
Instantaneous	$\delta(t)$	$\mathrm{e}^{\nu_{\mathrm{trap}}\tau}\mathrm{e}^{-\nu_{\mathrm{loss}}^{(\mathrm{trap})}t}\delta(t)$
Fixed delay	$\delta\left(t-\nu_{\mathrm{detrap}}^{-1}\right)$	$\mathrm{e}^{-\nu_{\mathrm{loss}}^{(\mathrm{trap})}t}\frac{\left(\nu_{\mathrm{trap}}\tau\right)^{\nu_{\mathrm{detrap}}t}}{\Gamma\left(1+\nu_{\mathrm{detrap}}t\right)}\mathrm{III}_{\nu_{\mathrm{detrap}}^{-1}}(t)$ †
Poisson process	$\nu_{\mathrm{detrap}}\mathrm{e}^{-\nu_{\mathrm{detrap}}t}$	$\delta(t)+\frac{1}{t}\mathrm{e}^{-\nu_{\mathrm{detrap}}t}\sqrt{\nu_{\mathrm{trap}}\tau\nu_{\mathrm{detrap}}t}I_1\left(2\sqrt{\nu_{\mathrm{trap}}\tau\nu_{\mathrm{detrap}}t}\right)$ ‡
Multiple trapping model	$\alpha\nu_0\left(\nu_0 t\right)^{-\alpha-1}\gamma(\alpha+1,\nu_0 t)$	$\mathrm{e}^{-\nu_{\mathrm{loss}}^{(\mathrm{trap})}t}\left[\frac{1}{t_\alpha}l_\alpha\left(\frac{t}{t_\alpha}\right)*g(t)\right]$ §

† The Dirac comb of period T is defined

$$\mathrm{III}_T(t) \equiv \sum_{n\in\mathbb{Z}} \delta(t-nT). \tag{B.1}$$

‡ The modified Bessel function of the first kind of order ν is defined

$$I_\nu(z) \equiv \sum_{n\geq 0} \frac{\left(\frac{z}{2}\right)^{2n+\nu}}{n!\Gamma(1+n+\nu)}. \tag{B.2}$$

§ The characteristic time t_α is defined

$$\nu_0 t_\alpha \equiv \sqrt[\alpha]{\frac{\alpha\pi}{\sin\alpha\pi}\nu_{\mathrm{trap}}\tau}, \tag{B.3}$$

we define in Laplace space the one-sided Lévy density

$$l_\alpha(p) \equiv \mathrm{e}^{-p^\alpha}, \tag{B.4}$$

and in Laplace space

$$g(p) \equiv \exp\left[-\alpha\Phi_{\mathrm{Lerch}}\left(-\frac{p}{\nu_0}, 1, -\alpha\right)\right], \tag{B.5}$$

where the Lerch transcendent $\Phi_{\mathrm{Lerch}}(z, s, a)$ is given by Eq. (A.3).

C

Approximating higher-order velocity moments

In Sec. 5.4.1, we use first-order momentum transfer theory to obtain expressions for the drift velocity, Eq. (5.46), and mean energy, Eq. (5.47), of charged particles defined by the generalised Boltzmann equation (5.1). These velocity moments are each expressed in terms of the higher-order velocity moments of energy flux $\boldsymbol{\xi} \equiv \langle \epsilon \mathbf{v} \rangle^{(0)}$ and mean squared energy $\langle \epsilon^2 \rangle^{(0)}$. Here, we use zeroth-order momentum transfer theory to approximate these higher-order moments in terms of the lower-order ones.

In Sec. 3.4, we write the solution of the generalised Boltzmann equation (5.1) for the case of constant process frequencies as a Chapman-Enskog expansion in Fourier-transformed velocity space. Assuming process frequencies that are independent of energy is functionally equivalent to performing zeroth-order momentum transfer theory. By considering the first term of this expansion, we find an approximate solution that is valid near the steady, spatially uniform state:

$$f(t, \mathbf{r}, \mathbf{v}) \approx n(t, \mathbf{r}) \left[\omega_{\text{coll}}(\varepsilon) \, \hat{w}(\alpha_{\text{coll}}, \mathbf{v}) + \omega_{\text{trap}}(\varepsilon) \, \hat{w}(\alpha_{\text{detrap}}, \mathbf{v}) \right], \tag{C.1}$$

where the convex combination weights $\omega(\varepsilon)$ are defined as relative collision and trapping frequencies by Eqs. (5.32) and (5.33). Here, the separate processes of collision scattering and detrapping have resulted in a solution containing non-Maxwellian velocity distributions of the form

$$\hat{w}(\alpha, \mathbf{v}) \equiv w(\alpha, v) \frac{\sqrt{\pi}}{\sqrt{2}\alpha W} \text{erfcx}\left(\frac{1 - \alpha \mathbf{v} \cdot \alpha \mathbf{W}}{\sqrt{2}\alpha W} \right), \tag{C.2}$$

where $w(\alpha, v)$ is the Maxwellian velocity distribution defined by Eq. (5.5), $\mathbf{W}$ is the drift velocity from zeroth-order momentum transfer theory, defined in Eq. (3.61), and the scaled complementary error function is defined as $\mathrm{erfcx}(z) \equiv \frac{2}{\sqrt{\pi}} \mathrm{e}^{z^2} \int_z^\infty \mathrm{d}\zeta\, \mathrm{e}^{-\zeta^2}$.

As expected, taking velocity moments of this solution (C.1) reproduces the zeroth-order momentum transfer theory expressions for drift velocity $\mathbf{W}$, Eq. (5.36), and mean energy ε, Eq. (5.37). In the same vein, we can find approximations for higher-order velocity moments written in terms of these lower-order moments, $\mathbf{W}$ and ε. For the energy flux we find

$$\boldsymbol{\xi} \approx \left(\frac{5}{3}\varepsilon + \frac{4}{3} m W^2 \right) \mathbf{W}, \tag{C.3}$$

and for mean squared energy:

$$\left\langle \epsilon^2 \right\rangle^{(0)} \approx \frac{5}{3} \left[\omega_{\mathrm{coll}}(\varepsilon)\, \varepsilon_{\mathrm{coll}}^2 + \omega_{\mathrm{trap}}(\varepsilon)\, \varepsilon_{\mathrm{detrap}}^2 \right] + \frac{13}{3} \left(m W^2 \right)^2, \tag{C.4}$$

which is written in terms of the separate mean energies of $\tilde{w}(\alpha_{\mathrm{coll}}, \mathbf{v})$ and $\tilde{w}(\alpha_{\mathrm{detrap}}, \mathbf{v})$, given respectively:

$$\varepsilon_{\mathrm{coll}} \equiv \frac{3}{2} k_{\mathrm{B}} T_{\mathrm{coll}} + m W^2, \tag{C.5}$$

$$\varepsilon_{\mathrm{detrap}} \equiv \frac{3}{2} k_{\mathrm{B}} T_{\mathrm{detrap}} + m W^2. \tag{C.6}$$

D

Detrapping given trap-based recombination

D.1 Constant recombination frequency

Chapter 3 presents a phase-space model for charge transport that considers collisions, trapping, detrapping and recombination. In this section, we ascertain the rate at which particles in this model leave traps, given that some trapped particles undergo recombination instead of detrapping.

In this model, free particles are trapped at a rate proportional to their number density $n(t, \mathbf{r})$:

$$\left(\frac{\partial n}{\partial t}\right)_{\text{trap}} = -\nu_{\text{trap}} n(t, \mathbf{r}) . \tag{D.1}$$

Trapped particles then undergo recombination at the constant frequency $\nu_{\text{loss}}^{(\text{trap})}$:

$$\left(\frac{\partial n_{\text{trap}}}{\partial t}\right)_{\text{recomb}} = -\nu_{\text{loss}}^{(\text{trap})} n_{\text{trap}}(t, \mathbf{r}) . \tag{D.2}$$

Consider initially consider traps of a fixed duration τ. Without any recombination, particles detrap at the same rate that they initially became trapped at according to Eq. (D.1):

$$\left(\frac{\partial n}{\partial t}\right)_{\text{detrap}} = \nu_{\text{trap}} n(t - \tau, \mathbf{r}) . \tag{D.3}$$

With recombination present, the detrapping rate decays alongside the number of trapped particles according to Eq. (D.2), resulting in an exponential decrease:

$$\left(\frac{\partial n}{\partial t}\right)_{\text{detrap}} = \nu_{\text{trap}} n\left(t-\tau, \mathbf{r}\right) \mathrm{e}^{-\nu_{\text{loss}}^{(\text{trap})}\tau}. \tag{D.4}$$

Finally, accounting for a distribution of trapping times, $\phi\left(t\right)$, results in

$$\begin{aligned}\left(\frac{\partial n}{\partial t}\right)_{\text{detrap}} &= \int_0^t \mathrm{d}\tau \phi\left(\tau\right) \nu_{\text{trap}} n\left(t-\tau\right) \mathrm{e}^{-\nu_{\text{loss}}^{(\text{trap})}\tau} \\ &= \nu_{\text{trap}} \Phi\left(t\right) * n\left(t, \mathbf{r}\right), \end{aligned} \tag{D.5}$$

where we have introduced the effective waiting time distribution $\Phi\left(t\right) \equiv \phi\left(t\right) \mathrm{e}^{-\nu_{\text{loss}}^{(\text{trap})}t}$. This is the detrapping rate used in the generalised Boltzmann equation (3.1) and in the resulting generalised diffusion equation (3.89).

D.2 Time-varying bimolecular recombination frequency

Chapter 6 develops a two-dimensional semiconductor device simulation by using, in part, the generalised diffusion equation (3.89) derived in Chapter 3 to describe the transport of charge carriers. In this simulation, the bimolecular recombination of charge carriers is considered, resulting in a detrapping rate that differs from what appears in Chapter 3 and in Eq. (D.5) above.

As this simulation makes use of the generalised diffusion equation (3.89), electrons are trapped at a rate proportional to their number density $n\left(t, \mathbf{r}\right)$:

$$\left(\frac{\partial n}{\partial t}\right)_{\text{trap}} = -\nu_{\text{trap}} n\left(t, \mathbf{r}\right). \tag{D.6}$$

Trapped electrons then undergo transport-limited bimolecular recombination with free holes of number density $p\left(t, \mathbf{r}\right)$:

$$\left(\frac{\partial n_{\text{trap}}}{\partial t}\right)_{\text{recomb}} = -\frac{\mu_p}{\mu_p + \mu_n} \beta p\left(t, \mathbf{r}\right) n_{\text{trap}}\left(t, \mathbf{r}\right), \tag{D.7}$$

where μ_n and μ_p are electron and hole mobilities, β is the bimolecular recombination coefficient and $n_{\text{trap}}\left(t, \mathbf{r}\right)$ is the number density of trapped electrons. As was done in the previous section, we initially consider traps of a fixed duration τ. In this case, trapped particles return from traps at the same rate they entered in Eq. (D.6):

$$\left(\frac{\partial n}{\partial t}\right)_{\text{detrap}} = \nu_{\text{trap}} n\left(t-\tau, \mathbf{r}\right). \tag{D.8}$$

Introducing bimolecular recombination causes the number of trapped particles to decay according to Eq. (D.7), alongside the detrapping rate:

$$\left(\frac{\partial n}{\partial t}\right)_{\text{detrap}} = \nu_{\text{trap}} n\left(t-\tau,\mathbf{r}\right) \exp\left(-\frac{\mu_p}{\mu_p+\mu_n}\beta\int_0^\tau \mathrm{d}z p\left(z,\mathbf{r}\right)\right), \tag{D.9}$$

For a distribution of electron trapping times, $\phi_n\left(t\right)$, this becomes

$$\begin{aligned}\left(\frac{\partial n}{\partial t}\right)_{\text{detrap}} &= \int_0^t \mathrm{d}\tau \phi_n\left(\tau\right) \nu_{\text{trap}} n\left(t-\tau,\mathbf{r}\right) \exp\left(-\frac{\mu_p}{\mu_p+\mu_n}\beta\int_0^\tau \mathrm{d}z p\left(z,\mathbf{r}\right)\right) \\ &= \frac{\phi_n\left(t\right) * \left[n\left(t,\mathbf{r}\right)\exp\left(\frac{\mu_p}{\mu_p+\mu_n}\beta\int_0^t \mathrm{d}\tau p\left(\tau,\mathbf{r}\right)\right)\right]}{\exp\left(\frac{\mu_p}{\mu_p+\mu_n}\beta\int_0^t \mathrm{d}\tau p\left(\tau,\mathbf{r}\right)\right)}.\end{aligned} \tag{D.10}$$

A similar detrapping rate expression can be derived for holes that trap with a distribution of times, $\phi_p\left(t\right)$:

$$\left(\frac{\partial p}{\partial t}\right)_{\text{detrap}} = \frac{\phi_p\left(t\right) * \left[p\left(t,\mathbf{r}\right)\exp\left(\frac{\mu_n}{\mu_p+\mu_n}\beta\int_0^t \mathrm{d}\tau n\left(\tau,\mathbf{r}\right)\right)\right]}{\exp\left(\frac{\mu_n}{\mu_p+\mu_n}\beta\int_0^t \mathrm{d}\tau n\left(\tau,\mathbf{r}\right)\right)}. \tag{D.11}$$

E

Numerical techniques

This appendix elaborates upon the various techniques used in the numerical solution of the two-dimensional semiconductor device model specified by Eqs. (6.66)–(6.79).

E.1 Finite volume method

In this section, we describe the finite volume method and use it to outline a solution to the charge carrier continuity equations (6.66)–(6.69).

Consider the one-dimensional classical continuity equation

$$\frac{\partial n}{\partial t} + \frac{\partial \Gamma}{\partial x} = 0, \tag{E.1}$$

for number density $n(t,x)$ and arbitrary flux $\Gamma(t,x)$. The finite volume method splits the domain up into indexed cells $x \in [(i-1)\Delta x, i\Delta x]$ and considers the average number density within each:

$$\bar{n}_i(t) \equiv \frac{1}{\Delta x} \int_{\left(i-\frac{1}{2}\right)\Delta x}^{\left(i+\frac{1}{2}\right)\Delta x} \mathrm{d}x n(t,x). \tag{E.2}$$

Applying this average to the above continuity equation yields the system of ordinary differential equations

$$\frac{\mathrm{d}\bar{n}_i}{\mathrm{d}t} = \frac{1}{\Delta x}\left[\Gamma_{i-\frac{1}{2}}(t) - \Gamma_{i+\frac{1}{2}}(t)\right]. \tag{E.3}$$

That is, the rate of change of the average number density in each finite volume cell is equal to its net inward flux at its boundaries. The continuity equation (E.1) can then be solved by time integration of this system of ODEs.

This same approach can be extended to provide a solution to the two-dimensional continuity equations in Chapter 6. In this case, the finite volume method splits the problem domain into indexed rectangles $x \in [(j-1)\,\Delta x, j\Delta x]$, $y \in [i\Delta y, (i-1)\,\Delta y]$ and considers the following average number density within each:

$$\bar{n}_{ij}\,(t) \equiv \frac{1}{\Delta x \Delta y} \int_{(j-\frac{1}{2})\Delta x}^{(j+\frac{1}{2})\Delta x} \mathrm{d}x \int_{(i+\frac{1}{2})\Delta y}^{(i-\frac{1}{2})\Delta y} \mathrm{d}y n\,(t,x,y)\,. \tag{E.4}$$

The solution can then be found, as in one dimension, given the rectangle boundary fluxes, $\Gamma_{i,j\pm\frac{1}{2}}$ and $\Gamma_{i\pm\frac{1}{2},j}$.

E.2 WENO method

In the previous section, we describe the finite volume method, via Eq. (E.3), describes how the average number density within each finite volume cell changes due to the fluxes at its boundaries.

Consider applying the finite volume method to the simple case of a one-dimensional advective flux:

$$\Gamma\,(t,x) = Wn\,(t,x)\,, \tag{E.5}$$

where the velocity W is taken to be positive. Evidently, evaluating this flux at cell boundaries also requires knowledge of the number density at these boundaries:

$$\Gamma_{i+\frac{1}{2}} = Wn_{i+\frac{1}{2}}. \tag{E.6}$$

As the finite volume method only provides information regarding the average number densities $\bar{n}_i$ within each cell, we need to infer the point number densities $n_{i+\frac{1}{2}}$ from these averages. This can be achieved by defining a polynomial $p\,(x)$ that satisfies adjacent cell averages and evaluating this polynomial at the cell boundary. For example, linear polynomials can be used to provide the following second-order accurate reconstructions of the boundary number density $n_{i+\frac{1}{2}}$:

$$n^{(1)}_{i+\frac{1}{2}} = -\frac{1}{2}\bar{n}_{i-1} + \frac{3}{2}\bar{n}_i, \tag{E.7}$$

$$n^{(2)}_{i+\frac{1}{2}} = \frac{1}{2}\bar{n}_i + \frac{1}{2}\bar{n}_{i+1}, \tag{E.8}$$

$$n^{(3)}_{i+\frac{1}{2}} = \frac{3}{2}\bar{n}_{i+1} - \frac{1}{2}\bar{n}_{i+2}. \tag{E.9}$$

It is important when applying the above approximations to take into account the flow of information in the problem. Since the velocity W is positive, there is no way for $n_{i+\frac{1}{2}}$ to be affected by the downwind averages $\bar{n}_{i+1}$ and $\bar{n}_{i+2}$, and thus using the approximation $n^{(3)}_{i+\frac{1}{2}}$ results in a numerical scheme that is unconditionally unstable. For this reason, we must choose between the upwind approximations $n^{(1)}_{i+\frac{1}{2}}$ and $n^{(2)}_{i+\frac{1}{2}}$.

Another possible approximation pitfall occurs when there are rapid changes or discontinuities in the number density. In such scenarios the second-order approximations (E.7)–(E.7), and other higher-order approximations, can extrapolate to number densities outside the range of physical validity. For example, the approximations (E.7) and (E.9) can potentially yield negative number densities. Additionally, all three approximations (E.7)–(E.7) can potentially result in large fluxes (E.6) that cause more number density to leave a cell than is contained within it. For these reasons, approximations beyond first order accuracy often cause spurious oscillations to occur in the solution.

The weighted essentially non-oscillatory (WENO) method of Liu *et al.* [151] avoids these oscillations by performing a weighted sum of the approximations under consideration and weighing trustworthy approximations higher than those that are likely to be invalid. In this case, we have the WENO approximation

$$n_{i+\frac{1}{2}} \approx w_1 n^{(1)}_{i+\frac{1}{2}} + w_2 n^{(2)}_{i+\frac{1}{2}}, \tag{E.10}$$

where $w_1 + w_2 \equiv 1$. We would like the weights to be small $w_j \approx 0$ in the cases where $n^{(j)}_{i+\frac{1}{2}}$ is reconstructed from a region containing a sharp change or discontinuity. In the case that all regions are smooth and free from discontinuities, we would like to choose $w_j = \gamma_j$, where γ_j increases the accuracy of the approximation as much as possible. In this case, $\gamma_1 = \frac{1}{3}$ and $\gamma_2 = \frac{2}{3}$ are optimal in that they result in an approximation that is accurate to third order. WENO weights satisfy all of these requirements and take the form:

$$w_j = \frac{\omega_j}{\omega_1 + \omega_2}, \quad \omega_j = \frac{\gamma_j}{(\varepsilon + \beta_j)^2}, \tag{E.11}$$

where ε is a small positive number to avoid division by zero (typically taken to be $\varepsilon = 10^{-6}$) and β_j are smoothness indicators for each approximation region. For these, we use the smoothness indicators of Jiang and Shu [152], which in this case are

$$\beta_0 = (\bar{n}_{i+1} - \bar{n}_i)^2, \tag{E.12}$$

$$\beta_1 = (\bar{n}_i - \bar{n}_{i-1})^2. \tag{E.13}$$

E.3 Finite difference method

In this section, we apply finite differences to solve Poisson's equation (6.71):

$$\frac{\partial}{\partial \mathbf{r}} \cdot \left[\varepsilon(\mathbf{r}) \frac{\partial}{\partial \mathbf{r}} V(t, \mathbf{r}) \right] = -\rho(t, \mathbf{r}). \tag{E.14}$$

Explicitly writing this in two dimensions, x and y, gives:

$$\frac{\partial}{\partial x} \left[\varepsilon(x, y) \frac{\partial}{\partial x} V(t, x, y) \right] + \frac{\partial}{\partial y} \left[\varepsilon(x, y) \frac{\partial}{\partial y} V(t, x, y) \right] = -\rho(t, x, y). \tag{E.15}$$

Expanding the LHS yields:

$$\frac{\partial \varepsilon}{\partial x}\frac{\partial V}{\partial x}+\frac{\partial \varepsilon}{\partial y}\frac{\partial V}{\partial y}+\varepsilon\left(x,y\right)\left(\frac{\partial^2 V}{\partial x^2}+\frac{\partial^2 V}{\partial y^2}\right)=-\rho\left(t,x,y\right). \tag{E.16}$$

Note that we can write this as

$$\frac{\partial l}{\partial x}\frac{\partial V}{\partial x}+\frac{\partial l}{\partial y}\frac{\partial V}{\partial y}+\frac{\partial^2 V}{\partial x^2}+\frac{\partial^2 V}{\partial y^2}=f\left(t,x,y\right), \tag{E.17}$$

where, for brevity, we define

$$l\left(x,y\right)\equiv\ln\varepsilon\left(x,y\right), \tag{E.18}$$

$$f\left(t,x,y\right)\equiv-\frac{\rho\left(t,x,y\right)}{\varepsilon\left(x,y\right)}. \tag{E.19}$$

We now make use of the following second order centred finite difference discretisations in the x-direction:

$$\frac{\partial}{\partial x}f\left(x,y\right) = \frac{f\left(x+\Delta x,y\right)-f\left(x-\Delta x,y\right)}{2\Delta x}+O\left(\Delta x^2\right), \tag{E.20}$$

$$\frac{\partial^2}{\partial x^2}f\left(x,y\right) = \frac{f\left(x+\Delta x,y\right)-2f\left(x,y\right)+f\left(x-\Delta x,y\right)}{\Delta x^2}+O\left(\Delta x^2\right), \tag{E.21}$$

and similarly in the y-direction. These can be written succinctly using discrete indices i and j for the x and y directions, respectively:

$$\left(\frac{\partial f}{\partial x}\right)_{ij} = \frac{f_{i+1,j}-f_{i-1,j}}{2\Delta x}+O\left(\Delta x^2\right), \tag{E.22}$$

$$\left(\frac{\partial^2 f}{\partial x^2}\right)_{ij} = \frac{f_{i+1,j}-2f_{ij}+f_{i-1,j}}{\Delta x^2}+O\left(\Delta x^2\right), \tag{E.23}$$

Applying the above discretisations to Poisson's equation (6.71) yields the following system of linear equations:

$$a_{ij}V_{ij}+b_{ij}V_{i-1,j}+c_{ij}V_{i+1,j}+d_{ij}V_{i,j-1}+e_{ij}V_{i,j+1}=f_{ij}, \tag{E.24}$$

with coefficients

$$a_{ij} \equiv 2\left(\frac{1}{\Delta x^2}+\frac{1}{\Delta y^2}\right), \tag{E.25}$$

$$b_{ij} \equiv -\frac{1}{\Delta y^2}\left(1+\frac{l_{i-1,j}-l_{i+1,j}}{4}\right), \tag{E.26}$$

$$c_{ij} \equiv -\frac{1}{\Delta y^2}\left(1-\frac{l_{i-1,j}-l_{i+1,j}}{4}\right), \tag{E.27}$$

$$d_{ij} \equiv -\frac{1}{\Delta x^2}\left(1-\frac{l_{i,j+1}-l_{i,j-1}}{4}\right), \tag{E.28}$$

$$e_{ij} \equiv -\frac{1}{\Delta x^2}\left(1+\frac{l_{i,j+1}-l_{i,j-1}}{4}\right). \tag{E.29}$$

For example, for the particular case of a 3×3 discrete grid of potentials, the above system of equations in matrix form is

$$\begin{bmatrix} a_{11} & c_{11} & 0 & e_{11} & 0 & 0 & 0 & 0 & 0 \\ b_{21} & a_{21} & c_{21} & 0 & e_{21} & 0 & 0 & 0 & 0 \\ 0 & b_{31} & a_{31} & 0 & 0 & e_{31} & 0 & 0 & 0 \\ d_{12} & 0 & 0 & a_{12} & c_{12} & 0 & e_{12} & 0 & 0 \\ 0 & d_{22} & 0 & b_{22} & a_{22} & c_{22} & 0 & e_{22} & 0 \\ 0 & 0 & d_{32} & 0 & b_{32} & a_{32} & 0 & 0 & e_{32} \\ 0 & 0 & 0 & d_{13} & 0 & 0 & a_{13} & c_{13} & 0 \\ 0 & 0 & 0 & 0 & d_{23} & 0 & b_{23} & a_{23} & c_{23} \\ 0 & 0 & 0 & 0 & 0 & d_{33} & 0 & b_{33} & a_{33} \end{bmatrix} \begin{bmatrix} V_{11} \\ V_{21} \\ V_{31} \\ V_{12} \\ V_{22} \\ V_{32} \\ V_{13} \\ V_{23} \\ V_{33} \end{bmatrix} = \begin{bmatrix} f_{11} \\ f_{21} \\ f_{31} \\ f_{12} \\ f_{22} \\ f_{32} \\ f_{13} \\ f_{23} \\ f_{33} \end{bmatrix}. \tag{E.30}$$

In general, we have the linear system

$$\mathbf{LV} = \mathbf{f}, \tag{E.31}$$

where $\mathbf{L}$ is a sparse block tridiagonal matrix. In practice, this system can be solved efficiently at each time step by precomputing and utilising the LU factorisation of $\mathbf{L}$.

E.4 Schur complement method

As described in Section 6.1.2, the computational domain of Poisson's equation is bounded by a zero-field condition radially distant from the device. Ideally, this condition should be placed as far from the device as possible to satisfy the actual boundary condition (6.31) at infinity. This quickly becomes computationally prohibitive, however, as the size of the linear system (E.31) grows with the area of the computational domain. In fact, any direct solution of Poisson's equation via Eq. (E.31) is not ideal, as the solution includes the electric potential in the air surrounding the device, while only the electric field within the device is required to evaluate the fluxes (6.74) and (6.75). In this section, we resolve this problem by devising a Dirichlet boundary condition around the edges of the device that is equivalent to the distant Neumann boundary condition (6.31).

To begin with, we write the linear system (E.31) in block matrix form:

$$\begin{bmatrix} \mathbf{A} & \mathbf{B} & \mathbf{0} \\ \mathbf{C} & \mathbf{D} & \mathbf{E} \\ \mathbf{0} & \mathbf{F} & \mathbf{G} \end{bmatrix} \begin{bmatrix} \mathbf{V}_{\text{semi}} \\ \mathbf{V}_{\text{edge}} \\ \mathbf{V}_{\text{air}} \end{bmatrix} = \begin{bmatrix} \mathbf{f}_{\text{semi}} \\ \mathbf{f}_{\text{edge}} \\ \mathbf{0} \end{bmatrix}, \tag{E.32}$$

where we have grouped electric potential elements as

- "air" — unnecessary air elements that we would like to eliminate

- "edge" — elements on the outer edge of the semiconductor *and* any air elements adjacent to electrodes, which we require to evaluate surface integrals for the conduction current (6.78) and charge (6.79)
- "semi" refers to the remaining elements of interest within the semiconductor

Performing block Gaussian elimination on the above system results in the following smaller system, containing only the elements of interest:

$$\begin{bmatrix} \mathbf{A} & \mathbf{B} \\ \mathbf{C} & \mathbf{D} - \mathbf{E}\mathbf{G}^{-1}\mathbf{F} \end{bmatrix} \begin{bmatrix} \mathbf{V}_{\text{semi}} \\ \mathbf{V}_{\text{edge}} \end{bmatrix} = \begin{bmatrix} \mathbf{f}_{\text{semi}} \\ \mathbf{f}_{\text{edge}} \end{bmatrix}. \tag{E.33}$$

The block $\mathbf{D} - \mathbf{E}\mathbf{G}^{-1}\mathbf{F}$ is called a Schur complement and this technique of eliminating unnecessary elements is a type of domain decomposition technique called the Schur complement method. Figure E.1 illustrates the effect of the Schur complement method on the size and structure of the Poisson matrix.

In practice, the Schur complement $\mathbf{D} - \mathbf{E}\mathbf{G}^{-1}\mathbf{F}$ can be evaluated efficiently by first performing the LU factorisation $\mathbf{G} = \mathbf{L}_\mathbf{G}\mathbf{U}_\mathbf{G}$ and then performing forward and backward substitution:

$$\mathbf{D} - \left(\mathbf{E}\mathbf{U}_\mathbf{G}^{-1}\right)\left(\mathbf{L}_\mathbf{G}^{-1}\mathbf{F}\right). \tag{E.34}$$

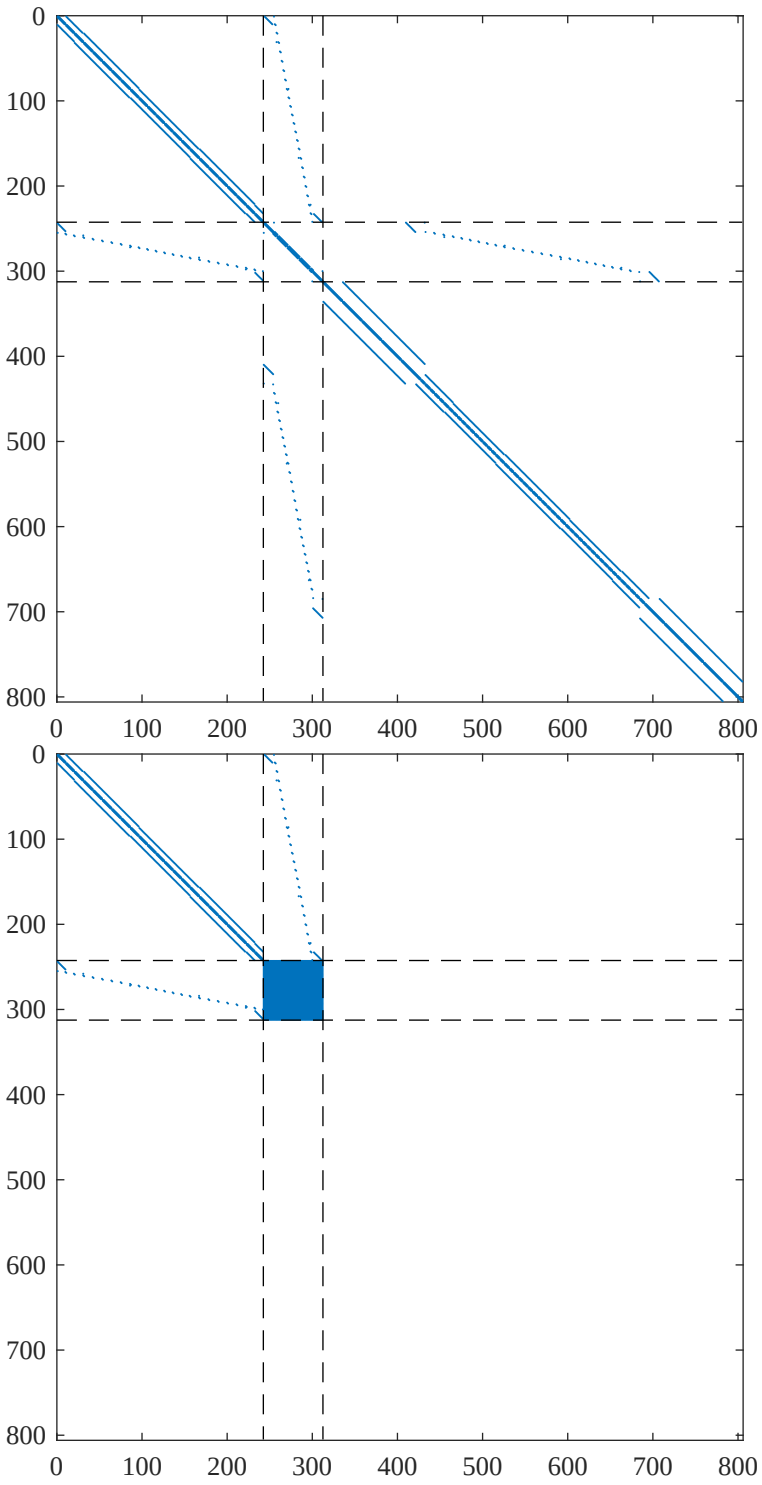

Figure E.1: Sparsity visualisation of the Poisson system $\mathbf{L}$ ordered in block form, as in Eq. (E.32), before and after Gaussian elimination. The result after elimination is a much smaller system, containing a dense block corresponding to the Schur complement $\mathbf{D} - \mathbf{E}\mathbf{G}^{-1}\mathbf{F}$, in Eq. (E.33).